An Investigation of the Interlayer Adhesion Strength between the Granular Base and Lightly Cemented Subbase and Its Influence on the Pavement Performance

By
Naphtal Ntirenganya

Thesis presented in fulfilment of the requirements for the degree of Master of Engineering in the Faculty of Engineering at Stellenbosch University

Supervisor: Dr Marius De Wet
Senior Lecturer: Geotechnical Engineering, Stellenbosch University

Co-Supervisor: Dr Denis Kalumba
Senior Lecturer: Geotechnical Engineering, University of Cape Town

March 2015

DECLARATION

By submitting this thesis electronically, I declare that the entirety of the work contained therein is my own, original work, that I am the sole author thereof (save to the extent explicitly otherwise stated), that reproduction and publication thereof by Stellenbosch University will not infringe any third party rights and that I have not previously in its entirety or in part submitted it for obtaining any qualification.

December 2014

ABSTRACT

Long term performance of a road pavement structure is significantly influenced by its potential to distribute traffic loading from the surface to the natural subgrade. The interlayer adhesion conditions play a substantial role in the induced stress-strain distribution across all layers of the entire structure. For layers constructed in stages like a granular base (GB) and a cement treated subbase (CTSB), the state of adhesion is questionable. Therefore a detailed investigation on the achievable adhesion and its influence on pavement performance is essential.

In this study, the direct shear test was used to assess the interlayer adhesion strength in terms of resistance of the GB layer to slide on top of the CTSB. To evaluate the level of achieved shear strength, the interlayer shear results were compared to the inlayer strength for a granular base and cemented subbase. The shear test results were presented in terms of relationships between shear stress and displacement, shear stress and normal pressure and vertical and horizontal displacements.

Based on frictional and dilatant approaches, shear test results demonstrated that the interlayer adhesion strength between the GB and CTSB is significantly influenced by the roughness conditions of the CTSB before placing the GB. Compacting materials of the base layer on top of the scarified CTSB produces a unified compound structure due to intimate interaction between the two layers. Moreover, the achievable adhesion depends on the maximum grain size available in the CTSB layer, confining pressure and moisture condition. The increase in maximum aggregate size deepens the interaction zone between the GB and scarified CTSB which results in high shear resistance. Ingress of water induces lubricant behaviour and weakens the shear resistance.

In the design example, it was shown that the assumption of full adhesion between pavement layers, currently used in many design methods, over-estimates the pavement life. The routine construction process of placing the GB on top of quasi-smooth CTSB induces poor adhesion between the layers which therefore affects stress-strain distribution behaviour across all layers of the pavement structure and then reduces the life of every single layer. According to the design example, the granular base layer is the most susceptible to early failure due to its stress-dependent behaviour.

The significant difference between pavement life when full adhesion is considered and when partial adhesion is allowed indicates that the achievable adhesion should be considered during the design of the structure rather than assuming full adhesion. Furthermore, the development of practical specifications and technical guidelines for improving the anticipated conditions in the field is recommended.

OPSOMMING

Die langtermyngedrag van ’n plaveiselstruktuur word tot ’n groot mate beïnvloed deur die vemoë daarvan om om verkeerslaste vanaf af die oppervlakte na die natuurlike grondlaag te verprei. Die adhesie tussen die plaveisellae speel ’n belangrike rol in die verspreiding van spannings en vervormings deur al die lae van die struktuur. In lae wat in fases gebou word, soos ‘n grofkorrelrige kroonlaag (GB) en ‘n sementgestabiliseerde stutlaag (CTSB), is die adhesie onder verdenking. ‘n Detailondersoek van die adhesie wat behaal kan word, en die invloed daarvan op plaveiselgedrag, is daarom noodsaaklik.

In hierdie ondersoek is die direkte skuiftoets gebruik om die tussenlaag-adhesie vas te stel in terme van die weerstand van die GB-laag om oor die CTSB-laag te skuif. Om die vlak van skuifsterkte wat behaal kan word, te bepaal, is die tussenvlakskuifsterkte vergelyk met die interne skuifweerstand van die grofkorrelrige laag en van die gestabiliseerde laag. Die skuiftoetsresultate is uitgedruk in terme van die verbande tussen skuifspanning en skuifverplasing, tussen skuifspanning en normaalspanning en ook tussen vertikale en horisontale verplasings.

Gebaseer op skuifweerstand en dilatansie het skuitoetsresultate gedemonstreer dat adhesie tussen die GB- en CTSB-lae baie beïnvloed word deur die ruheid van die CTSB voordat die GB gebou word. Indien die GB-laag bo-op ‘n grofgemaakte CTSB-laag geplaas word, word ‘n baie goeie verband en interaksie tussen die twee lae verkry. Die beskikbare adhesie hang ook af van die maksimum korrelgrootte in die CTSB-laag, die inperkspanning en die waterinhoud. Die toename in maksimum aggregaatgrootte maak die interaksiesone tussen die GB en die grofgemaakte CTSB dieper en dit lei tot hoër skuifweerstand. Infiltrasie van water dien as smeermiddel wat die weerstand verlaag.

In die ontwerp-voorbeeld is gedemonstreer dat die aanname van volle adhesie tussen plaveisellae, soos wat tans in baie ontwerpmetodes gedoen word, tot oorskatting van die leeftyd van die plaveisel lei. Die normale konstruksiemetode waarin die GB-laag bo-op ‘n semi-gladde CTSB-laag geplaas word, lei tot swak adhesie tussen die lae wat verspreiding van spannings en vervormings deur die plaveisel minder gunstig maak en die leeftyd van alle lae in die plaveisel verlaag. Volgens die ontwerp-voorbeeld is die grofkorrelrige kroonlaag die vatbaarste vir voortydige faling as gevolg van die sy spannings-vervormingsgedrag.

Die beduidende verskil tussen plaveiselleeftyd wanneer volle adhesie aanvaar of slegs gedeeltelike adhesie toegelaat word, illustreer dat die werklike haalbare adhesie gebruik moet word eerder as om volle adhesie te aanvaar. Verder word die onwikkeling van praktiese spesifikasies en tegniese riglyne om die verwagte toestande in die plaveisel beter in ag te neem, voorgestel.

To

Uwimana Marie Chantal Fabiola

Isheja Shingiro Elvis

And

Imena Sangwa Hector

I'm proud to be part of you.

ACKNOWLEDGMENT

I would like to express my sincere gratitude to The Almighty for guidance, strength and endurance to successfully complete this task.

I am also grateful to the following persons and institutions:

- Dr Marius de Wet (Stellenbosch University) and Dr Denis Kalumba (University of Cape Town), my study leaders. I am deeply appreciative for your time, advice and mentorship throughout. Your effort, guidance and interest in this research are highly appreciated. I am thankful to Dr Kalumba for being actively involved in this study. Furthermore, the financial support from Dr de Wet is also acknowledged.
- Prof Kim Jenkins (Stellenbosch University), Prof Andre Molenaar and Prof Martin van de Ven (Delft University of Technology). I appreciate your input and interest in this research. I am also gratified for your pavement courses which laid a good foundation on the subject.
- My special acknowledgments go to the University of Cape Town for allowing me to use their geotechnical laboratory especially Shear Trac III system machine.
- La Farge Tygerberg Valley for providing aggregate materials.
- Alex Mbaraga, Riaan Briedenhann, Chantal Rudman and Fabrice Barisanga. Your brilliant hands in this research are sincerely appreciated.
- Workshop and laboratory personnel Dion Viljoen, Gavin Williams and Colin Isaacs.
- Maggie and Jurie Goosen for encouragement and fellowship. You made Stellenbosch a home away from home.
- My parents, brother and in-laws for your prayers and encouragement.
- The government of Rwanda for loaning my studies.
- My working place, IPRC-Kigali for different facilitations.
- Rwanda High Commission in South Africa for smooth and timely assistance.
- I owe a lot of gratitude to my beloved wife Uwimana Marie Chantal Fabiola. Your strong heart and endurance encouraged me to persevere. You are my better half for ever.
- My two angels Isheja Shingiro Elvis and Imena Sangwa Hector. Thanks for enduring these two long years being far away from Dad.

“Nyagasani abahe umugisha mwese”

TABLE OF CONTENT

DECLARATION i

ABSTRACT ii

OPSOMMING iii

ACKNOWLEDGMENT v

TABLE OF CONTENT vi

LIST OF FIGURES x

LIST OF TABLES xiv

LIST OF SYMBOLS AND ABBREVIATIONS xvi

Chapter 1

INTRODUCTION 1

1.1. BACKGROUND OF THE RESEARCH 1

1.2. PROBLEM STATEMENT 2

1.3. RESEARCH OBJECTIVES 3

1.4. SCOPE AND LIMITATION 4

1.5. LAYOUT OF THE RESEARCH 5

Chapter 2

ROAD PAVEMENT DESIGN, RESPONSE ANALYSIS AND PERFORMANCE PREDICTION 6

2.1. INTRODUCTION 6

2.2. GENERAL OVERVIEW ON ROADS AND THEIR CLASSIFICATION 6

2.2.1. BRIEF HISTORY ON DEVELOPMENT OF ROADS 6

2.2.2. ROAD PAVEMENT CATEGORIES 8

2.2.3. FLEXIBLE PAVEMENT STRUCTURE 9

2.3. FLEXIBLE PAVEMENT DISTRESSES 11

2.4. THE PHILOSOPHY OF FLEXIBLE PAVEMENT DESIGN 15

2.4.1. PAVEMENT STRUCTURE RESPONSES 15

2.4.2. FLEXIBLE PAVEMENT PERFORMANCE 21

2.4.3. OVERVIEW OF SOUTH AFRICAN MECHANISTIC DESIGN METHOD (SAMDM) 22

Chapter 3

LITERATURE REVIEW ON PREVIOUS RESEARCH 30

3.1. INTRODUCTION 30

3.2. ADHESION IN FLEXIBLE PAVEMENT STRUCTURE 30

3.3. PRINCIPLES OF INTERLAYER ADHESION TESTING 33

3.3.1. DESTRUCTIVE TESTS 33

3.3.2. NON-DESTRUCTIVE TESTS (NDT) 42

3.4. DIRECT SHEAR INVESTIGATION 44

3.5. EFFECT OF INTERLAYER ADHESION ON PAVEMENT PERFORMANCE ESTIMATION 46

3.6. SUMMARY OF THE LITERATURE REVIEW 54

Chapter 4

RESEARCH MATERIALS, APPARATUS AND METHODOLOGY 56

4.1. INTRODUCTION 56

4.2. RESEARCH MATERIALS 56

4.2.1. GRADING 56

4.2.2. ATTERBERG LIMITS AND LINEAR SHRINKAGE 58

4.2.3. DRY BULK DENSITY, APPARENT RELATIVE DENSITY AND WATER ABSORPTION OF AGGREGATE. 59

4.2.4. MODIFIED AASHTO COMPACTION 59

4.2.5. SOAKED CBR 60

4.2.6. FLAKINESS INDEX 60

4.2.7. AGGREGATE CRUSHING VALUE (DRY AND WET) 60

4.2.8. UNCONFINED COMPRESSIVE STRENGTH (UCS) AND INDIRECT TENSILE STRENGTH (ITS) 61

4.3. DIRECT SHEAR INVESTIGATION 62

4.3.1. SAMPLE PREPARATION 64

4.3.2. INTERLAYER SHEAR TESTING 70

Chapter 5

TEST RESULTS AND DISCUSSION 75

5.1. INTRODUCTION 75

5.2. MATERIAL CHARACTERISATION TESTS RESULTS 75

5.2.1. SIEVE ANALYSIS 75

5.2.2. ATTERBERG LIMITS AND LINEAR SHRINKAGE 76

5.2.3. APPARENT AND BULK RELATIVE DENSITY (ARD AND BRD) AND WATER ABSORPTION 76

5.2.4. MODIFIED AASHTO COMPACTION 76

5.2.5. SOAKED CBR 77

5.2.6. FLAKINESS INDEX (FI) 78

5.2.7. AGGREGATE CRUSHING VALUE, ACV (DRY AND WET) 78

5.2.8. UNCONFINED COMPRESSIVE STRENGTH (UCS) AND INDIRECT TENSILE STRENGTH (ITS) 79

5.3. DIRECT SHEAR TEST RESULTS 81

5.3.1. SHEAR STRESS – HORIZONTAL DISPLACEMENT RELATIONSHIP 81

5.3.2. SHEAR STRESS – NORMAL PRESSURE RELATIONSHIP FOR INTERLAYER AND INLAYER TESTS 86

5.3.3. VERTICAL AND HORIZONTAL DISPLACEMENTS RELATIONSHIP 91

5.3.4. COMPARATIVE ANALYSIS ON INTERLAYER AND INLAYER SHEAR PERFORMANCE 95

5.3.5. QUANTITATIVE EFFECTS OF INVESTIGATED VARIABLES ON INTERLAYER SHEAR STRESS 103

5.4. SUMMARY OF MAIN FINDINGS 105

5.4.1. RESEARCH MATERIALS 105

5.4.2. INTERLAYER SHEAR INVESTIGATION 105

Chapter 6

PRACTICAL SIGNIFICANCE 108

6.1. INTRODUCTION 108

6.2. CORRELATION CHART FOR INTERLAYER ADHESION RATIO AND INTERLAYER FRICTION PARAMETER 108

6.3. PAVEMENT DESIGN EXAMPLE 110

6.3.1. OVERVIEW 110

6.3.2. ROAD CATEGORY AND LOADING CONDITIONS 111

6.3.3. TYPICAL STRUCTURE AND MATERIAL PROPERTIES 112

6.3.4. BEARING CAPACITY ESTIMATION 113

6.4. CONCLUDING SUMMARY 125

Chapter 7

CONCLUSIONS AND RECOMMENDATIONS 128

7.1. CONCLUSIONS 128

7.2. RECOMMENDATIONS 130

REFERENCES 131

APPENDICES 137

LIST OF FIGURES

Figure 2-1: Typical Roman Pavement (Macaulay, 1974 as presented in SAPEM, 2013) 7
Figure 2-2: Sir Lowry's pass 8
Figure 2-3: Typical cross sections of pavement structures 8
Figure 2-4: Different types of flexible pavement structure (Molenaar, 2007). 10
Figure 2-5: Flexible pavement distresses related to structural deterioration 12
Figure 2-6: Pavement distresses related to lack of interlayer adhesion 14
Figure 2-7: Conceptual representation of shear flow at the interface 16
Figure 2-8: Elastoplastic behaviour and resilient modulus of granular materials (Jenkins, 2013). 18
Figure 2-9: Axisymmetric stress state in elastic half space (Papagiannakis & Masad, 2008) 19
Figure 2-10: Schematic representation of stress distribution in two layers system (adapted from (Papagiannakis & Masad, 2008). 20
Figure 2-11: Fw factor for computing surface deflection at the centreline of a circular imprint carrying uniform stress (Papagiannakis & Masad, 2008). 21
Figure 2-12: Schematic diagram of Mechanistic – Empirical Design procedure (Theyse & Muthen, 2000). 23
Figure 2-13: Analysis Positions for Critical Parameters in a Flexible Pavement Structure (Adapted from SAPEM, 2013). 26
Figure 3-1: Beam analogy - different carrying capacity: (a) with compound- homogeneous beam; (b) without compound - three beams. (*b: Thickness of the cross section; E: Modulus of elasticity; h: Beam height, Iy: Inertia moment; L: Beam length; P: Force; W1: Deflection*), (Adapted from Tschegg *at al.,* 1995) 31
Figure 3-2: Conceptual illustration of interlock between two specimen structures (Raab *et al.*, 2012) 32
Figure 3-3: Schematic representation of separation mode (Muslich, 2010b) 33
Figure 3-4: Illustration of tensile bonding test with different failure modes 34
Figure 3-5: UTEP pull-off device (Tashman *et al.*, 2006) 35
Figure 3-6: Illustration diagram of the laboratory based manual torque bond test developed by Choi, *et al.* (2005) 36
Figure 3-7: Schematic representation of ASTRA interface shear apparatus (Canestrari & Santagata, 2005) 38
Figure 3-8: Illustration diagram of Louisiana State Interface Shear Strength Tester (Mohammad *et al.,* 2009) 39

Figure 3-9: Basic configuration of shear fatigue test developed by Romanoschi & Metcalf (2002) 40
Figure 3-10: Photograph and schematic illustration of the modified Leutner device (Choi *et al.,* 2005)..... 41
Figure 3-11: Schematic illustration of different load and clamping device in the LPDS test (Raab & Partl, 1999) 42
Figure 3-12: Photographic illustration of PSPA (Strategic Highway Research Program, s.a.). 43
Figure 3-13: Results of direct shear tests. (a) Shear stress ratio; (b) Dilation and (c) Dilation rate against horizontal displacement for tests on loose sand, medium dense sand and medium dense sand-gravel mixture (Simoni & Houlsby, 2006) 45
Figure 3-14: Schematic illustration of saw-tooth model (Adapted from Rowe, 1962) 46
Figure 3-15: Schematic illustration of four layer structure analysed by Romain (Adapted from Uzan *et al.*, 1978)..... 47
Figure 3-16: Graphical representation of stress, strain and deflection distribution in the second, third and fourth layer (Romain, 1968) 49
Figure 3-17: Schematic representation of the flexible pavement structure analysed by Uzan *et al.* (1978)..... 50
Figure 3-18: Increase of radial stress at the bottom of surfacing due to change of interface condition (Adapted from Uzan *et al.* 1978) 51
Figure 3-19: Distribution of radial strain throughout the entire pavement structure (Adapted from Uzan *et al.* 1978..... 51
Figure 3-20: Schematic illustration of pavement structure analysed by Kruntcheva *et al.* (2005) 52
Figure 3-21: Influence of bond condition on life to failure of flexible pavement structure (Kruntcheva *et al.* 2005)..... 53
Figure 3-22: Influence of horizontal load on life to failure of debonded interface expressed as percentage of full bonded (Kruntcheva *et al.*, 2005) 54
Figure 4-1: General overview of the experimental investigation..... 57
Figure 4-2: Sieves set up used for materials separation 58
Figure 4-3: Mechanical compaction machine located in SU soil lab..... 59
Figure 4-4: Aggregate Crashing Value (ACV) testing procedure 61
Figure 4-5: UCS and ITS testing configuration and analysis..... 61
Figure 4-6: Flowchart of shear test experimental design 63
Figure 4-7: Laboratory vertical shaft mixer 64
Figure 4-8: Schematic of vibratory compaction machine and appropriate marking of the compaction heights 66

Figure 4-9: SU vibratory compaction machine 67
Figure 4-10: Illustration of CTSB compaction details 67
Figure 4-11: Photograph of CTSB surface roughness before casting the granular base..... 68
Figure 4-12: Illustration of the curing process 68
Figure 4-13: Illustration of sample preparation and handling process 69
Figure 4-14: Photograph of Shear Trac-III 71
Figure 4-15: Photographic illustration of specimen set up in the Shear Trac-III load frame. 73
Figure 5-1: Wet Sieve analysis for G2 and G5 materials from Lafarge quarry 75
Figure 5-2 : Typical compaction curve 77
Figure 5-3: 7days UCS and ITS tests results 79
Figure 5-4: Shear stress versus horizontal displacement for interlayer tests 82
Figure 5-5: The effect of the normal pressure and CTSB surface condition on the interlayer shear stress 83
Figure 5-6: Shear stress versus horizontal displacement for inlayer tests with 19mm maximum aggregate 85
Figure 5-7: The Relationship between Shear Stress and Normal Stress for Interlayer Tests 87
Figure 5-8: Impact of CTSB surface roughness, interface saturation and CTSB maximum aggregate on interlayer friction and cohesion 90
Figure 5-9: The Relationship between Shear and Normal Stresses for Inlayer Tests with 19mm aggregate size 90
Figure 5-10: Dilatancy effect on CTSB and GB interlayer shear tests 92
Figure 5-11: Influence of aggregate size, saturation condition and normal pressure on dilatancy of scarified CTSB layer 93
Figure 5-12: Influence of aggregate size, CTSB roughness and testing condition on dilation angle 95
Figure 5-13: Comparative analysis of inlayer and interlayer shear stress and relative horizontal displacement to failure for the unsaturated condition. 97
Figure 5-14: Comparative analysis of inlayer and interlayer shear stress and relative horizontal displacement to failure for the saturated condition. 98
Figure 5-15: Comparative analysis of inlayer and interlayer failure envelopes for the unsaturated condition 99
Figure 5-16: Comparative analysis of inlayer and interlayer failure envelopes for the saturated condition 101
Figure 5-17: Comparative analysis of dilation between inlayer and interlayer shear test for the unsaturated condition 103

Figure 5-18: General trends of interlayer shear stress at failure for investigated parameters 106
Figure 5-19: General trends of interlayer friction and dilation angle for investigated parameters..... 107
Figure 6-1: Correlation chart for interlayer adhesion ratio and interlayer friction parameter for the interface between GB and CTSB 110
Figure 6-2: Typical cross section of the pavement. (a) Loading conditions, (b) Critical positions of failure 112
Figure 6-3: Vertical and horizontal strain distribution curve across the pavement structure with variation in interlayer friction 114
Figure 6-4: Vertical and horizontal stress distribution across the pavement structure with variation in interlayer friction..... 115
Figure 6-5: The influence of interlayer friction conditions on the life of the asphalt layer... 118
Figure 6-6: Deviator stress distribution in the base layer with variation in interlayer friction 119
Figure 6-7: The influence of interlayer friction conditions on the life of the granular base layer; (a) estimated life when failure is localised in the middle of the layer; (b) estimated life if failure is localised in the weakest sub-layer..... 121
Figure 6-8: The influence of interlayer friction conditions on the performance of the CTSB layer..... 123
Figure 6-9: Life of the subgrade layer according to different interlayer friction conditions . 125
Figure 6-10: Comparison of total number of load repetitions for scarified and quasi-smooth CTSB 126

LIST OF TABLES

Table 2-1: Pavement categories and material usage (Ebels, 2008) 9
Table 2-2: Pavement materials and respective behavioural analysis theories (Adapted from (Jenkins, 2013). 17
Table 2-3: South African pavement structure materials with their material codes (TRH14, 1985). 24
Table 3-1: Relative results of four - layer pavement structure with different interface conditions analysed by Romain (Adapted from Uzan *et al.*, 1978) 48
Table 5-1: BRD, ARD and water absorption for G2 and G5 materials retained on a 4.75 mm sieve. 76
Table 5-2: Mod AASHTO test results for research materials 77
Table 5-3: CBR results for G5 materials 77
Table 5-4: Flakiness Indices for selected G2 fractions 78
Table 5-5: ACV test result for wet and dry G2 materials 78
Table 5-6: Summary of material characterisation tests and the comparison with the recommended values 80
Table 5-7: Summary of the achieved shear stress and associated horizontal displacement for the interlayer direct shear test. 84
Table 5-8: Summary of shear stress-horizontal displacement results for the inlayer tests 86
Table 5-9: Achieved interlayer friction and cohesion 89
Table 5-10: Dilatancy effect on interlayer shear for the scarified CTSB layer 92
Table 5-11: Dilation angle 94
Table 5-12: Inlayer and interlayer shear results in terms of shear stress and horizontal displacement for the unsaturated condition 96
Table 5-13: Inlayer and interlayer shear results in terms of shear stress and horizontal displacement for the saturated condition 98
Table 5-14: Friction coefficients and cohesion for the unsaturated condition 99
Table 5-15: Friction coefficients and cohesion for the saturated condition 101
Table 5-16: Average dilation angle for the unsaturated condition 102
Table 5-17: Factorial design analysis for the interlayer shear stress 104
Table 6-1: Interlayer adhesion ratio β for shear, friction and dilation responses 109
Table 6-2: Interlayer adhesion ratios correlated to the interlayer friction parameters along with associated ALK values 111
Table 6-3: Mechanical properties of materials used to model pavement layers 113
Table 6-4: Shear properties of granular base material (SAPEM, 2013) 113

Table 6-5: Critical parameter and fatigue life of the asphalt layer with variation in interlayer friction between GB and CTSB 116
Table 6-6: Critical parameter and life of the granular base layer with variation in interlayer friction 120
Table 6-7: Critical parameter and life of the lightly cemented subbase with variation in interlayer friction..... 122
Table 6-8: Critical parameter and life of the subgrade layer with variation in interlayer friction 124

LIST OF SYMBOLS AND ABBREVIATIONS

SYMBOLS

μ	Coefficient of friction
μƐ	Micro strain
μm	Micrometre
∞	Infinite
c	Cohesion
Dr	Relative density
Ɛ	Stain
E	Stiffness
Ks	Interlayer shear reaction modulus
Mr	Resilient modulus
υ	Poisson's ratio
α	Interlayer friction parameter
β	Interlayer adhesion ratio
σ	stress
ϕ	Angle of internal friction
Ψ	Dilation Angle
Ʈ	Shear stress

ABBREVIATIONS

AASHTO	American Association of State Highway and Transportation Officials
AC	Asphalt Concrete
ACV	Aggregate Crushing Value
AD	*"Anno Domini"* or in the Christian era
ALK	Reduced spring compliance
APT	Accelerated Pavement Testing
ARD	Apparent Relative Density
BC	Before Christ
BRD	Bulk Relative Density
CTSB	Cement Treated Subbase
DIN	*"Deutsches Institut für Normung"* or German Institute for Standardization
FACT	Fines Aggregate Crushing Test
FI	Flakiness Index
FWD	Falling Weight Deflectometer
GB	Granular Base
GM	Grading Modulus
GPR	Ground Penetrating Radar
HVS	Heavy Vehicle Simulator
ITS	Indirect Tensile Strength
LL	Liquid Limit
LVDT	Linear Variable Differential Transformer
MDD	Maximum Dry Density
NDT	Non-Destructive Testing
OMC	Optimum Moisture Content
PI	Plastic Index
PL	Plastic Limit

SABS	South African Bureau of Standards
SAMDM	South African Mechanistic Design Method
SAPEM	South African Pavement Engineering Manual
SED	Strain Energy Distortion
SG	Subgrade
SU	Stellenbosch University
TMH	Technical Methods for Highways
TRH	Technical Recommendations for Highways
UCS	Unconfined Compressive Strength
UCT	University of Cape Town
UK	United Kingdom
US	United Sates
WA	Water Absorption

Chapter 1

INTRODUCTION

1.1. BACKGROUND OF THE RESEARCH

A road pavement structure is defined as a set of layers arranged one on top of other, all supported by a natural or improved subgrade. This configuration dates from the Roman era whereby a layered system made of stones and gravel were adopted to provide durable and resistant roads against the wheel pressure of chariots and wagons. The modern pavement structure comprises a surfacing layer, base and subbase courses, selected layers and natural subgrade. The main purpose of this configuration is to provide the most effective structure with adequate potential to distribute traffic loading from the surface to the natural subgrade with minimum damage. Researchers have shown that this purpose can only be achieved if all layers work as one compound (Hariyadi *et al.*, 2013; Kruntcheva *et al.,* 2005; Uzan, 1976; Uzan *et al.,* 1978; Ziari & Khabiri, 2007).

Basically, road pavement performance is governed by the strength and stiffness of the materials available in each individual layer which enable it to endure traffic induced stress and strain throughout the service life of the road. The failure mechanism of main pavement construction materials has been well documented from many years ago and fairly well understood by pavement engineers. According to Theyse *et al.* (1996), three main causes of pavement structural deterioration are fatigue, crushing and permanent deformation. Each layer in the pavement structure exhibits one of the failure modes mentioned above according to constitutive materials and associated stress-strain distribution behaviour.

In most developing countries, it is quite normal to experience potholes, ruts, cracks and other types of road pavement deterioration. These are generally linked to lack of maintenance and pavement overloading. However, the lack of mutual interaction between layers has also been identified to influence the pavement response against traffic induced stress and strain across the entire structure, and consequently affects the pavement performance. Researchers like Kruntcheva *et al.* (2005) used theoretical analysis to establish the impact of interlayer adhesion on stress-strain distribution throughout the pavement structure. They analysed a pavement structure using a multi-layered linear elastic program by considering various degrees of interface adhesion between pavement layers. The results indicated that the interlayer adhesion condition can reduce the life of a pavement structure by up to 80%. They also conducted static linear and nonlinear two-dimensional finite element analyses and similar results were found.

Practically, in South Africa and other parts of the world, premature failures of pavement structure due to interlayer adhesion problems have been reported (De Beer *et al.,* 2012; Hu & Walubita, 2010; Khweir & Fordyce, 2003; Netterberg & de Beer, 2012). Cores extracted from the trafficked and early deteriorated roads pavements have shown signs of layer debonding.

After realizing the severity of the interface condition on the pavement performance, researchers have devoted most of their attention to develop the most reliable quantification method. Different laboratory and *in situ* testing methods have been developed in different countries to assess the degree of adhesion between two layers. Since the interface was admitted to fail by shear, most of the testing approaches were typically based around shear testing. However, tensile and torsional testing were proposed and used to characterize bonding strength of the tack coat used as binder agent in bituminous layers.

From the comparative study conducted by Raab *et al.* (2009), the direct shear test was selected as the most reliable and effective method for testing interlayer adhesion strength in the pavement structure. Since two distinct setups of shear testing are available (i.e. devices with or without normal load), the apparatus allowing testing with the application of normal pressure has been recommended for testing granular materials. The shear testing with normal pressure was selected because it considers the dilatancy effect which is common in granular materials.

1.2. PROBLEM STATEMENT

The Mechanistic Design Method is one of the most popular structural design approaches used in South Africa and all other the world. The method is based on computation of stress and strain distribution in pavement layers. Most of the computation approaches used assumes full friction between layers. However, researchers have shown that this assumption is not realistic and results in over-estimation of pavement life (Kruntcheva *et al.* 2005; Sutanto *et al.*, 2006; Uzan *et al.,* 1978; Whiffin & Lister, 1962).

Characterisation of interlayer adhesion between pavement layers has been a point of concern for many years. Several studies have been conducted for acquiring deep understanding on real status of bonding in pavement layers (Collop *et.al.*, 2003; Crispino *et al.*, 1997; Hariyadi *et al.,* 2013). However, the reviewed literature has shown that most of the analyses performed were only focused on top asphaltic layers even though bonding challenges are just as noticeable in deeper layers, like base and subbase, as in top ones (Khweir & Fordyce, 2003; Kruntcheva *et al.*, 2005; Raab & Partl, 2004). Therefore the knowledge-gap on the adhesion condition between deeper layers is enormous. .

Deep-seated layers of a typical South African pavement structure are granular base and cement treated subbase. Both layers are laid below a thin asphaltic layer, all supported by a natural or improved subgrade. The routine construction processes of the cemented subbase involves mixing the material with the required amount of cement and water, compacting and curing the layer for at least seven days before laying the base layer. The theory of cement stabilization in the South African pavement structure has been well documented and understood since the 1940s (SAPEM, 2013), but the emphasis is confined to how this staged process affects the adhesion condition of the base course, laid on top of stiff hardened cemented subbase layer. In fact, cementation process starts immediately after the soil gets in contact with the cement and the compaction water. This results in development of compressive and tensile strength inside the layer. At the time of laying the base layer, the cement stabilized subbase is already hardened in such a way that the unification between layers became questionable. Moreover, a smooth wheel roller used for the subbase compaction creates a quasi-smooth surface which might hinder interlock between two layers.

The key focus of this study was to investigate the achievable adhesion strength between granular base and cement treated subbase when the above mentioned routine construction process is followed. The direct shear test with normal pressure was used. Extensive shear tests were conducted on samples prepared under procedures reflecting the actual field conditions.

1.3. RESEARCH OBJECTIVES

The influence of material properties on pavement performance has been well understood from a couple of years ago. Recently, much effort was dedicated to the impact of interlayer adhesion conditions on road pavement effectiveness. Various theoretical and laboratory based approaches have been developed to acquire understanding of the subject. However, according to the published literature, the knowledge gap is still wide as far as adhesion in deeper layers is concerned. This, therefore, provided a solid basis to conduct this study.

The main objective of the study was to investigate the state of interlayer adhesion between granular base and lightly cemented subbase in a typical South African pavement structure and assess its influence on the predicted pavement life. The characterisation was based on shear resistance between two layers whereby direct shear tests were performed on laboratory prepared specimens simulating the actual conditions in the field. To achieve the main objective, the following secondary objectives were formulated:

- Characterisation of research materials in conformity with South African road construction material guidelines,
- Development of a specimen preparation procedure which simulates the actual pavement construction process in the field,
- Conducting laboratory testing to assess the influence of material properties, construction practice and pavement working condition, on the interlayer shear strength, and
- Use of multi-layered linear elastic design software, BISAR to understand the influence of interlayer adhesion on long term performance of the South African pavement structure, especially the interface between granular base and lightly cemented subbase. The analysis was based on the routine construction practice used in the field.

This study analysed the interlayer shear strength by taking into account various testing conditions. Moreover, the interlayer shear results were compared with the inlayer shear strength test results conducted on both, granular and lightly cemented materials used to make both layers. To this end, it is important to clarify the difference between "*interlayer*" and "i*nlayer*" shear strength. For the purpose of this study, the interlayer shear strength refers to the maximum shear stress obtained with the direct shear box when shear plane was between granular base and cement treated subbase. Likewise, the inlayer shear strength corresponds to the maximum shear stress when the shear plane is localised within one of the layers (i.e. granular base or cement treated subbase).

1.4. SCOPE AND LIMITATION

Laboratory investigation related to the research materials was limited to assorted standard tests recommended by SAPEM (2013) and TRH 14 (1985) for graded crashed stone G2 and natural gravel G5. Detailed analysis about cement stabilisation was not covered. Only UCS and ITS tests were run to determine the optimum cement content to be used for stabilisation.

The direct shear investigation conducted in this study was only limited to four factors namely, maximum aggregate size in cement treated subbase, testing normal pressure, moisture conditions and cement treated subbase roughness before laying the top granular base. The analysis was based on frictional and dilatant criteria.

1.5. LAYOUT OF THE RESEARCH

Chapter 1: Introduction

The first chapter describes the general background of interlayer adhesion. The chapter highlights what has been covered on the subject and where the knowledge gap is. It also outlines the research objectives and scope.

Chapter 2: Road Pavement Design, Response Analysis and Performance Prediction

The second chapter gives a general overview on road pavement characteristics and design. The chapter highlights the worldwide historical background of roads and especially the South African context. It also demonstrates theoretical approaches used to estimate stress-strain distribution across a multi-layered pavement structure, and empirical relationships used to estimate the pavement performance. The South African Mechanistic Design Method (SAMDM) is also discussed in this chapter.

Chapter 3: Literature Review on Previous Research

This chapter presents a summary of published literature on interlayer adhesion strength in a pavement structure. It also exhibits theoretical and laboratory based approaches developed by various researchers.

Chapter 4: Research Materials, Apparatus and Methodology

The adopted research methods and the laboratory investigation program are outlined in this chapter. Standard tests conducted to characterise research materials are presented. Moreover different procedures followed for the direct shear investigation are also demonstrated in the chapter.

Chapter 5: Test Results and Discussion

Test results and discussion are presented herein. The chapter presents results for material characterisation test and direct shear investigation.

Chapter 6: Practical Significance

The influence of interlayer adhesion strength on pavement performance is presented in this chapter.

Chapter 7: Conclusions and Recommendations

The chapter presents general conclusions of the study and provides recommendations for further studies.

Chapter 2

ROAD PAVEMENT DESIGN, RESPONSE ANALYSIS AND PERFORMANCE PREDICTION

2.1. INTRODUCTION

Traffic loading induces progressive deterioration of the road pavement over its service life. The potential of the road to withstand traffic induced damage depends on the physical and mechanical properties of the pavement construction materials used. However, the accurate and realistic design approach plays a significant role on the pavement performance. According to the expected traffic, the structural design method must carefully analyse factors like stress-strain distribution and failure mode of pavement material, which influence the structural and functional performance of the road pavement.

This chapter provides a detailed overview of road pavement characteristics and performance behaviour.

The chapter is divided into four parts. The first part discusses a general perspective of the road pavement system and classification. The second section describes different pavement distresses related to structural failure while in the third, the design approach of the flexible pavement is discussed. An overview of the South African Mechanistic Design Method appears in the fourth part.

2.2. GENERAL OVERVIEW ON ROADS AND THEIR CLASSIFICATION

2.2.1. BRIEF HISTORY ON DEVELOPMENT OF ROADS

Sustainability of transport services is considered as one of the major indicators of a country's development. According to Trade and Industrial Policy Secretariat's report (Naudé, 1999), road transport dominates other transport modes as far as moving people and goods are concerned. For instance, in 1995, freight transport by road was estimated at 72.2 per cent in Europe and 80 per cent in South Africa. This, highlights how important road infrastructure is, and justifies more effort in detailed analysis design and construction of roads.

Thorough analysis of road development history from the remote ages is a key element to consider when trying to understand how pavements developed. Initially, pavements were nothing more than simple-bridle paths leading people and animals to places of food and drink. Population growth and urban development facilitated interaction between different groups of people in terms of trade, warfare and socialising. This occurred around 3500 BC

as mentioned in SAPEM (2013). Since then, layered structures, constructed with materials of better quality were used to protect the subgrade against wheel damage of chariots and wagons invented during that period. This gave rise to the pavement structure we commonly use today.

Early records acknowledge a road built in Egypt by the Pharaoh Cheops around 2500 BC as the first paved road ever constructed (Shirley, 2012). It was approximately 1,000 Metres long and 20 Metres wide. In Europe, the first modern roads were built by Romans, with a network of not less than 100,000 kilometres of roads built between 400 BC and 400 AD (SAPEM, 2013). The Roman roads were sloped upward in the centre of the cross section to drain out rainwater. They were constructed on a foundation of large stones with a surfacing course of smaller stones and gravel, confined between raised stone kerbs as shown in Figure 2-1.

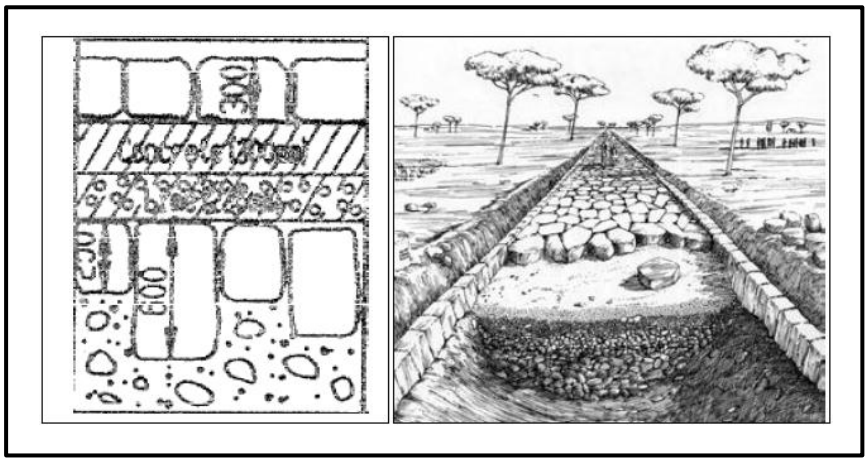

Figure 2-1: Typical Roman Pavement (Macaulay, 1974 as presented in SAPEM, 2013)

In South Africa, road development originated from hundreds of mountain passes developed by indomitable road pioneers of the remote ages, with considerable engineering feats. They provided ways through and over the natural barriers in the area; giving access to communities, and offering the infrastructure that makes for a thriving economic and social life.

Ross (2004) gave an account of about fifty of the best and well-known mountain passes of the greater Cape Area. He highlighted extensive work done by Andrew Bain, Thomas Bain, Charles Michell, John Montagu, Adam de Smidt, Patrick Fletcher and many other pioneers of the era, to transform mountain passes into roads, which are able to carry heavy traffic for a long period without failure. Some of them, given the required maintenance, are currently still in use (SAPEM, 2013). A good example is Hottentots Holland Kloof pass - now called Sir Lowry's pass, located on N2 national road near Somerset West in the Western Cape Province (see Figure 2-2)

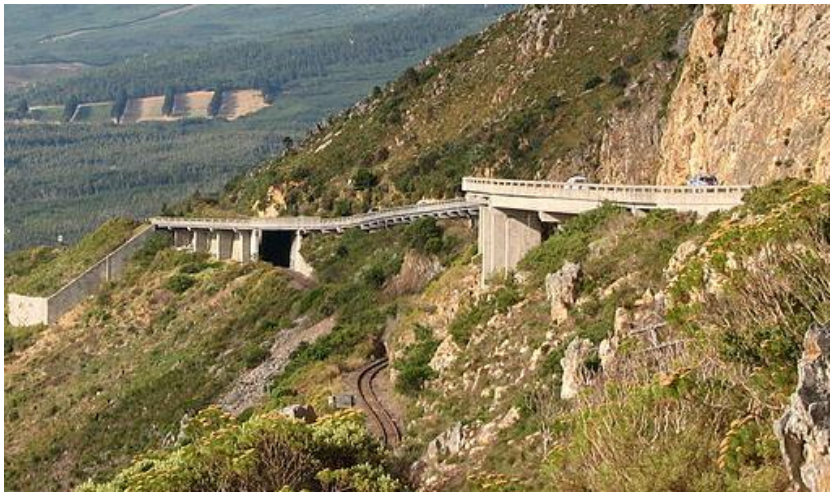

Figure 2-2: Sir Lowry's pass

Population growth and advances in transportation technology from non-motorised to motorised transport required improved roads built with high quality materials and sound construction practices. These roads are required to provide a pavement structure that can withstand high traffic loading with minimum damage.

2.2.2. ROAD PAVEMENT CATEGORIES

Generally, the classification of pavement types is merely based on the type of materials used to build upper layers, since deeper layers are more or less the same for given factors like traffic volume, maintenance requirements, climate conditions and so forth (SAPEM, 2013). Consequently, two distinct categories are routinely recognized:

- Flexible pavement, and
- Rigid pavement.

Figure 2-3 illustrates typical cross sections of the pavement categories mentioned above.

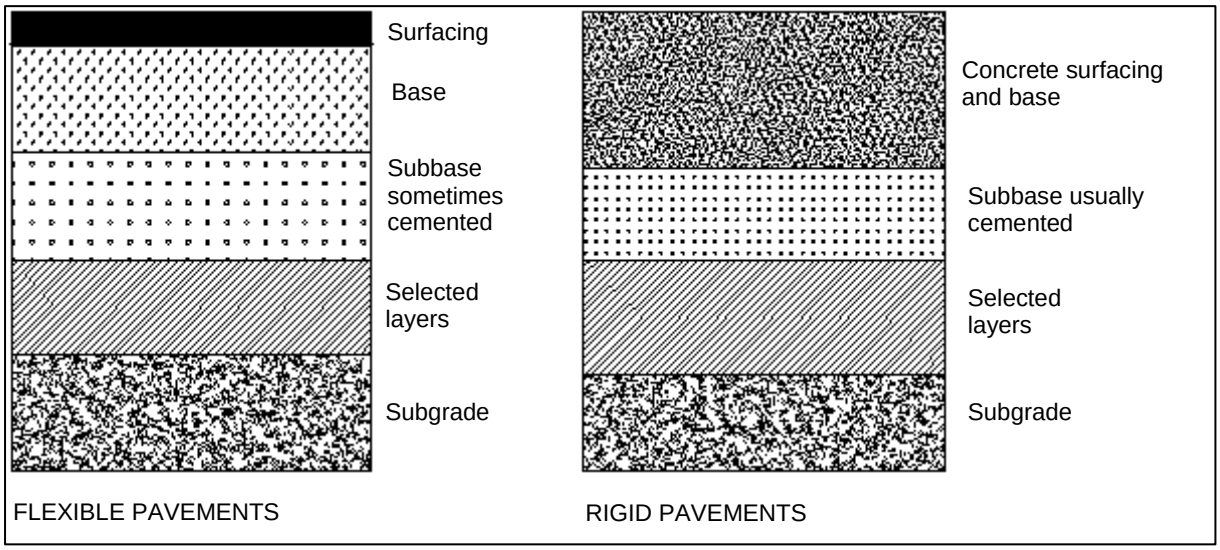

Figure 2-3: Typical cross sections of pavement structures

It is important to note that the above mentioned classification is generally used in developed countries. In developing countries, however, large parts of the road networks comprises of unsurfaced roads. Since they are constructed using different materials in the top layers, comparing them to flexible and rigid pavements, they are added as a third category. Table 2-1 shows the different materials used for various layers of a specific pavement type.

Table 2-1: Pavement categories and material usage (Ebels, 2008)

	UNSURFACED	FLEXIBLE PAVEMENT				RIGID PAVEMENT
SURFACING	Granular	Bituminous				Concrete
BASE		Granular		Bituminous		
SUBBASE		Granular	Cemented	Granular	Cemented	Cemented

Unsurfaced roads are typically constructed using only granular materials over the full depth of the pavement structure. Rigid pavement materials are comparatively, straight forward; i.e concrete surfacing on top of a cemented subbase, with a possibility of granular layers below. On the other side, flexible pavements exhibit the largest variety of material usage. It frequently consists of various combinations of bituminous, cemented and granular materials. This might cause variable performance in some cases. Therefore, extensive research and analysis are needed to be able to characterise the performance of these combinations of materials.

Flexible pavements are characterised by a bituminous surfacing layer marked as thick or thin asphalt pavement. Thicker surfacing layers are more common in Europe and North America in comparison to Africa, both for road pavements and airport runway pavements (Molenaar, 2007). Thin asphalt pavements generally consist of only a bituminous surfacing (typically not more than 50 mm) laid at the top of a granular base layer as shown in Figure 2-4 (I and II). This configuration is widely used in South African pavement structures, and in many other surrounding developing countries.

2.2.3. FLEXIBLE PAVEMENT STRUCTURE

A pavement structure is defined as a combination of different layers made of different materials, placed on top of natural subgrade to support the traffic load and distribute it to the roadbed with minimum damage (Transportation Officials, 1993).

The typical South African flexible pavement structure is not far from the Roman's confuguration mentioned in Section 2.2.1; It consists of a thin asphalt top layer constructed on top of a high quality crushed stone base layer and stiff cemented (stabilised) subbase.

Since granular materials exhibit stress dependence behaviour, stiff support from the cemented subbase enables stiffer behaviour of the granular base. In contrast, less stiff behaviour will be seen in the same layer should a granular subbase be used. This configuration causes the traffic loading to be endured by a granular base and cement treated subbase (structure II of Figure 2-4), while the asphalt top layer provides a smooth riding surface and skid resistance.

The high performance of two typical South African pavement structures shown in Figure 2-4, comes from the high quality available granular materials used for base and subbase layers, and the high level of compaction achieved (Molenaar, 2007). Structure II, cement treated subbase and granular base is discussed further in this study. The investigation of adhesion strength between two layers, and how this can affect the predetermined pavement life is covered. This structure was chosen since adhesion was suspected to be comparatively weak due to heterogeneity of materials making up the two layers. Moreover, adhesion strength between cemented subbase and granular base, in that particular structure, is doubtful due to the fact that both layers are constructed in stages. Stage construction may reduce adhesion between the layers.

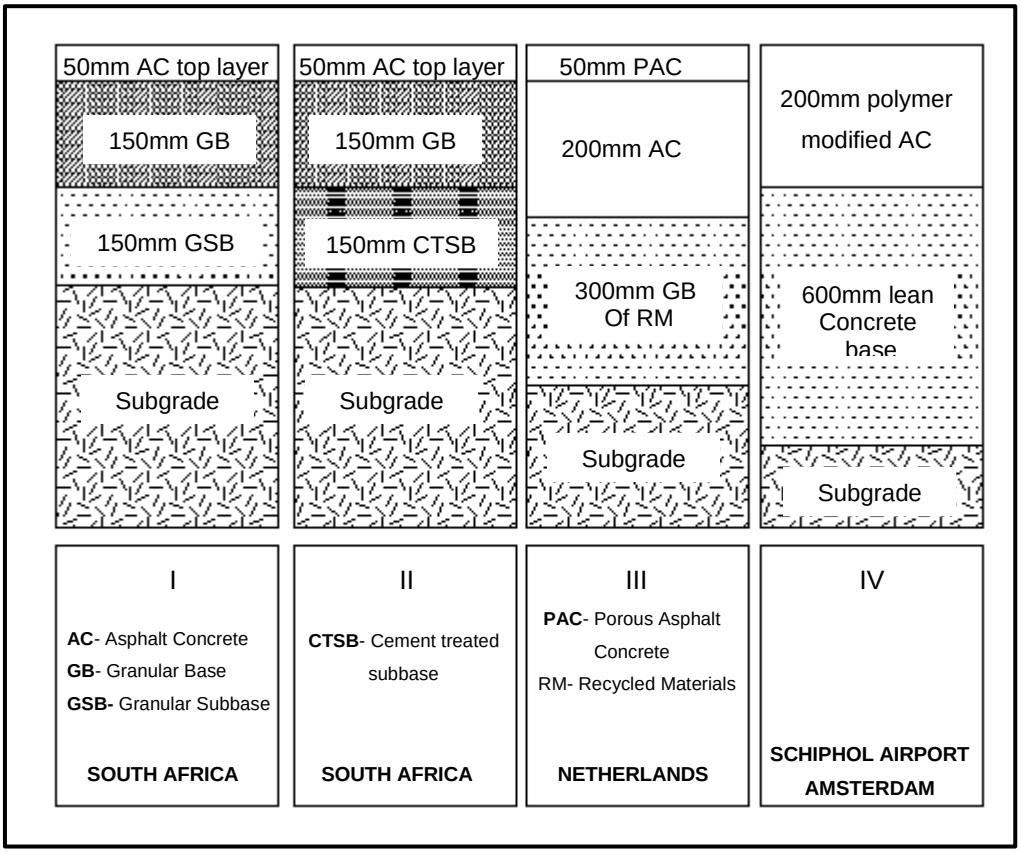

Figure 2-4: Different types of flexible pavement structure (Molenaar, 2007).

Practically, the main objective of combining different materials in a layered system is to provide a pavement with the desired functional and structural service levels over its design life. To achieve this, the upper structural layers, which carry a huge stress emanating from tyre pressure, must be constructed with the highest quality materials and proper techniques. This is done to ensure the necessary spreading of load from the surface to the *insitu* subgrade. However, Khweir & Fordyce (2003) noticed early pavement failure even though individual layers exhibit reasonably high dynamic stiffness modulus values, high permanent deformation resistance and high fatigue resistance properties. These failures were induced by the weak interface between layers. It is therefore, important to recognize that pavement performance can be seriously affected by interface problems, even though the performance of an individual layer may be very high.

2.3. FLEXIBLE PAVEMENT DISTRESSES

Flexible pavement distresses can be classified as surface, drainage, functional, and pavement structural distresses (SAPEM, 2013).

Surface distresses refer to the top apparent deterioration related to surface texture, potholing, surfacing cracks, aggregate loss and general condition of the binder. It is important to mention that surface deterioration could allow water ingress which results in structural weakening and early deterioration.

Drainage distresses result from water ingress due to poor surface and subsurface drainage system. It is manifested by ponding, vegetation alongside the road resulting in sand build up and entrapment of water in the pavement.

Functional distresses are related to how comfortable and safe the road user is, while driving on a particular section of the road. Various indicators are used to assess functional distresses of a section like riding quality, skid resistance, edge drop and bush encroachment.

All types of distresses mentioned above are relatively easy to identify and less expensive to rehabilitate if maintenance measures like resurfacing and drainage system rehabilitation are implemented in real time. However, pavement structural defects are the most difficult to identify and more expensive to repair.

Structural distresses are related to deeper deterioration of the pavement structure, mainly due to traffic loading, drying shrinkage and environmental hazards. Traffic induced distresses are normally confined to the wheel paths and are caused by ineffective distribution of stress and strain across the pavement structure. In Figure 2-5, various structural related distresses are shown as adapted from SAPEM (2013).

(a) Crocodile cracking

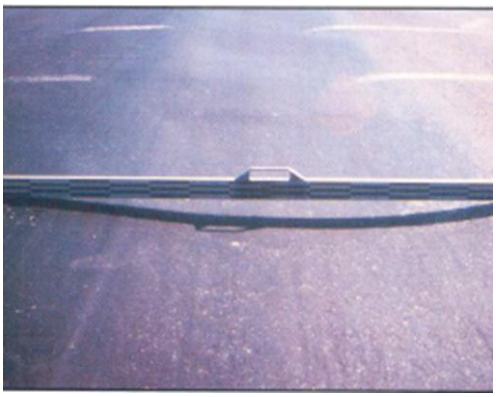

(b) Rutting

(c) Undulation

(d) Pumping

(e) Pothole

(f) Patching

Figure 2-5: Flexible pavement distresses related to structural deterioration (SAPEM, 2013).

Structural deterioration of a pavement has been linked to progressive weakening of the pavement layers due to stress – strain development within the layer. However, researchers have identified the impact of interlayer adhesion on structural deterioration of a pavement (Willis & Timm, 2007; Atkinson & Gordon, 1989).

Willis & Timm (2007) have reported the case of structural deterioration due to lack of bonding between the top asphaltic layers (see Figure 2-6(a)). Failure was induced by the increase of radial stress and strain at the bottom of each layer which thereafter developed fatigue cracking as shown in Figure 2-6(a).

In addition to fatigue cracking in asphaltic layers, reflective cracks and material erosion in cement treated layers were reported by Atkinson & Gordon (1989) on a full scale pavement track trial constructed with various cement treated layers. Accelerated Loading Facility was used to simulate pavement conditions in a short period of time and this allowed long term comparison of the performance with normal traffic loading and environmental conditions. After a series of trials, a core was taken through the pavement layers to identify distress and to determine any failure modes which may be present. The core indicated extensive debonding between cement treated layers, which prompted layers to act as individuals rather than as a thick bonded unit. This therefore, induced high tensile stress at the bottom of layers which resulted in vertical crack initiation. Cracks started at the debonded interface in deeper layers and propagated vertically upwards to the surface as formulated by Willis & Timm (2007). Moreover, the core showed material erosion between layers caused by water ingress. Figure 2-6(b) illustrates a typical cross section of the cracking pattern observed.

Recently, extensive studies have been conducted to characterize bonding conditions between top asphaltic layers and identify their influence on the structural deterioration of the road pavement. However, more research is needed to investigate interface strength in deeper layers (i.e. base and subbase) and how it influences pavement deterioration. Willis & Timm (2007) mentioned poor bonding conditions between base and subbase in a slab taken from a Swiss motorway as shown in Figure 2-6(c), but no information whether any structural failure (i.e. rutting or cracking) was attributed to base and subbase debonding (Raab & Partl, 2004).

Lack of literature on structural deterioration due to poor bonding of deeper layers does not negate its negative impact on overall performance of the pavement structure.

(a) Fatigue cracking due to poor bonding between pavement layers

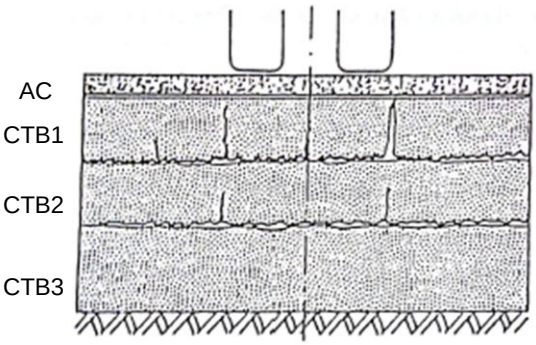

(b): Crack propagation and interlayer erosion due to interface separation

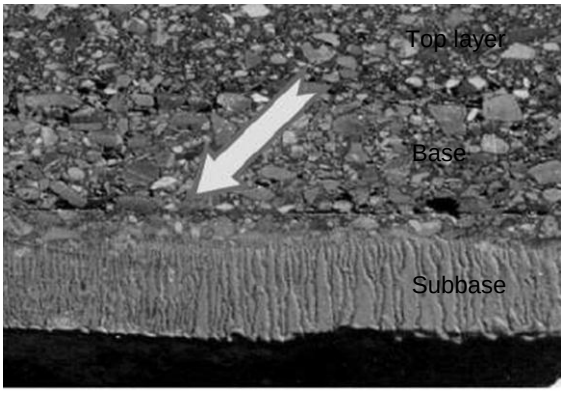

(c): Interlayer adhesion problem between base and subbase layers

(d): Illustration of weak interface between pavement layers after HVS test

Figure 2-6: Pavement distresses related to lack of interlayer adhesion (Willis & Timm, 2007; Atkinson & Gordon, 1989; Raab & Partl, 2004; De Beer *et al.*, 2012).

De Beer *et al.* (2012) discussed the adverse effects of weak layers, interlayers, lamination and weak interfaces in South African pavement structures incorporating lightly cemented layers. Theoretical analysis was based on Strain Energy of Distortion (SED) model, developed by Timoshenko & Goodier (1951). The model highlights the use of the quantity of strain energy stored per unit volume of the material, to determine the limiting stress at which failure might occur. Generally, the increased value of SED was found in debonded layers which demonstrated a high potential for damage in the pavement layers to occur.

Practically, on the other hand, De Beer *et al.* (2012) used full-scale Heavy Vehicle Simulator (HVS) tests to validate mechanistic analysis. Field tests were conducted on selected pavements with lightly cemented layers. HVS tests showed that the development of surface distresses was induced by debonding and weak interlayers as shown by field cores taken after testing (see Figure 2-6(d)).

The influence of interlayer critical conditions on the general performance of pavement structure has been adequately demonstrated and documented through many years as mentioned previously. Mechanistic modelling showed the negative impact of poor adhesion on stress and strain distribution in the pavement structure. Similarly, theoretical analysis has been validated by full scale HVS tests whereby signs of debonding and weak interface were reported to induce pavement deterioration. However, all reviewed literature only focused on characterisation of interlayer conditions between bituminous top layers and how this influences the general pavement behaviour. It is therefore, important to mention lack of insightful knowledge on interlayer conditions in deeper granular and lightly cemented layers even though different researchers (Raab & Partl, 2004; Romain, 1968; Ziari & Khabiri, 2007) have reported the reduction of pavement life by up to 62% due to poor adhesion between base and subbase layers (Kruntcheva *et al.*, 2005).

2.4. THE PHILOSOPHY OF FLEXIBLE PAVEMENT DESIGN

2.4.1. PAVEMENT STRUCTURE RESPONSES

Structural design of a flexible pavement is based on how it responds when exposed to traffic. This response is recorded as stress, strain and vertical deflection in each of the pavement layers. Even though stress, strain and deflection are distributed throughout the pavement structure, only critical values are localized at specific locations. These have a significant effect on the pavement's performance (Ullidtz, 1987).

2.4.1.1. Source of Stress and Strain in Granular Materials

The National Highway Institute of the United States pointed out the severity of the moving wheel on the development of vertical, shear and bending stresses and strains in each layer of the pavement (Peshkin, 1994). Other researchers, however, mentioned the great influence of the pavement materials' properties, the layers' arrangement and the typical distribution of load- related stress and strain in the pavement structure, on the rate and degree of pavement deterioration (Brown, 1996) as cited by Edwards (2007). Additionally, different researchers mentioned the complexity of stress patterns due to a moving wheel load (LeKarp *et al.,* 2000), and the unclear understanding of the nature of deformation mechanism of aggregates in granular layers. All these uncertainties are explained by the

high variety of road construction materials in terms of mechanical properties and thus, dissimilar wheel load-related responses.

From the theoretical analysis point of view, Peshkin (1994) introduced three main types of wheel load-related stress and strain to be considered when analysing the pavement structure:

i. Vertical Stress and Strain

Vertical stress developed under the wheel path of the moving vehicle causes compressive stress in the pavement structure. At a certain point, this induces permanent deformation of granular layers like subgrade, and therefore results in rutting of the top surface of the pavement. It is important to mention that the rate of permanent deformation depends on the strength characteristics of the pavement materials.

ii. Shear stress and Strain

Theoretically, granular materials are assumed to fail by shear. In that context, a moving wheel on top of a thin-surfaced pavement creates a shearing action in the pavement, especially on a steep gradient or in a section of the road where the vehicle usually accelerates, brakes or turns (Muslich, 2010a). This can then be transferred to the interface between the base and subbase beneath. Figure 2-7 illustrates the conceptual distribution of shear movement from the base course to the interface with the subbase beneath, which is known as shear flow.

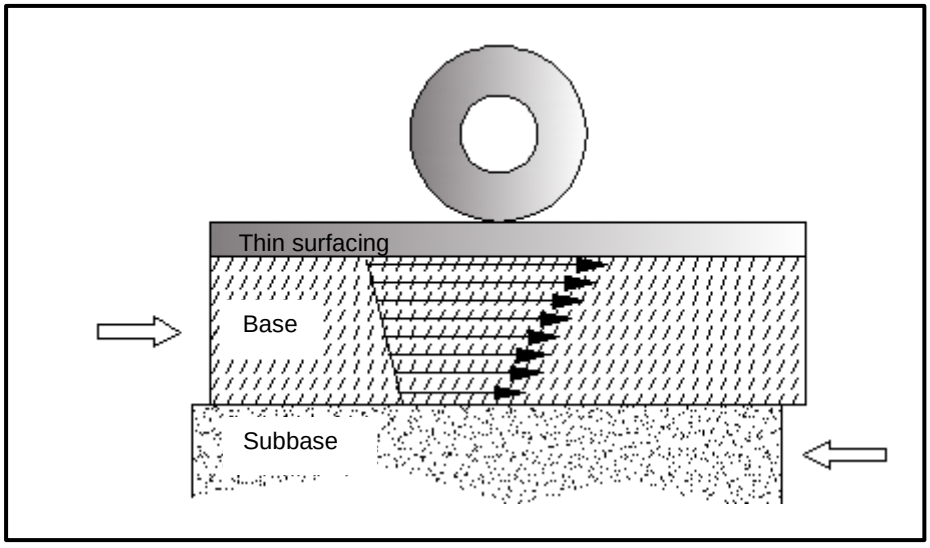

Figure 2-7: Conceptual representation of shear flow at the interface

iii. Horizontal/ Radial Stress and Strain

Under the wheel path, the pavement layers deform in a manner similar to the bending of partially bonded beams. Horizontal stress occurs at the bottom of each beam in the system and may be either compressive or tensile. In the pavement structure, this response is due to the fact that pavement layers are not fully bonded to one another, and therefore, develops interlayer horizontal stress due to bending.

2.4.1.2. Estimation of Flexible Pavement Responses

Estimation of pavement structure response is an essential process towards accurate prediction of pavement performance. Normally, there are three fundamental theories used to estimate material responses, i.e. elasticity, plasticity and viscosity (Jenkins, 2013). However, very few materials conform to one specific theory. Therefore, the most accurate estimation involves combining two or three approaches according to the type of materials. Table 2-2 shows different materials with corresponding characterisation theories. Later in this section elasto-plastic behaviour of granular materials is discussed.

Table 2-2: Pavement materials and respective behavioural analysis theories (Adapted from (Jenkins, 2013).

Pavement materials	Analysis theory
Cement/ Concrete	Elasticity
Granular materials	Elasto-plasticity
Bituminous materials	Visco-elasticity
Asphalt	Visco-elasto-plasticity

i. Elasto-Plastic behaviour of granular materials

Granular materials used in pavement structures do not behave as purely elastic or purely plastic. Their responses upon cyclic loading and unloading entails a recoverable (i.e. elastic) and permanent (i.e. plastic) deformation component. This behaviour is referred as elasto-plastic and is schematically detailed on Figure 2-8.

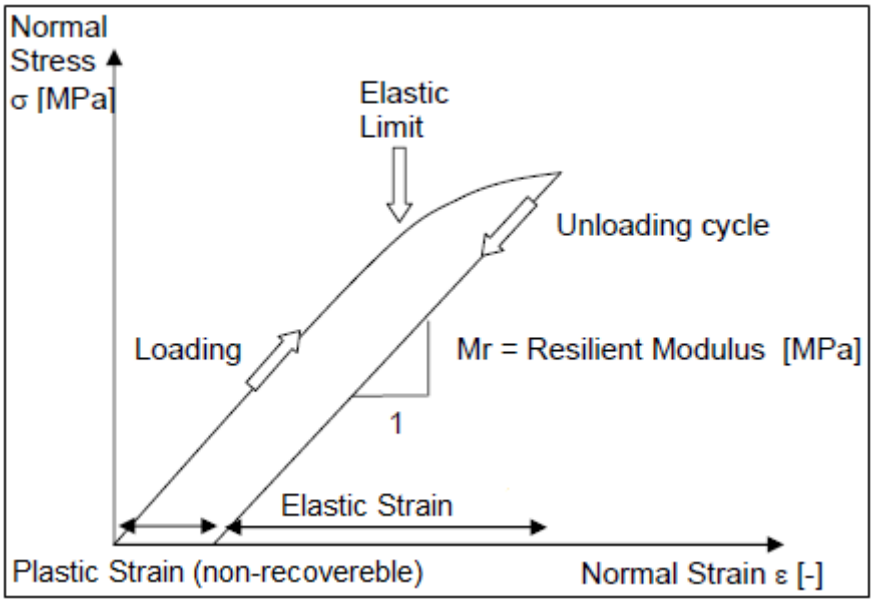

Figure 2-8: Elastoplastic behaviour and resilient modulus of granular materials (Jenkins, 2013).

ii. Stress in a single homogeneous layer

Point Load

Figure 2-9, illustrates the simplest loading condition of a single point load, P applied to a homogeneous half space. At a depth z below the surface, stress in three directions (i.e. z, r and θ) can be calculated by using Boussinesq relationships shown in Equation 2-1, Equation 2-2 and Equation 2-3 respectively. Vertical deflection is calculated by Equation 2-4.

$$\sigma_z = -\frac{P}{2\pi}\frac{3z^3}{(r^2+z^2)^{5/2}} \quad \textbf{(2-1)}$$

$$\sigma_r = -\frac{p}{2\pi}\left[\frac{3r^2 z}{\left(r^2+z^2\right)^{5/2}} - \frac{1-2\mu}{r^2+z^2+z\sqrt{r^2+z^2}}\right] \quad \textbf{(2-2)}$$

$$\sigma_\theta = \frac{p}{2\pi}(1-2\mu)\left[\frac{z}{\left(r^2+z^2\right)^{3/2}} - \frac{1}{r^2+z^2+z\sqrt{r^2+z^2}}\right] \quad \textbf{(2-3)}$$

$$\omega = \frac{P(1-\mu^2)}{\pi E r} \quad \textbf{(2-4)}$$

In a similar way, the corresponding strain components can be calculated from the stress components through the generalized Hook's Law as shown in Equation 2-5 and Equation 2-6.

$$\varepsilon_z = \frac{1}{E}[\sigma_z \quad \mu(\sigma_r + \sigma_\theta)] \qquad \textbf{(2-5)}$$

$$\varepsilon_r = \frac{1}{E}[\sigma_r \quad \mu(\sigma_z + \sigma_\theta)] \qquad \textbf{(2-6)}$$

Where:

σ_z and ε_z: Vertical stress and strain respectively,

σ_r and ε_r: Radial normal stress and strain respectively

ω: Vertical deflection at the surface

μ: Poisson's ratio

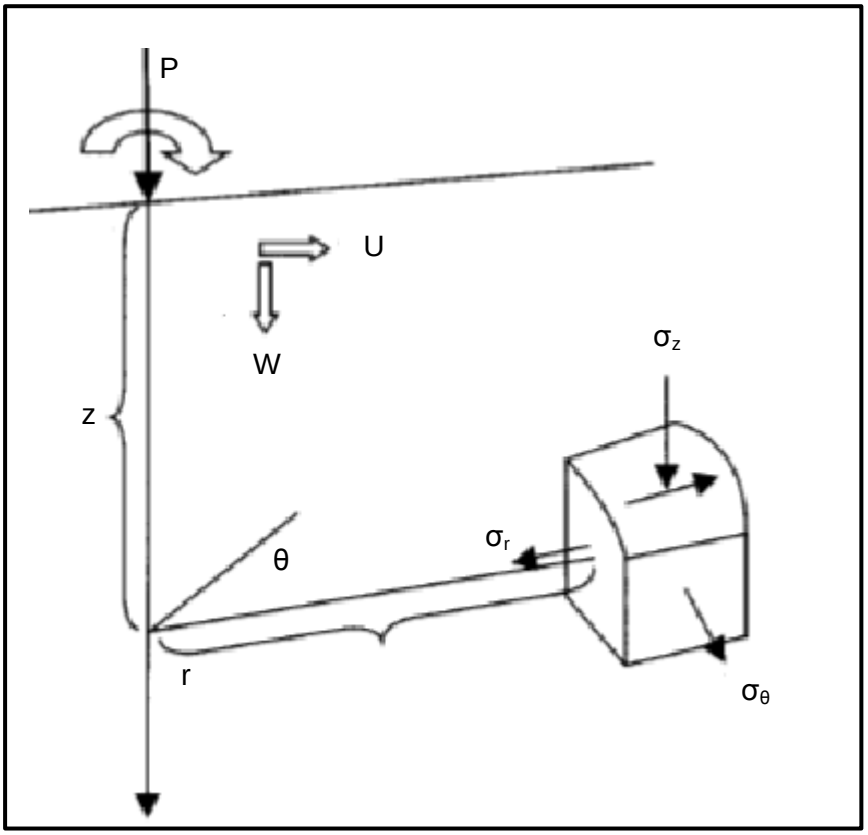

Figure 2-9: Axisymmetric stress state in elastic half space (Papagiannakis & Masad, 2008)

Circular Load with Uniform Vertical Stress

The pavement response under the centre of the wheel load with uniformly distributed stress, p on a circular loading area of radius a, is expressed by Equation 2-7 and Equation 2-8. Associated vertical deflection at the surface is given by Equation 2-9.

$$\sigma_z = p\left[-1+\frac{z^3}{(a^2+z^2)^{3/2}}\right] \quad \textbf{(2-7)}$$

$$\sigma_r = \sigma_\theta = \frac{p}{2}\left[-(1+2\mu)+\frac{2(1+\mu)z}{\sqrt{a^2+z^2}} \quad \frac{z^3}{(a^2+z^2)^{3/2}}\right] \quad \textbf{(2-8)}$$

$$\omega = 2pa\frac{(1-\mu^2)}{E} \quad \textbf{(2-9)}$$

iii. Stress in a two-layer system

A two-layer configuration is adapted to encounter high stress due to the wheel load in the half space. The system comprises a stiffer finite- thickness layer, placed on the top of an infinite layer for the safer distribution of stress in the pavement system as shown in Figure 2-10 (Papagiannakis & Masad, 2008).

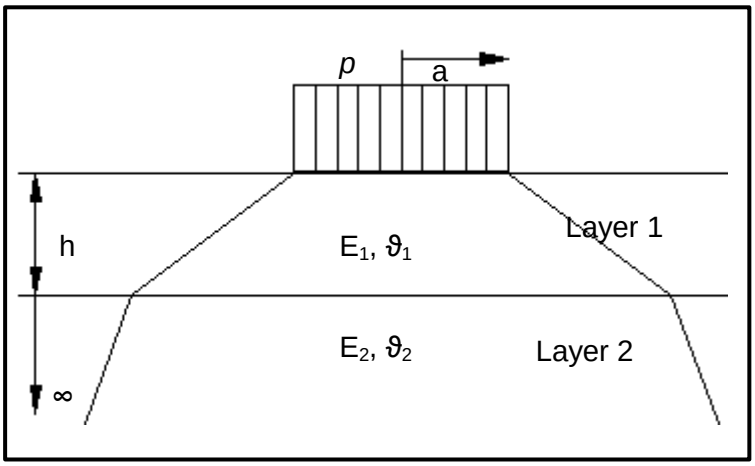

Figure 2-10: Schematic representation of stress distribution in two layers system (adapted from Papagiannakis & Masad, 2008).

Burmister was the first researcher who developed a solution for stress in a two-layer system (Molenaar, 2007). He built up a model of the surface deflection under the centreline of uniformly distributed stress *p* over a circular area of radius *a*, with an assumption of Poisson's ratio of 0.5. Equation (2-10) shows the condensed form of the model as cited by Papagiannakis & Masad (2008).

$$\omega = \frac{1.5pa}{E_2}F_w\left[\frac{a}{h},\frac{E_2}{E_1}\right] \quad \textbf{(2-10)}$$

In addition to the mathematical model, Burmister produced a chart for F_w, which is a function of a/h and E_2/E_1. The chart is presented in Figure 2-11.

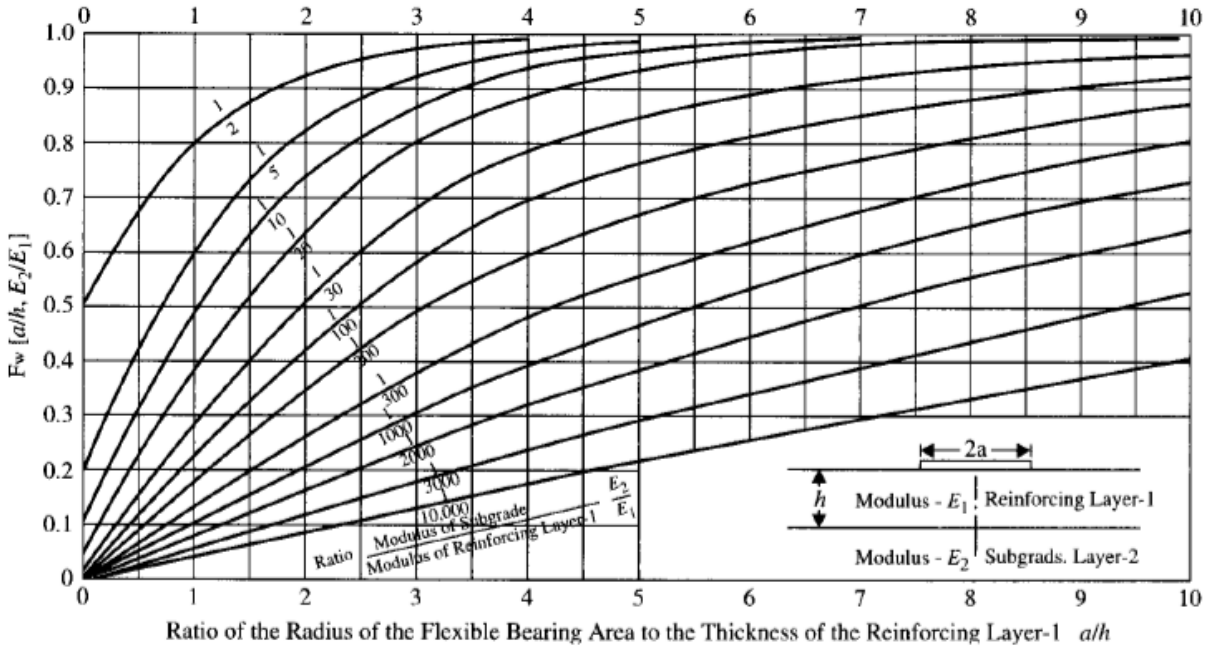

Figure 2-11: Fw factor for computing surface deflection at the centreline of a circular imprint carrying uniform stress (Papagiannakis & Masad, 2008).

iv. Stress in multilayers system

Practically, the pavement system is composed by more than two finite thickness layers resting on the infinite subgrade. The assessment of stress-strain distribution should address the structure as a multi-layered system. Even though the response analysis for this system is not far from the Burmister's principle for two layers, it is complicated to analyse the table and graphs that derive stress in different positions of the pavement structure. Therefore, the use of multilayer computer software is strongly recommended for accurate and easy calculations of stress, strain and deflection.

A variety of computer programs are currently in use and most of them are based on Burmister's analytical approach. Well known programs are CIRCLY, KENLAYER, BISAR, mePADS and WESLEA (Molenaar, 2007). BISAR, however, is generally accepted as the reference to which all other programs can be compared. This is due to high mathematical stability, accurate and realistic results, and more importantly, its ability to model different interface conditions (Molenaar, 2007).

2.4.2. FLEXIBLE PAVEMENT PERFORMANCE

Prediction of flexible pavement performance is based on how it can withstand traffic loading before the development of failure signs like cracking, rutting and permanent deformation.

At present, most design procedures use a mechanistic-empirical method for linking the pavement performance with the traffic induced responses in terms of stress, strain and

deflection. As indicated by the name, this method consists of two parts: the analytical and the empirical. The analytical approach consists of calculating pavement responses by using analytical relationships as described in section 2.4.1 and thereafter, using their results as input values in the empirical relationship to estimate the future performance of the pavement structure. Predefined empirical models, also known as transfer functions are used to estimate the number of load repetitions required to produce a certain amount of failure in the pavement structure. Transfer functions have been developed and calibrated to specific types of materials and respective modes of failure under simulated traffic loading.

A mechanistic-empirical method is widely used in different parts of the world and a South African version has been developed to meet the local most commonly used pavement materials. The general overview is discussed below.

2.4.3. OVERVIEW OF SOUTH AFRICAN MECHANISTIC DESIGN METHOD (SAMDM)

2.4.3.1. Introduction

Among many other design methods available in the South African pavement industry (De Beer & Van der Merwe, 1991; SAPEM, 2013), the SAMDM has been the most popular design method in South Africa for many years (Theyse & Muthen, 2000).

Like other mechanistic-empirical design methods, SAMDM estimates the bearing capacity of the pavement structure into two stages. The first one consists of modelling material responses according to their resilient and strength properties regarding the pavement loading conditions. This is mostly done by using software packages like BISAR, ELSYM5, mePADs, etc. Output of the analysis provides stress and strain at critical locations of the pavement structure and these are therefore used as input values for the second stage of the design. This consists of simulating pavement performance by means of transfer functions developed and calibrated for specific material types and associated modes of failure. The structural capacity of the pavement is, therefore, expressed as the total number of load repetitions that a specific layer can sustain before reaching its terminal conditions. Figure 2-12 illustrates the different steps followed for the mechanistic- empirical design procedure.

The popularity of the method stems from its ability to accommodate a wide range of local materials and to suit different pavement types. In this regard, extensive research was conducted to characterize South African road building materials (Jooste, 2004; Theyse *et al.,* 1995; Theyse *et al.*, 1996) and a range of typical specifications were published for being used as input values for the SAMDM. However, various weaknesses of the system have been illustrated by some researchers (Jooste, 2004; SAPEM, 2013).

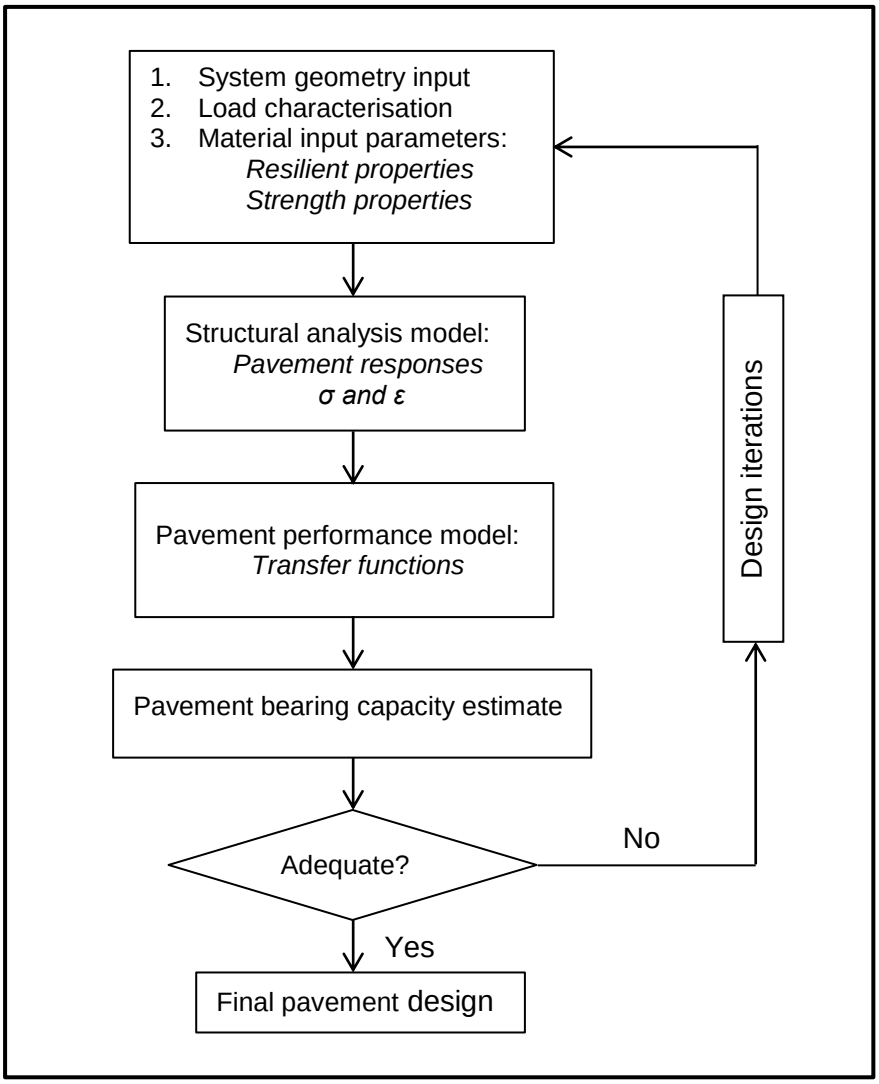

Figure 2-12: Schematic diagram of Mechanistic – Empirical Design procedure (Theyse & Muthen, 2000).

2.4.3.2. South African Material Characterisation for SAMDM

Official classification of South African pavement construction materials is found in TRH14 (1985) where materials are grouped according to their source, treatment, and usage in pavement structures. Consequently, four main categories are available:

1. Natural soils and gravels,
2. Crushed gravels and rocks,
3. Chemically stabilised materials, and
4. Portland Cement Concrete (PCC).

Table 2-3 illustrates the standard unbound granular materials and lightly cemented gravel accompanied by respective codes and engineering specification as presented in TRH14 (1985). Note that GM denotes the Grading Modulus.

Table 2-3: South African pavement structure materials with their material codes (TRH14, 1985).

Symbol	Code	Material	Main specifications
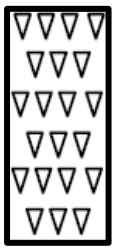	G1	Graded crushed stone	Dense-graded, unweathered crushed stone, Max size 37,5mm, 88% apparent density, PI < 4.0 (min 6 tests)
	G2	Graded crushed stone	Dense-graded, crushed stone, Max size 37,5mm, 100 – 102 % mod. AASHTO or 85% bulk density, PI < 6.0 (min 6 tests)
	G3	Graded crushed stone	Dense-graded, crushed stone and soil binder, Max size 37,5mm, 98 – 100 % mod. AASHTO PI < 6.0
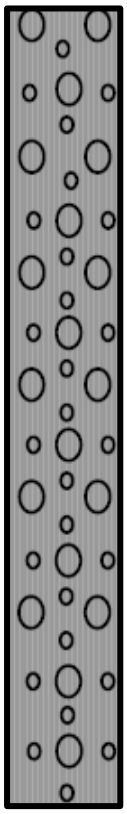	G4	Natural Gravel	CBR ≥ 80, Max size 53mm, 98 – 100 mod. AASHTO, PI < 6, Swell 0.2 at 100% mod. AASHTO
	G5	Natural Gravel	CBR ≥ 45, Max size 63mm or 1/3 of the layer thickness; density as prescribed for layer of usage; PI < 10; Swell 0.5 at 100% mod. AASHTO
	G6	Natural Gravel	CBR ≥ 25, Max size 63mm or 1/3 of the layer thickness; density as prescribed for layer of usage; PI < 12 or 2(GM)+10; Swell 1.5 at 100% mod. AASHTO
	G7	Natural Gravel	CBR ≥ 15, Max size 1/3 of the layer thickness; density as prescribed for layer of usage; PI < 12 or 2(GM) +10; Swell 1.5 at 100% mod. AASHTO
	G8	Gravel - soil	CBR ≥ 10 at *in situ* density; Max size 1/3 of the thickness; density as prescribed for layer of usage; PI < 12 or 2(GM) +10; Swell 1.5 at 100% mod. AASHTO
	G9	Gravel - soil	CBR ≥ 7 at *in situ* density; Max size 1/3 of thickness; density as prescribed for layer of usage; PI < 12 or 2(GM) +10; Swell 1.5 at 100% mod. AASHTO
	G10	Gravel - soil	CBR ≥ 3 at *in situ* density; Max size 1/3 of thickness; density as prescribed for layer of usage or 90% mod. AASHTO
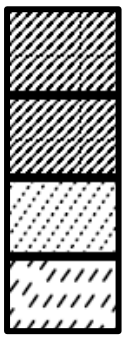	C1	Cemented crushed stone or gravel	UCS 6 – 12 MPa at 100% mod. AASHTO compaction; at least G2 before treatment
	C1	Cemented crushed stone or gravel	UCS 3 – 6 MPa at 100% mod. AASHTO compaction; at least G2/G4 before treatment
	C3	Cemented natural gravel	UCS 1.5 – 3.0 MPa and ITS ≥ 250 kPa at 100% mod. AASHTO; Max size 63mm; PI ≤ 6 after treatment
	C4	Cemented natural gravel	UCS 0.75 – 1.5 MPa and ITS ≥ 200 kPa at 100% mod. AASHTO; Max size 63mm; PI ≤ 6 after treatment

$GM = \frac{P_{2mm} + P_{0.425mm} + P_{0.075}}{100}$ And P_{2mm} etc., indicate the percentage retained on the indicated sieve size.

The exceptional performance of the SAMDM is not only based on the accurate modelling of pavement materials but also to the proper understanding of the failure mechanism of each material in the pavement structure. This therefore gives a general overview on how a particular material will perform.

2.4.3.3. Stress-strain distribution across the pavement structure

Distribution of stress and strain in the pavement structure depends on various parameters like the resilient and strength properties of each individual layer, structural loading condition, system geometry, analysis points, and interaction between layers. The most effective analysis method should consider these parameters carefully.

It should be noted that the elastic multi-layered computer program, BISAR software fulfils the above mentioned requirements.

One of the potential features of BISAR software is the capacity to consider the partial friction between pavement layers. This type of calculation is conducted with the aid of the shear spring compliance AK. The designers of BISAR software defined the AK parameter as the inverse of the shear reaction modulus at the interface between adjacent layers and it is expressed by Equation 2-11. More details on the shear reaction modulus of interface are presented in Appendix C.

$$AK = \frac{\text{relative horizontal displacement between layers}}{\text{shear stress acting at the interface}} \quad m^3/N \qquad \textbf{(2-11)}$$

The relationship is treated mathematically by the parameter α defined in Equation 2-12.

$$\alpha = \frac{AK}{AK + \frac{1+\mu}{E} \cdot a} \qquad \textbf{(2-12)}$$

In which:

a: radius of the load, (m), E: modulus of the layer above the interface, (Pa)

μ: Poisson's Ratio of that layer, α: friction parameter, with $0 \leq \alpha \leq 1$

(α = 0 means full friction, α = 1 means complete slip)

The parameter -α can also be expressed in terms of reduced shear spring compliance, ALK as shown in Equation 2-13.

$$ALK = \frac{\alpha}{1-\alpha} * a \qquad \textbf{(2-13)}$$

It should be noted that one of the values between AK and ALK is entered in the software and the value of interlayer friction parameter, α is derived from them (Shell, 1998).

2.4.3.4. Pavement Performance Estimation Models

The SAMDM is based on the critical layer approach whereby the structural bearing capacity of the entire system is determined by the most critical layer (Theyse & Muthen, 2000). Each single layer is analysed according to the assumed failure mechanism of the material involved. Bearing in mind the impact of layers' interaction on the overall performance of the pavement, the critical layer approach might, however not take into consideration the interaction of layers in terms of unison. In fact, every single layer may exhibit substantial structural capacity while the entire system demonstrates marginal performance due to lack of interlayer adhesion.

In the light of performance estimation, each layer is modelled according to the type of material involved. Generally, South African pavement materials comprise asphalt, granular, cemented and subgrade materials. Each type of material exhibits a specific failure mode upon loading which is assessed by a critical parameter determined at a specific location in the pavement structure. Figure 2-13 summarizes the critical parameters and locations used for a typical South African pavement structure.

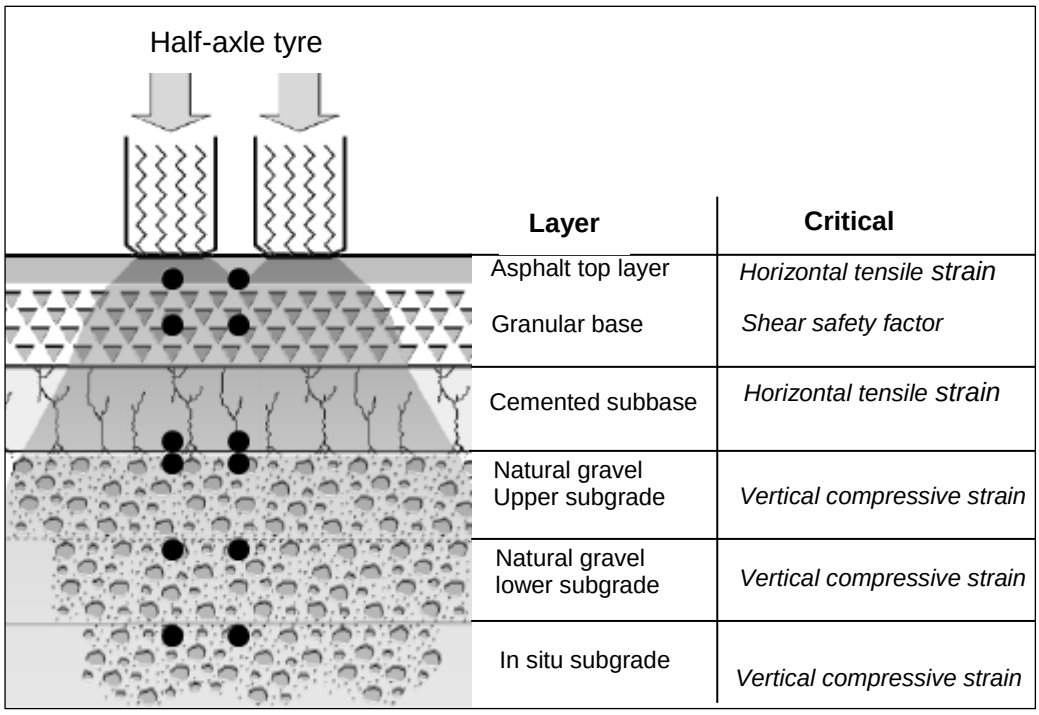

Figure 2-13: Analysis Positions for Critical Parameters in a Flexible Pavement Structure (Adapted from SAPEM, 2013).

The structural capacity of a specific material type in the pavement structure is calculated according to the corresponding critical parameters. Corresponding transfer functions are used to link values of critical parameters with the number of load applications that can be sustained before the specific material type will fail in a particular way.

Various transfer functions have been developed for different South African road categories but for the purpose of illustration, this analysis was only limited to Category A roads.

Failure Modes, Critical Parameters and Transfer Functions for Pavement Materials

i. Hot Mix Asphalt material

A hot mix asphalt layer fails by fatigue cracking under a series of repeated loading. The critical parameter for the analysis is the tensile strain, $\varepsilon_t(\mu\varepsilon)$ at the bottom of or within the layer. SAMDM provides specific transfer functions for thin asphalt layers (<50 mm) and thick asphalt layers (>75 mm). However, due to the fact that thin asphalt top layers are widely used in developing countries, it was considered in this study.

The transfer function for the continuous graded asphalt surfacing layer of Category A road is given in Equation 2-14

$$N_f = 10^{17.40\left(1-\frac{\log\varepsilon_t}{3.40}\right)} \quad \textbf{(2-14)}$$

Where:

- N_f: Total number of load applications that the asphalt layer can withstand before reaching terminal conditions
- ε_t : Tensile strain at the bottom of or within the layer $(\mu\varepsilon)$

ii. Granular Material

An unbound granular layer is assumed to fail by shear and the critical position is localized in the middle of the layer (SAPEM, 2013). Maree (1978), as reviewed by Theyse *et al.* (1996) linked the failure conditions to the safety factor defined as the ratio between shear strength of the material and shear stress developed in the middle of the layer (see Equation 2-15). The stress ratio is, therefore used in the transfer function shown in Equation 2-16 to estimate the structural bearing capacity of the layer for Category A road.

$$F = \frac{\sigma_3\left[K\left(\tan^2\left(45+\frac{\phi}{2}\right)-1\right)\right]+2KC\tan\left(45+\frac{\phi}{2}\right)}{(\sigma_1-\sigma_3)} \quad \text{or}$$

$$F = \frac{\sigma_3\phi_{term}+C_{term}}{(\sigma_1-\sigma_3)} \quad \textbf{(2-15)}$$

$$N = 10^{(2.605122F+3.480098)} \quad \textbf{(2-16)}$$

Where:

- $\sigma_{1,}\sigma_3$: Major and minor principal stresses acting in the middle of the granular layer,
- c and ϕ : Cohesion and angle of internal friction respectively,
- K:constant depending on moisture, (0.65 for saturated, 0.8 for moderate and 0.95 for normal,
- ϕ_{term} and c_{term}: values depending to the type of materials and moisture condition (Theyse *et al.,* 1996).
- N: Number of equivalent standard axles before shear failure
- F: Stress ratio or safety factor.

It is important to note that the stiffness in the granular layer is highly dependent on the strength of the supporting layer. The stronger the supporting layer, the stiffer the granular layer (Molenaar, 2007).

iii. Cement Treated Material

Normally, lightly cemented materials are analysed for two consistency states. At the first stage, cemented materials are considered as bound materials whereby two critical parameters are investigated, namely vertical compression stress at the top of the layer, which control crushing and maximum tensile strain, which causes effective fatigue at the bottom of the layer. Effective fatigue life represents the number of standard axle loads required to cause cracks in the layer to the extent that it has similar effective stiffness as the unbound granular layer (Theyse *et al.*, 1996). Equation 2-17 and Equation 2-18 provide transfer functions for both cases.

When the cemented layer reaches the end of its effective fatigue life, it enters the second state in which it is considered as an unbound granular layer. At that time its performance is estimated by using granular materials transfer functions. The overall life of the layer is calculated by considering both phases (Theyse *et al.*, 1996).

$$N_{eff} = SF * 10^{c\left(1-\frac{\varepsilon}{d\varepsilon_b}\right)} \quad \textbf{(2-17)}$$

SF = 1 for t < 102,

= 10^ (0.00285t – 0.293) for 102mm ≤ t 319mm

= 8 for t > 419mm

$$N_{ci/ca} = 10^{a\left(1-\frac{\sigma_v}{b*UCS}\right)} \quad \textbf{(2-18)}$$

Where:

- N_{eff} : Effective fatigue life
- SF: Shift factor for crack propagation

- ε: Horizontal tensile strain at the bottom of layer (με)
- ε_b: Strain at break, which is equal to 125 for C3 and 145 for C4
- $N_{ci/ca}$: Standard axles to crack initiation or advanced crushing
- σ_v: Vertical compressive stress at top of layer
- UCS: Unconfined compressive strength (kPa)
- a, b, c and d: constants which depend on the category of the road
- t: layer thickness

iv. Subgrade Material

Permanent deformation is the failure mode of the subgrade material which results in the vertical deformation (i.e. rutting) of the road surface. The critical parameter of the subgrade material is the vertical strain $\varepsilon_v(\mu\varepsilon)$ at the top of the layer. Equation 2-19 provides the transfer function for two terminal rut conditions, 10 mm and 20 mm rut.

$$N = 10^{(A-10\log\varepsilon_v)} \quad \textbf{(2-19)}$$

Where:

- N: the total number of standard axles that the subgrade can withstand before failure
- ε_v : vertical strain at the top of subgrade layer $(\mu\varepsilon)$
- For Category A road, A=33.3 for 10mm rut and 36.3 for 20mm rut.

The SAMDM is a performance-based design method whereby pavement damage is quantified according to material response under simulated loading. Despite its many advantages, different publications revealed the weakness of the method, for instance, high sensitivity to minor changes of the input variables, theory of materials characterisation and more importantly the accuracy of transfer functions used to estimate damages in different pavement layers (Jooste, 2004; Theyse *et al.*, 1996; Theyse *et al.,* 2011). This is why, from its development, the method was kept more dynamic and different calibrations was done to enhance accuracy and realistic estimation of the pavement performance (Jooste, 2004).

Chapter 3

LITERATURE REVIEW ON PREVIOUS RESEARCH

3.1. INTRODUCTION

From the 1960's, a number of studies have been conducted to assess bonding conditions between pavement layers and its influence on the general pavement performance (Romain, 1968; Uzan, 1976; Uzan *et al.*, 1978) From the theoretical point of view, mathematical models have shown that poor bonding between layers induces quick deterioration of the pavement (Khweir & Fordyce, 2003). However, the reviewed literature has shown that most of the research performed was only focused on the top asphaltic layers even though bonding challenges are also noticeable in deeper layers as in top ones.

Quantification of interlayer adhesion strength has been conducted by using different approaches. Various testing methods like pull off, torsion and shear tests have been proposed but still, the choice of the adequate testing setup remains the point of discussion.

In this chapter, an overview of previous, publications on the subject is outlined. The chapter itself is divided into four sections. The first section provides a general status quo of adhesion conditions in the pavement structure while the second outlines different testing methods and the application of each. In the third section, the approach of using direct shear test for assessing interlayer adhesion is discussed. The fourth part of this chapter represents an overview of previous studies on the effect of adhesion on pavement performance and estimated life.

3.2. ADHESION IN FLEXIBLE PAVEMENT STRUCTURE

Traffic loading develops stress and strain across the pavement structure. The load bearing potential of a pavement is significantly affected by its general configuration. The multi-layered structure causes the pavement to act in a similar way as a partially bonded beam illustrated by Tschegg *et al.* (1995) and schematically presented in Figure 3-1. They demonstrated that the deflection of three unbonded beams is nine times higher than that of fully bonded beams.

From the beam analogy shown in Figure 3-1, it is clear that the strength and stiffness of each individual layer does not guarantee effective performance of the entire structure. The unison interaction between them is also essential.

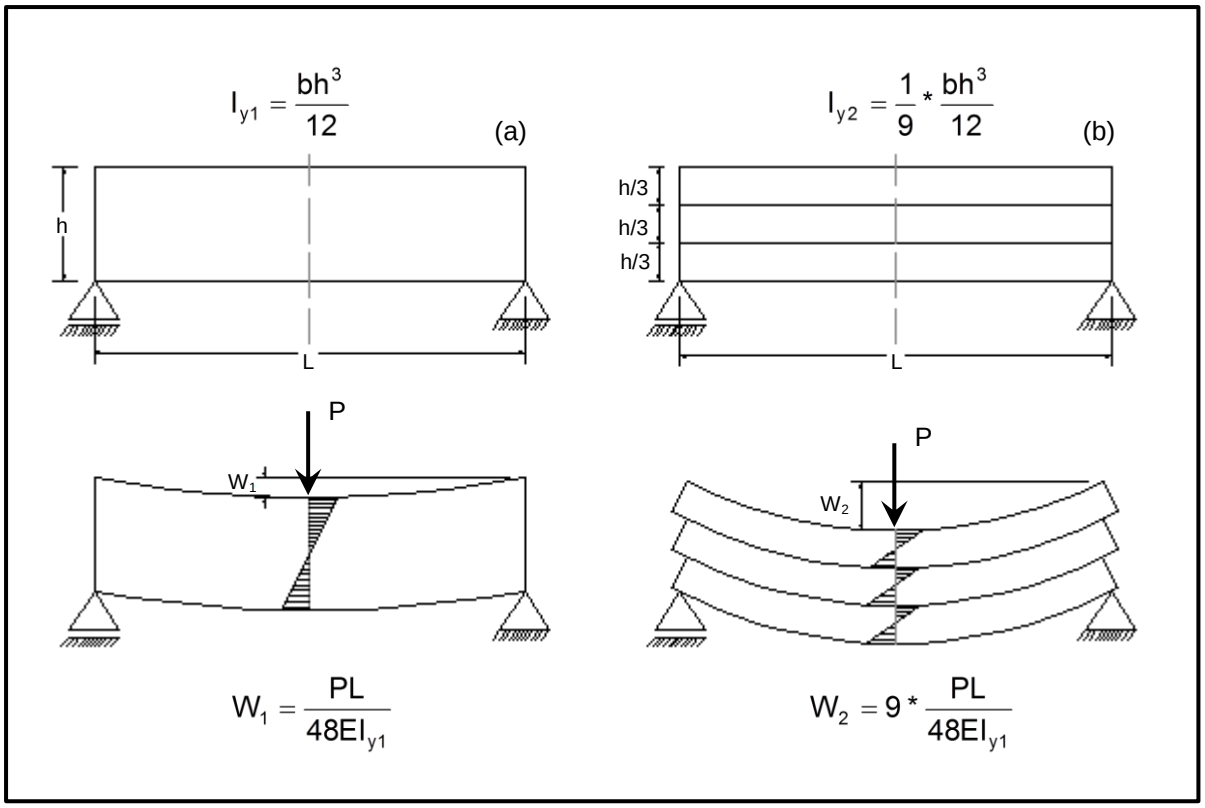

Figure 3-1: Beam analogy - different carrying capacity: (a) with compound- homogeneous beam; (b) without compound - three beams. (*b: Thickness of the cross section; E: Modulus of elasticity; h: Beam height, Iy: Inertia moment; L: Beam length; P: Force; W1: Deflection*), (Adapted from Tschegg *et al.,* 1995)

Most pavement structural design methods are based on the calculation of stress and strain distribution in layers. To ease the computation, many of them assume full bondage between layers or otherwise, modelling the interface between two extreme conditions: full bond or full slip (no bond). Different researchers have shown that, under real conditions, the exact state of interlayer adhesion is unknown, and are exclusively ranging from full to zero adhesion depending on material properties and construction practice (Kruntcheva *et al.*, 2005).

Generally, pavement layers are neither perfectly bonded nor perfectly unbonded (Uzan *et al.,* 1978; Whiffin & Lister, 1962). In the study conducted by Sutanto *at al*. (2006) they demonstrated that the assumption of full bond between pavement layers does not represent the real condition in the pavement structure since a number of failures have been reported. Also full slip was reported to be unrealistic because some friction due to granular particles may still exist at the interface between adjacent layers.

Practically, to achieve the maximum adhesion between pavement layers, it is important to acquire insight knowledge about the different factors which influence the interlayer behaviour. Parameters like aggregate size, compaction practice, moisture content, stress condition and material type have been identified by researchers to have a direct effect on achievable bond in the field (Jaskuła, 2014; Raab *et al.*, 2012; Sutanto *et al.,* 2006).

Raab *et al.* (2012) conducted a study to assess the influence of geometrical interlock and combination of aggregate sizes on the shear strength between layers. Different layer combinations simulated by simple model materials consisting of steel balls with assorted sizes, were tested by using different shear box apparatus. From the study results, they concluded that it was possible to achieve different adhesion conditions depending on the steel ball combination. The highest shear strength values were achieved for the combination of small balls on top of big ones. This can be explained by the interlock effect between balls whereby the small balls on top filled up the gaps between the big balls and formed a unified structure as conceptualised in Figure 3-2. The second combination was small/small, followed by big/big and lastly big/small.

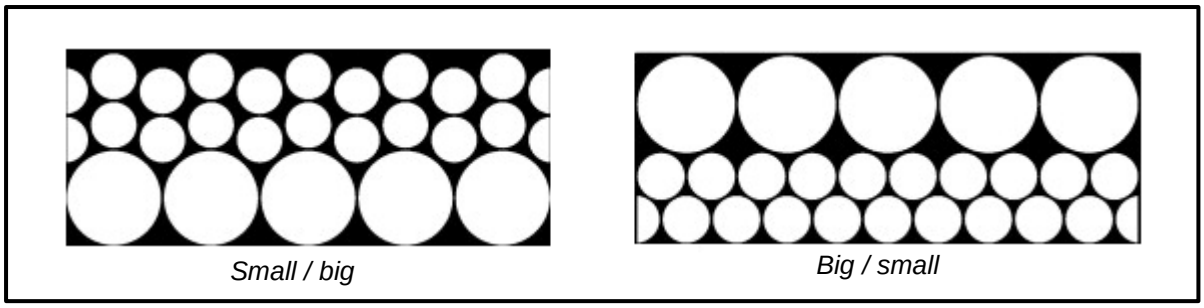

Figure 3-2: Conceptual illustration of interlock between two specimen structures (Raab *et al.*, 2012)

After the analysis conducted by Jaskuła (2014) about the influence of compaction effectiveness on interlayer bonding between asphalt layers, he concluded that the achievable bond between layers is strongly dependent on the compaction techniques used. From the results of the analysis, the highest values were achieved with gyratory compaction while the lowest values were linked to a static roller. Similar values were detected for laboratory and vibrating rollers.

The type of compaction technique used to compact the bottom layer determines the attained surface texture. A smooth roller results in a quasi-smooth surface while the knobby wheels roller compactor generates a relatively rough surface. When the top layer is compacted on a rough surface, the achieved interlock induces the two layers to act as a single unit and therefore high shear strength between them develops. It is important to mention that the amount of confining stress, which is defined by the lateral support of the road pavement (e.g. road kerbs), induces the achievable compaction degree and adhesion strength for granular materials.

3.3. PRINCIPLES OF INTERLAYER ADHESION TESTING

From the previous literature on pavement interlayer testing, it is clear that different test methods and various devices have been developed in different parts of the world. In fact, the working principle of most of them is based on three main modes of layer separation as depicted by Muslich (2010b) and presented in Figure 3-3 (i.e. shear, tensile and a combination of the two). The choice of the specific testing method and device therefore depends on the anticipated mode of failure which is, consequently, governed by the type of material (e.g. bound or unbound, particle size, etc.) and the geometric location of the sample (e.g. top or deeper layers). Moreover, specimen shape and size, type of application (e.g.*in situ* or laboratory), as well as the purpose of the testing (research or routine quality assurance) are considered for the selection of testing approach.

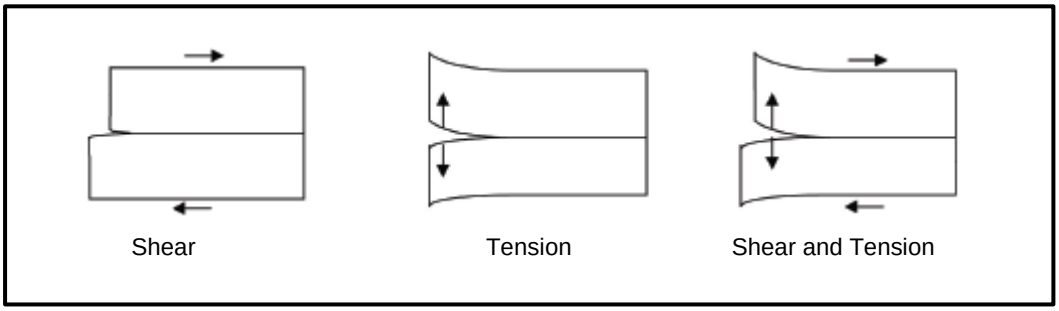

Figure 3-3: Schematic representation of separation mode (Muslich, 2010b)

Although the development of several testing methods contributed much to interlayer bond testing, consistent guidelines and standardization of the evaluation and testing is frequently not available. This, therefore, results in a lack of comprehensive information and if available, they are not comparable or cannot be used for computational modelling (Raab *et al.*, 2009)

In this section, interlayer testing methods are discussed in two broad categories: destructive (i.e. sample destroyed after testing) and non-destructive (i.e. sample recovered) tests.

3.3.1. DESTRUCTIVE TESTS

According to the testing place, destructive testing can be categorised as *in situ* or laboratory tests. The *in situ* test is usually carried out in the field with a sample or core extracted from the existing, ordinarily trafficked pavement structure. It is important to note that the traffic can also be simulated by Accelerated Pavement Testing (APT) techniques whereby a controlled wheel load is applied to the pavement structure for the purpose of simulating the effect of long-term in service loading conditions in a compressed time period (Hugo & Martin, 2004).

On the other hand, a laboratory based test is conducted on a core extracted from the existing pavement structure or laboratory prepared specimen.

3.3.1.1. Tensile Testing

The tensile bond (pull-off) test is commonly used to examine the bonding strength between the top thin asphaltic layer and the layer beneath it with the main purpose of determining the optimum tack coat application rate. This test can be performed in the laboratory or *in situ* whereby a steel plunger is glued to a prepared testing surface and pulled off after a partial core has been cut around the plunger as shown on Figure 3-4(a)

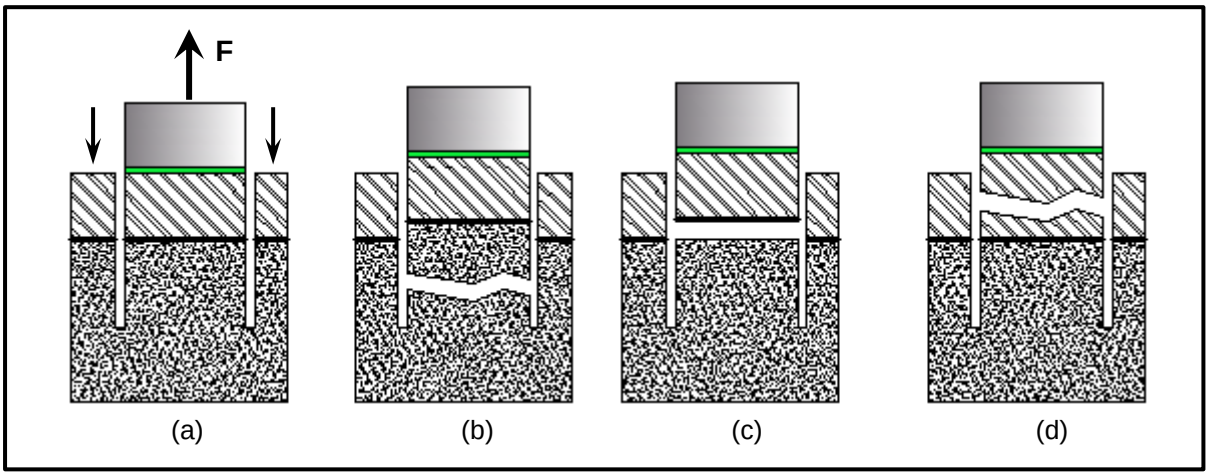

Figure 3-4: Illustration of tensile bonding test with different failure modes

Figure 3-4(b), (c), and (d) shows the failure modes that can occur. Inlayer failure indicates that bond strength is greater than the tensile strength of the layer, while failure at the interface provides a measurement of interlayer tensile bonding strength.

The tensile bond test is currently used as a standard method for testing interlayer tensile bond strength in various countries like Australia (Roffe & Chaignon, 2002) UK (British Standards Institution, 2003), and Germany (DIN, 2003). This involved the development of a wide range of related devices for *in situ* and laboratory based investigation (Raab & Partl, 1999; Raab & Partl, 2004). Figure 3-5 illustrates a device developed at the University of Texas at El Paso (UTEP), which Tashman *et al.* (2006) used to measure the tensile strength of the tack coat before placing a new layer. Thirty minutes after the application of the tack coat, the device was placed on the surface and the torque wrench was rotated clockwise until the contact plate touched the tack coated surface. To ensure total setting of the plate, 88kg load was placed and maintained on the weight key for at least ten minutes before testing. When the contact plate was firmly set with the surface, the load was removed and the torque wrench was rotated in the counter clockwise direction to pull off the plate from the tack coated surface. The torque required to detach the plate was recorded and then converted to tensile strength. It is important to mention that the device shown in Figure 3-5 can be used for both *in situ* and laboratory testing.

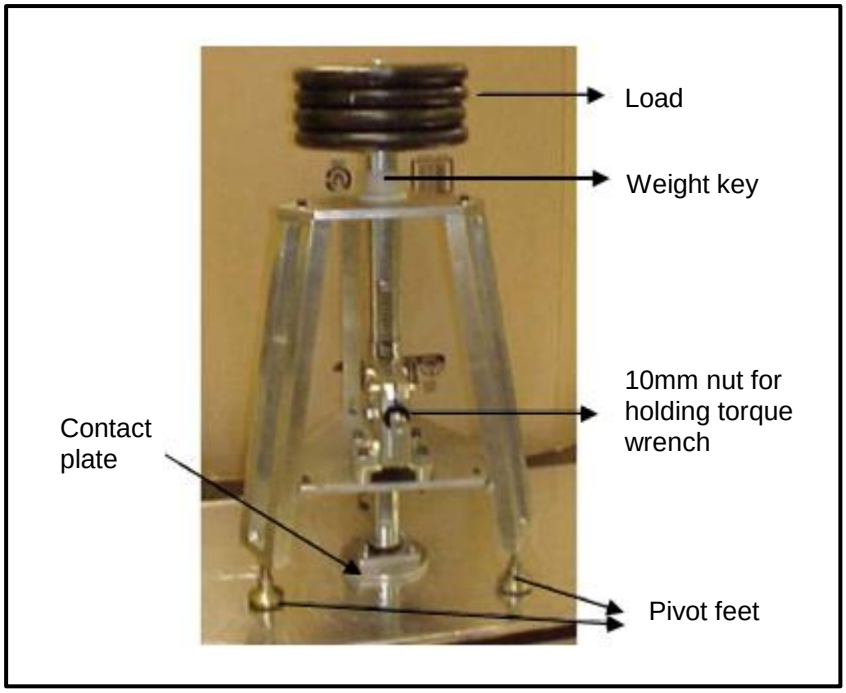

Figure 3-5: UTEP pull-off device (Tashman *et al.*, 2006)

3.3.1.2. Torque Testing

The torque bond test is generally conducted by twisting the top of a bituminous core specimen at a constant rotation rate to induce twisting shear failure at the interface. This is subsequently converted into the shear strength of the interface, by using the relevant mathematical equations (Muslich, 2010b).

The first torque bond device was developed in Sweden (Walsh & Williams, 2001) whereby manual torque was applied on the top of the core to investigate the *in situ* bonding condition. However, this procedure involved challenges in controlling the torque rate which, later on encouraged Choi *et al.* (2005) to modify the device by synchronizing the movement of the torque dial gauge with the second hand of an analogue clock. This consequently yielded a constant torque rate of 600Nm/minute.

Choi *at al.* (2005) developed a laboratory based manual torque bond device (Figure 3-6), which is able to test interface shear strength of a full depth core, under a more controlled environment. The testing procedures consist of clumping the core below the interface and, carefully applying torsion force until the interface fails. Figure 3-6 illustrates a schematic and pictorial representation of the device. Additionally, it is important to mention that some changes on the device were recommended by researchers (Muslich, 2010b) to reduce variability of the result and increase accuracy.

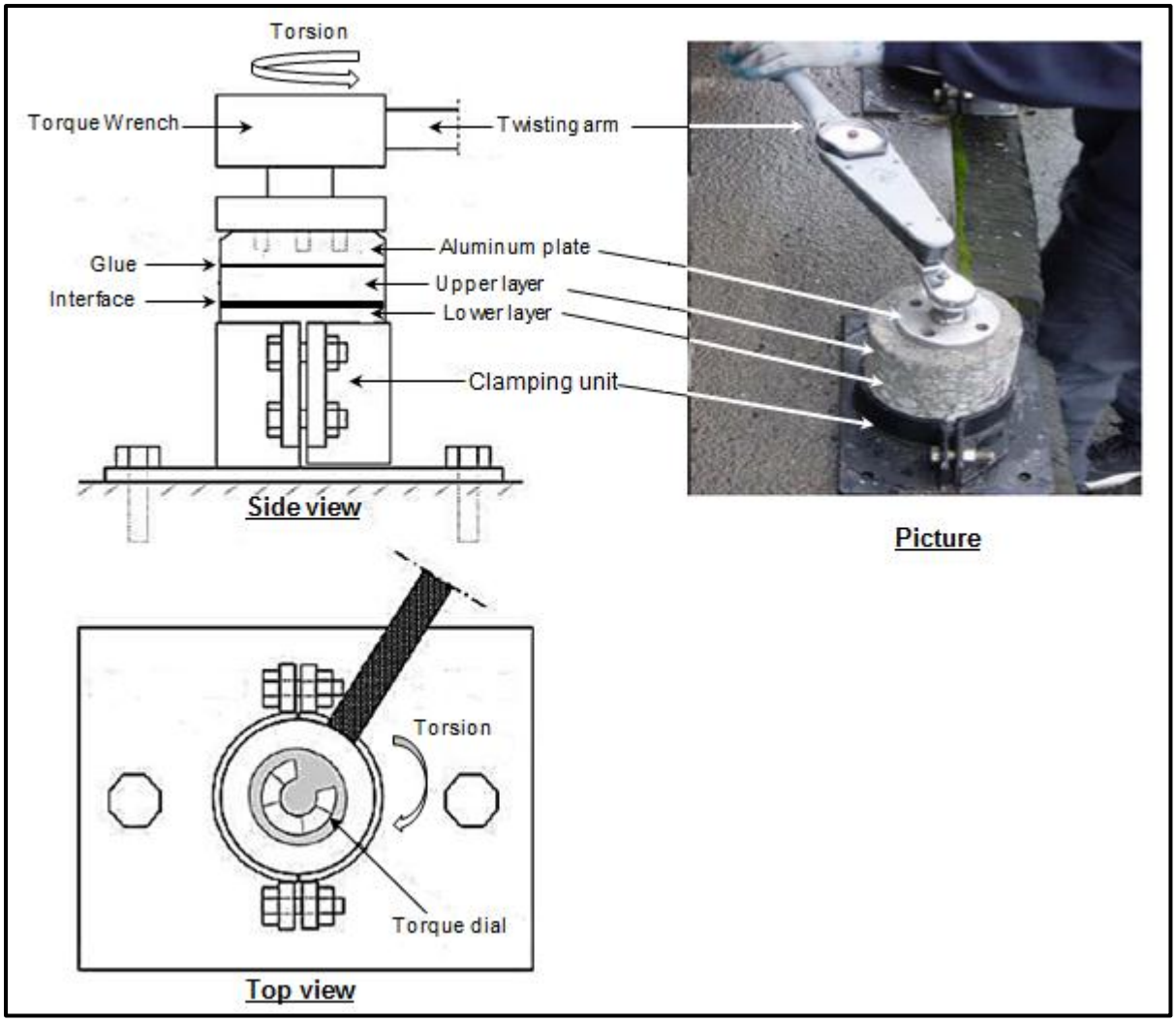

Figure 3-6: Illustration diagram of the laboratory based manual torque bond test developed by Choi, *et al.* (2005)

Apart from the manual testing device developed in the UK, a number of mechanically controlled testing methods and apparatus were designed all over the world. The Carleton In situ Shear Strength Test (CISST) apparatus, developed in Carleton University, Canada (Abd El Halim *et al.*, 1997) is able to determine the *in situ* shear strength of the surfacing material as well as the interface torque strength between the surface and the layer beneath. Torsion Vibration and In Situ Testing (TVIST) equipment developed by the Swiss Federal Laboratories for Materials Testing and Research (EMPA) (Raab & Partl, 1999) can measure the interface torque bond strength by applying both torsion and vertical loadings and particularly, it is available in both *in situ* and laboratory versions. Diakhaté *et al.* (2007) also developed an automatic torque bond setup which has a quality of accurate control of the loading rate. This apparatus has been improved by Muslich (2010b) by designing a similar device with the capability to perform a series of repeated torque bond tests in a more controlled environment and loading conditions.

Considering both aforementioned testing setups, it is important to note that none of them can be used to assess the effect of aggregate interlock at the interface; they only measure the tensile and torsion bond strength of binder or thin bituminous layers. Therefore, they cannot be used to characterize the interface conditions in deeper pavement layers made of unbound or lightly cemented materials.

3.3.1.3. Direct Shear Testing

The direct shear test is one of the oldest strength tests for soils, which was first used by Coulomb in 1776 (Lambe & Whitman, 1969). With the normal shear testing, the sample is held in a box that is split across its middle and a confining force is applied, along with the shear force to cause relative displacement between the two parts of the box.

The use of the direct shear test in pavement interlayer testing dates from the 1970's. Uzan *et al.* (1978) used a basic direct shear apparatus to investigate the adhesion properties of the asphaltic pavement layers. Later on, comparative analysis on different testing methods showed that direct shear test is the most reliable and effective method for testing interlayer adhesion properties in the pavement structure (Raab *et al.*, 2009).

The literature review on interlayer shear test devices presents many variants of direct shear apparatus developed in different countries. Based on their general set up, available direct shear test methods can be divided into two broad categories: the testing method with normal load and the one without. The main difference between the two categories is that the testing setup with normal load takes into account dilatancy effects due to interface roughness between layers, which is not considered in the test without normal load (Muslich, 2010b).

According to the published literature, the laboratory testing apparatus used by Uzan *et al.* (1978) seems to be the benchmark of other interlayer shear tests operating with normal load. The setup was composed by: (a) the lower and upper parts of a shear mould, 49.5mm and 30mm high respectively, (b) four deflectometers used to measure horizontal and vertical displacement, (c) a frame for applying vertical load, and (d) a motor coupled with a ring device for applying and reading horizontal force. This apparatus was used by Uzan *et al.* (1978) to investigate interface properties between bituminous layers with laboratory prepared samples, whereby a double layered specimen of 150 mm x 100 mm was sheared at a constant horizontal displacement of 2.5 mm/min. The impact of tack coat application rate, temperature and normal pressure was investigated.

Similar testing equipment presented in Figure 3-7 was developed at the Polytechnic University of Marche (Italy) (Santagata *et al.*, 2009) and named Ancona Shear Testing Research and Analysis (ASTRA). This device has been used by different researchers

(Canestrari & Santagata, 2005; Santagata *at al.,* 2009) to characterize interface bonding conditions in bituminous pavement layers. A double-layered specimen is prepared by statically compacting one layer on top of the other and subsequently, shearing it from the interface at the rate of 2.5 mm/min and specific normal pressure until the total failure of the interface.

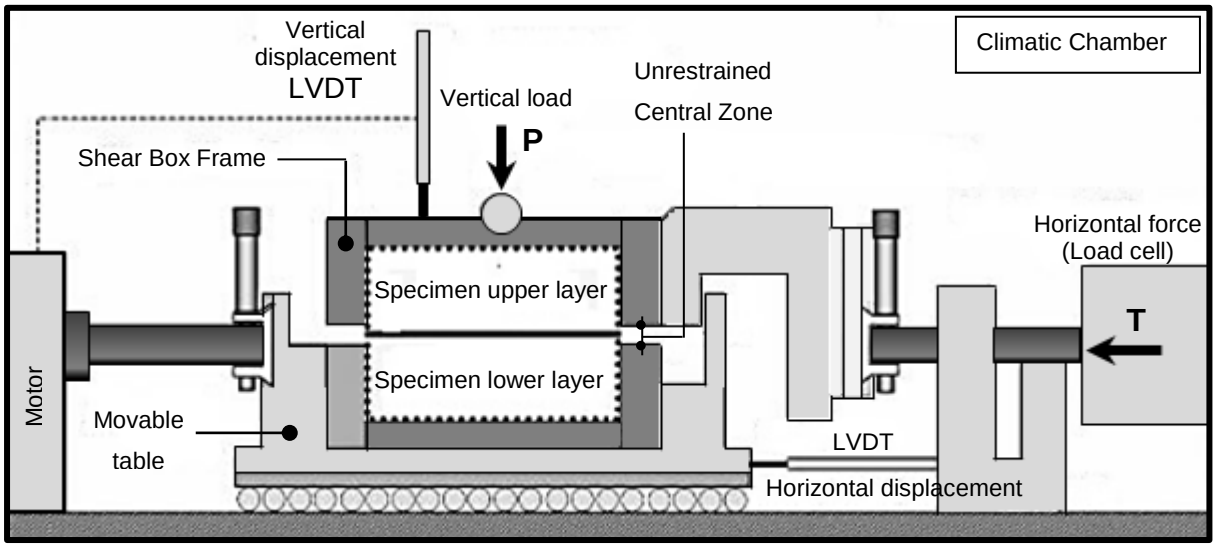

Figure 3-7: Schematic representation of ASTRA interface shear apparatus (Canestrari & Santagata, 2005)

Mohammad *et al.* (2009) developed a portable interface shear device called Louisiana State Interface Shear Strength Tester (LISST) which is shown in Figure 3-8. The device is designed to be mounted in an existing load frame which is used to apply shear loading while testing. Bituminous cylindrical specimens of either 100 mm or 150 mm can be sheared at the rate of 2.54 mm/min. Normal pressure can be applied while testing and the gap between the shearing and the reaction frame is maintained at 12.7 mm. It is important to mention that the LISST setup allows accurate setting of the failure plane to be at the interface.

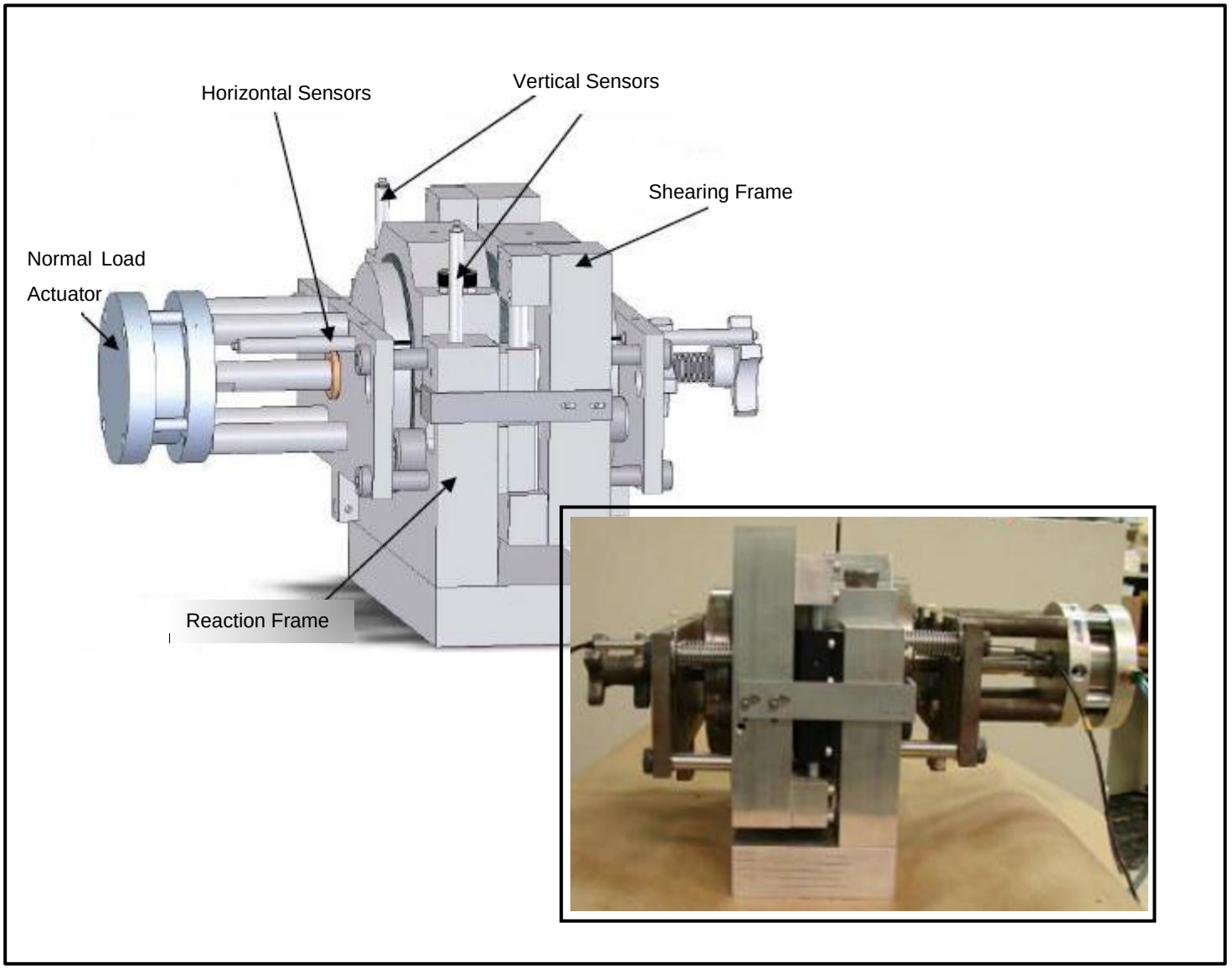

Figure 3-8: Illustration diagram of Louisiana State Interface Shear Strength Tester (Mohammad *et al.*, 2009)

While many shear tests allow only static testing, few devices were designed to undertake testing in a static and a dynamic mode which simulates the repetitive loading of the moving vehicles (Ascher & Wellner, 2007). The shear fatigue test developed by Romanoschi & Metcalf (2002) was used for fatigue tests on bituminous layer interfaces. The configuration of the apparatus depicts the inclination of the shear plane to 25.5^0 from the horizontal (Figure 3-9). During the test, a vertical load is applied with a frequency of 0.5Hz which corresponds to the total period of 0.2 sec and the length of the pulse of 0.05 sec. This simulates the pass of a vehicle at 50km/h (Raab, 2011). The corresponding normal pressures at the interface are 0.5; 0.75; 1 and 1.25MPa, which are closer to the actual values for the top interfaces of roads and airfield pavement structures (Raab, 2011).

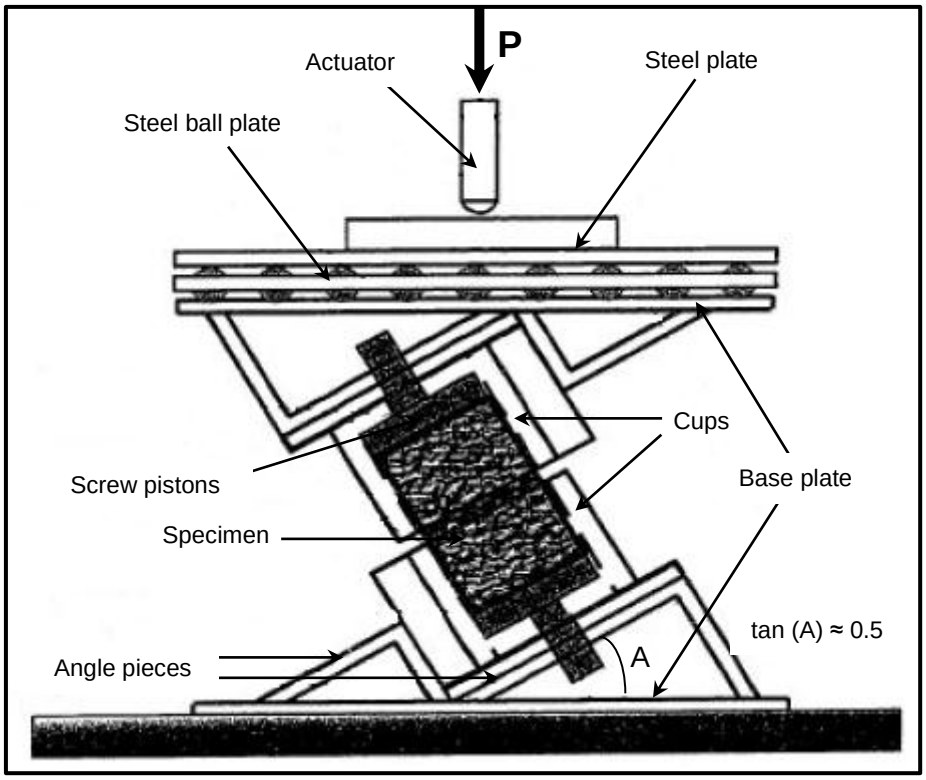

Figure 3-9: Basic configuration of shear fatigue test developed by Romanoschi & Metcalf (2002)

Different versions of the direct shear test apparatus have been employed by researchers to characterize interlayer bonding conditions in the pavement structure. This testing method was found to be the most reliable among several candidate tests, especially, in research based projects (Choi *at al.,* 2005; Collop *et al.*, 2003). However, its experimental complexity related to the application of normal and shear loads prevents this method from being used as a routine standard test (Muslich, 2010b). Therefore, the simplified direct shear test without the application of normal load was adopted to simplify the experimental setup.

According to the literature, the simplified direct shear test developed by Leutner (1979) seems to be the first device designed without a normal load application setup. The test is conducted on a cylindrical 150 ± 2 mm diameter specimen comprising at least two bonded layers. The testing method involves the application of the shear displacement across the interface whereby shear stress and relative displacement are recorded until the interface fails. The test is typically conducted at a standard displacement rate of 50 ± 3 mm/min and a standard testing temperature of 20 ± 1^{o} C. It is important to mention that from its conception, the Leutner device has been continually improved and the latest version is shown in Figure 3-10.

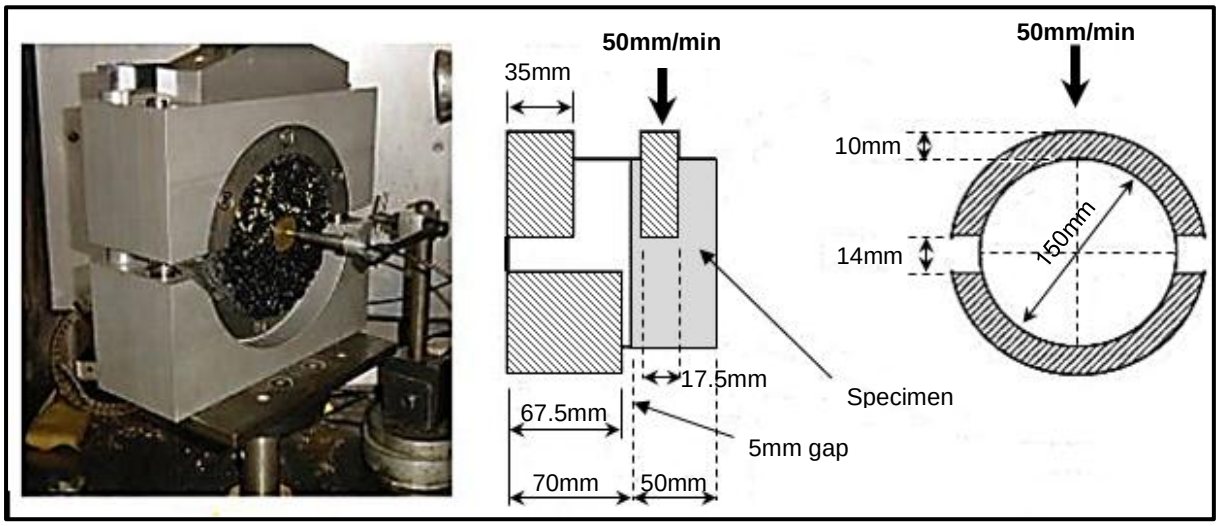

Figure 3-10: Photograph and schematic illustration of the modified Leutner device (Choi *et al.*, 2005)

In Switzerland, a modified version of the Leutner test was developed by EMPA and named the Layer Parallel Direct Shear (LPDS) test (Raab & Partl, 1999). The general setup and working principle of the LPDS test is similar to the Leutner test but the difference is the availability of a wide range of interchangeable loading and clamping devices shown in Figure 3-11 which facilitate the testing of specimens of different diameter. From the comparative study conducted by Raab & Partl (1999), the results obtained using the Leutner test, were almost similar to those of the LPDS test with U-shaped loading and clamping device.

In Australia (FSV, 1999), Spain (Recasens, 2005), France (Diakhaté, 2007) and US (Sholar *et al.*, 2004) different versions of the direct shear test without a normal load were designed and some of them were confirmed as national standard tests. However, their general layouts resemble the Leutner apparatus, with minor changes like testing temperature, specimen size, and the gap width between the shearing rings. In addition, it is important to mention that, since most direct shear devices without normal load were designed to be mounted in a

servo-hydraulic Marshall testing machine, tests were generally set as deformation controlled at the rate of 50 mm/min.

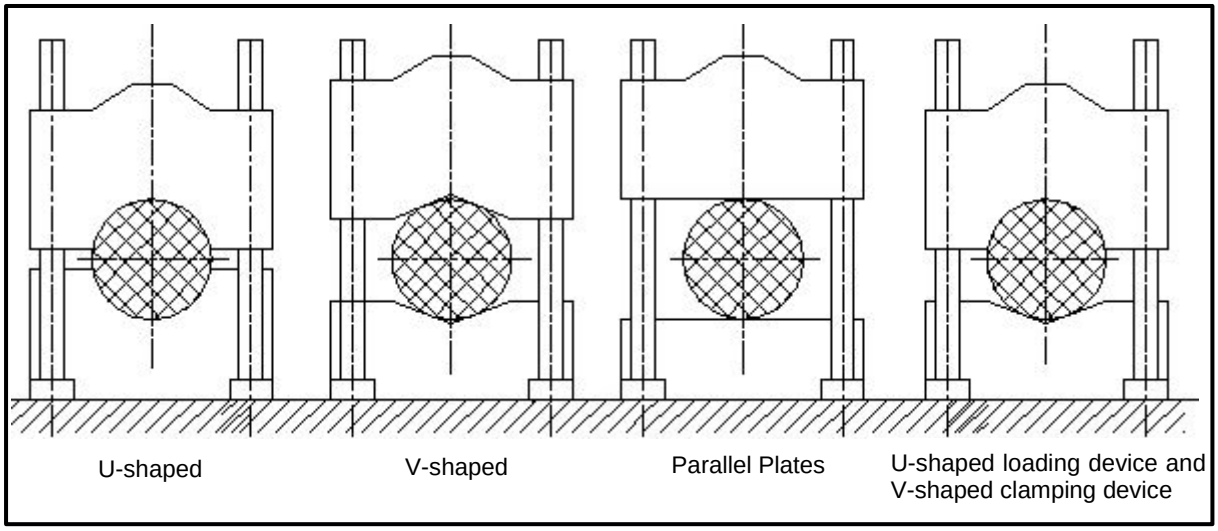

Figure 3-11: Schematic illustration of different load and clamping device in the LPDS test (Raab & Partl, 1999)

From the 1970's, interlayer testing has been developed quickly as the issue of poor bonding between pavement layers became pertinent. Even though different destructive testing methods have been developed, a large effort of research has also been devoted to the aspect of non-destructive testing (NDT) methods for quantifying bond conditions in the pavement structure.

3.3.2. NON-DESTRUCTIVE TESTS (NDT)

The use of NDT methods in pavement assessment dates more than 40 years ago (Kruntcheva *et al.,* 2004). Currently, the Falling Weight Deflectometer (FWD) is widely used to evaluate the structural capacity of the pavement. The FWD is designed to transmit a load pulse to the pavement surface, which simulate traffic loading, and integrated deflection sensors (i.e. geophones) measure the deformation of the pavement which is therefore used to calculate stiffness-related parameters of the pavement by using a backcalculation process (Al Hakim, 1997). In addition to deflection measurement, other type of measurement like Ground Penetrating Radar (GPR), Collograph, and Lightweight vibrator are also used in pavement structure evaluation (Saarenketo & Scullion, 2000).

Lepert *et al.*, (1992) conducted an extensive experiment on a special test section with different predefined interface conditions. The main purpose of the project was to investigate the potential of different NDT equipment to detect interface debonding. Among the deflection and dynamic measurements performed, none of them was relevant for detecting interface debonding.

The Seismic Pavement Analyser (SPA) developed by Nazarian *et al.* (1993), and later on reduced into a smaller portable device, the Portable Seismic Pavement Analyser (PSPA), shown in Figure 3-12, was used to explore the upper pavement layers. The working principle of the PSPA is based on generating stress waves in the pavement structure and then analysing its responses. This device was used by researchers to perform laboratory and site investigation of interlayers between bituminous layers (Kruntcheva *et al.*, 2004). It was found that for layers of similar properties, the device can only estimate bonding conditions for interfaces deeper than 100mm from the pavement surface.

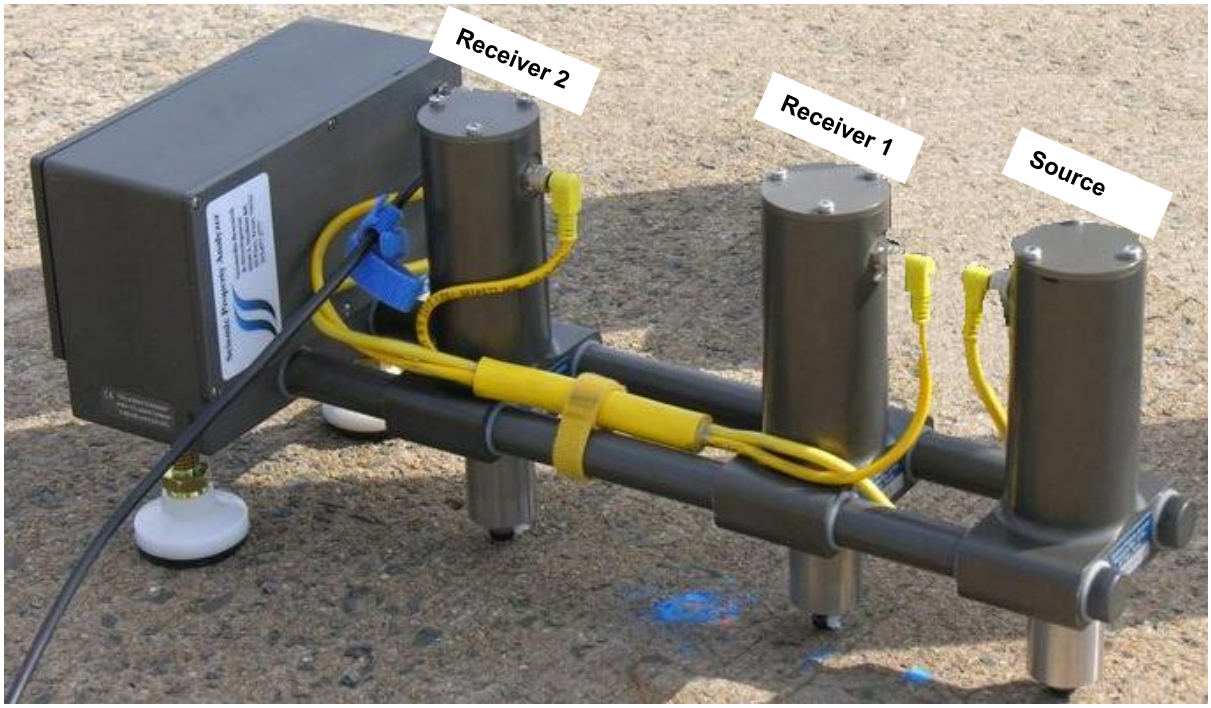

Figure 3-12: Photographic illustration of PSPA (Strategic Highway Research Program, s.a.).

Kruntcheva *et al.* (2004) conducted a laboratory and theoretical study to develop a NDT technique named Impulse Hammer Test (IHT) which can be used to test interface conditions in the flexible pavement structure. The working principle was based on different responses of bonded, debonded and partially bonded structures upon impulse loads applied to the pavement surface. During their study, they analysed different pavement structures and later on, cores were extracted from specific points for comparative laboratory tests. The results from the Leutner shear test showed a high correlation with the predicted bond conditions from the IHT. Moreover, the results of the finite element analysis conducted for deep understanding of the method, confirmed the Leutner and IHT results.

Many other NDT techniques were developed and successfully used, like the "*Colibry*" device developed in France (Lepert *et al.*, 1992; Simonin & Maisonneuve, 1998). Moreover, new back analysis techniques were also developed (Abd El Halim *et al.,* 1997) and used for

rough estimation of bonding conditions between thicker layers, deeper in the pavement structure (Kruntcheva *et al.*, 2000).

The use of the NDT method for the characterisation of the interlayer conditions in the pavement structure has shown well-defined advantages like covering long distances in a short time and being non-destructive as well. However, discernable deficiencies were reported, for instance, muffled accuracy (Kruntcheva *et al.*, 2004; Muslich, 2010b) coverage of only thicker layers (Kruntcheva *et al.*, 2004) and performance highly dependent on the actual condition of the pavement (Kruntcheva *et al.*, 2004). This is why the method was recommended for preliminary investigation, and should be supplemented by destructive tests.

The literature review on the interlayer adhesion testing has shown different test methods used to assess adhesion conditions in the pavement structure. It has also exposed eminent applicability of the direct shear test with normal load, especially for testing specimens made of unbound granular materials. The direct shear test with normal load has been recommended to test rough interfaces to consider the dilatancy effect.

3.4. DIRECT SHEAR INVESTIGATION

Most of the direct shear setups which have been used to assess the interlayer shear strength were limited to 150 mm x 150 mm in cross section for square apparatus and 150 mm in diameter for circular apparatus. The advance in technology and high necessity of acquiring the deep understanding of the interface shear behaviour, involved the development of automated and bigger shear testing devices. Apart from being less laborious, they allow researchers to undertake the shear test of relatively big specimens made of aggregate size equivalent to those used in a typical pavement structure.

A 254 mm x 152 mm shear box has been used by Simoni & Houlsby (2006) to investigate the shear strength and dilatancy of sand-gravel mixtures. The purpose was to determine the frictional and dilatant contributions to the strength of the mixtures according to their relative density. Testing variables were limited to the mixture relative density, maximum grain size and gravel fraction.

According to the shear test results shown In Figure 3-13, they concluded that as the gravel fraction increased, a substantial increase in peak shear/normal stress ratio (τ/σ_v) was noticed. Also the dilation behaviour of the mixture increased. The same behaviour was observed when the relative density was changed from 0.22 to 0.54 as shown in Figure 3-13.

Siang *et al.* (2013) observed similar results for a study conducted on the effect of the morphology of sand on the relationship between shear strength and dilatancy effects.

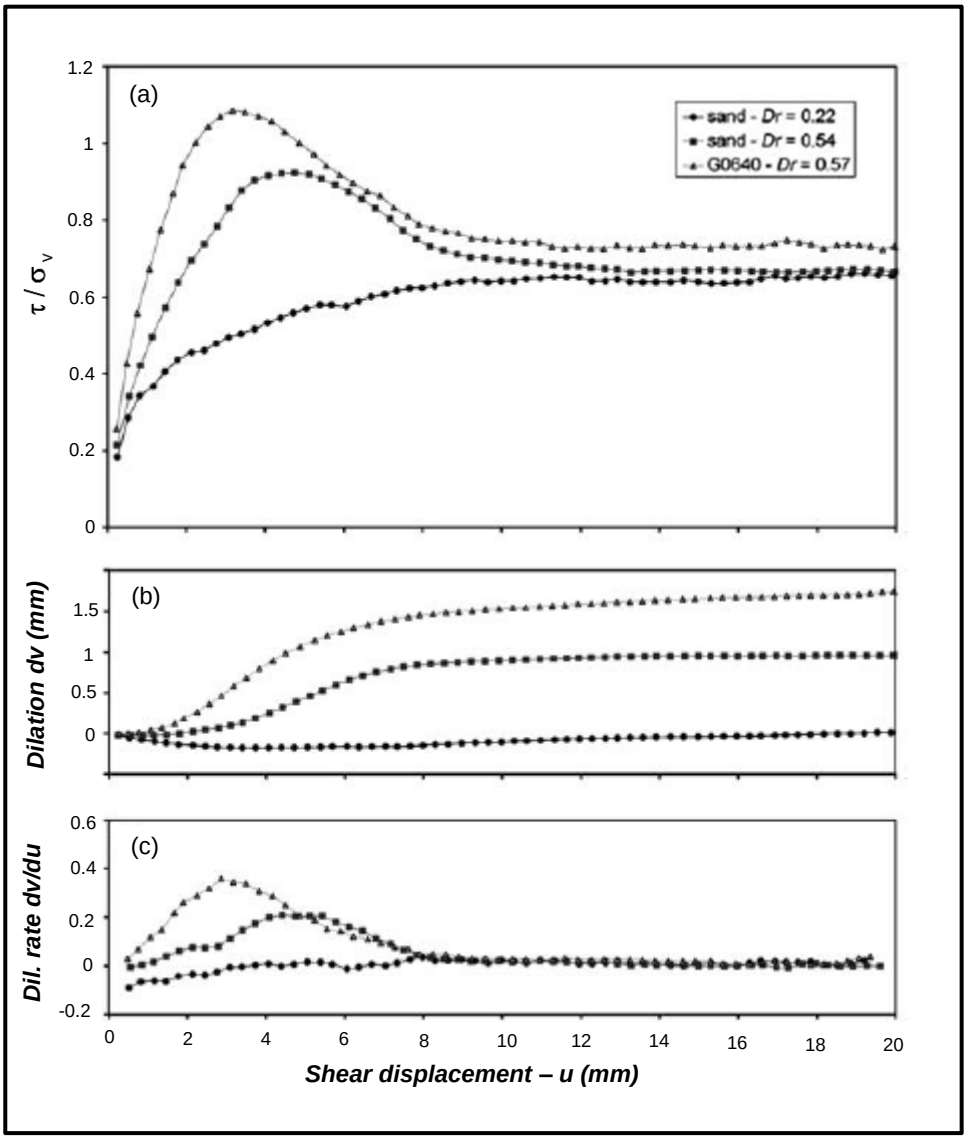

Figure 3-13: Results of direct shear tests. (a) Shear stress ratio; (b) Dilation and (c) Dilation rate against horizontal displacement for tests on loose sand, medium dense sand and medium dense sand-gravel mixture (Simoni & Houlsby, 2006)

In fact, the increase of gravel fraction in the sand-gravel mix increases the maximum aggregate size of the mixture. When such a sample is compacted, small particulars of sand interpose in the gaps between large gravel particles and form a dense and interlocked parking. The associated direct shear behaviour is characterised by a significant vertical movement of the top half of the sample due to the interlock-slip phenomenon induced by the repeated process of strong and weak interaction between the coarse and angular shaped gravel particles. This phenomenon is described as *saw tooth* interaction and it is conceptualised in Figure 3-14.

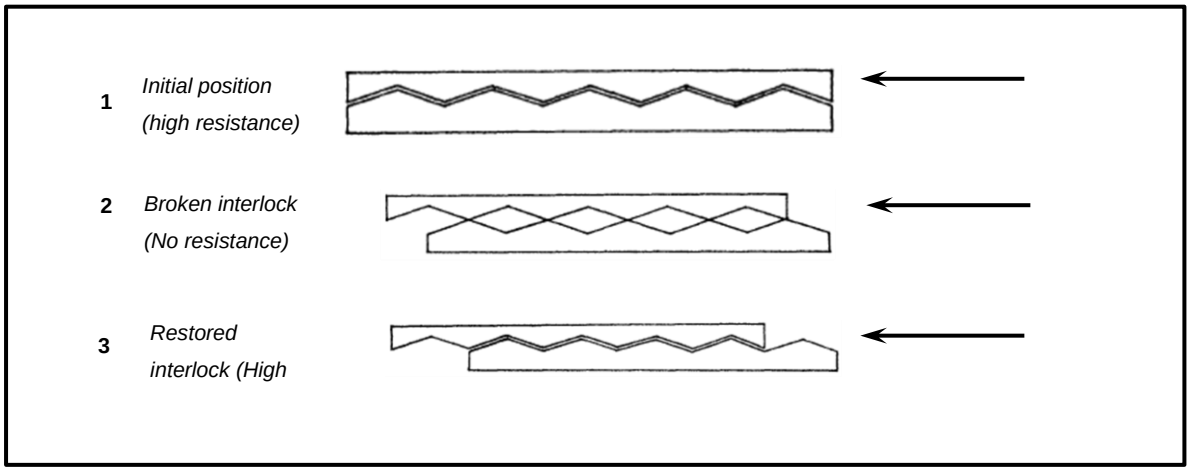

Figure 3-14: Schematic illustration of *saw-tooth* model (Adapted from Rowe, 1962)

3.5. EFFECT OF INTERLAYER ADHESION ON PAVEMENT PERFORMANCE ESTIMATION

The influence of interaction between pavement layers on the overall performance has been discussed since the 1960's (Romain, 1968; Uzan, 1976). Recently, researchers have analytically demonstrated how the long-term structural capacity of the road is seriously affected by interface conditions in general and particularly by the interlayer adhesion (Hariyadi *et al.*, 2013; Kruntcheva *et al.*, 2005).

Apart from the analytical point of view, the pertinent influence of interface conditions on the prediction of flexible pavement life has been reported by different researchers all over the world (Khweir & Fordyce, 2003; Ziari & Khabiri, 2007). This was discussed by Uzan (1976) beforehand whereby he analysed the influence of the interface condition on stress distribution in the pavement structure. He demonstrated the negative impact of poor bonding on the distribution of radial and vertical stresses and the deflection bowl as well. Therefore, this alteration of stress distribution through the pavement structure was reported to reduce the estimated pavement life.

Basically, the prediction of flexible pavement life is based on the distribution of stress, strain and deflection in the multi-layered pavement system. According to the theory of simple bending, it can be shown that stress distribution across the multi-layered structure is highly influenced by the adhesion conditions between layers. In this regard, a number of studies have quantified how each interface condition in the whole system (including base and subbase) influences the overall pavement performance in terms of response distribution (Kruntcheva *et al.*, 2005; Romain, 1968; Uzan *et al.*, 1978).

The research conducted by Romain (1968) seems to be among the foremost published studies about the influence of interlayer bonding conditions in the pavement structure. He carried out an extensive study on the influence of interlayer adhesion on the distribution of stress, strain and deflection in a four-layer pavement structure presented in Figure 3-15.

By using Burmister's theory on stress and displacement in a multi-layered system, the structure was modelled with full bond and full slip interface conditions. Table 3-1 illustrates the variation of stress, strain and deflection according to three cases of different interface conditions relative to stress, strain and deflection computed for the case of full adhesion at all interfaces.

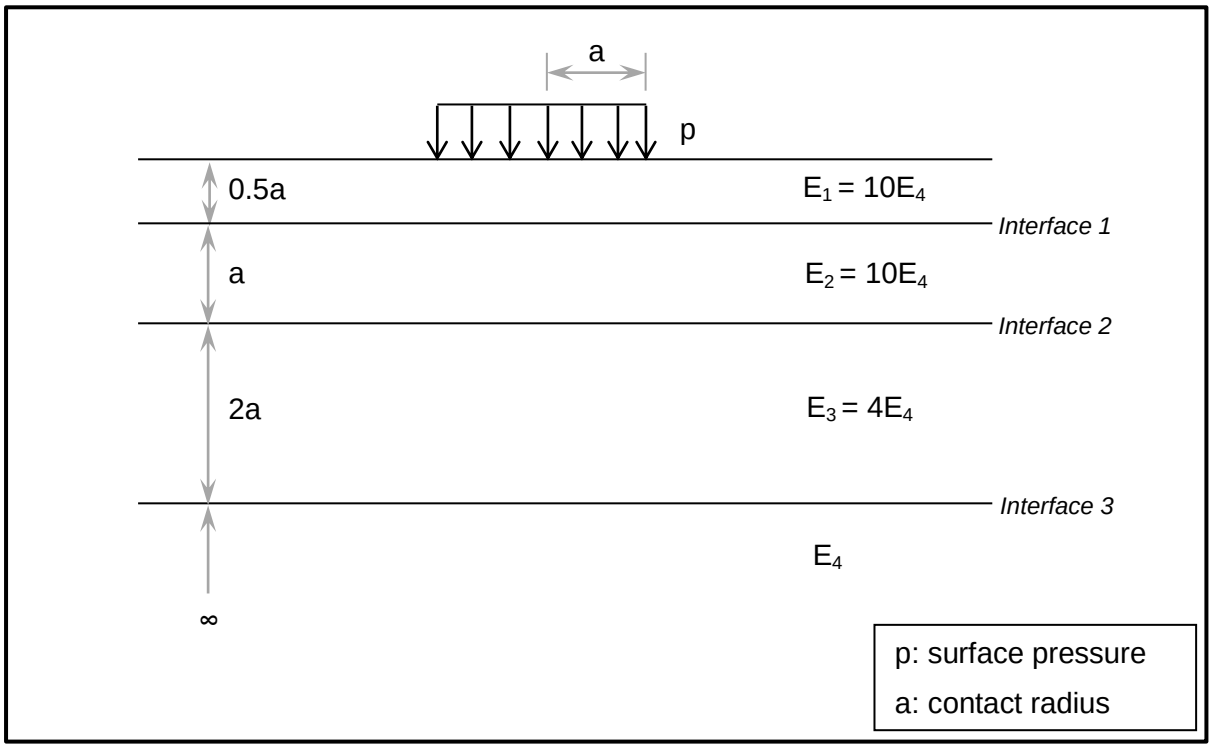

Figure 3-15: Schematic illustration of four layer structure analysed by Romain (Adapted from Uzan *et al.*, 1978)

Table 3-1: Relative results of four - layer pavement structure with different interface conditions analysed by Romain (Adapted from Uzan *et al.*, 1978)

	Bonding Conditions			
	Interface 1	**Smooth**	**rough**	**Smooth**
	Interface 2	**rough**	**smooth**	**Smooth**
	Interface 3	**rough**	**rough**	**Rough**
First Layer	Max. compressive stress	0.79	1.07	0.89
	Max. tensile stress	2.19	1.92	2.69
	Max. compressive strain	2.83	1.07	3.07
	Max. tensile strain	1.93	1.10	2.07
	Deflection	1.20	1.19	1.43
Second Layer	Max. compressive stress	1.74	0.98	1.81
	Max. tensile stress	1.08	2.26	2.73
	Max. compressive strain	1.27	1.72	2.25
	Max. tensile strain	1.30	1.44	1.89
Third Layer	Max. compressive stress	1.55	1.48	2.29
	Max. tensile stress	1.38	1.23	1.77
	Max. compressive strain	1.28	0.92	1.18
	Max. tensile strain	1.22	0.92	1.29
Fourth Layer	Max. compressive stress	1.40	1.79	2.40
	Max. compressive strain	1.37	1.37	1.97
	Max. tensile strain	1.19	1.39	1.58

The pavement structure shown in Figure 3-15 presents 3 interfaces: surface-base (Interface 1), base-subbase (interface 2) and subbase-subgrade (interface 3). According to the objectives of the current study, Figure 3-16 illustrates the effect of the second and third interface conditions on pavement responses in terms of stress, strain and deflection distribution in the second, third and fourth layer of the pavement structure analysed by Romain (1968). It can be seen that the change of interface conditions induced the overall pavement response relative to the response when full bond is considered at all interfaces. It is of special interest to underline the rapid increase in maximum tensile stress in the second layer, along with maximum compressive stress in the subgrade, when the second interface changes from rough to smooth. This may, therefore cause the second and fourth layers (i.e. subgrade) to fail more rapidly than other layers.

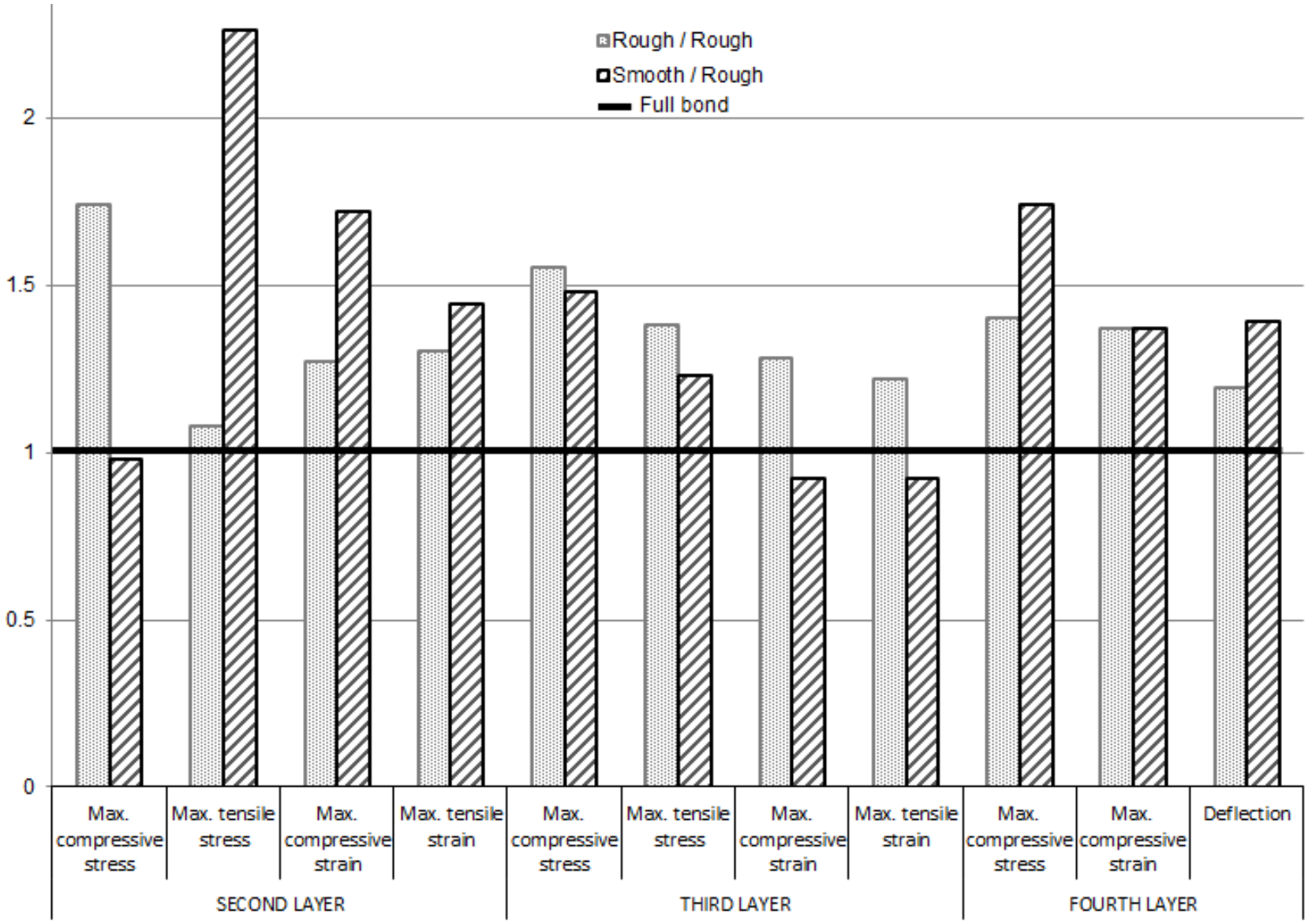

Figure 3-16: Graphical representation of stress, strain and deflection distribution in the second, third and fourth layer (Romain, 1968)

Uzan *et al.* (1978) analysed the influence of bonding between the surfacing and binder courses in a four-layer pavement structure (Figure 3-17). The analysis was done using the BISAR computer program whereby full adhesion between the two last interfaces was assumed while bonding between the surface and binder course was kept variable.

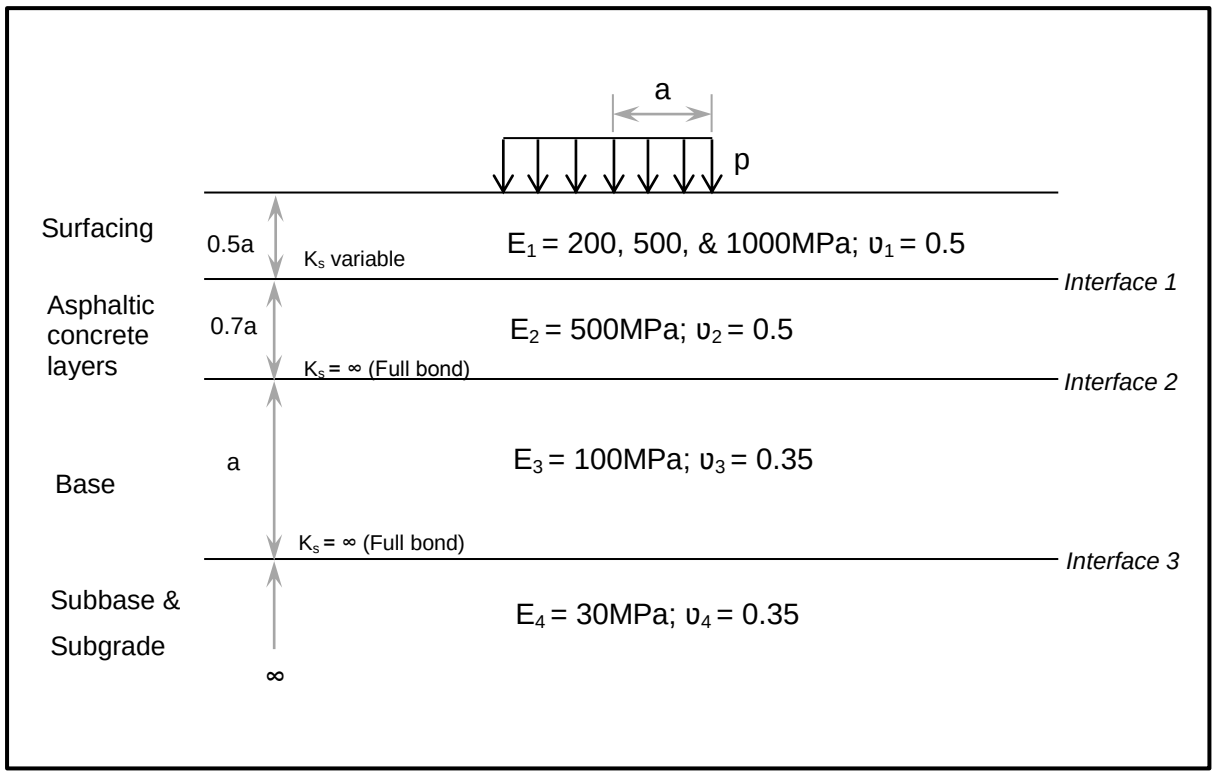

Figure 3-17: Schematic representation of the flexible pavement structure analysed by Uzan *et al.* (1978)

The results of the analysis showed high variability of radial stress at the bottom of the surfacing when shear reaction modulus, K_s changes between 1 and 100 MPa/mm (Figure 3-18). This can induce fatigue cracking at the bottom of the layer. Moreover, they investigated the influence of surfacing – binder courses interface conditions on the distribution of horizontal strain through the entire pavement structure.

As presented on Figure 3-19, the change of interface condition from full bond to perfectly smooth induced a substantial increase of horizontal tensile strain at the bottom of the base layer. This therefore could cause early failure of the layer and the whole structure as well. It is important to underline that this analysis was done under the assumption of full bond between base and subbase layer which is not, practically, the case. Consequently, the change of base – subbase interface conditions might indeed worsen stress and strain distribution behaviour.

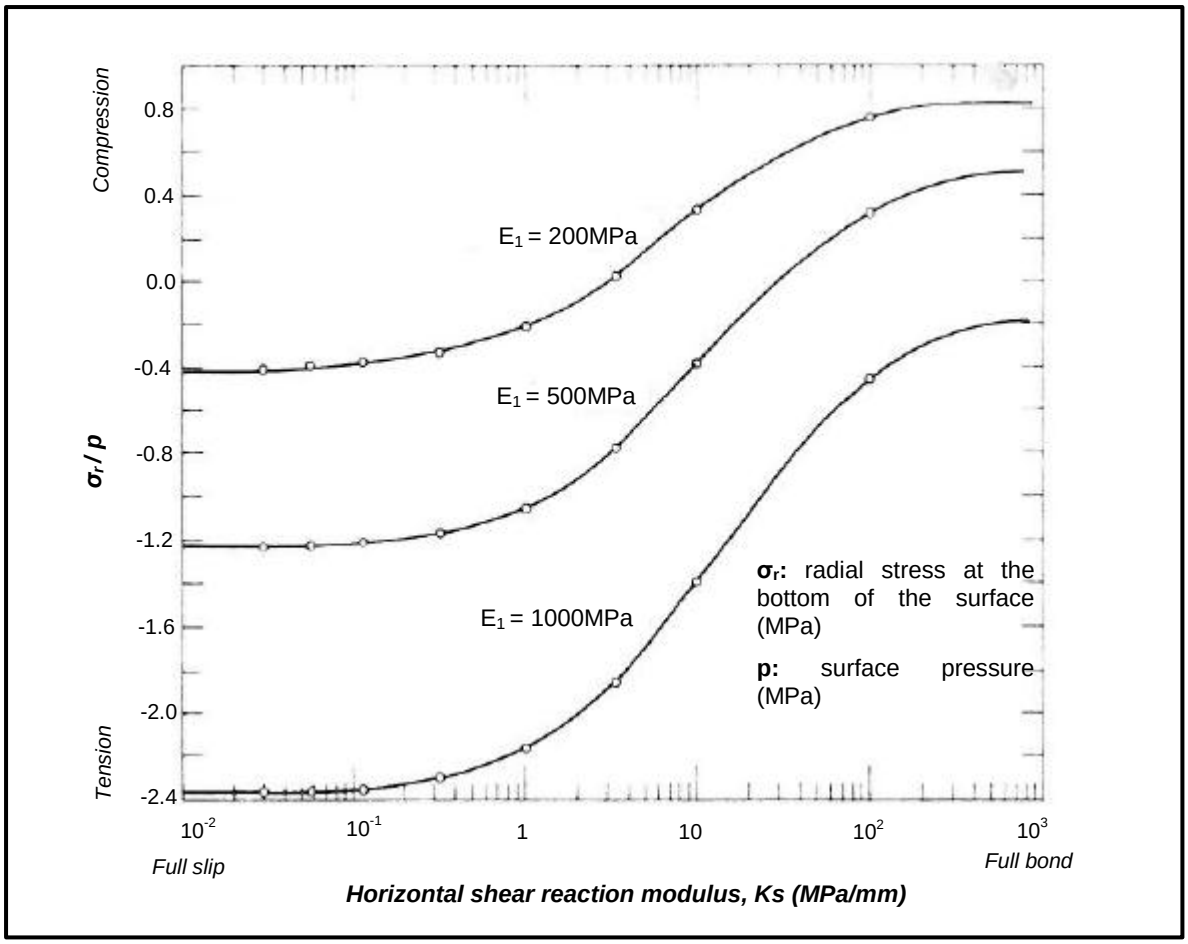

Figure 3-18: Increase of radial stress at the bottom of surfacing due to change of interface condition (Adapted from Uzan *et al.* 1978)

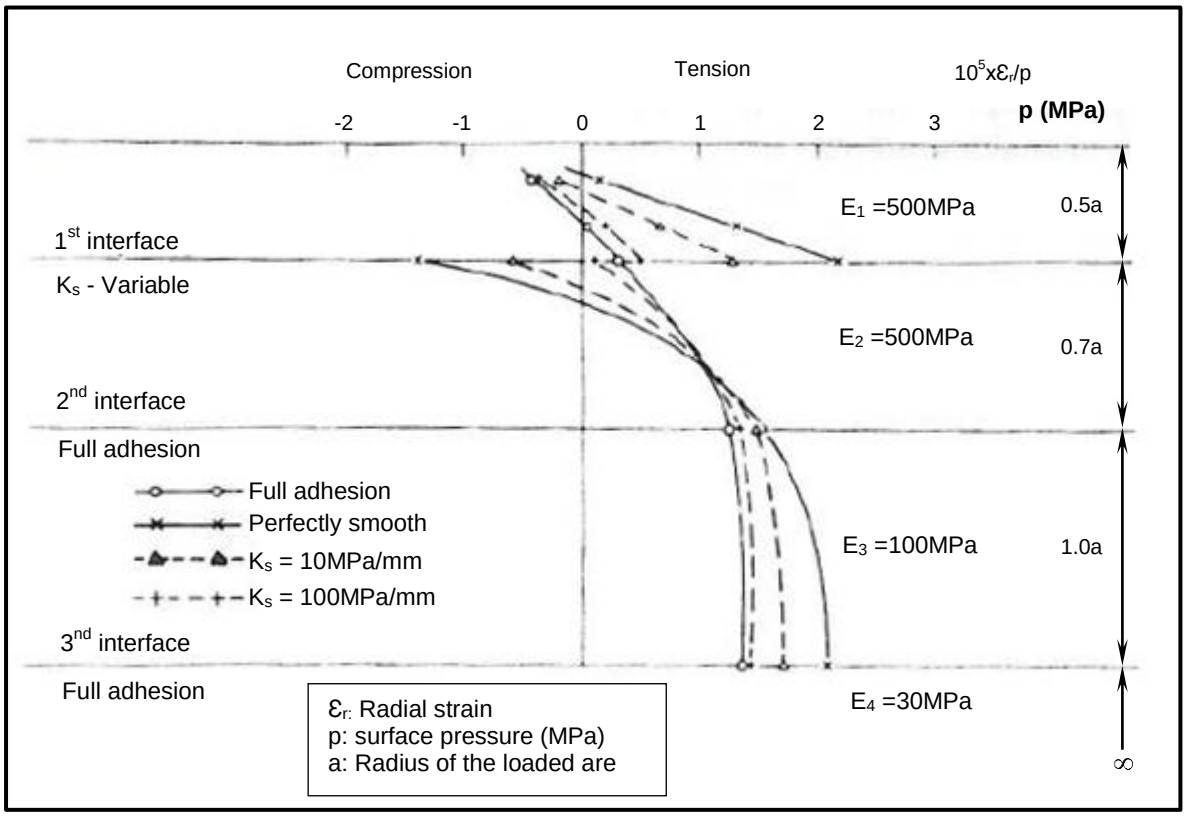

Figure 3-19: Distribution of radial strain throughout the entire pavement structure (Adapted from Uzan *et al.* 1978

Kruntcheva *et al.* (2005) used the BISAR computer program to investigate the influence of interlayer bond conditions on the pavement life to failure. A five layer pavement structure shown in Figure 3-20 was modelled with two types of loading conditions: a standard vertical dual-wheel loading combined with horizontal loads simulating friction forces due to breaking, scuffing of tyres around sharp corners, accelerating and cornering. Two friction directions were examined: parallel to trafficking and at 45^0 to this direction.

Figure 3-21 illustrates the pavement lives to failure expressed as a percentage of full bond life for different debonded interface with subgrade stiffness, $E_{subgrade}$ = 20MPa. The life to failure for fatigue and the life to failure for deformation are denoted as fatigue life N_f and deformation life N_d, respectively. The notations k1/2, k2/3 and k3/4 after N_f and N_d stand for partial slip between layer 1 and 2, layer 2 and 3 and layer 3 and 4, respectively. Additionally, the solid line corresponds to deformation lives whereas the dashed lines represent the fatigue lives, all expressed as a percentage of full bond.

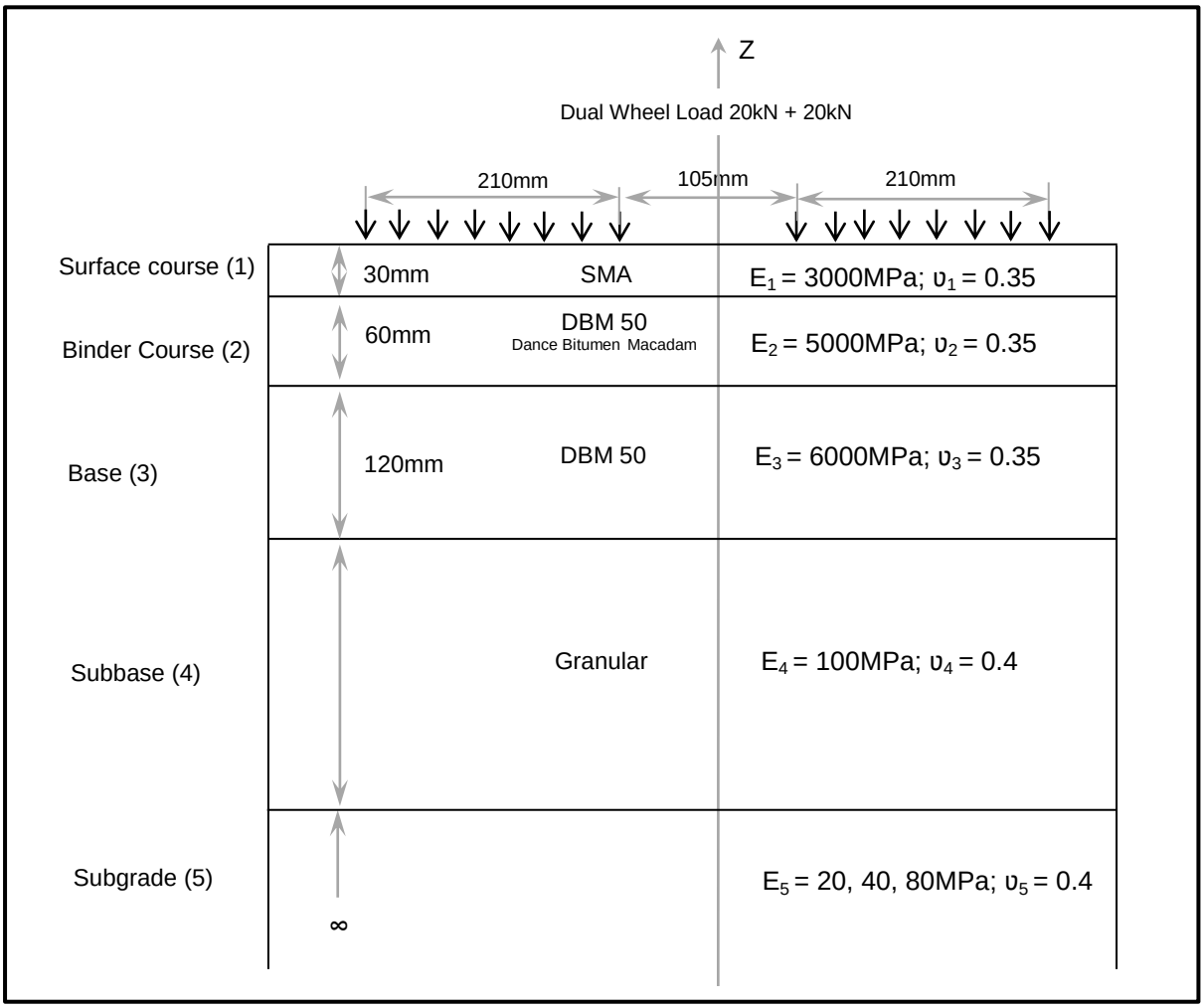

Figure 3-20: Schematic illustration of pavement structure analysed by Kruntcheva *et al.* (2005)

From the results of the analysis, as summarized in Figure 3-21, Kruntcheva *et al.* (2005) concluded that the interface between the binder course and base layer is the most critical since the failure life can be reduced by up to 80% when full slip is considered. However, the results also showed that poor adhesion at the interface between base and subbase reduces the pavement failure life by 62% from full-bond life, but this depends on the supporting foundation. Furthermore, the presence of horizontal loads significantly reduces the failure life as compared to the life to failure when only vertical load is considered (Figure 3-22).

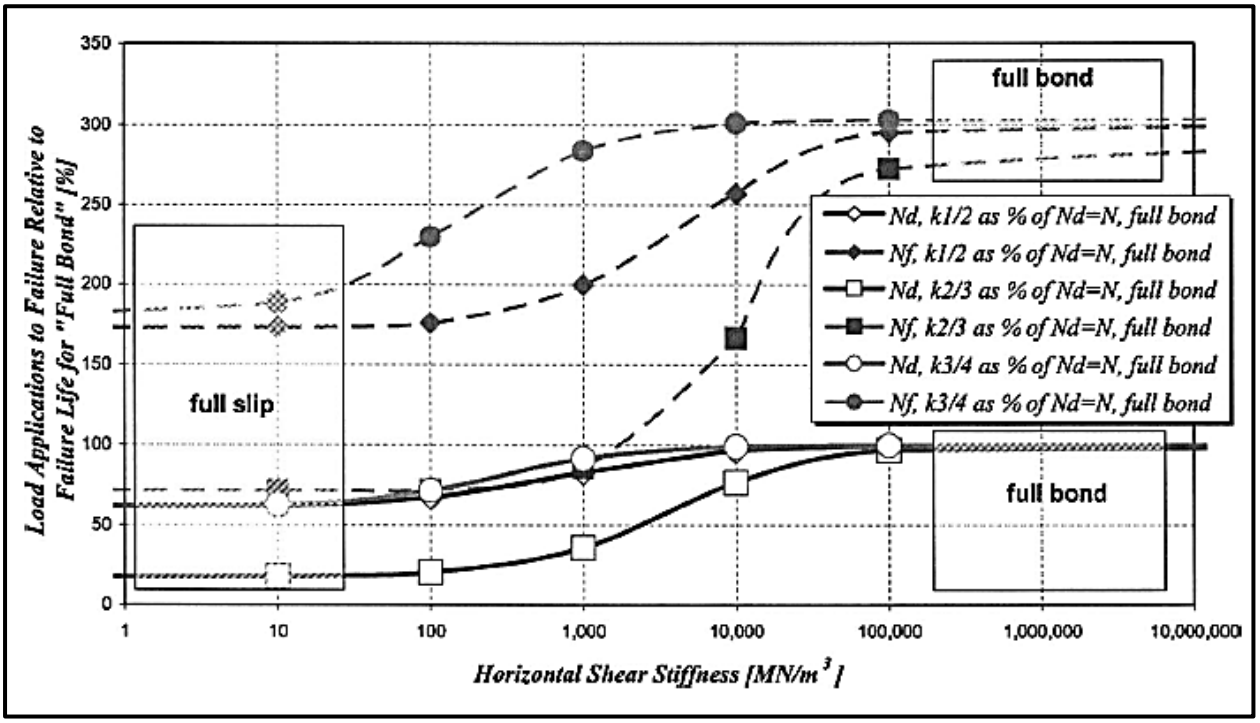

Figure 3-21: Influence of bond condition on life to failure of flexible pavement structure (Kruntcheva *et al.* 2005)

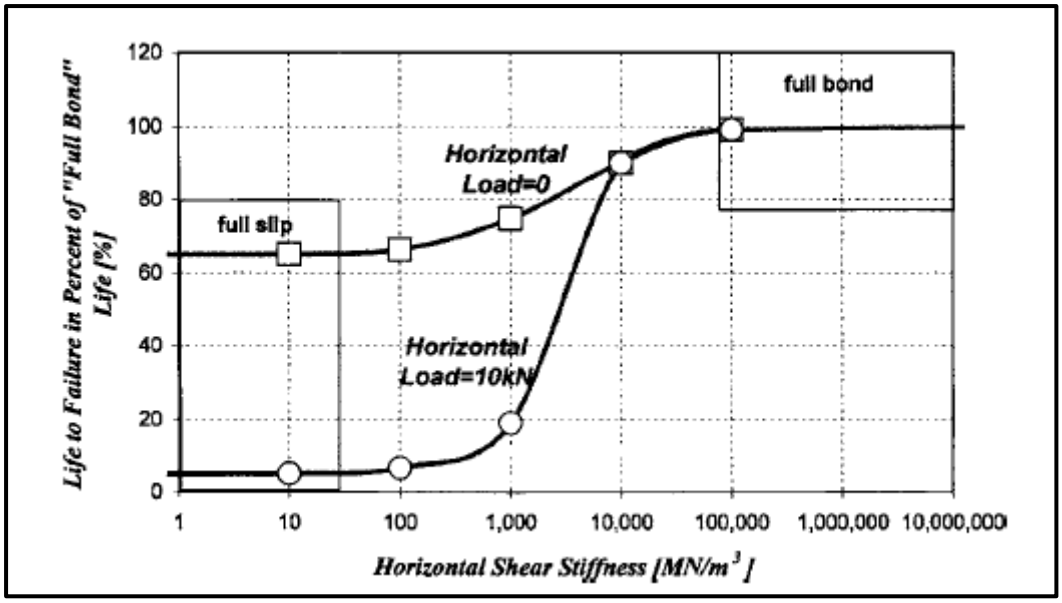

Figure 3-22: Influence of horizontal load on life to failure of debonded interface expressed as percentage of full bonded (Kruntcheva *et al.*, 2005)

3.6. SUMMARY OF THE LITERATURE REVIEW

The advance in technology has stimulated an increase of traffic volume, maximum axle load and the tire pressure applied on road pavements. To address the associated damage, extensive research has been conducted to acquire a thorough understanding on how different materials perform in a multi-layered pavement structure. Significant concern was devoted to the structural performance of each individual layer in the pavement system. However, past literature revealed the influence of the interaction between layers on pavement distresses to occur.

The state of interlayer adhesion has been admitted to influence the performance of road pavements according to previous literature. Various failure cases and decrease of pavement life discussed in this chapter have disclosed the impact of poor adhesion between asphaltic top layers, or asphalt and granular base layers, on early deterioration of the pavement structure. Yet, a limited number of publications has also identified the same problem in deeper layers like granular and cemented layers but a detailed understanding of the failure mechanism and the quantification approach remain a point of discussion.

According to previous publications discussed in this chapter, the interlayer bonding strength between bituminous layers has been tested by using various devices. Direct shear apparatuses working without normal load have been identified to suit asphaltic materials due to their simplicity and possibility to be mounted in the normal servo-hydraulic Marshall testing machines available in many pavement and geotechnical laboratories. However, due to their unbound behaviour, granular materials cannot be tested with direct shear devices without

normal load. Therefore, the machine allowing the application of normal load while testing was selected for this study.

To consider the big aggregate particles available in typical pavement materials, a large shear box (i.e. 300 mm x 300 mm cross section) was adopted.

Direct shear test results have been used by researchers to assess the interaction response of granular materials. Influential parameters like aggregate size and relative density were investigated. To this end, frictional and dilatant behaviour of the interlayer between granular and cement treated layers were used to investigate their adhesion condition. Basically, the resistance of a layer to slide on top of another indicates significant interaction between them thus effective adhesion. Similarly, an increase of specimen volume throughout the shear phase shows intimate contact between layers due to interlock.

Chapter 4

RESEARCH MATERIALS, APPARATUS AND METHODOLOGY

4.1. INTRODUCTION

This chapter discusses the methodology used in this study. The chapter is divided into two main parts: research material characterisation and direct shear investigation.

Characterisation of the research material was done according to various standard tests and this chapter highlights these. The direct shear investigation comprises a detailed description of sample preparation, direct shear apparatus and testing procedure. All the results are presented in Chapter 5.

Figure 4-1 illustrates a flowchart of the experimental investigation followed.

4.2. RESEARCH MATERIALS

Two types of granular materials were used for this study: crushed hornfels stone G2 for the Granular Base (GB) layer, and blended G5 as the parent material for the Cement Treated Subbase (CTSB) layer. Material selection was based on recommended materials for base and subbase layers of a typical South African pavement structure (SAPEM, 2013; TRH 14, 1985). Both of them were collected from Lafarge quarry located in Tygerberg valley in the Western Cape / South Africa.

Since the laboratory investigation was set to reflect the routine road construction practice in the field, the research materials were required to be characterized according to the South African road construction materials guidelines. Therefore various characterization tests were run with respect to SAPEM (2013) and TRH 14 (1985) requirements.

This section presents a series of standard characterisation tests performed and relative methods followed.

4.2.1. GRADING

In order to ensure consistency and accurate blending of materials during specimen preparation, air-dried G2 and G5 materials were separated and stored into different fractions, by means of sieving. The G2 and G5 materials were sieved into thirteen and seven fractions, respectively. Figure 4-2 depicts the sieving set up used.

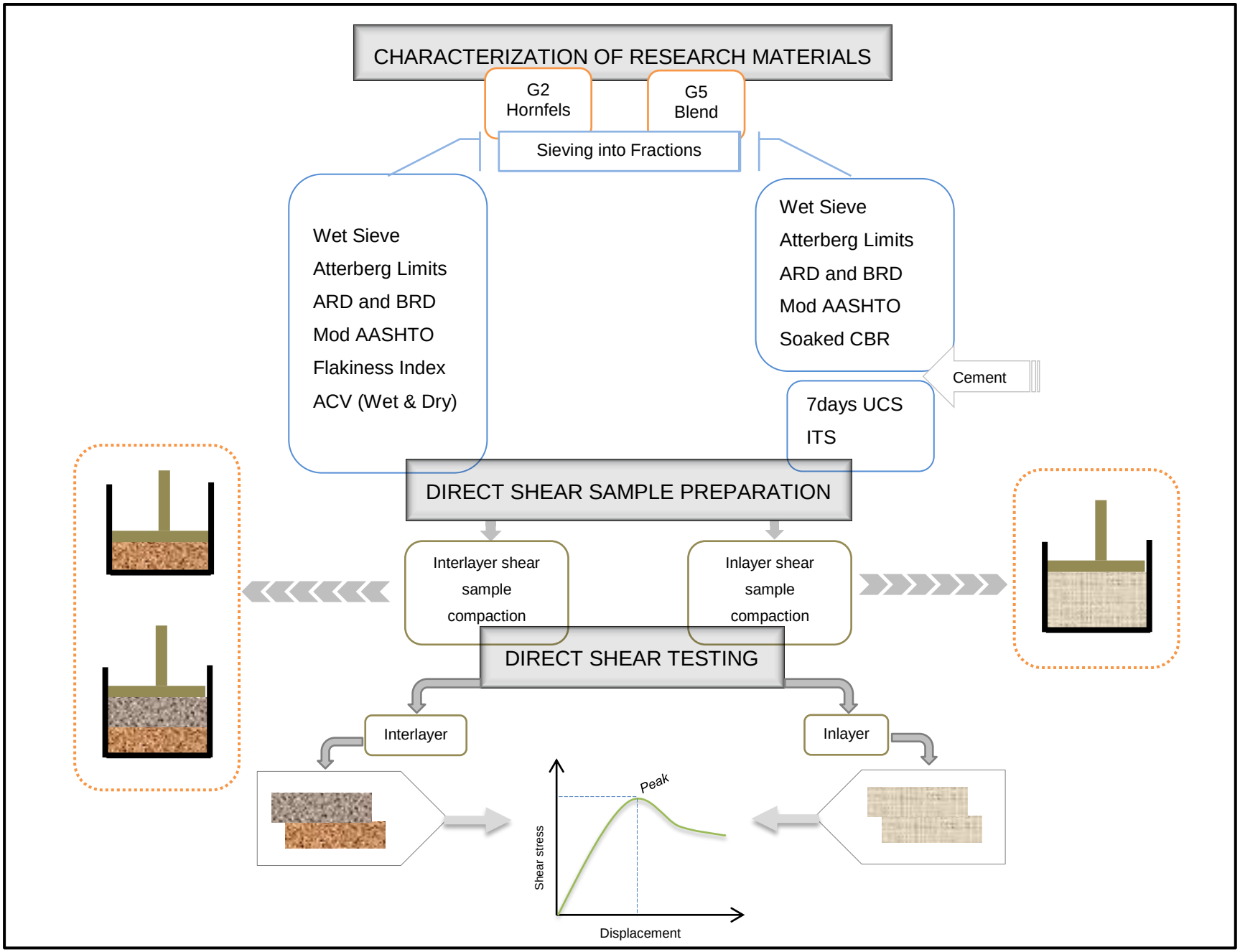

Figure 4-1: General overview of the experimental investigation

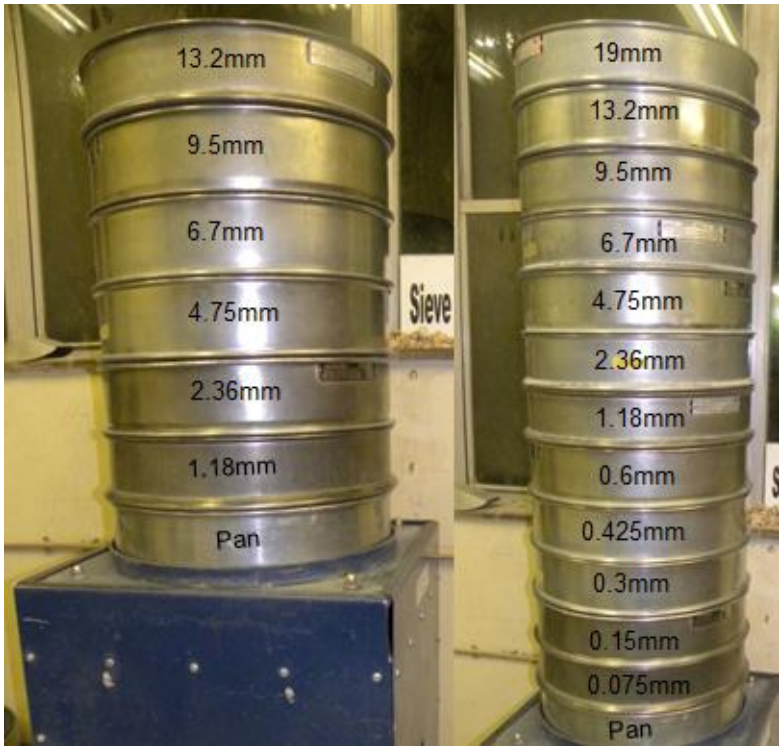

(a) Sieve set for G5 (b) Sieve set for G2

Figure 4-2: Sieves set up used for materials separation

The blend composition was designed for G2 and G5 materials using Fuller's equation shown in Equation 4-1. Subsequently, wet sieving was carried out for both materials to determine the grading modulus for G5 and locate the G2 grading curve in the grading envelop required by TRH 14 (1985). TMH1 Method 1(a) standard was followed.

$$P = \left(\frac{d}{D}\right)^{n} \qquad \textbf{(4-1)}$$

With P: % passing a sieve with aperture d

D: Maximum particle size and

n ranging between 0.25 and 0.45. For this study 0.45 was used since it was found to give densest packing (SAPEM, 2013).

4.2.2. ATTERBERG LIMITS AND LINEAR SHRINKAGE

The Atterberg limits tests give basic information regarding the material's plasticity and sensitivity to water. The Plastic Index (PI), obtained by subtracting the Plastic Limit (PL) from the Liquid Limit (LL), provides a clear indication of the material's performance. The lower the PI, the better the material. On the other side, the Linear Shrinkage (LS) indicates the material's sensitivity to water.

For this study, TMH1 Method A2 and Method A3 were followed for the determination of Liquid Limit and Plastic Limit respectively, for G2 and G5 materials.

4.2.3. DRY BULK DENSITY, APPARENT RELATIVE DENSITY AND WATER ABSORPTION OF AGGREGATE.

Usually, the density of particles is defined as the mass of the aggregate particles divided by their volume. If this volume includes only impermeable (internal) voids and excludes permeable (surface) and inter-particle voids, the yield density is termed as apparent relative density (ARD). On the other hand, if the volume includes impermeable (internal), and permeable (surface) voids, but excluding the inter-particle voids, the yield density is called dry bulk density or bulk relative density (BRD) (SAPEM, 2013).

The BRD is considered as a field compaction reference test for G2 and G3 quality material and the ARD gives an indication of the specific gravity of an aggregate.

For this study, TMH1 Method B14 was followed for testing G2 and G5 materials.

4.2.4. MODIFIED AASHTO COMPACTION

Generally, the Mod AASHTO test is used to determine the laboratory Maximum Dry Density (MDD) and Optimum Moisture Content (OMC) for road construction materials. In this study, the test was done according to TMH1 Method A7, and the mechanical compaction equipment shown in Figure 4-3 was used. The MDD and OMC determined for G2 and G5 (natural or cemented) materials were used as benchmark during compacting specimens for CBR, UCS, ITS and direct shear test samples.

Figure 4-3: Mechanical compaction machine located in SU soil lab

4.2.5. SOAKED CBR

The soaked California Bearing Ratio (CBR) is a standard strength test for gravel and soils of G4 and lesser quality to be used for road construction purposes (SAPEM, 2013).

The test is carried out on a compacted specimen of the material after soaking it for 4 days. The general principle involves pushing the plunger into the soil sample with a specific displacement rate and the load that is needed to obtain that displacement is monitored. The load-displacement curve obtained in this way is compared to the curve of a reference material.

THM1 Method A8 was followed for this study.

4.2.6. FLAKINESS INDEX

The Flakiness Index (FI) is defined as the quantitative measure of coarser aggregate shape related to a degree of flatness. Practically, this parameter has a direct effect on particle arrangement in a compacted layer of the pavement structure.

The manual procedure adopted to determine the FI for crushed gravel to be used as base and subbase layer consists of gauging all particles of a specific fraction size through slots of specific width. The index is expressed as the percentage of the total mass of the aggregates that passes through the slots. Various test standards are available for FI test but Method B3 of the TMH1 standard was followed for this study.

4.2.7. AGGREGATE CRUSHING VALUE (DRY AND WET)

Aggregate Crushing Value (ACV) is one of the recommended tests for aggregates to be used in subbase and base layers. The test itself aims to assess the strength properties of the aggregates whereby a prepared confined aggregate sample is crushed under a specified, gradually applied compressive load. According to SABS Method 842, “ACV of the aggregate is defined as a percentage of the test sample which is crushed to - 2.36 mm sieve when a sample of - 13.2 mm + 9.5 mm sieve is subjected to crushing under a gradually applied compressive load of 400 kN”. Similarly, the load in kN required to crush the same sample so that 10 % will pass a 2.36 mm sieve is defined as 10% FACT. However, 10% FACT is only recommended for weaker materials.

Additionally, the ACV test can be used to assess aggregate durability. The test is conducted on a soaked sample of aggregate and the ACV value for wet and dry are compared. SAPEM (2013) recommends the wet/dry ratio not less than 75% for adequate durability of crushed stone base (G3 and better). Figure 4-4 contains photographs of the overall testing procedure followed for this study as required in SABS Method 842.

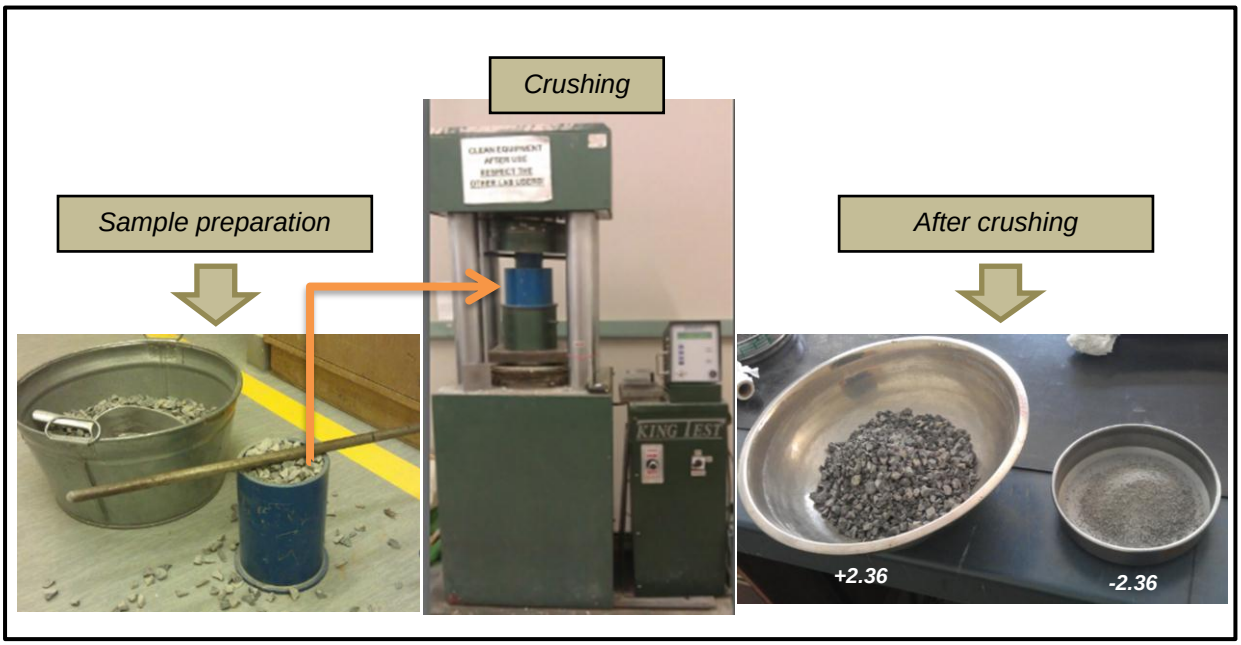

Figure 4-4: Aggregate Crashing Value (ACV) testing procedure

4.2.8. UNCONFINED COMPRESSIVE STRENGTH (UCS) AND INDIRECT TENSILE STRENGTH (ITS)

UCS and ITS tests are standard strength tests for stabilised road construction materials. The testing procedure involves displacement controlled loading to a 7 days cured cylindrical specimen, 127 mm high and 150 mm in diameter, up to failure. ITS and UCS specimens are loaded diametrically and axially respectively and characteristic strengths are defined as the maximum stress applied to the specimen during testing. Figure 4-5 illustrates the test setups and typical maximum stress curve.

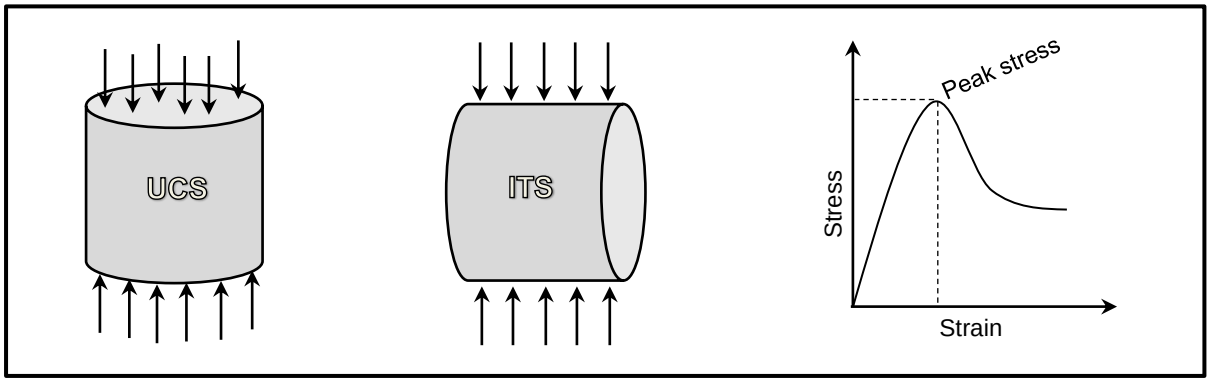

Figure 4-5: UCS and ITS testing configuration and analysis

For this study, UCS and ITS tests were conducted as part of the mix design procedure to obtain the optimum stabiliser content. Two specimens were tested for each cement content, and three cement contents were chosen either for UCS or ITS tests. TMH1, Method A14 and Method A16T were used for UCS and ITS tests respectively.

4.3. DIRECT SHEAR INVESTIGATION

The automated direct shear testing was run on 300 mm x 300 mm laboratory compacted samples. The typical specimen was made of two different layers; one compacted on top of another. Both layers were compacted at 100% Mod AASHTO.

To achieve the research objectives, two qualitative factors and one quantitative factor influencing interlayer adhesion strength were examined. Qualitative factors include Cement Treated Subbase (CTSB) surface roughness condition and testing moisture condition. The quantitative factor considered is the applied normal pressure. Each of the three factors has at least two levels of analysis; Two surface roughness conditions of the CTSB were considered: scarified and quasi-smooth, two testing moisture conditions: saturated and unsaturated, and at least two identical values of normal pressures (i.e. 50 and 100 kPa) for all possible combinations. Additionally, extra experimental runs were conducted to assess the effect of the maximum size of the aggregate in the CTSB whereby the maximum size was changed from 19 mm to 26 mm. This trial was only limited to the scarified CTSB surface under saturated and unsaturated conditions with three normal pressures.

In order to better understand the degree of shear resistance between Granular Base (GB) and CTSB layers, two extreme strength conditions were selected and compared with the normal interlayer shear strength. The best condition was represented by the inlayer shear strength whereby the shear plane was localised within one of the layers. Consequently, a set of inlayer tests was conducted for both types of materials. Saturated and unsaturated conditions were considered and three values of normal pressure were examined. On the other hand, the worst case scenario was simulated by shearing the interface while two layers were separated by a 500 µm thick plastic sheet, placed between them. Figure 4-6 presents the overall layout of the shear test experimental design.

It is important to mention that at least two specimens were tested for each combination in order to detect the outliers.

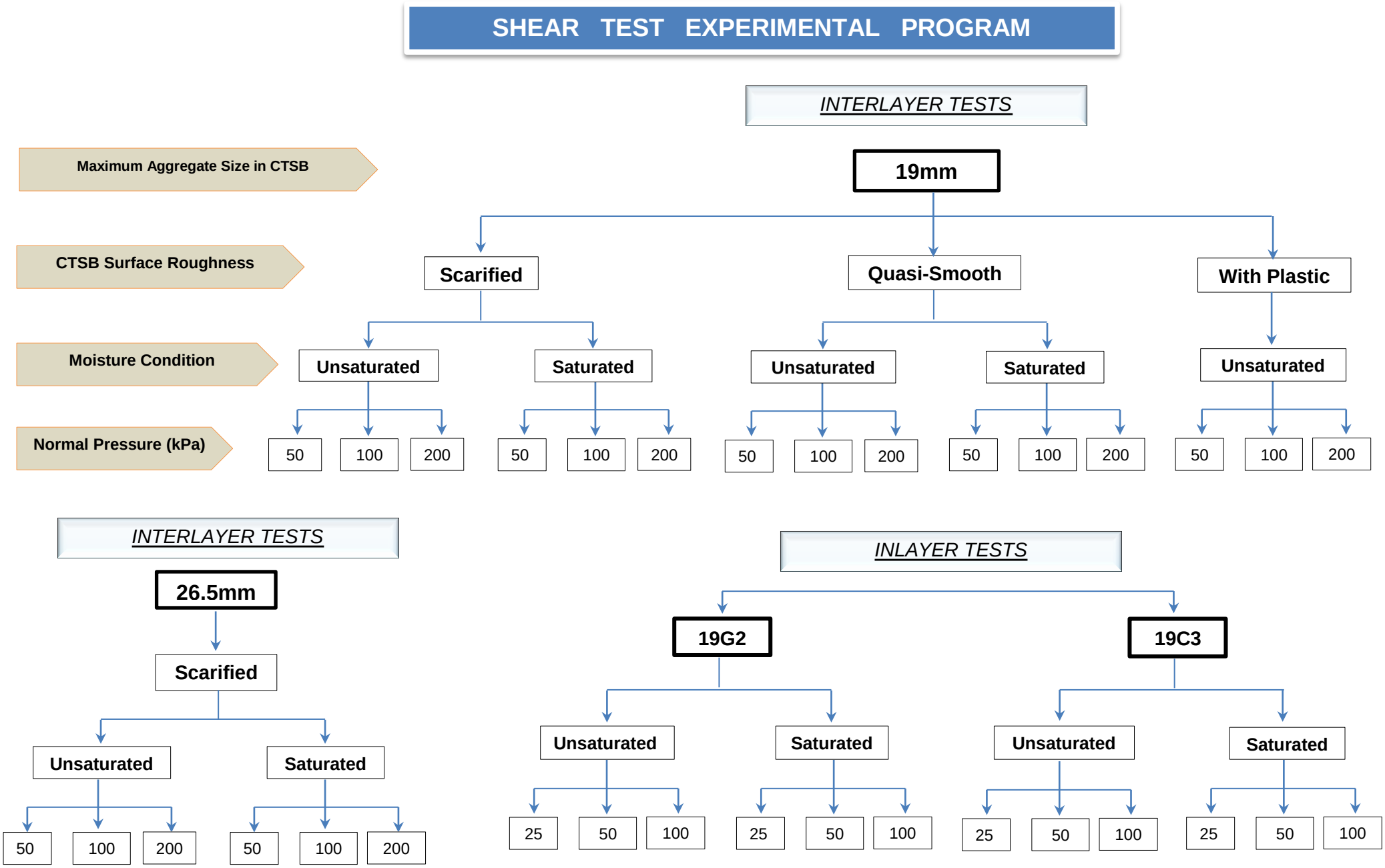

Figure 4-6: Flowchart of shear test experimental design

4.3.1. SAMPLE PREPARATION

As mentioned before, the typical specimen was made of two layers: the GB compacted on top of the CTSB. Therefore, the specimen preparation was accomplished in two broad stages:

4.3.1.1. Mix Design and Compaction of the CTSB layer

The CTSB was made of G5 granular material, stabilised by 1.8% of cement. The amount of materials required to make a layer was calculated based on the target MDD obtained from the Mod AASHTO test and the volume of the layer. To ensure accuracy and uniformity, various fractions of G5 materials were weighed off and blended accordingly. The laboratory mixer shown in Figure 4-7 was used to mix the computed quantity of granular materials, cement and water until the proper consistency was achieved.

Figure 4-7: Laboratory vertical shaft mixer

The SU vibratory compactor was used to compact the specimen to the target density (see and Figure 4-8 Figure 4-9). The machine mainly consists of four parts:

1. Two electric vibratory motors fixed in a steel framework,
2. Supporting steel column and guides,
3. Compaction mould, and
4. Concrete slab and air bellows

By switching on the machine, high frequency vibrations of two electric motors are transmitted to the steel compaction plate through triple pillars and to the concrete slab through the supporting steel column. The concrete slab is suspended on four rubber air bellows. Since the compaction mould is fixed on the concrete slab, specimen compaction is controlled by

the vibrating effect of both the top dead weight of the machine and the concrete slab. This has the advantage of producing a uniform compaction throughout the specimen. A block and tackle chain is used for vertical movement of the top dead weight of the machine.

The process of specimen compaction started by mounting four sides of the steel compaction mould around the wooden base and fixing them to the concrete slab by means of bolts and nuts.

Prior to compaction, three levels were marked on the supporting steel column to define the essential compaction heights of the layer. Since the entire layer of 80 mm was compacted in two equal sub-layers, the steel column was marked at 0 mm reference level which corresponded to the lowest level of the steel compaction plate when it was touching the wooden plate inside the empty steel mould (see Figure 4-8A). From that reference level, 40 and 80 mm were properly marked as the top levels of the first and second sub-layers respectively (Figure 4-8B).

During the compaction exercise, the complete interlock between two sub-layers was achieved by scarifying the top surface of the first completed sub-layer before casting the second one. Scarification was done using manual scarifying tool and electric drill.

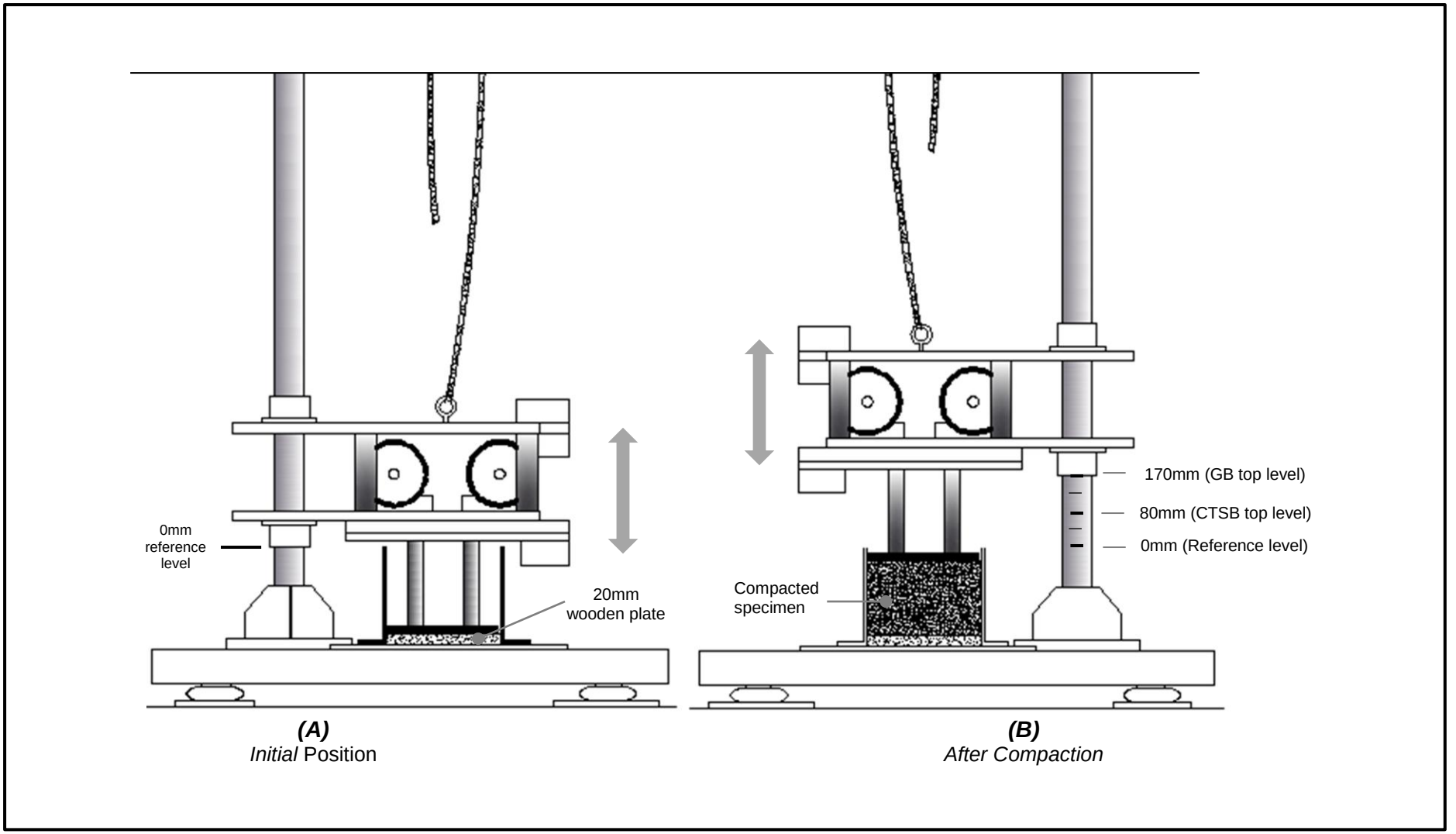

Figure 4-8: Schematic of vibratory compaction machine and appropriate marking of the compaction heights

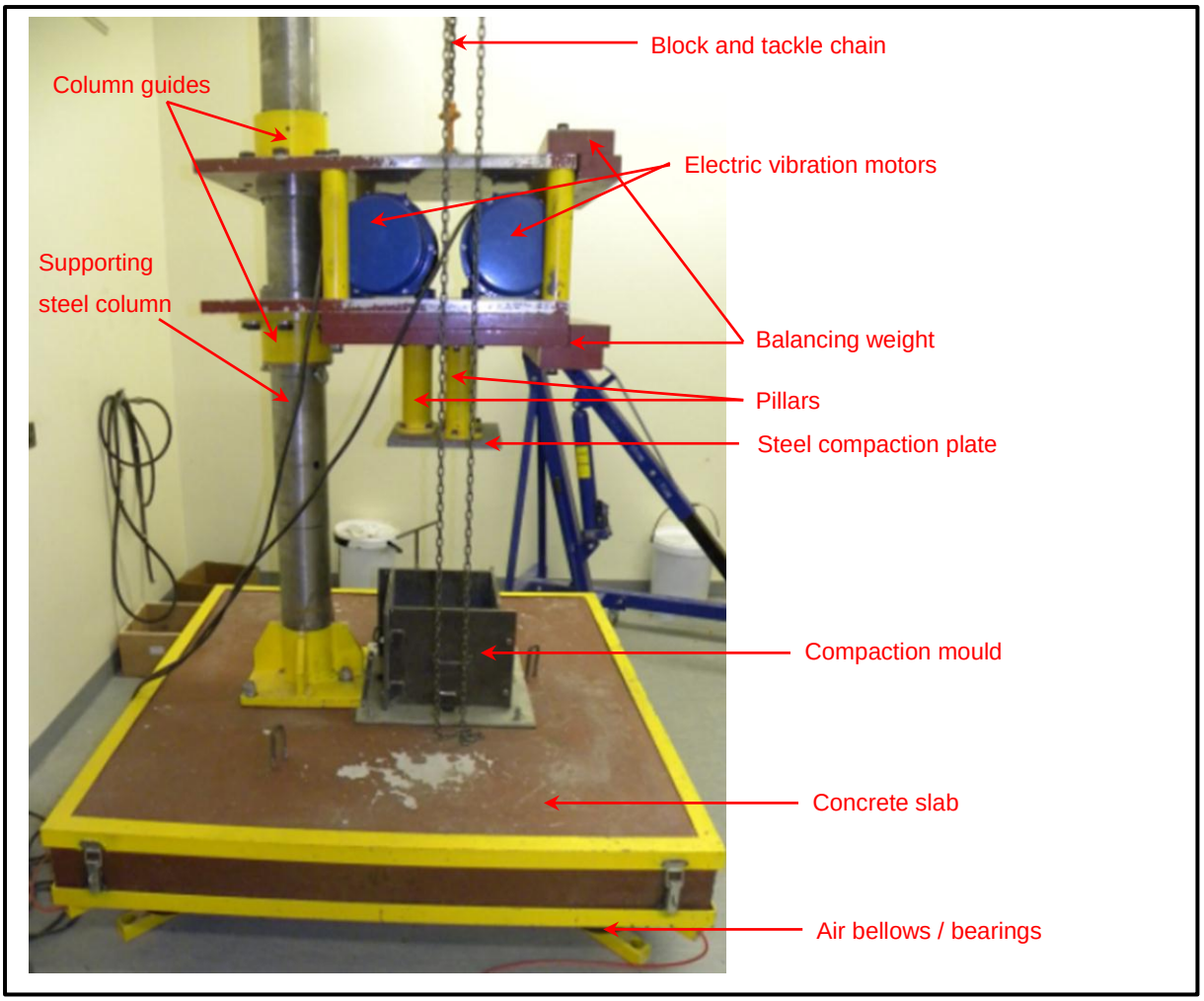

Figure 4-9: SU vibratory compaction machine

After the compaction of the second sub-layer, the surface was scarified or left quasi-smooth (see Figure 4-11) according to the experimental design requirements. Figure 4-10 contains a photograph and a diagram of the CTSB layer in the compaction mould after compaction.

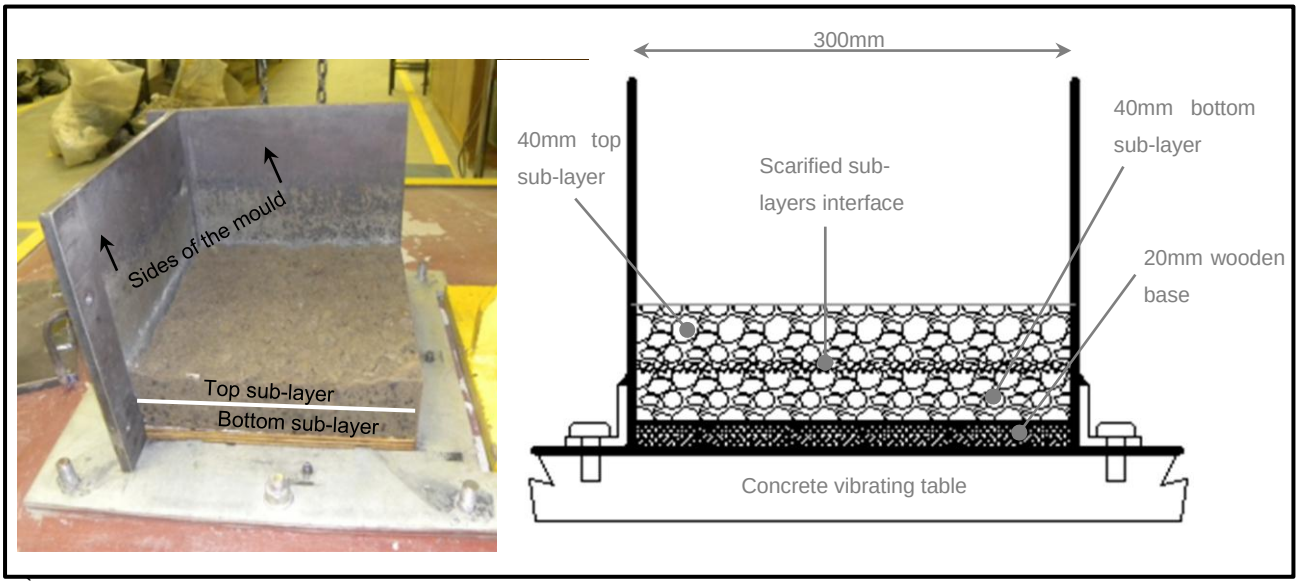

Figure 4-10: Illustration of CTSB compaction details

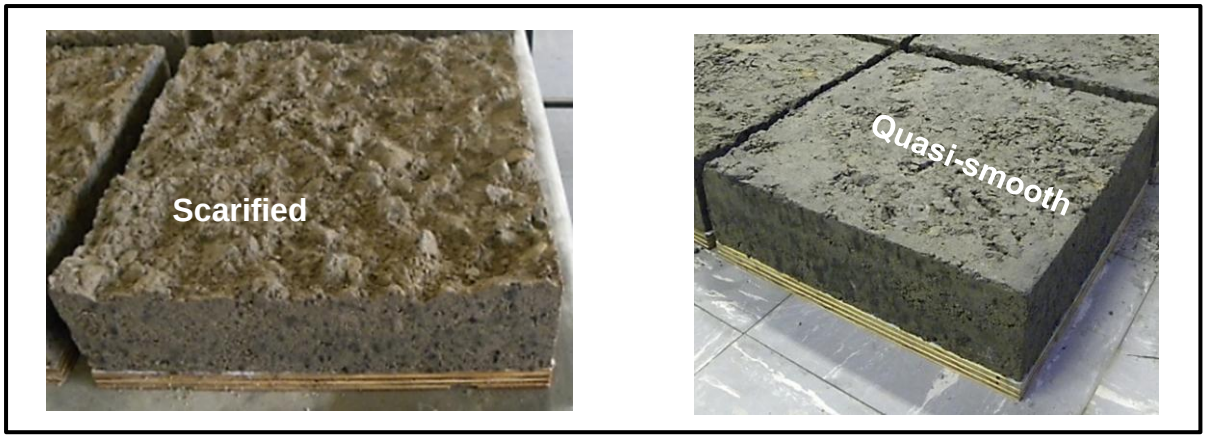

Figure 4-11: Photograph of CTSB surface roughness before casting the granular base

4.3.1.2. Curing of the CTSB and Compaction of the GB

The required strength of the cement stabilized material is achieved through hydration processes which involve the combination of water, soil and cement. At the end of compaction, the material's moisture content is not enough to accomplish the hydration process, therefore additional water is required. This is accomplished through a curing process.

In this study, the curing practice involved keeping the CTSB specimen under a wet blanket and spray water for four days prior to laying the GB materials. Practically, this simulated what is normally done in the field whereby, after compaction of the CTSB layer, it is kept damp for up to seven days by frequent surface watering or by covering it with another pavement layer. It has been reported that premature drying prevents the development of strong cementitious bonding and enhances shrinkage cracking (TRH 13, 1986; Jenkins, 2013). Figure 4-12 shows the specimens during the curing process.

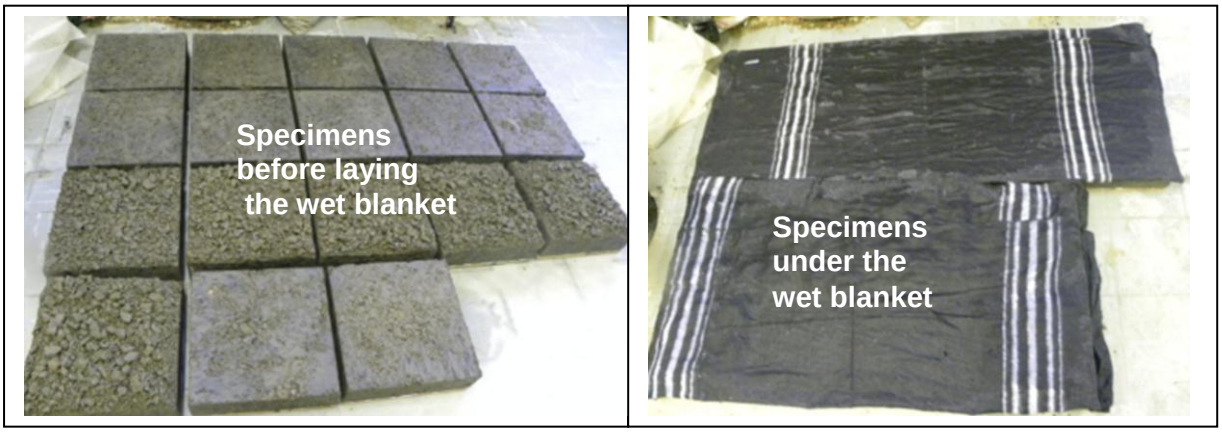

Figure 4-12: Illustration of the curing process

Mixing and compaction of the G2 granular base was done in a similar way as the cemented G5 subbase. Computed quantities of G2 fractions were weighed and mixed with a calculated amount of water required to achieve the optimum moisture content. The standard laboratory vertical shaft mixer shown in Figure 4-7 was used for mixing. When the required consistency was achieved, the materials were immediately sealed in a plastic bag to prevent evaporation and were allowed to stand for half an hour before compaction so that the moisture may become evenly distributed.

When the material was ready for compaction, four sides of the compaction mould were set around the CTSB layer and firmly fastened with bolts and nuts. To enhance specimen uniformity, the entire GB layer was compacted into two identical sub-layers with proper scarification between them as well. Since the layer was 90 mm high, two more levels were marked on the supporting column to identify the accurate compaction height of the layer. Therefore, from the 0 mm reference mark, 125 mm and 170 mm were properly marked to represent the top of the first and second sub-layers respectively (see Figure 4-8).

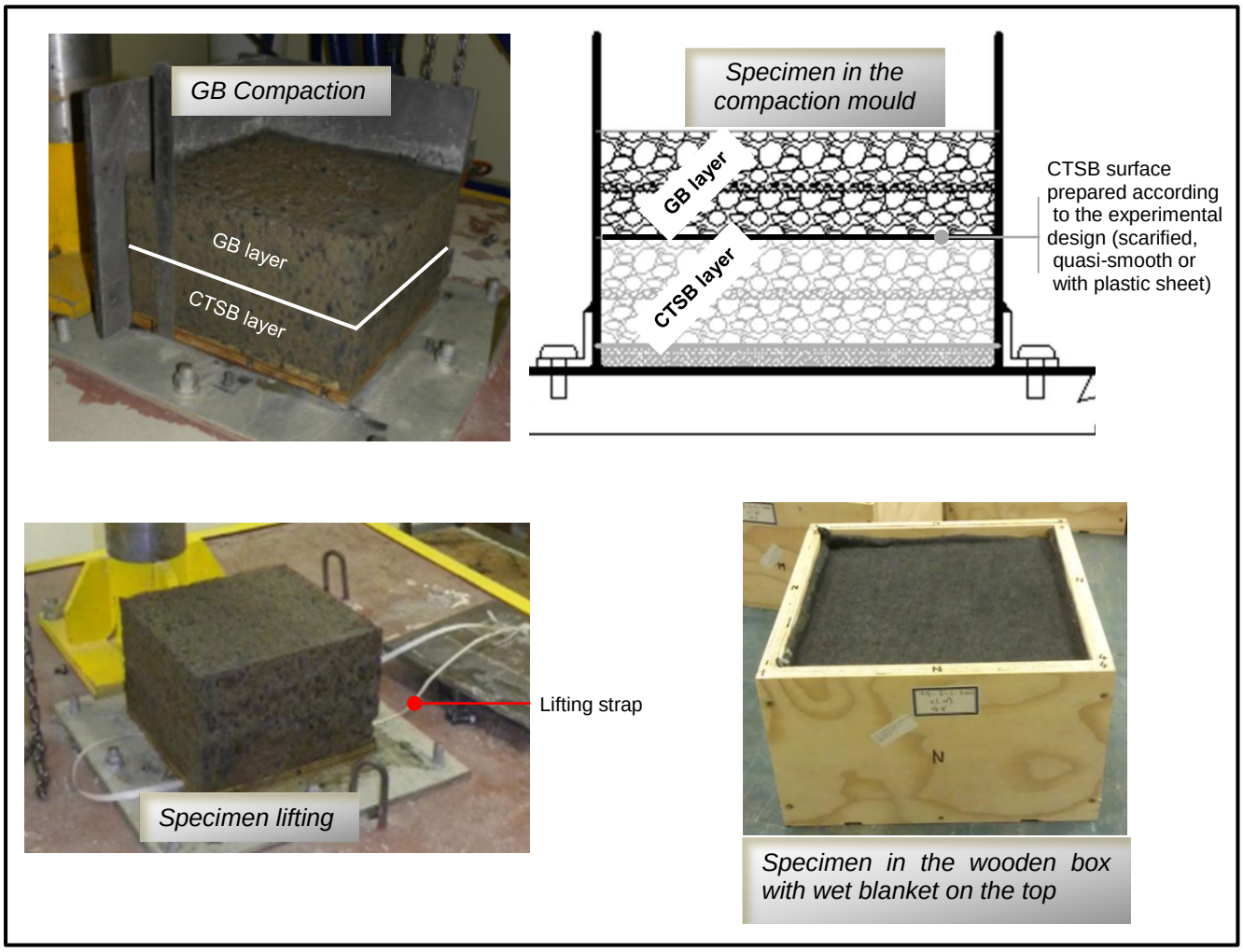

Figure 4-13: Illustration of sample preparation and handling process

After compaction of the GB on top of the CTSB layer, the full specimen was taken out of the mould and carefully confined in a wooden box for transportation purposes. Thereafter, it was kept at a temperature of 25^0C for a period of three more days before testing. This was done to complete 7 days curing time of CTSB recommended by the literature (TRH 13, 1986, Jenkins, 2013) and to allow homogeneous moisture distribution in the GB. Normally, the laboratory 7 days curing process involves keeping the specimen in a sealed plastic bag but the approach used in this study was selected to simulate the field practice and to facilitate transport and handling of the samples. Figure 4-13 shows the sample preparation and handling process.

4.3.2. INTERLAYER SHEAR TESTING

The automated direct shear machine named: Shear Trac-III system, was used in this research to investigate the interlayer shear behaviour. The machine is based in the geotechnical laboratory of the University of Cape Town (UCT).

The Shear Trac-III system was designed to test the shear strength of the soil and interface shear strength between soil and geosynthetics. However, if the specimen is properly prepared and accurately fitted in the shear box, the machine can also test the interlayer shear strength of the pavement layers, but difficulties related to specimen preparation and set up prevents the use of the machine as a routine testing method. It is rather recommended for research projects which normally allow extended time.

Even if static loading of the direct shear test does not accurately simulate horizontal dynamic loading of the pavement structure, the test was identified as the most reliable for characterization of interlayer shear strength as previously mentioned in Chapter 3. In comparison with other shear devices used for interlayer shear testing, Shear Trac-III system has the following advantages:

- The size of the shear box allows the accommodation of materials with a big particle size,
- It provides fully automated testing, and
- It presents the possibility to apply normal load which simulates the vertical component of the traffic loading.

4.3.2.1. General Configuration of the Shear Trac-III System

Figure 4-14 contains a photograph of the Shear Trac-III system. The system consists of a Shear Trac-III load frame and computer system, equipped with a network card and software called SHEAR, which is used to control the test and create a report of the results.

The Shear Trac-III load frame consisted of:

- A water bath box which holds the shear box, maintains water around the specimen for saturated tests and moves horizontally during the shear phase of the test;
- A shear box for holding the sample,
- Two high precision micro stepper motors that control the loading mechanism for horizontal and vertical load,
- Sensors for measuring loads and displacements, and
- Two embedded controllers for test control and data acquisition (Geocomp, 2012).

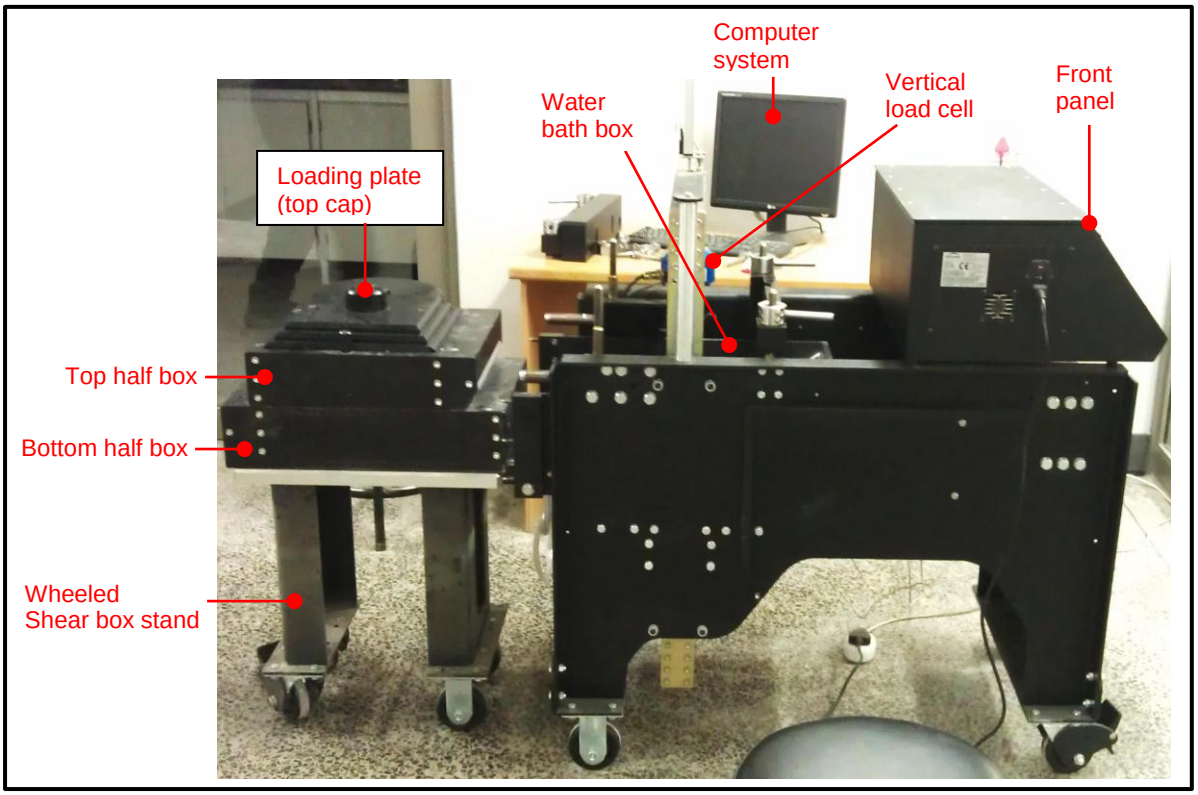

Figure 4-14: Photograph of Shear Trac-III

The SHEAR software contained menus and property pages that were used to define different testing conditions. Specific information for the sample could be inserted for inclusion on the tabulated or graphed results (Geocomp, 2012).

4.3.2.2. Specimen Setup in the Shear Testing Machine

Various trials were attempted to determine the fit-for-purpose technique to be adopted for setting up the specimen in the shear box. Figure 4-15 illustrates the most appropriate process which was used for this study.

The process involved six consecutive steps:

1. Once the sample was ready for testing, four sides of the wooden box were unscrewed and removed. The bottom wooden plate was grooved to accommodate two 500µm thick lifting straps. Hence a pair of straps was slipped in and fastened with suitable buckles,
2. Since the specimen was quite heavy, it was first lifted up and carefully kept on the stool prior to be inserted in the shear box,
3. The shear box was made with 2 mm allowance on each side. This made easy to slide in the 300 mm x 300 mm specimen by means of the 500 µm thick strap. The bottom and top halves of the shear box remained aligned and fixed with alignment screws,
4. When the specimen was firmly placed in the shear box, the lifting straps were removed, the loading plate was placed and the wheeled shear box stand was carefully pushed to the Shear Trac-III load frame,
5. After lining up the front of the shear box with the water bath, it was carefully slid in,
6. Finally, when the shear box was properly mounted inside the Shear Trac-III housing, all set up accessories, including the top box end, the front container panel, the flange nuts and the cross beam, were fixed.

Extra care was devoted to the specimen preparation process and set up to accurately align the shear plane with the interface between CTSB and GB. The shear plane was at the level of 100 mm from the inner bottom of the box. However, few specimens were found with the interlayer plane located at 1 to 6 mm less due to over compaction of the CTSB or material trimming out by the scarification process. In that case, steel spacer plates were laid below the specimen to raise the height up to the required level. On the other hand, specimens with interlayer height above 100 mm were discarded.

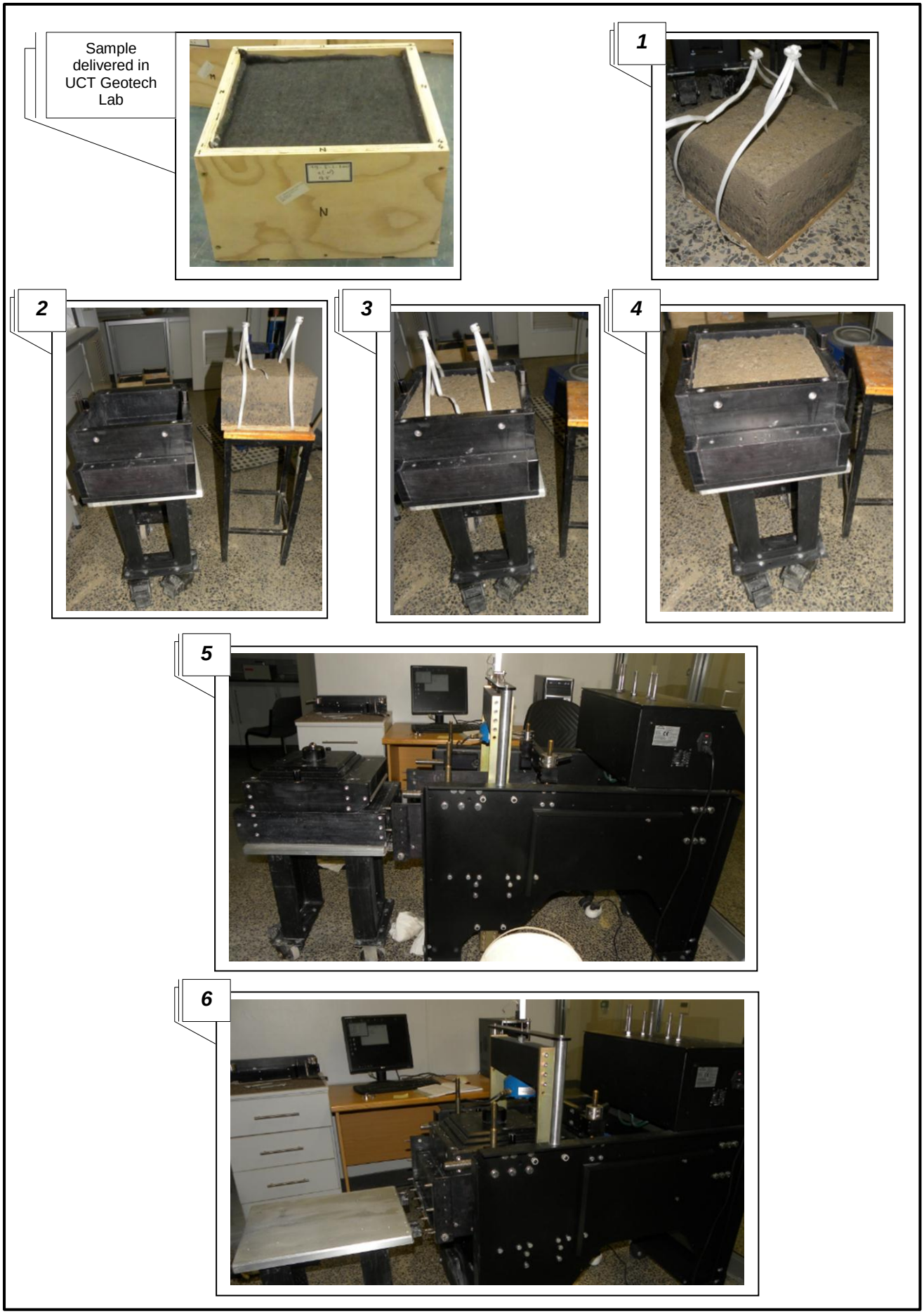

Figure 4-15: Photographic illustration of specimen set up in the Shear Trac-III load frame

4.3.2.3. Testing Procedure

According to the testing conditions, two types of tests were conducted: saturated and unsaturated testing.

During the saturated test, the specimen was allowed to stand in water for 40 minutes before testing. 40 minutes was admitted to allow total saturation of the interlayer between CTSB and GB. Additionally, before and during the test, the water level was kept at 25 mm above the shear plane to ensure saturation consistency between the two layers.

Prior to shearing the interface, a one directional consolidation phase was run to bring the specimen to the equilibrium state. Vertical displacement due to consolidation ranged between 0 and 4 mm for all tested samples. Since each specimen was adequately compacted and properly positioned in the shear box, slight movement due to consolidation pressure was localised at the top loading plate which did not affect the alignment between the shear plane and the specimen interlayer.

After the consolidation phase, a gap of 5 mm was created between the two half-boxes to eliminate any possibility of metal to metal friction.

The unsaturated tests were conducted in a similar way but the sample was not soaked in water before and during test.

Selection of the shear rate was based on previous studies. However, material type and sample size were also considered. According to the research done on interlayer shear testing with the application of normal pressure, the horizontal displacement rate ranged between 1.27 and 3 mm/min (Canestrari & Santagata, 2005; Canestrari *et al.,* 2005; D'Andrea *et al.,* 2013; D'Andrea & Tozzo, 2012; Uzan *et al.,* 1978). Note that all the above listed studies involved bituminous materials and relatively small devices comparing to the Shear Trac-III system.

With knowledge of the unbound behaviour of granular materials and the large size of the sample, the shear rate of 1 mm/min was decided on to provide detailed records for the unsaturated testing. For the saturated tests, the rate was reduced to 0.6 mm/min to allow for the total saturation of the interface as shearing proceeds.

For each level of test variables, a minimum of two tests was performed and the average values of the converged curves were studied. During each direct shear test, the measured parameters were the vertical and horizontal displacement and the horizontal stress. All parameters were recorded every 6 seconds corresponding to the horizontal displacement increment of 0.1 mm for unsaturated testing and 0.06 mm for saturated testing. This provided a detailed record of the results.

Chapter 5

TEST RESULTS AND DISCUSSION

5.1. INTRODUCTION

Test results, analyses and discussions are presented in this Chapter. The content includes material characterisation and direct shear tests results.

5.2. MATERIAL CHARACTERISATION TESTS RESULTS

5.2.1. SIEVE ANALYSIS

Figure 5-1 illustrates grading curves for G2 and G5 materials with 19 mm maximum aggregate size. According to the grading modulus (i.e. 2.4) and visual inspection, the G5 material was classified as coarsely graded and therefore qualified for road construction (SAPEM, 2013). On the other hand, grain size distribution curve of the G2 material fitted well in the recommended grading curve.

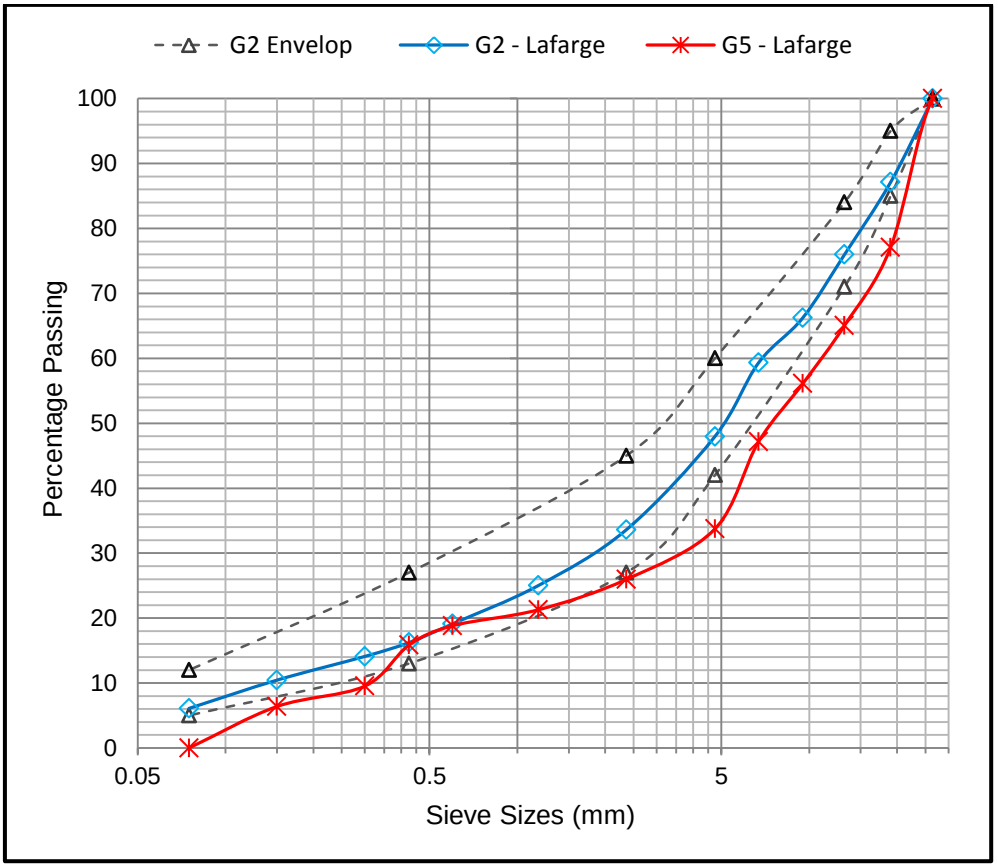

Figure 5-1: Wet Sieve analysis for G2 and G5 materials from Lafarge quarry

5.2.2. ATTERBERG LIMITS AND LINEAR SHRINKAGE

According to SAPEM (2013), if the material has a Linear Shrinkage (LS) below 0.5%, it is considered as “non-plastic” and if the LS ranges between 0.5% and 1%, the material is then considered as “slightly- plastic”. The bar linear shrinkage test on G2 and G5 materials confirmed their non-plasticity as they shrunk by 0.3 and 0.5% respectively.

The Atterberg Limits tests conducted on the material smaller than 0.425 mm showed that both G2 and G5 materials were non-plastic. The determination of the Plastic Limit was not achieved since the moist sample was cohesionless, which prevented the sample from being moulded into a ball.

Typically, a natural G5 material should possess some plasticity according to TRH 14 (1985). But, since the G5 collected from the commercial quarry was a blend of crushed stone and natural soil, it showed non-plastic behaviour; therefore did not require stabilisation. Nonetheless, the material was stabilised for the purpose of this research.

5.2.3. APPARENT AND BULK RELATIVE DENSITY (ARD AND BRD) AND WATER ABSORPTION

Table 5-1 illustrates the results of the bulk relative density, apparent relative density and water absorption of the G2 and G5 materials retained on a 4.75 mm sieve. From the results, it can be observed that G2 material exhibits a high density compared to G5 material. Both materials have shown negligible water absorption behaviour.

Table 5-1: BRD, ARD and water absorption for G2 and G5 materials retained on a 4.75 mm sieve.

	G2	G5
BRD	2.524	2.328
ARD	2.734	2.705
Water absorption (%)	0.0	0.1

5.2.4. MODIFIED AASHTO COMPACTION

The results of Mod AASHTO compaction are presented in Table 5-2. The maximum dry density (MDD) and optimum moisture content (OMC) for G2, G5 and cemented G5 are shown.

Generally, the addition of cement to the soil leads to the increase of fines, which in turn, increases the water absorption property of the material. Additionally, the hydration process during modification and cementation reactions increase the amount of water required to

bring the material at its densest state. Therefore, all these parameters could have been resulted in the decrease of MDD and the increase of OMC of the cemented G5.

From the results shown in Table 5-2, the MDDs of G2 and G5 are approximately equal. This can be explained by the quality of G5 materials as discussed in Section 5.2.2. The MDD of cemented G5 was less than that of natural G5 as was expected, but it was achieved at the same moisture content. The amount of cement added and the type of G5 material explain this behaviour. Figure 5-2 shows a typical compaction curve obtained on G5 material.

Table 5-2: Mod AASHTO test results for research materials

Material type	MDD (kg/m^3)	OMC (%)
G2	2332	5.4
G5	2349	5.2
Cemented G5	2301	5.2

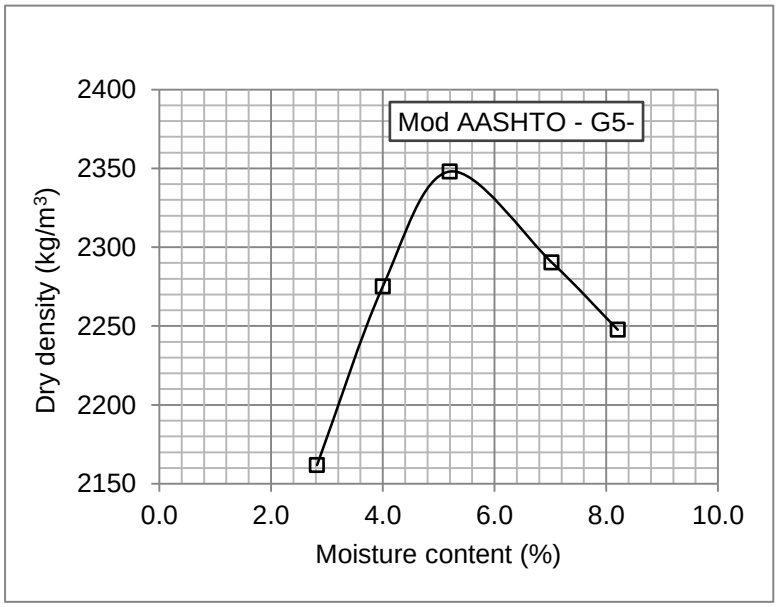

Figure 5-2 : Typical compaction curve

5.2.5. SOAKED CBR

The results of California Bearing Ratio test for G5 materials are presented in Table 5-3. The CBR values at 2.5 mm penetration are presented against relative compaction density.

Table 5-3: CBR results for G5 materials

Relative Compaction (% Mod AASHTO)	CBR at 2.5 mm penetration (%)
100	72
95	65
90	62

According to SAPEM (2013), and TRH14 (1985) recommendations, the CBR value for a typical G5 material should not be less than 45% at 95% Mod AASHTO density. However, since a blended G5 material was used for this study, high penetration resistance was achieved as shown in Table 5-3. It is also important to mention that the material showed non-swelling behaviour.

5.2.6. FLAKINESS INDEX (FI)

Table 5-4 shows the results of FI tests conducted on two fractions of G2 materials as recommended by SAPEM (2013).

Table 5-4: Flakiness Indices for selected G2 fractions

Fraction size (mm)	Total Weigh (g)	Weight passing (g)	FI (%)
Passing 19, Retained 13.2	3500	475.7	13.6
Passing 26.5, Retained 19	4000	660.9	16.5

Particle shape is one of the parameters which have a direct effect on particle arrangement to achieve the highest density of the layer during the compaction procedure. It also influences the strength and durability of the compacted layer. In fact, flat and/or elongated particles are susceptible to breakage when a load is applied perpendicular to the flat side. When this happens over and over, it increases the fine content and decreases the resilient behaviour of the granular materials.

According to TRH14 (1985) recommendations for the G2 material, the FI determined on -19 mm, +13.2 mm and -26.5 mm +19 mm fractions should not exceed 35%. The results of both fractions as presented in Table 5-4 fall well below this value, therefore the material qualifies for the base course.

5.2.7. AGGREGATE CRUSHING VALUE, ACV (DRY AND WET)

The results of ACV tests for wet and dry materials are presented in Table 5-5.

Table 5-5: ACV test result for wet and dry G2 materials

	10% FACT (kN)	ACV (%)
Dry	454	8.8
Wet	415	9.6
Wet/Dry ratio %	91	

From the results shown in Table 5-5; the G2 materials showed a high resistance to crushing comparing with the recommended values presented in Table 5-6. This is justified by the unweathered state of the hornfels parent rock. The wet/dry ratio is also far greater than the recommended value (see Table 5-6). This shows high durability of the material.

5.2.8. UNCONFINED COMPRESSIVE STRENGTH (UCS) AND INDIRECT TENSILE STRENGTH (ITS)

For the purpose of this study, the UCS and ITS tests were only used for the selection of optimum stabilizer content. Figure 5-3 illustrates the UCS and ITS test results.

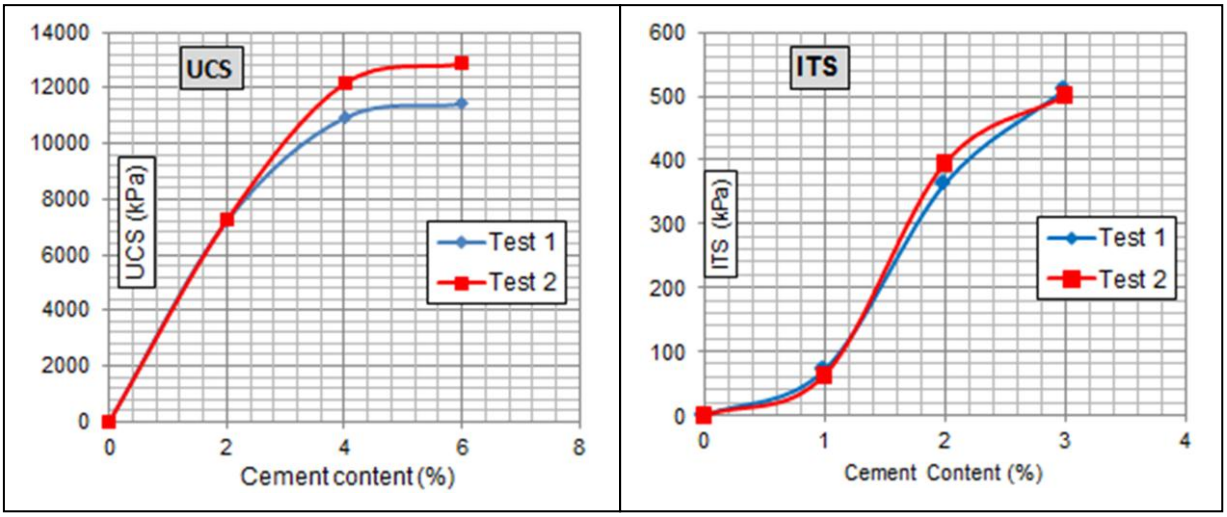

Figure 5-3: 7days UCS and ITS tests results

Among the four standard categories of cement stabilised materials used in South African pavement structures as mentioned in Chapter 2, C3 was selected for this study. This selection was based on the TRH14 (1985) recommendation for subbase materials. Recommended values for C3, according to TRH14 (1985) are 1500 to 3000 kPa for UCS and ITS not less than 250 kPa. However, since the G5 parent material used was a blend of crushed stone and natural gravel, the sample had a high compressive strength even at relatively low cement content as shown in Figure 5-3. Therefore, the tensile criteria were adopted to select the appropriate cement content. Practically, the higher the cement content in the layer, the more brittle the layer will be and will consequently be more susceptible to cracking. From the ITS results shown in Figure 5-3, 1.8% cement was selected to be the most suitable. This corresponds to approximately 320kPa ITS and 6700kPa UCS.

From the results of extensive tests conducted on the research materials as summarised in Table 5-6, it should be concluded that both G2 and G5 materials used for this study met all necessary requirements for road construction materials. However, it is worth mentioning that the blended G5 showed high strength compared to the normal G5 materials. But for the purpose of this study, it was used as it is.

The summary of test results shown in Table 5-6 presents also the recommended values for a specific test and the reference guideline document.

Table 5-6: Summary of material characterisation tests and the comparison with the recommended values

TEST	GUIDELINE DOCUMENT	RECOMMENDED VALUES		CURRENT VALUES		COMMENTS
		G2	G5/CTM*	G2	G5/CTM	
Grading	SAPEM 2013, TRH14	G2 envelope	GM>1.5	Within the envelope	GM=2.4	Requirements satisfied
Atterberg Limits	SAPEM 2013, TRH14	LL(Max) = 25 PI(Max) = 6 LS(Max) = 3%	LL(Max) = 30 PI(Max) = 10 LS(Max) = 5%	Material not plastic, LS = 0.3%	Material not plastic, LS = 0.5%	Material not plastic
ARD and BRD And Water absorption	SAPEM 2013	Not Applicable	Not Applicable	ARD = 2.734 BRD = 2.524 WA = 0.0%	ARD = 2.328 BRD = 2.705 WA = 0.1%	Good quality materials.
Mod AASHTO	SAPEM 2013, TRH14	Not Applicable	Not Applicable	MDD = 2332kg/m^3 OMC = 5.4%	MDD = 2349kg/m^3 (G5),2301 kg/m^3 (CTM) OMC =5.2%(G5&CTM),	High density of G5 material due to crushed stone content
Soaked CBR	SAPEM 2013	Not Applicable	CBR at 95%>45% Swell at 100%<0.5%	Not Applicable	CBR at 95% = 65% Swell at 100% = 0.0%	Requirements satisfied
Flakiness Index	SAPEM 2013, TRH14	FI for -19;+13.2 < 35% FI for -26.5;+19 < 35%	Not Required	FI for -19;+13.2 = 13.6% FI for -26.5;+19 = 16.5%	Not Required	Requirements satisfied
ACV and 10%FACT (Wet &Dry)	SAPEM 2013, TRH14	ACV :-Dry <29% -Wet < 29% 10%FACT:-Dry >110kN -Wet>110kN ACV Ratio (wet/dry) > 75%,	Not Required	ACV :-Dry = 9.6% -Wet = 8.8% 10%FACT:-Dry= 454kN -Wet = 415kN ACV Ratio (wet/dry) = 91%,	Not Required	Requirements satisfied
UCS	SAPEM 2013, TRH14	Not Applicable	1.5MPa<UCS<3MPa (only for CTM)	Not Applicable	UCS = 6.7MPa (CTM)	Since blended G5 was used, UCS is high but ITS is satisfactory
ITS	SAPEM 2013, TRH14	Not Applicable	ITS > 250kPa	Not Applicable	ITS = 320kPa	

*Cement Treated Material

5.3. DIRECT SHEAR TEST RESULTS

Three parameters were recorded and analysed during the direct shear investigation. These included shear loads required to mobilise the bottom half of the shear box to failure, the relative horizontal displacement, and the vertical displacement of the specimen due to dilation of the sample.

5.3.1. SHEAR STRESS – HORIZONTAL DISPLACEMENT RELATIONSHIP

5.3.1.1. Interlayer Testing

Figure 5-4 illustrates the relationship between shear stress and horizontal displacement for interlayer shear tests. Each of the tests was conducted at three normal pressures: 50, 100 and 200 kPa. However, the 200 kPa was reduced to 150 kPa for the scarified – unsaturated condition since the associated maximum shear stress was beyond the capacity of the loading cell.

The general observation from the shear test results shown in Figure 5-4 is that, the maximum shear stress increased with the increase of the normal pressure as it was expected. Moreover, it decreased as the interlayer gets saturated.

In Figure 5-4(a) (b) and (d), the relationship between interlayer shear stress and horizontal displacement for different CTSB surface conditions and normal pressures is represented. At constant normal pressure and unsaturated moisture condition, the interlayer shear resistance reached the highest value when the CTSB layer was scarified. For instance, at 100kPa normal pressure, the interlayer shear resistance was reduced from 299.7kPa to 191.7kPa due to laying the GB layer without scarifying the top surface of the CTSB. This is a 36% reduction. Likewise, more reduction of interlayer strength was recorded when intimate contact between two layers were interrupted by a thin plastic sheeting. This testing condition yields 94.2kPa at the same normal pressure. This represents a 69% reduction. In practical terms, this does not represent realistic conditions but it gives insight into the impact of intimate interaction upon shear resistance.

General trends of shear strength within the investigated zone are also presented in Figure 5-5 and the summary of the interlayer direct shear test results is presented in Table 5-7.

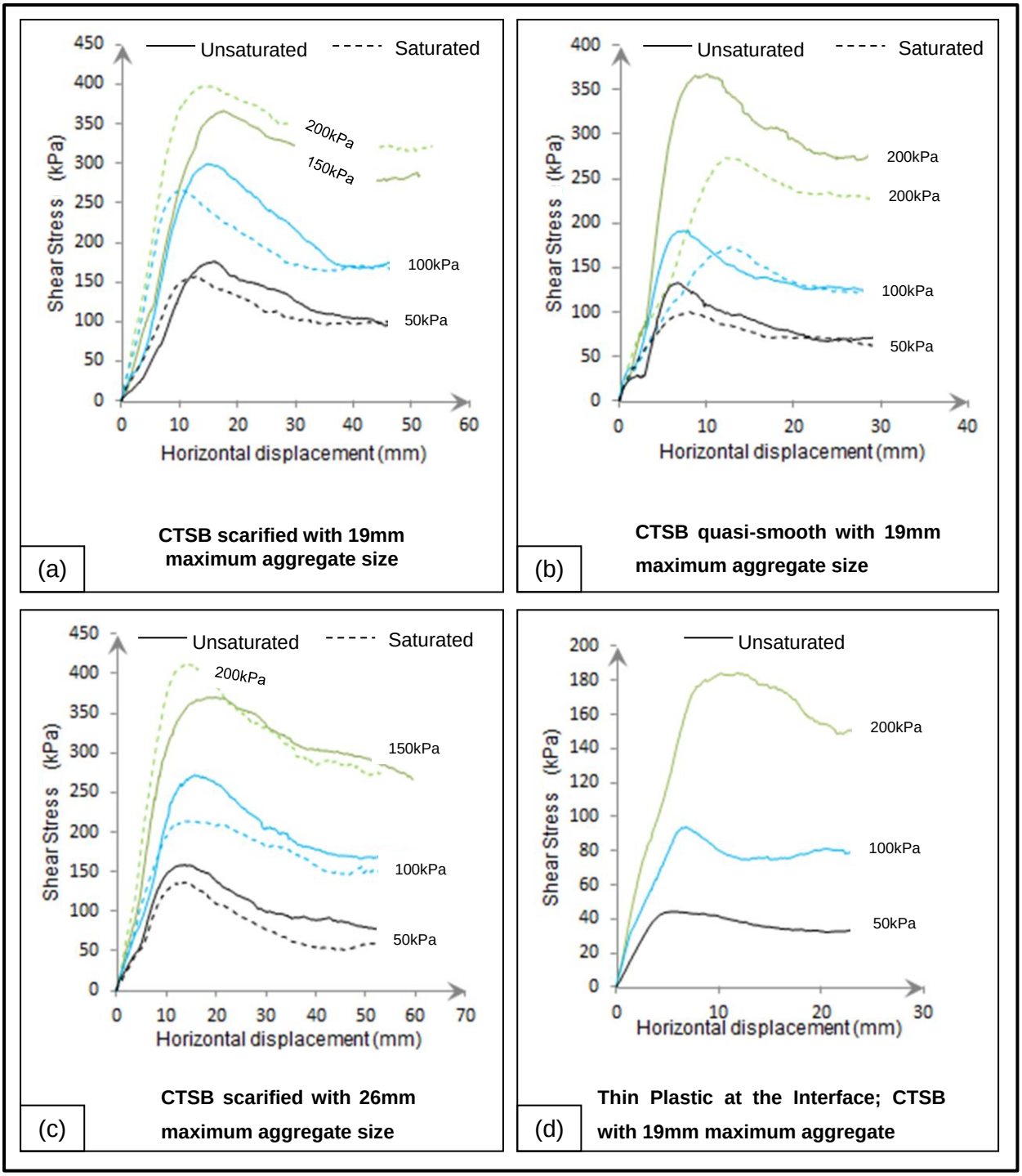

Figure 5-4: Shear stress versus horizontal displacement for interlayer tests

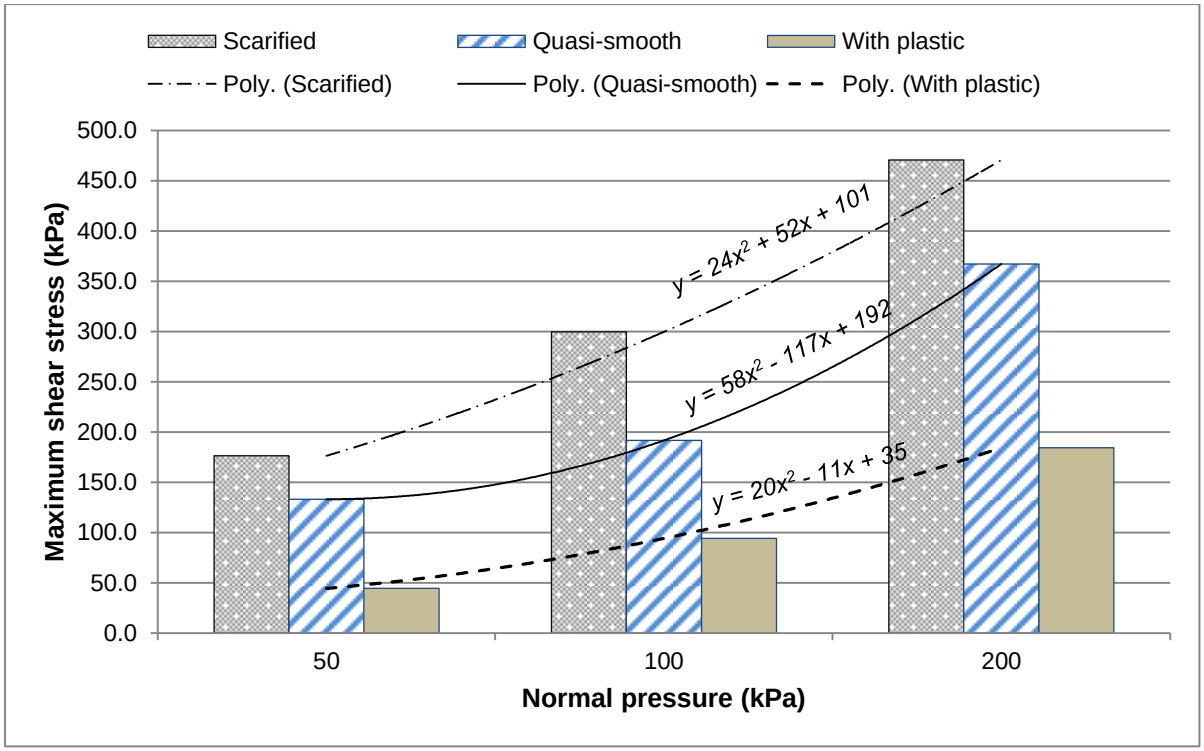

Figure 5-5: The effect of the normal pressure and CTSB surface condition on the interlayer shear stress

For the purpose of understanding the practice of scarification and how this influences the resistance against horizontal movement between two layers, the *"saw tooth model"* might provide more clarification.

Scarification of the CTSB layer after compaction creates a rough and ridged surface which is characterised by projecting aggregates on the top. During the cementation process, the overhanging aggregate particles develop strength and resistance against overturning. At the time of laying a granular base layer, free aggregate particles of the layer fill up valleys of the rigid CTSB and create a so called *"saw tooth"* interaction. In that condition, the resistance against horizontal movement of one layer relative to another is reinforced by overhanging rigid aggregate particles of the CTSB which root deeper in the layer. Moreover, other various parameters enhance shear resistance, namely the compaction practice of the GB, moisture content and working stress conditions.

The impact of the maximum aggregate size in the CTSB layer can be realised by comparing the shear results for a CTSB with 19 and 26 mm as maximum aggregate sizes as shown in Figure 5-4(a) and (c) respectively. At 50 and 100kPa, a slight reduction in the maximum shear stress was recorded when the maximum size of aggregate in the CTSB was changed from 19 mm to 26 mm. Friction theory was used to analyse and discuss the shear behaviour and more details are provided in Section 5.3.2.

Table 5-7: Summary of the achieved shear stress and associated horizontal displacement for the interlayer direct shear test.

Maximum Size of Aggregate in CTSB (mm)	CTSB surface condition	Testing moisture condition	Average compaction degree (%Mod AASHTO)		Normal stress (kPa)	Maximum shear stress (kPa)	Horizontal displacement at failure (mm)
			CTSB	GB			
19	Quasi-smooth	Unsaturated	99.3	100.1	50	133.1	6.8
			98.6	99.8	100	191.7	7.3
			99.9	100.3	200	367.2	10.2
		Saturated	98.9	99.7	50	100.3	8.0
			100.3	100.1	100	173.0	12.7
			100.1	100.2	200	273.6	12.2
	Scarified	Unsaturated	100.0	99.4	50	176.4	16.0
			99.9	98.5	100	299.7	15.0
			99.1	99.6	150	366.7	17.6
		Saturated	98.7	99.6	50	157.7	12.8
			99.1	98.6	100	267.1	10.2
			99.7	98.5	200	397.8	15.3
	Lined with thin plastic sheet	Unsaturated	100.9	101.2	50	44.4	5.5
			100.5	100.4	100	94.2	6.8
			100.7	100.3	200	184.3	11.8
26	Scarified	Unsaturated	99.9	99.1	50	158.9	13.7
			99.6	99.5	100	272.5	15.6
			99.7	99.3	150	370.2	20.1
		Saturated	99.5	99.5	50	136.8	13.5
			100.1	98.9	100	214.4	13.6
			100.0	99.4	200	413.0	14.2

5.3.1.2. Inlayer Testing

The relationship between shear strength and horizontal displacement for the inlayer shear tests of the CTSB and GB is presented in Figure 5-6(a) and (b) respectively. Each diagram shows the results of the saturated and unsaturated condition for 25, 50 and 100kPa normal pressure.

The relationship between shear stress and displacement of lightly cemented material (CTSB) is shown in Figure 5-6(a) whereby the solid and dashed lines present the unsaturated and saturated shear responses respectively. Contrary to the previous cases, the saturated and unsaturated trends are closer for a specific normal pressure. This demonstrates lack of saturation of the specimen prior to and during testing.

Additionally, the stress response of the cemented materials shows a rapid increase in the shear stress, followed by an immediate decrease after reaching the peak. This manifests the brittle behaviour of the materials in spite of its high stress at failure.

Figure 5-6(b) shows the shear stress- displacement behaviour of the granular material (GB) when the shear plane is located within the layer. Shear-displacement graphs show the increase in the maximum shear stress as the normal pressure increases. The saturated curves also show shear strength reduction due to water as might be expected.

Like other granular materials, shear stress-displacement graphs of the G2 inlayer shearing showed rough curves before the peak value was reached. This behaviour was influenced by the repeated process of build-up and collapse resistance to the horizontal movement, created by the interlock between the coarse and angular shaped granular material.

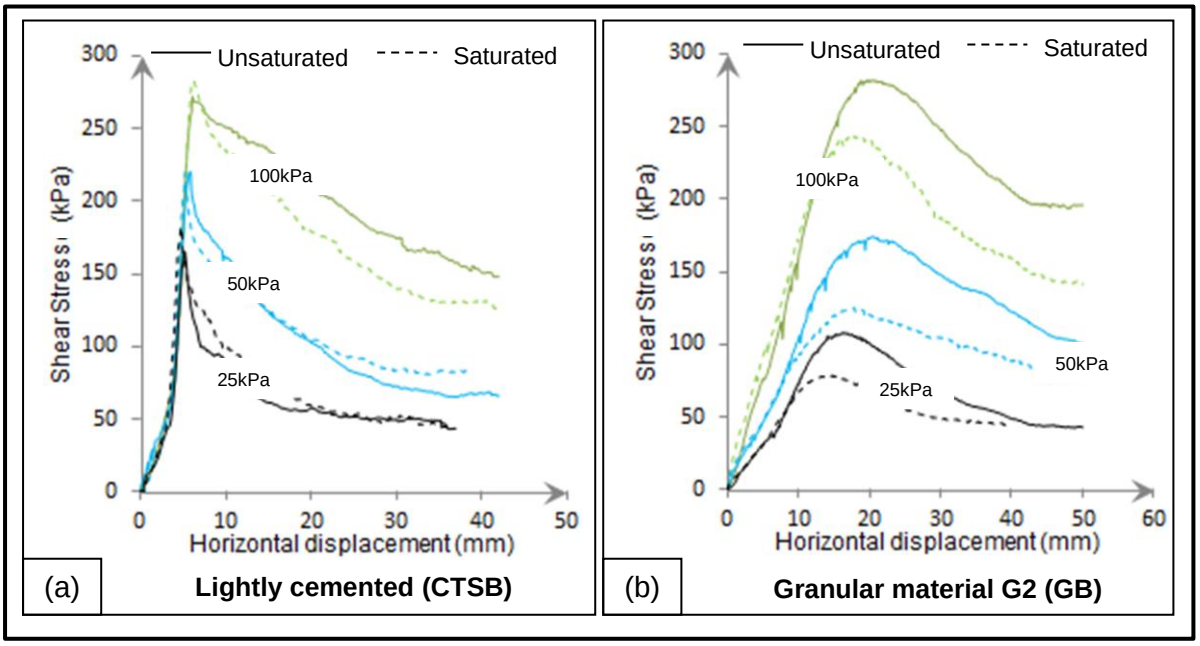

Figure 5-6: Shear stress versus horizontal displacement for inlayer tests with 19mm maximum aggregate

The tabulated summary of the inlayer test results for the CTSB and GB layers is presented in Table 5-8. The achieved shear stresses and related horizontal displacements are computed for different test variables as provided in the experimental design. The column of the achieved compaction degree in terms of percentage Mod AASHTO is also shown for CTSB and GB layers.

Table 5-8: Summary of shear stress-horizontal displacement results for the inlayer tests

Layer	Testing Moisture Condition	Average Compaction Degree (%Mod AASHTO)		Normal Stress (kPa)	Maximum Shear Stress (kPa)	Horizontal Displacement at Failure (mm)
		GB	CTSB			
GB	Unsaturated	100.5	Not Applicable	25	108.0	16.2
		100.4		50	174.2	20.5
		100.7		100	281.9	19.8
	Saturated	100.6		25	78.3	14.8
		100.7		50	125.2	17.8
		100.6		100	243.7	18.4
CTSB	Unsaturated	Not Applicable	101.0	25	165.4	5.2
			100.3	50	220.3	5.8
			100.9	100	271.9	6.1
	Saturated		100.7	25	182.0	4.9
			100.7	50	219.7	5.3
			100.5	100	283.1	6.2

5.3.2. SHEAR STRESS – NORMAL PRESSURE RELATIONSHIP FOR INTERLAYER AND INLAYER TESTS

This section describes the relationship between maximum shear stress and applied normal pressure.

For each testing variable, the maximum shear stresses were deduced from the graphs in Figure 5-4 (interlayer testing) and Figure 5-6 (inlayer testing), and plotted against their respective normal pressures. The best straight line fitted through three respective points corresponding to three normal pressures defined the Mohr-Coulomb failure envelope. Therefore, the tangent of their inclination angles defines the interlayer friction coefficient -μ while the intercept on the vertical axis gives the interlayer cohesion -c.

Figure 5-7 and Figure 5-9 present the Mohr-Coulomb failure envelopes for the interlayer and inlayer shear tests respectively. Each graph illustrates the unsaturated (solid lines) and saturated (dashed lines) test results with their respective friction coefficients and cohesion. The indices “unsat” and “sat” on the cohesion and friction terms stand for unsaturated and saturated testing conditions respectively.

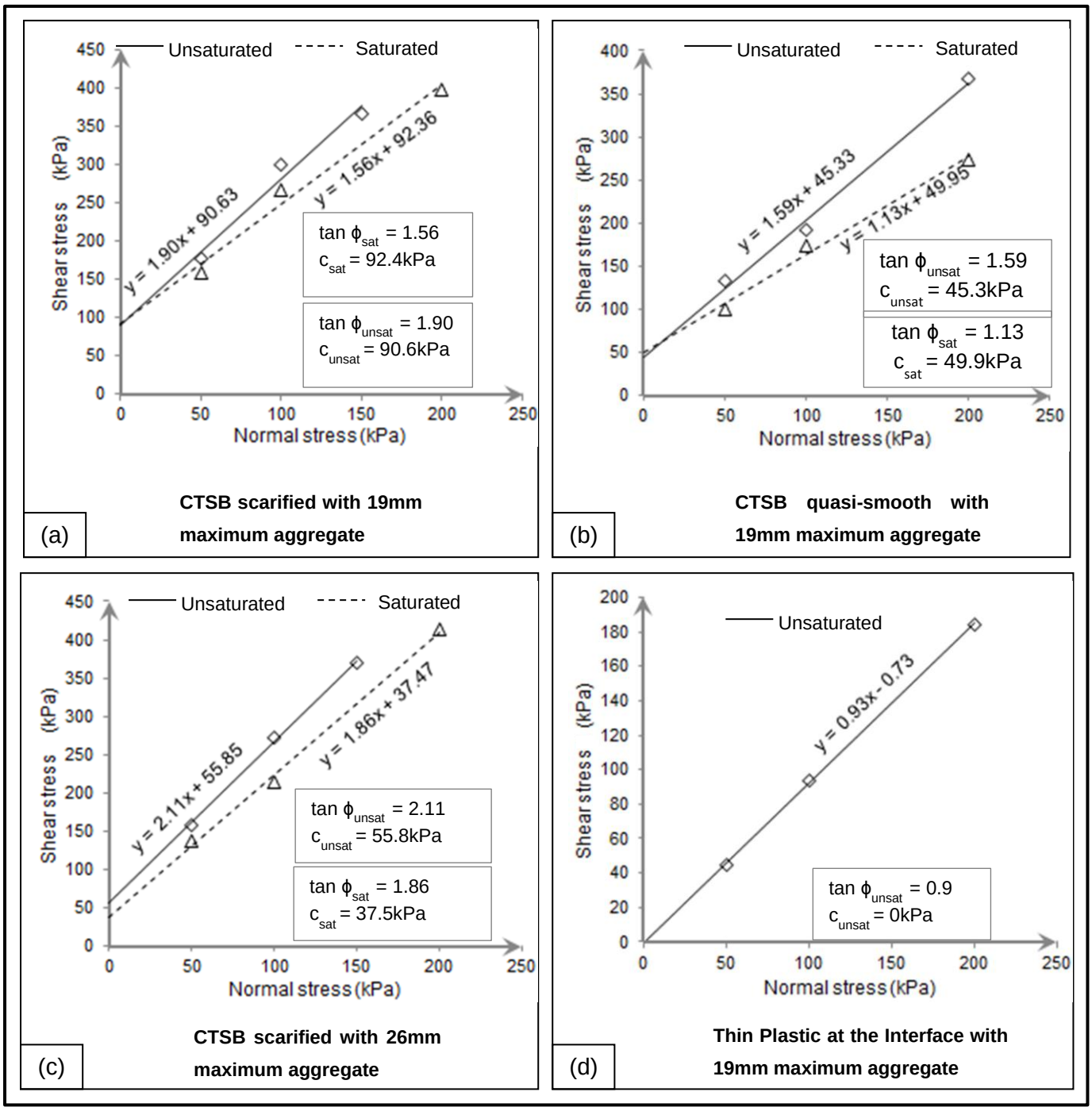

Figure 5-7: The Relationship between Shear Stress and Normal Stress for Interlayer Tests

Figure 5-7(a) and (b) show two graphs of the Mohr-Coulomb failure envelopes related to the interlayer shear tests when the CTSB layer was scarified before laying the GB and when it was quasi-smooth respectively. In both graphs, the trend lines for saturated and unsaturated tests converge to the same intercept on the vertical (shear stress) axis. This therefore, indicates the independency of the interlayer cohesion on the saturation condition as the normal pressure approaches zero. However, the water added during saturated testing, acted as lubricant throughout the shear phase. This caused the granular particles at the shear

plane to slide over one another quickly as shearing proceeded. The phenomenon resulted in the reduction in shear resistance which can be noticed in Figure 5-7(a) and (b) by the decrease of $\tan\phi$ coefficient.

In Figure 5-7(c) the shear stress-normal pressure relationship for 26 mm maximum aggregate in the CTSB is presented. It is worth to note the increase of shear resistance when the maximum aggregate size in the CTSB changes from 19 mm to 26 mm. This can be noticed by comparing the shear results in Figure 5-7(a) and (c).

In Figure 5-7(d) shear results for the most critical scenario are presented. It can be predicted that when there is no interaction between the CTSB and GB layers there is no cohesion between them. This is demonstrated by the failure line passing through the origin. It is important to realise that this case yielded the smallest $\tan\phi$ coefficient as was expected.

In Table 5-9 and Figure 5-8, the results of the interlayer friction and cohesion are summarized for different testing conditions. According to the results, the following observations were made:

- The CTSB surface conditions affected the interlayer friction coefficient. At unsaturated conditions, the value of $\tan\phi$ was reduced from 1.90 when the CTSB was scarified, to 1.59 for the case of quasi-smooth surface. This reduction represents roughly 16%. Moreover, the value of $\tan\phi$ reached 0.93 when the CTSB surface was lined with a thin plastic sheeting before laying the GB. This is equivalent to a 51% reduction.
- It seems apparent that there is no clear impact of moisture on the interlayer cohesion for 19 mm maximum size of aggregate in the CTSB layer. However, the added water induced the reduction of the friction coefficient from 1.90 to 1.56 for scarified CTSB and from 1.59 to 1.13 for non-scarified surface. These reductions represent approximately 18 and 29% respectively.
- An increase in the maximum aggregate size in the CTSB layer from 19 mm to 26 mm caused an increase in the interlayer friction coefficient from 1.90 to 2.11 which, corresponds to 11%, for the unsaturated condition and 1.56 to 1.86 or 19% for the saturated condition. Moreover, bigger size aggregates induced a reduction in the interlayer cohesion from 90.6kPa to 55.9kPa or 38% reduction for the unsaturated condition and 92.4kPa to 37.5kPa or 59% reduction for the saturated condition. This decrease can be explained by the general behaviour of the granular materials. In fact, the increase in maximum size of aggregate in the mix entailed the decrease of fines ratio and development of a coarse skeleton which has limited contact points. When such a type of mix is compacted and then scarified, the produced surface seems rougher and coarser compared to that of a material with a small size aggregate. Therefore, laying the

GB material on such a surface results in grain to grain contact which leaves open gaps between coarser particles. This therefore leads to an incoherent structure.

- A lack of intimate contact between CTSB and GB layers due to a smooth CTSB surface induced high reduction of the interlayer cohesion. A decrease from 90.6 to 45.3kPa was recorded for the unsaturated and 92.4 to 50kPa for the saturated conditions. These correspond to a 50% and 40% reduction respectively.

Table 5-9: Achieved interlayer friction and cohesion

Maximum aggregate size in CTSB (mm)	CTSB surface condition	Saturation condition	Label	Normal pressure (kPa)	μ=tan ϕ	ϕ (°)	c (kPa)
19	Scarified	Unsaturated	19-S-NS	50 100 200	1.90	62.2	90.6
		Saturated	19-S-S	50 100 200	1.56	57.3	92.4
	Quasi-smooth	Unsaturated	19-NS-NS	50 100 200	1.59	57.8	45.3
		Saturated	19-NS-S	50 100 200	1.13	48.5	50.0
	With plastic sheet	Unsaturated	19-WP-NS	50 100 200	0.93	42.9	0.7
26	Scarified	Unsaturated	26-S-NS	50 100 200	2.11	64.6	55.9
		Saturated	26-S-S	50 100 200	1.86	61.7	37.5

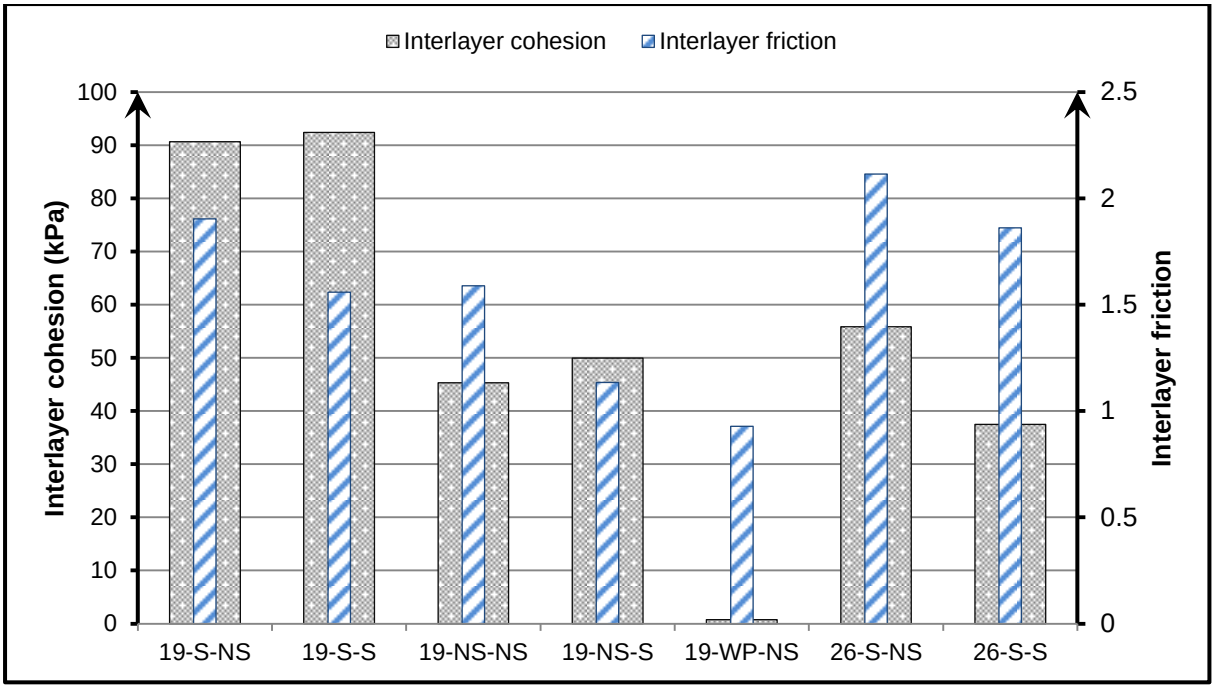

Figure 5-8: Impact of CTSB surface roughness, interface saturation and CTSB maximum aggregate on interlayer friction and cohesion

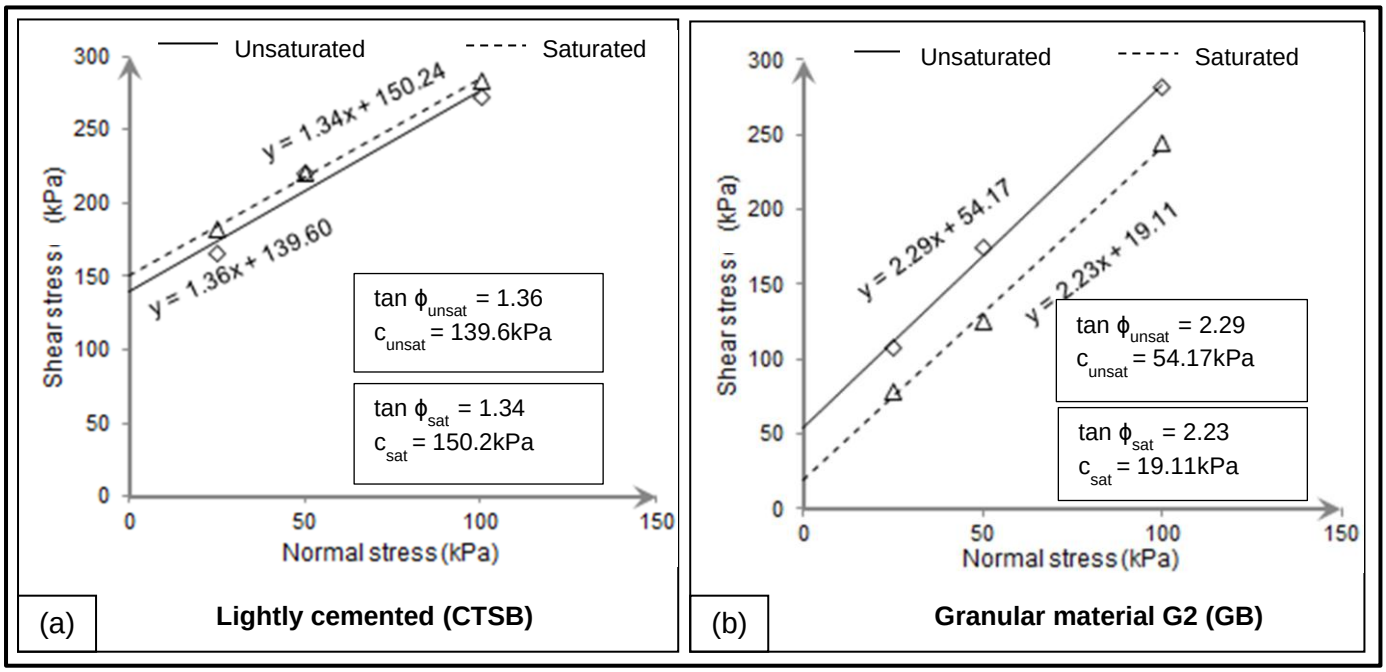

Figure 5-9: The Relationship between Shear and Normal Stresses for Inlayer Tests with 19mm aggregate size

Figure 5-9(a) and (b) presents the relationship between shear stress and normal pressure for the inlayer shear tests done separately on CTSB and GB materials in saturated and unsaturated conditions.

The results of the saturated and unsaturated failure envelopes of the CTSB layer presented in Figure 5-9(a) do not show a clear impact of water on the cohesion and friction resistance

for this particular case. This was induced by the short saturation time allowed. On the other hand, the results of the GB inlayer shear test presented in Figure 5-9(b) yielded a slightly higher friction resistance when compared to interlayer shear testing, either in saturated or unsaturated conditions, as was anticipated.

According to the results of the relationship between shear stress and normal pressure developed from the direct shear test, it seems evident that the interlayer friction resistance between the CTSB and GB layers is closer to the inlayer shear resistance of the GB when the top surface of the CTSB layer was scarified before laying the GB materials.

5.3.3. VERTICAL AND HORIZONTAL DISPLACEMENTS RELATIONSHIP

Trends in the recorded displacements throughout interlayer shear testing of the CTSB and GB layers are presented in Figure 5-10. For each set of testing parameters, the vertical displacement of the sample is plotted against the horizontal displacement of the bottom half of the shear box for both saturated and unsaturated testing conditions.

General trends show that the vertical movement of the sample during testing depends on the CTSB surface conditions and normal pressure. The scarified surface yielded high movement while the more confined samples dilated less.

In Figure 5-10, negative values of the vertical displacement indicate continuous expansion of the specimen during the shear process. However, at the critical state, shearing was done at constant volume.

5.3.3.1. Maximum Vertical Displacement

From Figure 5-10(a) and (c), it seems true that the marked volume change behaviour observed during the interlayer shear with scarified CTSB depends on the maximum size of aggregate in the CTSB, saturation condition and normal pressure. Table 5-10 summarizes the volume change behaviour of interlayer shear when the CTSB layer was scarified. A general trend is a decrease in vertical displacement as the normal pressure increases (Figure 5-11(a)). It also indicates the drop-off in volume change when the interface is saturated (Figure 5-11(a) and (b)). Moreover, the comparison of graph (a) and (b) in Figure 5-11 exhibits the bilateral increase of the vertical displacement when the maximum size of aggregate in the CTSB is changed from 19 mm to 26 mm.

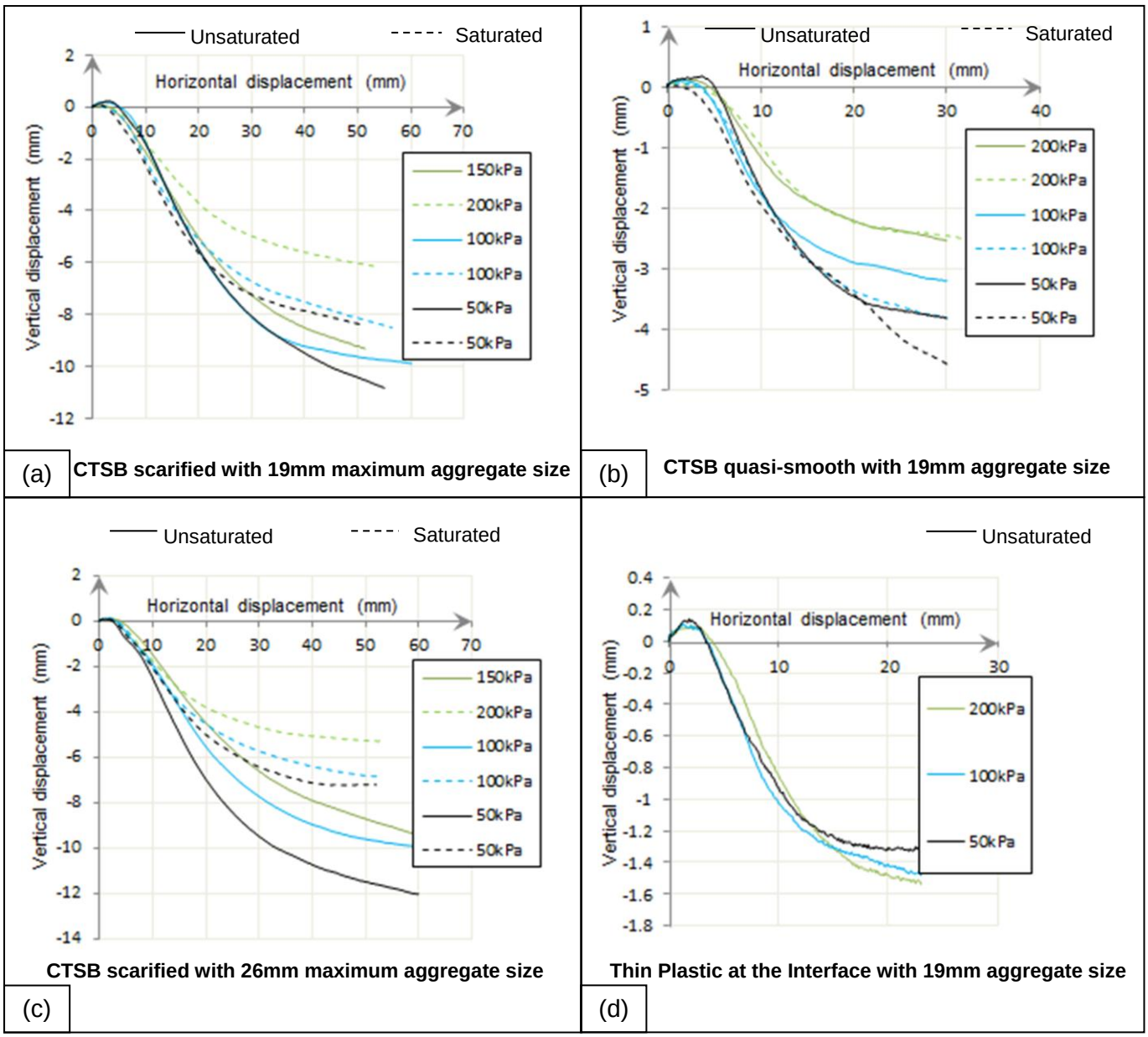

Figure 5-10: Dilatancy effect on CTSB and GB interlayer shear tests

Table 5-10: Dilatancy effect on interlayer shear for the scarified CTSB layer

Maximum size of aggregate in CTSB (mm)	Normal pressure (kPa)	Maximum vertical displacement (mm)	
		Saturated	Unsaturated
19	50	8.4	11.7
	100	8.5	9.9
	200(150*)	6.2	9.3
26	50	7.5	12.3
	100	6.9	10.4
	200(150*)	5.4	9.4

(*) Applied normal pressure for the unsaturated condition

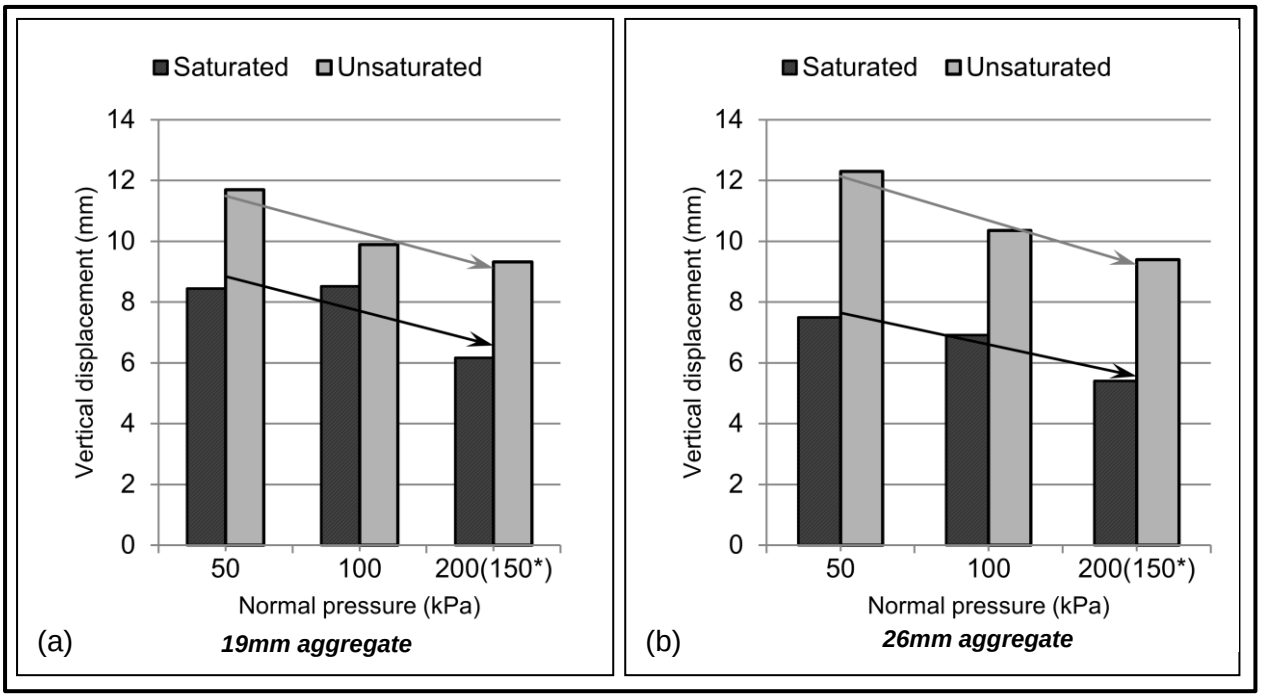

Figure 5-11: Influence of aggregate size, saturation condition and normal pressure on dilatancy of scarified CTSB layer

The above-mentioned interactions between the CTSB and GB layers are only discernable when the CTSB top surface is scarified. For the quasi-smooth surface, the maximum vertical displacement ranged between 2 and 4 mm (Figure 5-10(b)) and 1.2 to 1.6 for the interlayer shear with a thin plastic sheet at the interface (Figure 5-10(d)). In this case, the saturated conditions and normal pressure doesn't have a marked influence. This confirms the interaction between the CTSB and GB layers when the top surface of the CTSB is scarified. In addition, the interaction is more marked when the maximum size of aggregate in the CTSB layer increases.

5.3.3.2. Rate of Dilation and Dilation Angle

The rate of volume change required to mobilise the interlayer shear stress to a critical state was calculated from the respective interlayer shear responses (see Figure 5-10) and was plotted against the horizontal displacement (Appendix A.3). Maximum values of the dilation rate for the respective normal pressures were used to calculate the angle of dilation, in degrees, for each testing condition. Thereafter, the average dilation angles were presented in Table 5-11 and plotted in Figure 5-12.

Table 5-11: Dilation angle

Maximum size of aggregate in CTSB (mm)	CTSB surface condition	Saturation condition	Label	Average dilation angle (Ψ°)
19	Scarified	Unsaturated	19-S-NS	13.7
		Saturated	19-S-S	12.1
	Quasi-smooth	Unsaturated	19-NS-NS	6.5
		Saturated	19-NS-S	9.1
	With plastic	Unsaturated	19-WP-NS	4.5
26	Scarified	Unsaturated	26-S-NS	14.9
		Saturated	26-S-S	12.6

General trends indicated that the scarified CTSB layer produced the highest dilation angles, compared to the quasi-smooth surface. Shearing the interlayer while the top surface of the CTSB is lined with plastic sheeting provided the smallest dilation angle as shown in Table 5-11 and Figure 5-12.

According to the results shown in Table 5-11 and plotted in Figure 5-12, the followings were observed:

- The average angle of dilation was reduced by roughly 12% for the scarified CTSB layer containing 19 mm maximum aggregate size and approximately 15% for 26 mm maximum aggregate size due to the interlayer saturation during shear. This decrease was incited by the lubricant behaviour of the water at the interface between the CTSB and GB layers which softened the particle interlock, therefore resulting in straightaway particle sliding and rearrangement.
- Results of the unsaturated scarified interlayer shear test for 19 mm maximum aggregate in the CTSB offered 13.7^{O} average dilation angle while the one with 26 mm maximum aggregate yields 14.9^{O}. This increase of approximately 9% was induced by the increase in maximum aggregate size in the CTSB.
- Results of the unsaturated non-scarified interlayer shear test for 19 mm aggregate in the CTSB produced 6.5^{0} of average dilation angle while the scarified shear test, with the same aggregate size in the CTSB, produced 13.7^{0}. There was thus an approximate increase of 53% in the dilation angle due to scarification of the CTSB.
- The results of the non-scarified interlayer shear test with 19 mm aggregate size in the CTSB layer produced 6.5^{0} of average dilation angle while the scarified interlayer shear test with 26 mm maximum aggregate size produced 14.9^{0}. This makes the increase in

average dilation angle by 56% due to the increase in maximum aggregate size in the CTSB and surface scarification.

- The dilation angle can reduce up to 70% when the interaction between the CTSB and the GB is only characterised by simple friction without interlock as simulated by shearing with thin plastic at the interface.

All the above observations shed light on the intimate interaction between scarified CTSB layer and the GB due to particle interlock at the surface contact between the two layers.

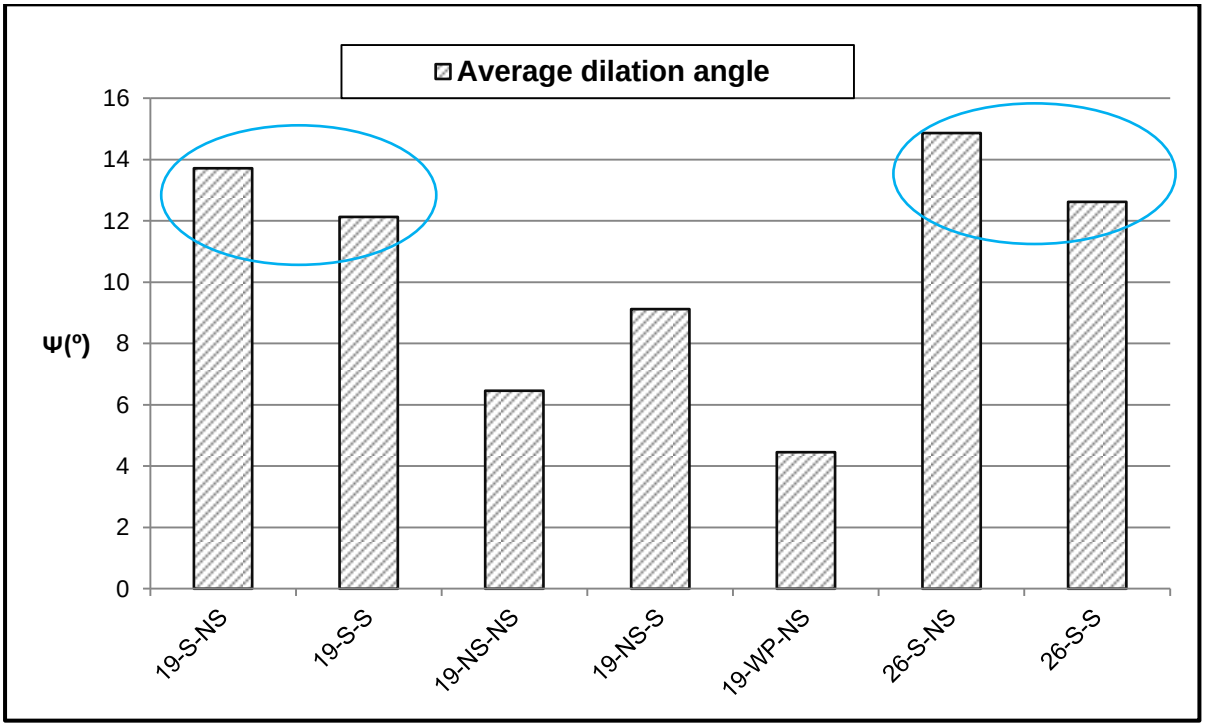

Figure 5-12: Influence of aggregate size, CTSB roughness and testing condition on dilation angle

5.3.4. COMPARATIVE ANALYSIS ON INTERLAYER AND INLAYER SHEAR PERFORMANCE

5.3.4.1. Shear Stress – Horizontal Displacement

i. Unsaturated Condition

In Table 5-12 and Figure 5-13, the results of the unsaturated inlayer and interlayer shear test are presented whereby maximum shear stress and relative horizontal displacement are tabulated and plotted according to different testing conditions. The maximum aggregate size in the CTSB for both inlayer and interlayer test was limited to 19 mm.

Table 5-12: Inlayer and interlayer shear results in terms of shear stress and horizontal displacement for the unsaturated condition

Type of shear test	CTSB surface condition	Normal pressure (kPa)	Label	Maximum shear stress (kPa)	Horizontal displacement to failure (mm)
Interlayer	Scarified	50	19-S-NS-50	176.4	16.0
		100	19-S-NS-100	299.7	15.0
	Quasi-smooth	50	19-NS-NS-50	133.1	6.8
		100	19-NS-NS-100	191.7	7.3
	With plastic	50	19-WP-NS-50	44.4	5.5
		100	19-WP-NS-100	94.2	6.8
Inlayer	Not applicable	50	19-G2-NS-50	174.2	20.5
		100	19-G2-NS-100	281.9	19.8
		50	19-C3-NS-50	220.3	5.8
		100	19-C3-NS-100	271.9	6.1

From the inlayer and interlayer test results shown in Figure 5-13 and Table 5-12, the prominent influence of the CTSB layer finishing on the interlayer shear resistance can be observed. When it comes to comparing the interlayer and inlayer shear resistance and the maximum displacement required to fully mobilise the shear stress, it was found that:

- The interlayer shear between the GB and scarified CTSB layer produced the maximum shear stress of 176.6kPa after 16 mm horizontal displacement. This was achieved at 50kPa normal pressure. At 100kPa normal pressure, the maximum shear stress of 299.7kPa was achieved after 15 mm horizontal displacement. For the inlayer GB test, the maximum shear stress of 174.2kPa was achieved after 20.5 mm horizontal displacement with 50kPa normal pressure. At 100kPa normal pressure, the shear stress at failure turned to 281.9kPa with 19.8 mm horizontal displacement. Comparing the results of inlayer and interlayer shear tests, it should be concluded that the interlayer shear between the GB and scarified CTSB layer offered approximately equal shear resistance with the inlayer GB layer at 50kPa normal pressure and slightly higher at 100kPa. However, the horizontal displacement required to fully mobilise the shear stress was low.
- The interlayer shear resistance between the GB and smooth CTSB was 133.1kPa at 50kPa normal pressure and 191.7kPa at 100kPa normal pressure. If one compares these results with those related to inlayer GB shear as presented in the previous paragraph, the decrease of 24% shear resistance for 50kPa normal pressure and 32% for 100kPa should be noticed. This reduction might reach 75% at 50kPa and 67% at 100kPa when the interlock between the GB and CTSB materials is lost as simulated in the worst case scenario.

- Inlayer shear results of the CTSB materials showed brittle behaviour compared to GB, i.e. the horizontal displacement to failure was very low.

The observations above confirmed that the interlayer shear response between GB and CTSB depends on the CTSB surface conditions and applied normal pressure. They also depict that if the CTSB layer is scarified before laying GB, the obtained interlayer shear resistance values are much closer to those attained when the shear plane is located in the middle of the GB layer.

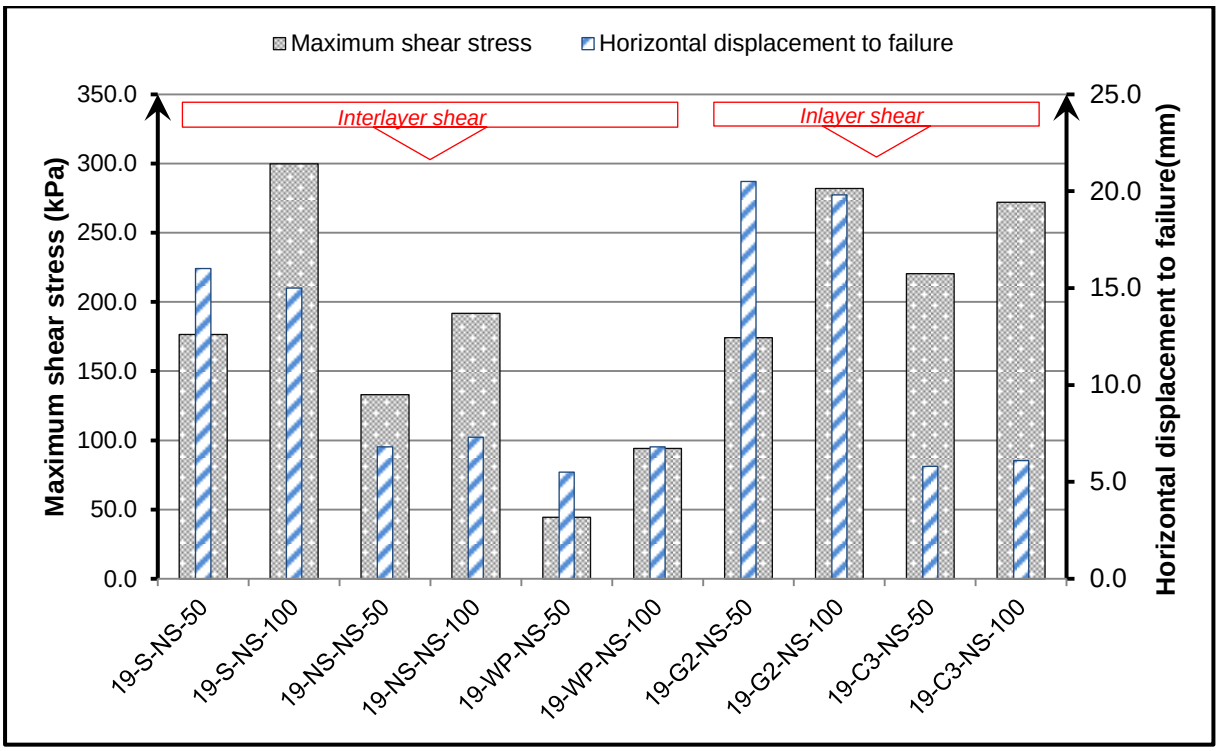

Figure 5-13: Comparative analysis of inlayer and interlayer shear stress and relative horizontal displacement to failure for the unsaturated condition.

ii. Saturated Condition

The summary of interlayer and inlayer shear test results for the saturated condition is presented In Table 5-13 and Figure 5-14. A similar comparison was done to characterise the interlayer shear performance between CTSB and GB relative to inlayer GB or CTSB behaviour. The following observations were made:

- When the top surface of CTSB was scarified before laying the GB layer, the saturated interlayer shear resistance was found to be higher than the inlayer shear resistance of the GB in saturated condition as it can be seen in Table 5-13 and Figure 5-14. In fact, since saturation of the top surface of the CTSB layer was not achieved as mentioned in Section 5.3.2, the interlayer shear involved sliding the saturated, but confined granular materials over the stiff and rough cemented surface of the CTSB layer. This

phenomenon promoted high shear resistance compared to the inlayer behaviour of fully saturated granular materials.

- The above-mentioned behaviour was not observed for the smooth CTSB surface because there was no interlock between the layers.

Table 5-13: Inlayer and interlayer shear results in terms of shear stress and horizontal displacement for the saturated condition

Type of shear test	CTSB surface roughness	Normal pressure (kPa)	Label	Maximum shear stress (kPa)	Horizontal displacement to failure (mm)
Interlayer	Scarified	50	19-S-S-50	157.7	12.8
		100	19-S-S-100	267.1	10.2
	Quasi-smooth	50	19-NS-S-50	100.3	8.0
		100	19-NS-S-100	173.0	12.7
Inlayer	Not applicable	50	19-G2-S-50	125.2	17.8
		100	19-G2-S-100	243.7	18.4
		50	19-C3-S-50	219.7	5.3
		100	19-C3-S-100	283.1	6.2

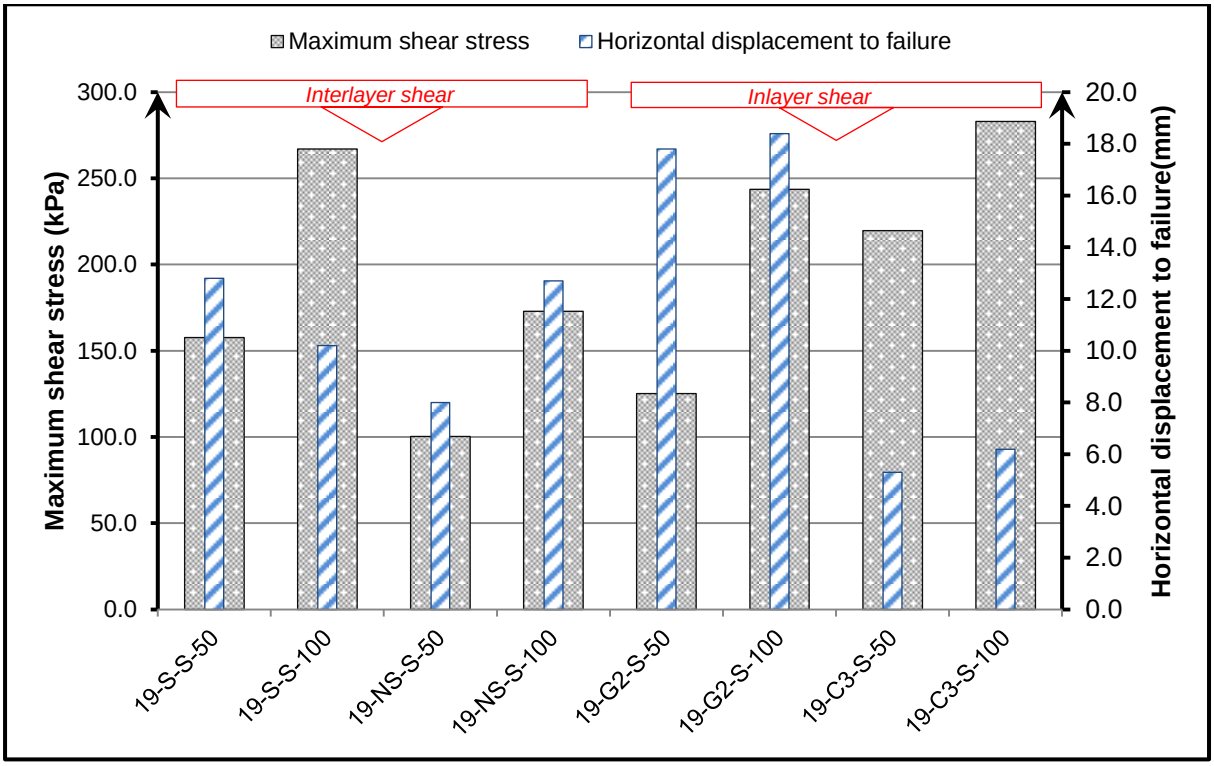

Figure 5-14: Comparative analysis of inlayer and interlayer shear stress and relative horizontal displacement to failure for the saturated condition.

5.3.4.2. Shear Stress – Normal Pressure

i. Unsaturated Condition

Table 5-14 presents the interlayer and inlayer friction coefficients and cohesions for the unsaturated condition. The values presented in Table 5-14 were derived from the shear stress-normal pressure relationships as presented in Figure 5-15 according to various testing conditions.

Table 5-14: Friction coefficients and cohesion for the unsaturated condition

Type of shear test	CTSB surface condition	Label	μ=tan ϕ	ϕ (^{0})	c (kPa)
Interlayer	Scarified	19-S-NS	1.90	62.2	90.6
	Quasi-smooth	19-NS-NS	1.59	57.8	45.3
	With plastic	19-WP-NS	0.93	43	0.7
Inlayer	Not applicable	19-G2-NS	2.29	66.4	54.2
		19-C3-NS	1.36	53.7	139.6

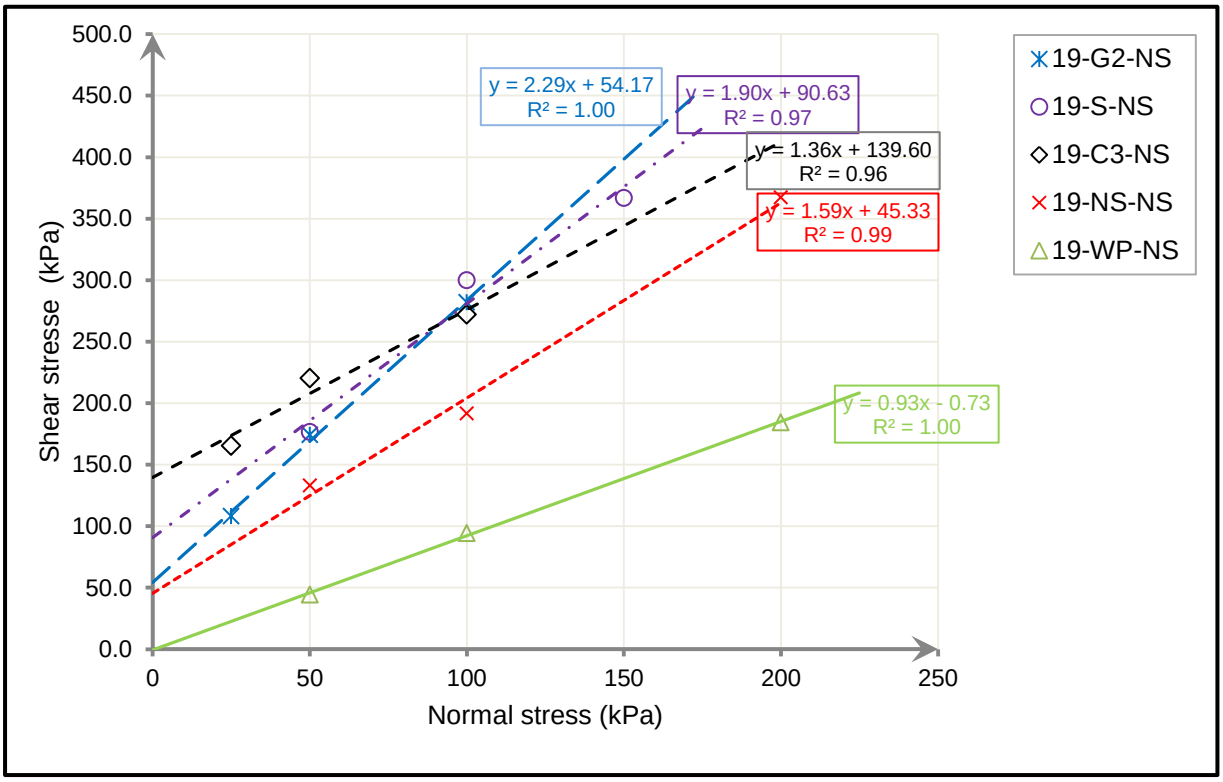

Figure 5-15: Comparative analysis of inlayer and interlayer failure envelopes for the unsaturated condition

The comparative analysis of inlayer and interlayer response upon shear demonstrated the active influence of the CTSB surface conditions and moisture condition.

From the Mohr-Coulomb failure envelopes plotted in Figure 5-15, the following observations were made:

- Cohesionless and full slip conditions were noticed for the interlayer shear response with thin plastic sheeting between the GB and CTSB layers as was expected. An interlayer friction coefficient of 0.93 and approximately zero cohesion were observed (see Figure 5-15).
- The highest friction was observed on the inlayer shear response of the GB material with friction coefficient of 2.29. The CTSB layer was found to be the most cohesive due to cementation.
- The failure envelope line of interlayer shear response for scarified CTSB and GB crosses the intersection between the two failure envelope lines of inlayer GB and CTSB shear and stays between them for a wide range of normal pressure (see Figure 5-15). Therefore, according to the observation presented in the previous paragraph, the failure envelope path of the scarified CTSB and GB structure seems to confirm that scarifying the CTSB layer before laying the GB provides the most efficient conditions in both cohesion and friction.
- It was found that at 94kPa normal pressure, CTSB, GB and scarified CTSB-GB structure have all the same maximum mobilised shear stress of 265kPa.
- The failure envelope of the interlayer shear between quasi-smooth CTSB and GB lay between two extreme conditions defined above. This implicated the reduction of interlayer friction coefficient by 30% compared to the highest friction conditions observed.

All the observations above supported the influence of CTSB surface scarification on the interlayer friction and cohesion behaviour between the GB and CTSB layers.

ii. Saturated Condition

Table 5-15 and Figure 5-16 show the friction and cohesion responses for the saturated inlayer shear condition of CTSB and GB layers. They also exhibit the interlayer shear response for CTSB-GB structure.

The general observation noticed from Figure 5-16 is that the failure envelope line of the GB layer intercepts the vertical axis far below the intercept of the smooth CTSB-GB failure envelope line. But still, the GB layer exhibits high friction resistance at high normal pressure, comparative to other testing conditions.

The failure envelope line for the interlayer shear strength between scarified CTSB and GB layers is far above the one for smooth CTSB-GB interlayer shear strength (see Figure 5-16). Therefore, it shows a high resistance compared to the smooth CTSB-GB structure.

Table 5-15: Friction coefficients and cohesion for the saturated condition

Type of shear test	CTSB surface roughness	Label	μ= tan ϕ	ϕ (^{0})	c (kPa)
Interlayer	Scarified	19-S-S	1.56	57.3	92.4
	Quasi-smooth	19-NS-S	1.13	48.5	50.0
Inlayer	Not applicable	19-G2-S	2.23	65.8	19.1
		19-C3-S	1.34	53.3	150.2

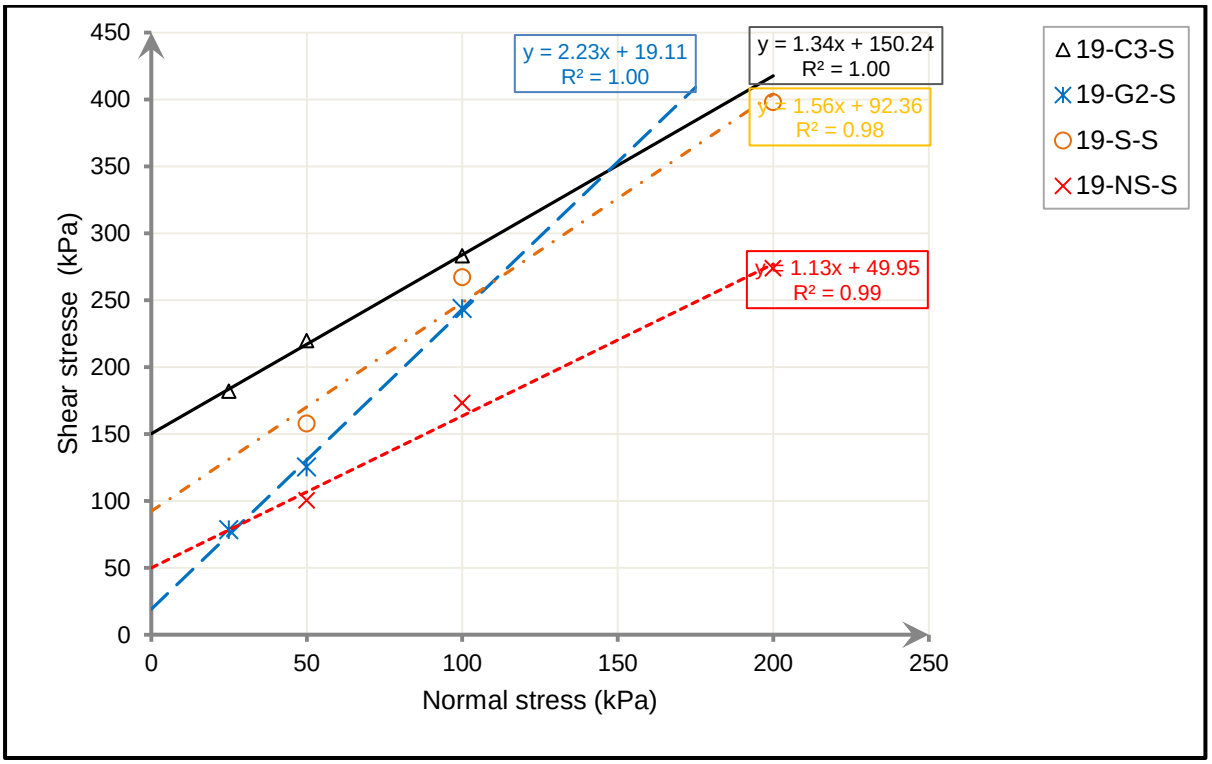

Figure 5-16: Comparative analysis of inlayer and interlayer failure envelopes for the saturated condition

From the above-mentioned observations linked to the relationship between maximum shear stress and normal pressure in unsaturated and saturated conditions, it is apparent that the interlayer cohesion and friction coefficients are both influenced by the surface roughness conditions of the CTSB before laying the GB and the saturation condition. It has also been found that the highest values of interlayer cohesion and friction coefficients were achieved when the CTSB surface was scarified. The obtained values were closer to the inlayer shear values for the GB and CTSB layers.

5.3.4.3. Vertical - Horizontal Displacements

In Table 5-16 and Figure 5-17, the average dilation angles are presented for the inlayer and interlayer shear tests. The values were previously deduced from the relationship between vertical and horizontal displacement throughout the shear tests as presented in Section 5.3.3.

The comparative analysis of dilation angles related to the interlayer and inlayer shear tests (Table 5-16 and Figure 5-17) highlighted the influence of the CTSB surface roughness, on its interaction with the GB layer. From Table 5-16 and Figure 5-17, the following were observed:

- For the interlayer shear test, the value of the highest dilation angle was 13.7^{o} which was achieved when the surface of the CTSB layer was scarified before laying the GB. This value was fairly close to the dilation angle obtained from the inlayer shear test of the GB layer which was 14.9^{o}.
- The value of the dilation angle corresponding to the interlayer shear test between quasi-smooth CTSB and GB was 6.5. When it is compared to the inlayer response of the GB, which has 14.9^{o} dilation angle, the smooth CTSB-GB structure reveals a reduction of dilation up to roughly 56%. When the comparison is done between inlayer GB (Ψ=14.9^{0}) and interlayer shear with plastic between the CTSB and GB (Ψ=4.5^{0}), a reduction of the dilation angle up to 70% can be observed.

Table 5-16: Average dilation angle for the unsaturated condition

Type of shear test	CTSB surface roughness	Label	Average dilation angle (Ψ^{o})
Interlayer	Scarified	19-S-NS	13.7
	Quasi-smooth	19-NS-NS	6.5
	With plastic	19-WP-NS	4.5
Inlayer	Not applicable	19-G2-NS	14.9
		19-C3-NS	9.4

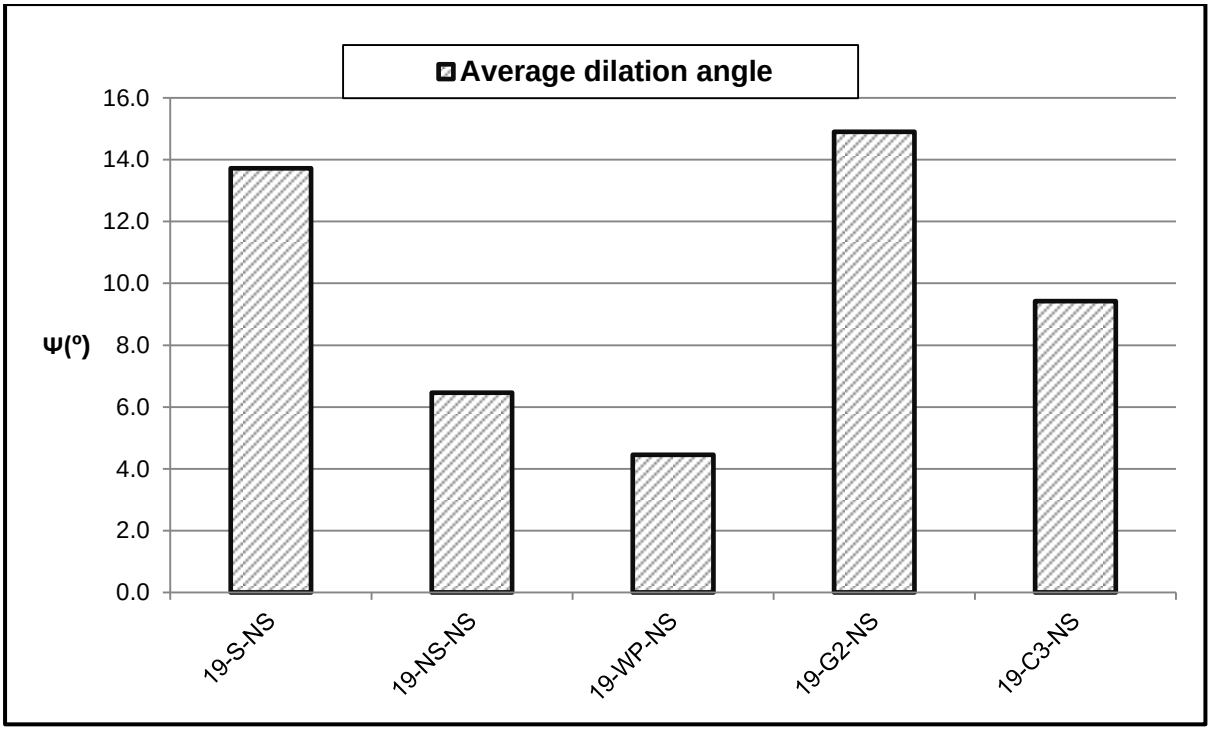

Figure 5-17: Comparative analysis of dilation between inlayer and interlayer shear test for the unsaturated condition

The dilation angles obtained from various testing conditions revealed the correlation between dilation behaviour and the adherence of the GB to the CTSB. Scarification of the CTSB exhibited a greater dilation angle which was closer to the value obtained for the GB inlayer shear test. Therefore, it should be concluded that when the surface of the CTSB layer is scarified before laying the GB layer, the yield interlayer shear resistance is much closer to the resistance in the middle of the GB layer.

5.3.5. QUANTITATIVE EFFECTS OF INVESTIGATED VARIABLES ON INTERLAYER SHEAR STRESS

Previous subsections of Section 5.3 shed light on the influence of various parameters on the interlayer shear resistance between the CTSB and GB layers. Investigated parameters include normal pressure, surface conditions of the CTSB, interlayer moisture condition, and the maximum size of the aggregate in the CTSB. Moreover, a comparative analysis between interlayer and inlayer shear stress was carried out and discussed in Section 5.3.4, whereby respective indicators, including the interlayer friction coefficient, cohesion and dilation angle were used to characterise the interlayer shear resistance according to the inlayer values.

From the reviewed literature, the maximum interlayer shear stress was frequently used to characterise the adhesion conditions in pavement layers (Collop *et al.,* 2003; Raab, 2011; Uzan *et al.,* 1978).

In this section, the main effect of CTSB scarification, moisture conditions and normal pressure, on the shear resistance was quantified by means of the factorial design method at two levels (2^3) (Box *et al.,* 2005). Additionally, interaction effects were also assessed. All calculation results are summarised in Table 5-17 and more details are given in Appendix B

Table 5-17: Factorial design analysis for the interlayer shear stress

Experimental run	CTSB scarification - A-	Moisture condition -B-	Normal pressure -C- (kPa)	Average Interlayer shear stress (kPa)	Variable	Effect
1	Quasi-smooth	Saturated	50	100.3		
2	Scarified	Saturated	50	157.7	A	75.7
3	Quasi-smooth	Unsaturated	50	133.1	B	25.7
4	Scarified	Unsaturated	50	176.4	A x B	-0.05
5	Quasi-smooth	Saturated	100	173.0	C	91
6	Scarified	Saturated	100	267.1	A x C	25.35
7	Quasi-smooth	Unsaturated	100	191.7	B x C	-0.05
8	Scarified	Unsaturated	100	299.7	A x B x C	7

Table 5-17 shows the main effects of the CTSB scarification (A), moisture condition (B) and normal pressure (C) on the interlayer shear stress. It also exhibits the two-factor interactions (i.e. A x B, A x C and B x C) and three-factor interaction (i.e. A x B x C). For the sake of analysis, the 1st experimental run of quasi-smooth CTSB in saturated condition and 50kPa normal pressure (see Table 5-17) was considered as a benchmark whereby its corresponding shear stress was compared to the yield stress at the 2nd up to 8th run. Experimental errors were not considered.

The main effects analysis presented in Table 5-17 shows that, the increase of the normal pressure from 50kPa to 100kPa resulted in the relative increase of the interlayer shear stress by 91kPa or about 90%. Scarification of the CTSB layer before laying the GB increased the maximum interlayer shear stress by 75.7kPa which is by about 75%. On the other hand, unsaturated condition of the interlayer increased only 25% to the interlayer shear stress.

The interaction effects analysis showed that the change in both, CTSB surface and moisture conditions to their most favourable levels (i.e. scarified and unsaturated respectively) does not affect the yield stress. A similar observation was made when, both moisture condition and normal pressure were changed to favourable levels (i.e. unsaturated and 100kPa respectively). However, the results highlight the increase of 25.35kPa in the interlayer shear stress when both CTSB condition and normal pressure are changed to their upper levels

(see Table 5-17). Three-factor interaction showed the increase of the yield by 7kPa or roughly 7%.

According to the results of the factorial design analysis shown in Table 5-17, it seems apparent that the main effect of normal pressure and the CTSB surface conditions is to increase the interlayer shear stress. The effect of moisture condition showed evidence of interaction with other variables as shown by two-factor interactions (see Table 5-17)

5.4. SUMMARY OF MAIN FINDINGS

This section presents a summary of the laboratory test results on the research materials and interlayer shear investigation. It also gives a concise discussion of the outcome.

5.4.1. RESEARCH MATERIALS

Material types were chosen according to TRH14 (1985) recommendations for base and subbase construction materials. A pavement structure made of G2 and C3 base and subbase materials, respectively, was selected for the purpose of this study.

Since the research materials were collected from a large supply commercial quarry, assorted laboratory tests had to be conducted to define their physical and mechanical properties and compare them with TRH14 (1985) and SAPEM (2013) recommended values. Table 5-6 in Section 5.2 presents the summary of the characterisation tests results and relevant comments according to TRH14 (1985) and SAPEM (2013) guidelines.

In general, the laboratory test results confirmed the physical and mechanical performance of the material. However, the amount of crushed stone found in the G5 materials developed high compression strength when it was compacted. This therefore required the use of low cement content for stabilisation to satisfy the tensile strength criteria and to achieve the purpose of this study.

5.4.2. INTERLAYER SHEAR INVESTIGATION

Figure 5-18 and Figure 5-19 summarise the effects of the assorted factors which influence the interlayer adhesion strength in the pavement structure. The analysis was mainly based on three shear responses:

- Interlayer shear stress at failure,
- Interlayer friction coefficient
- Average angle of dilation.

Figure 5-18 shows the general trends of interlayer shear stress at failure for the investigated factors. The bar chart depicts the stress dependency behaviour of the interaction between the granular base (GB) and cement treated subbase (CTSB) layers irrespective of the CTSB

surface finishing or interlayer saturation condition. This corresponds with the results obtained by Canestrari & Santagata (2005) on the increase of the peak shear stress between HMA layers when the normal pressure increases regardless of the interface treatment. Additionally, the bar chart reveals that at constant normal pressure, interlayer shear stress depends on the CTSB surface conditions and interlayer saturation state.

The decrease of shear resistance has been recorded when the maximum aggregate size in the CTSB layer changes from 19 mm to 26 mm (see Figure 5-18).

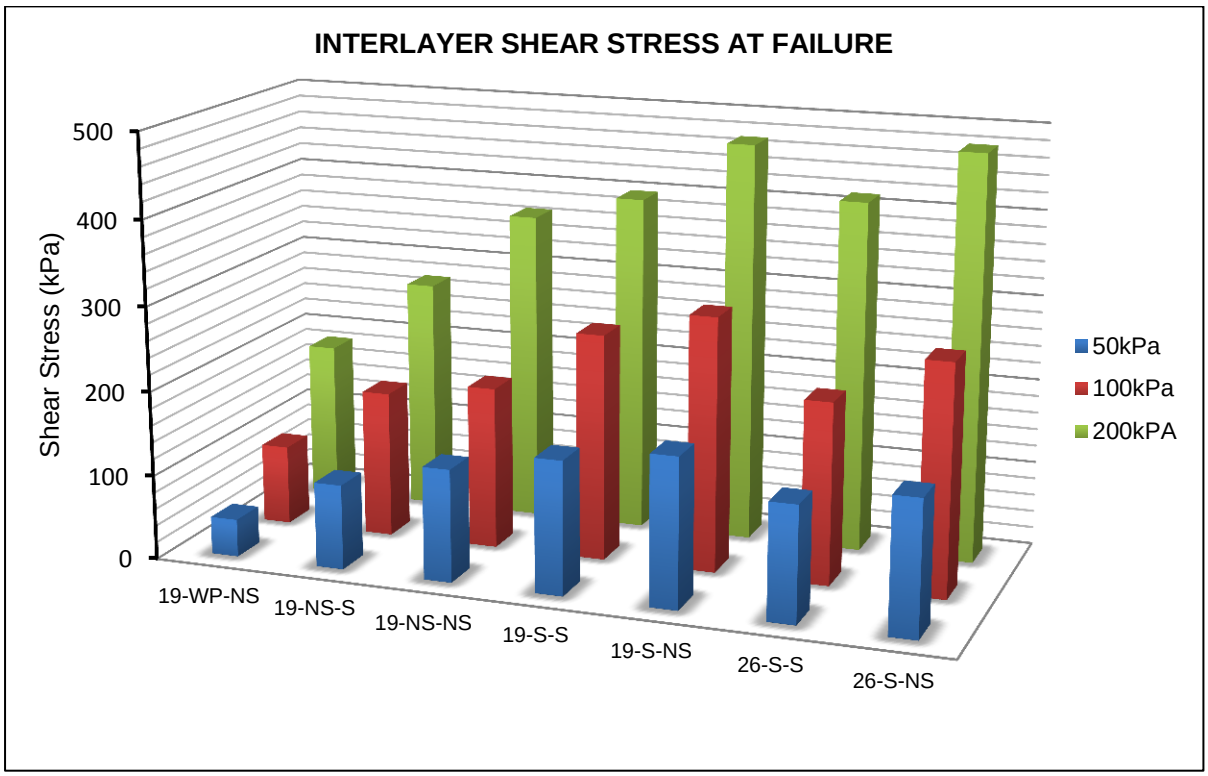

Figure 5-18: General trends of interlayer shear stress at failure for investigated parameters

In Figure 5-19 the interlayer friction coefficients and average dilation angles for different testing conditions are presented. The primary axis shows the average angle of dilations in degrees and the secondary axis shows the interlayer friction coefficients. The general trend for both parameters shows that at the same aggregate size in the CTSB layer, maximum values were achieved when the CTSB surface was scarified before laying the GB while minimum values were recorded for the interlayer shear with a thin plastic sheet at the interface between the two layers. This highlights the impact of the CTSB surface conditions on the interaction between the two layers. The trend also shows the decrease in the average dilation angle and interlayer friction coefficient when the interlayer is saturated. This is explained by the lubricant effect of water which influences particles at the interface to slide over one another quickly.

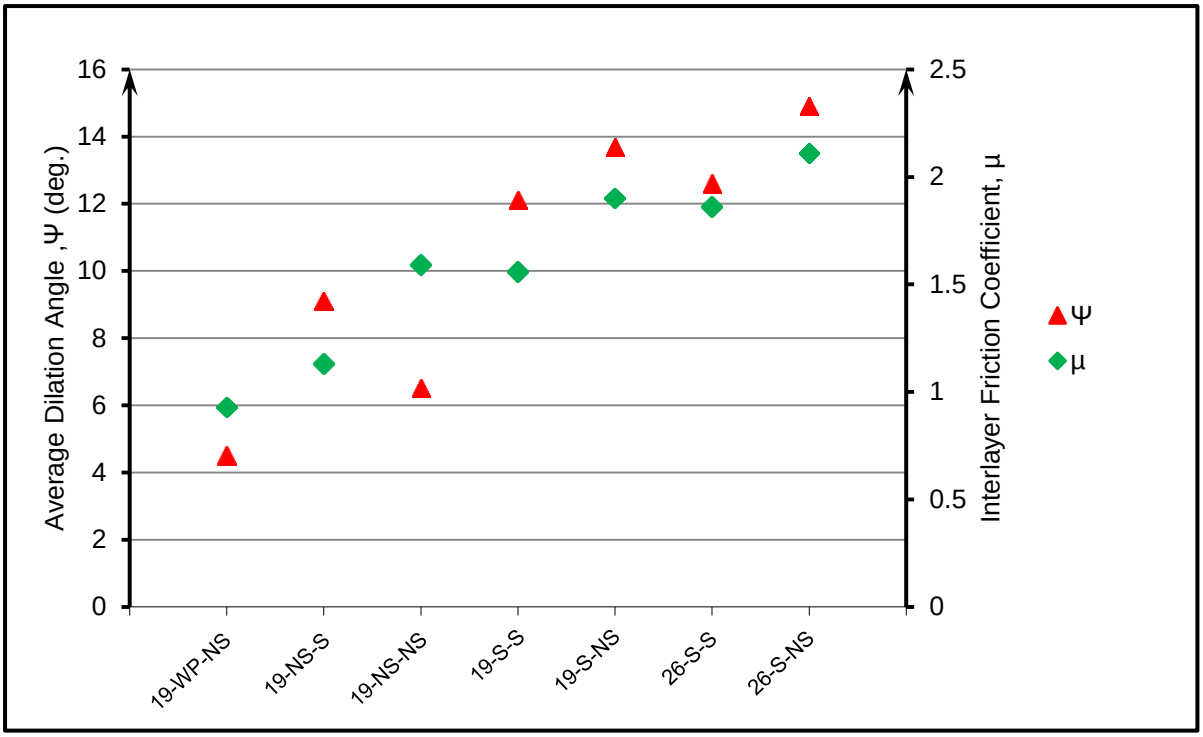

Figure 5-19: General trends of interlayer friction and dilation angle for investigated parameters

Chapter 6

PRACTICAL SIGNIFICANCE

6.1. INTRODUCTION

The general configuration of the pavement structure comprises a set of various layers arranged one on top of another. The main purpose of this configuration is to provide a cost-effective structure which offers sufficient strength to distribute traffic loading from the surface to the natural subgrade with minimum damage. To this end, the physical and mechanical properties of the material in each layer contribute to the overall performance of the whole structure. However the interaction between layers has been also identified to affect the distribution of stress and strain throughout the pavement structure (Burmister, 1945; Khweir & Fordyce, 2003; Kruntcheva *et al.,* 2000).

This chapter aims at illustrating the practical influence of frictional interaction between layers on the overall pavement performance. For the purpose of illustration, a typical design example was conducted on a Category A. The design principle, however, can equally be adopted for all other road categories. The analysis of stress-strain distribution throughout the pavement structure was carried out with BISAR software for various interlayer friction conditions. Finally, the total number of load repetitions that every layer can sustain before reaching specific terminal conditions was computed for each interlayer friction parameter. The computation was based on the material failure mode and relevant critical parameters as specified in the South African Mechanistic Design Method (SAMDM).

Using the results of this study, an attempt was made to develop a correlation chart between interlayer adhesion ratio β computed from the laboratory tests and interlayer friction parameter α which is used in BISAR software analysis.

6.2. CORRELATION CHART FOR INTERLAYER ADHESION RATIO AND INTERLAYER FRICTION PARAMETER

The direct shear tests conducted throughout this study to determine the interlayer shear strength would have been able to come up with specific values of reduced spring compliance if the determination of correction factors related to material type and displacement rate was achieved. This however, required many test runs which was not accomplished due to challenges related to the testing conditions and time frame. Therefore, the approach of correlating the achieved interlayer adhesion ratios and interlayer friction parameters was used for the analysis.

The approach consisted of computing the ratio between the achievable adhesion strength for different testing conditions and the maximum values simulated by the inlayer shear results. Interlayer adhesion ratios have been computed for the three main responses used in this study as highlighted in Chapter 5, namely: interlayer shear stress at failure, interlayer friction coefficient and average angle of dilation.

Table 6-1 presents the interlayer adhesion ratio β, calculated for three testing conditions of the Cement Treated Subbase (CTSB) layer, i.e. scarified, quasi-smooth and lined with a plastic sheet. The β values are presented for shear, friction and dilation responses. The results associated with an unsaturated condition were considered for the computation since the pavement is likely to work under moderate moisture condition rather than saturated.

Table 6-1: Interlayer adhesion ratio β for shear, friction and dilation responses

Interlayer adhesion ratio	β_{shear}	$\beta_{friction}$	$\beta_{dilation}$
Inlayer / Inlayer	1	1	1
Scarified / Inlayer	1	0.8	0.9
Quasi-smooth / Inlayer	0.7	0.7	0.4
With plastic / Inlayer	0.3	0.4	0.3

Interlayer shear tests conducted throughout this study covered the adhesion range from total friction (simulated by inlayer shear) to very low friction (shear with plastic at the interface). The intermediate friction conditions were also analysed such as scarifying or non-scarifying the CTSB before laying the Granular Base (GB). For correlating the results of the laboratory tests and the analytical approach used by BISAR software, reasonable partial friction parameters were selected between ideal (α = 0) and critical (α = 1) range. In Figure 6-1 the correlation chart is presented for interlayer shear, interlayer friction and dilation ratios. The chart relates the interlayer friction parameter α, and the interlayer adhesion ratio β.

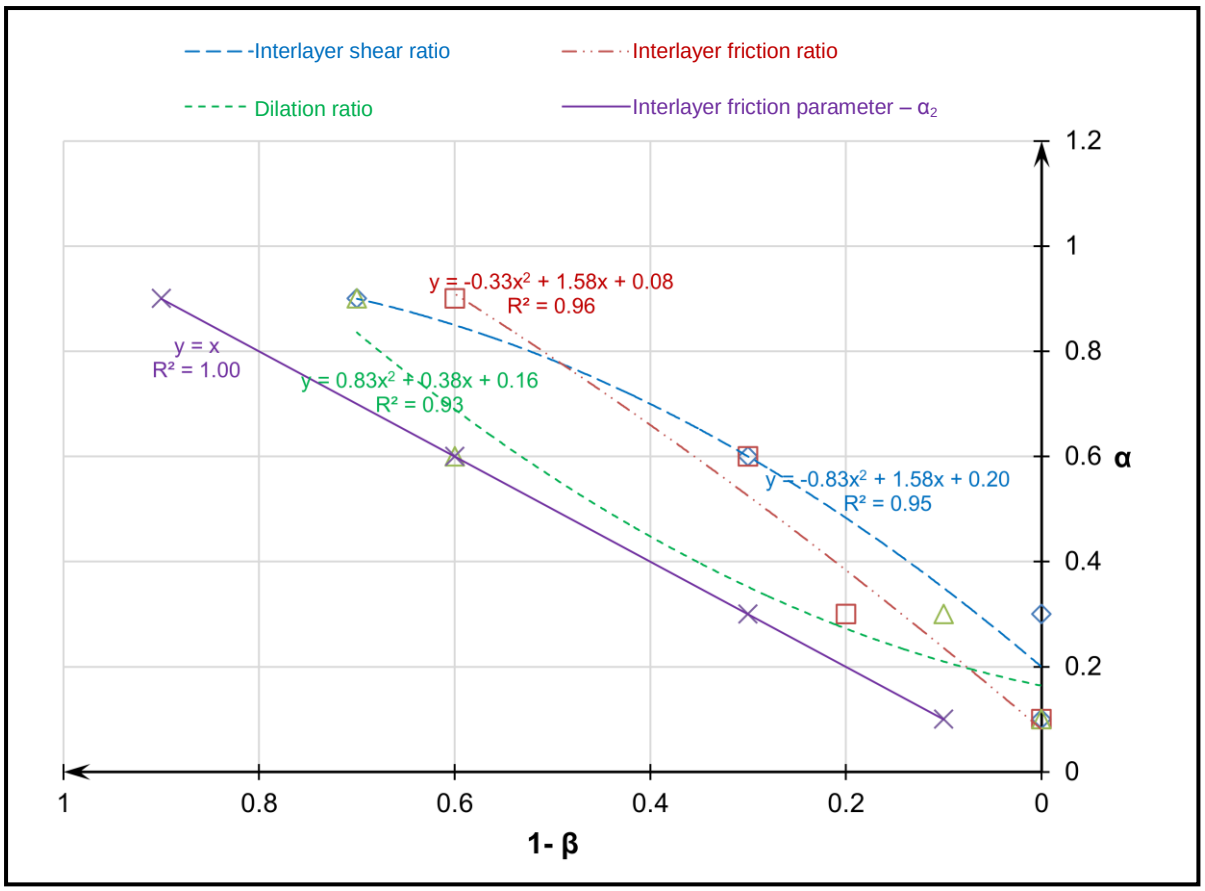

Figure 6-1: Correlation chart for interlayer adhesion ratio and interlayer friction parameter for the interface between GB and CTSB

6.3. PAVEMENT DESIGN EXAMPLE

6.3.1. OVERVIEW

This section illustrates the detailed design of a typical flexible pavement structure whereby various interlayer friction conditions between the GB and CTSB were taken into account. The design was carried out according to the SAMDM as discussed in Section 2.4.3 of the second chapter. The stress-strain distribution throughout the pavement structure was estimated by using the linear-elastic computer software BISAR.

Normally, the SAMDM assumes full friction between layers. However, this does not represent the real conditions as discussed in Chapter 2 and Chapter 3. The use of BISAR software allowed the modelling of the pavement structure with different interlayer friction conditions which were defined by the parameter - α (i.e. α = 0 means full friction and α = 1 means full slip). For the purpose of this analysis, a range of interlayer friction parameters was selected and then correlated to the actual conditions considered in this study. The correlation chart shown in Figure 6-1 was used. The selection of interlayer friction parameters was done in such a way that a sufficient range of partial friction between the GB and the CTSB layers was covered. Interlayer friction parameters were entered in the software as the reduced spring compliance (ALK), which was calculated by using Equation 2-13 relating the interlayer friction parameter α to the reduced spring compliance ALK

through the radius of loading a. Additionally, the worst case scenario was modelled whereby full slip was assumed between the Asphalt Concrete (AC) / GB and GB / CTSB interfaces. For all modelling cases, full bond was assumed between the CTSB and subgrade (SG) layers. Table 6-2 shows a range of interlayer friction parameters along with related adhesion ratios and reduced spring compliances. The α_1 and α_2 stand for the interlayer friction parameters for AC/GB and GB/CTSB interfaces respectively.

Table 6-2: Interlayer adhesion ratios correlated to the interlayer friction parameters along with associated ALK values

AC / GB - α_1	GB / CTSB - α_2	1-β			Reduced spring compliance, ALK (m)		GB / CTSB interface condition
		Shear	Friction	Dilation	ALK_1	ALK_2	
0.01	0.1	0	0	0	1.31E-03	1.44E-02	Full friction ↕ Full slip
	0.3	0	0.2	0.1		5.57E-02	
	0.6	0.3	0.3	0.6		1.95E-01	
	0.9	0.7	0.6	0.7		1.17E+00	
0.99	0.99				1.29E+01	1.29E+01	Worst case scenario

6.3.2. ROAD CATEGORY AND LOADING CONDITIONS

This design was conducted on a typical interurban road, specified as Category A in the South African road categories. It is characterised by a high volume of traffic, and many heavy vehicles. The design traffic loading for this category ranges between 3 and $10x10^6$ standard axle (80kN axles/lane) over 20 years. The approximate design reliability is 95%.

Knowledge of pavement loading conditions is a key element towards realistic design. The current South African design standard includes a dual wheel configuration spaced by 350mm centre to centre with 80kN static axle load and 650kPa tyre contact pressure (Theyse *et al.,* 2011). However, various surveys have shown severe overloading of pavements in many countries including South Africa (Molenaar, 2007; Morton *et al.,* 2004). This was induced by heavy and overloaded vehicles and different sizes and shapes of wheel loads which produced high inflation pressures.

Considering the above-mentioned facts, this analysis used the loading configuration comprising an 80kN axle with one super single tyre at each end instead of dual wheel. The tyre pressure was kept at 750kPa.

By assuming that the contact pressure and tyre pressure are equal, the relationship between wheel load and tyre pressure gave the radius of the contact area as 130 mm which was used to relate the interlayer friction parameter - α and the reduced spring compliance - ALK.

6.3.3. TYPICAL STRUCTURE AND MATERIAL PROPERTIES

Figure 6-2(a) illustrates the cross section of a Category A pavement structure which was analysed during this study. It is composed of four layers made of the following materials:

- Thin continuously graded asphalt top layer (AC),
- Granular G2 base layer (GB),
- Cement treated subbase layer C3 (CTSB),
- Infinite subgrade G10 (SG).

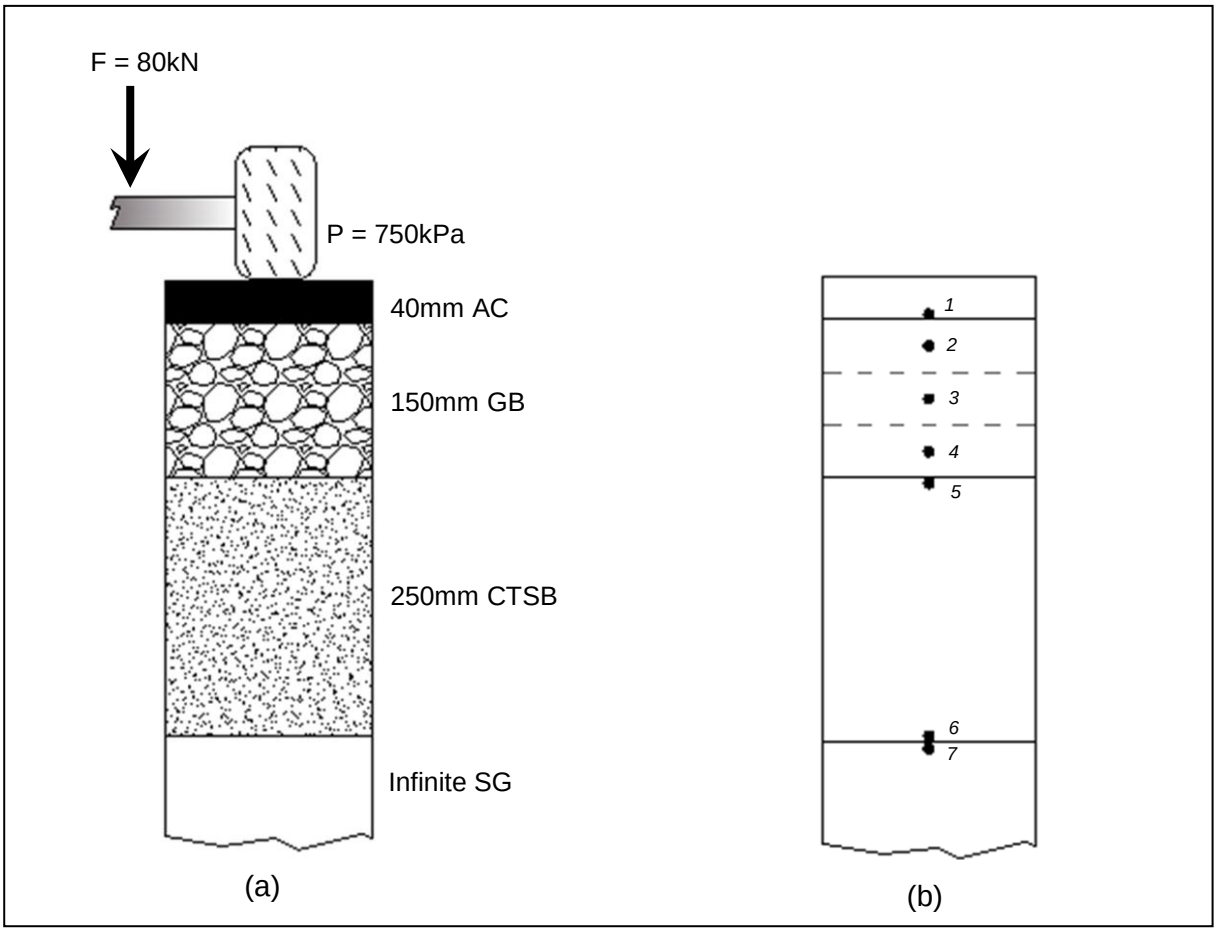

Figure 6-2: Typical cross section of the pavement. (a) Loading conditions, (b) Critical positions of failure

Mechanical properties of the materials used for the analysis are presented in Table 6-3 and Table 6-4.

Since no laboratory tests were carried out to assess the resilient behaviour, material stiffness used for this analysis was selected according to the values suggested by Freeme (1983) as presented in Theyse *et al.* (1996) (see Table 6-3). Layer thickness was selected from the South African design catalogue as presented in TRH4, (1996).

Table 6-3: Mechanical properties of materials used to model pavement layers

Layer	Type of material modelling	Thickness (mm)	E (MPa)	ν (-)
Asphalt	Linear elastic	40	2500	0.35
Granular base G2	Non-linear elastic	150	400	0.45
Cemented subbase C3	Linear elastic	250	1500	0.4
Subgrade G10	Linear elastic	Infinite	50	0.4

The types of material modelling shown in Table 6-3 were selected according their general behaviour. Except the unbound granular materials used in the base layer, all other materials were modelled as linear elastic. Table 6-4 presents the shear parameter utilised for granular materials.

Table 6-4: Shear properties of granular base material (SAPEM, 2013)

Material	c (kPa)	ϕ (°)	k_1 (kPa)	k_2 (-)
G2	50	52	9700	0.66

6.3.4. BEARING CAPACITY ESTIMATION

The bearing capacity of the pavement structure was evaluated according to the total number of load repetitions that each layer can withstand before reaching terminal conditions. This depends on the stress-strain distribution in each individual layer of the pavement.

6.3.4.1. Stress and Strain Distribution

According to the predefined interlayer friction conditions, reduced spring compliances have been computed (see Table 6-2) and introduced to BISAR software with other input parameters for the analysis. Figure 6-3 and Figure 6-4 illustrate stress and strain variation throughout the pavement structure when various friction conditions are considered. Note that α_1 and α_2 stand for interlayer friction parameters for AC/GB and GB/CTSB interlayers respectively.

In Figure 6-3, curves of vertical and horizontal strain distribution across the pavement structure are shown. It can be seen that more vertical strain is developed across the granular base and on top of the subgrade as interlayer friction diminishes. This behaviour has a direct influence on the permanent deformation of the layer and subsequently the deformation of the road surface.

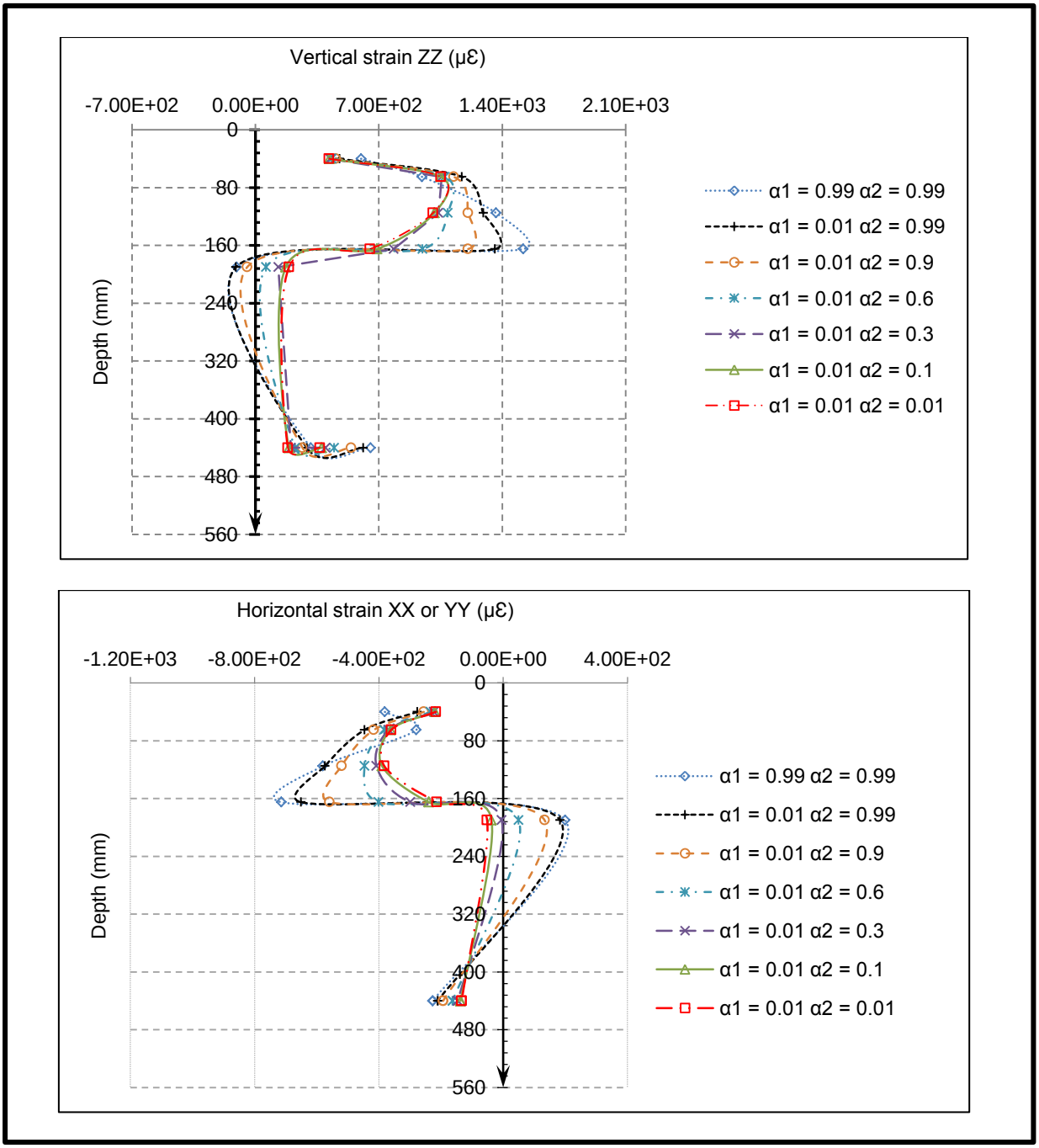

Figure 6-3: Vertical and horizontal strain distribution curve across the pavement structure with variation in interlayer friction

From the horizontal strain distribution curve one can observe the increase of tensile strain at the bottom or within the asphalt layer as friction between the layers diminishes. This indicates its influence on the structure's load spread behaviour. The direct effect of more strain in the AC layer is to speed up the development of fatigue cracks at the bottom or within the layer.

In addition, Figure 6-3 shows a rapid increase in horizontal tensile strain in the granular base as full friction between the GB and CTSB gets lost. This justifies the significant reduction in the layer's life (see Figure 6-7) since granular materials are weak in tension.

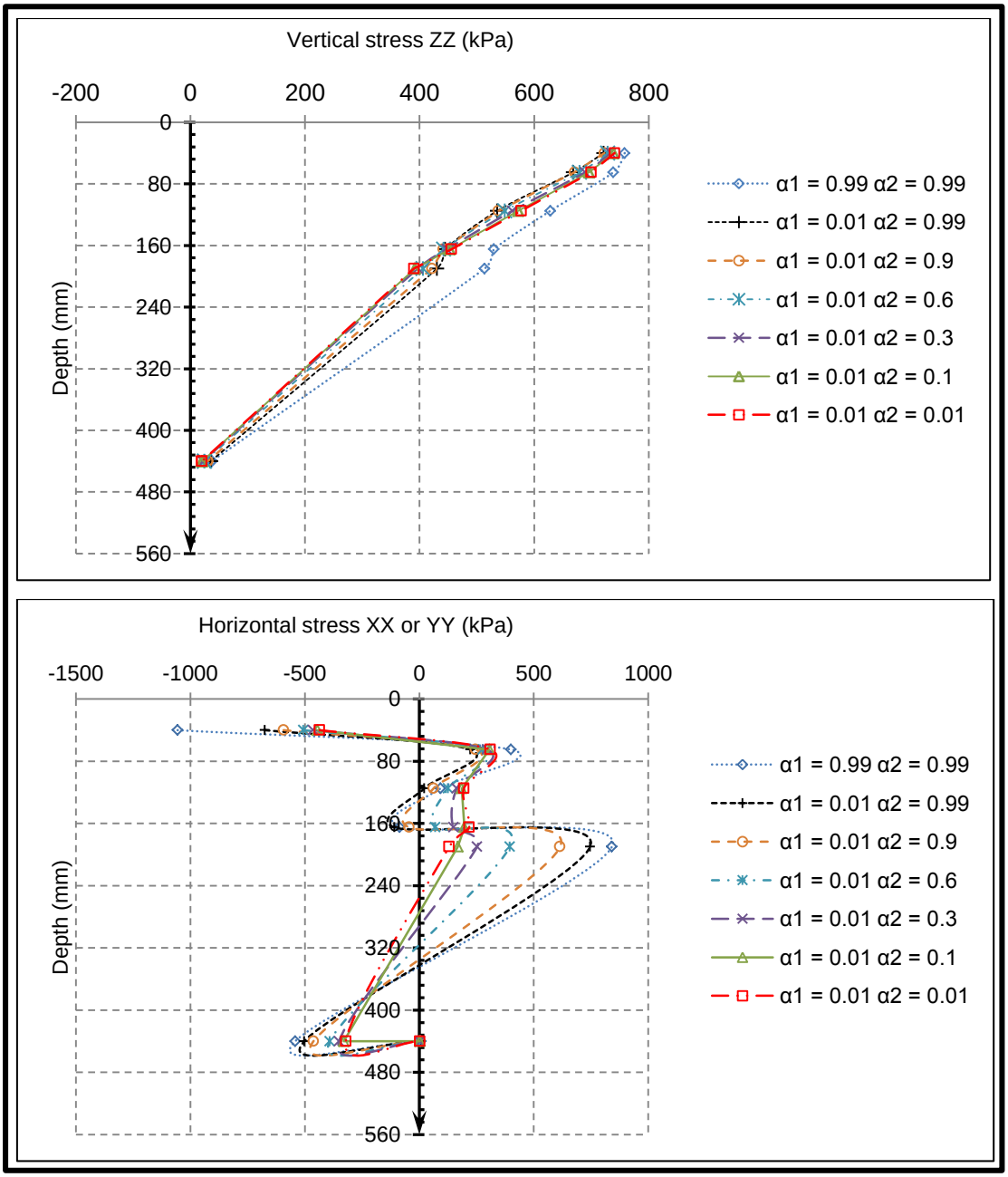

Figure 6-4: Vertical and horizontal stress distribution across the pavement structure with variation in interlayer friction

Figure 6-4 presents the vertical and horizontal stress distribution curves. The load spreading response of the pavement structure from the top to the subgrade can be observed in the vertical stress distribution curve, but the Influence of the interlayer friction conditions is not well established. On the other hand, the horizontal stress distribution curves, also shown in Figure 6-4 presents a marked increase in horizontal stress at the GB/CTSB interface as interlayer friction diminishes. This reaction might induce significant shear flow between layers and subsequently, interface shear failure.

From the stress-strain distribution analysis, it can be concluded that the interlayer friction conditions between the GB and the CTSB has a significant influence on material response in

the pavement structure. The granular base layer was observed to be more sensitive to traffic induced loading as the interlayer friction parameter changes from full friction ($\alpha = 0$) towards full slip ($\alpha = 1$). This sensitivity was attributed to the stress-dependency behaviour of granular materials.

6.3.4.2. Critical Parameters and Transfer Functions

In the typical South African pavement structure, each type of material exhibits a specific mode of failure associated with a critical parameter which is calculated at a specific position in the pavement structure as discussed in Chapter 2, Section 2.4.3. Figure 6-2(b) illustrates critical positions related to this analysis.

Mathematical relationships have been used to estimate the maximum number of load repetitions that a layer can sustain before reaching terminal conditions. These relationships link specific critical parameters of the layer to its performance.

I. Asphalt Layer

The hot mix asphalt layer exhibits fatigue cracking failure due to tensile strain at the bottom or within the layer. Table 6-5 contains the output values of tensile strain recorded on the corresponding critical position when the interlayer friction conditions are modelled from complete slip ($\alpha_1 = \alpha_2 = 0.99$) towards full friction ($\alpha_1 = \alpha_2 = 0.01$). The corresponding life of the layer has been calculated by using the transfer function for a Category A road and associated values are shown on the right-hand column of the table.

It is clear from Table 6-5 that the tensile horizontal strain in the asphalt layer increases as the interlayer adhesion reduces. This was earlier noticed and discussed in Section 6.3.4.1.

Table 6-5: Critical parameter and fatigue life of the asphalt layer with variation in interlayer friction between GB and CTSB

Interlayer friction parameter - α	Tensile strain in the asphalt layer ε_t ($\mu\varepsilon$)	Life of the layer, N_{eff}
$\alpha_1 = 0.99$, $\alpha_2 = 0.99$	3.81E+02	1.56E+04
$\alpha_1 = 0.01$, $\alpha_2 = 0.99$	2.77E+02	8.02E+04
$\alpha_1 = 0.01$, $\alpha_2 = 0.9$	2.55E+02	1.20E+05
$\alpha_1 = 0.01$, $\alpha_2 = 0.6$	2.34E+02	1.90E+05
$\alpha_1 = 0.01$, $\alpha_2 = 0.3$	2.24E+02	2.37E+05
$\alpha_1 = 0.01$, $\alpha_2 = 0.1$	2.19E+02	2.66E+05
$\alpha_1 = 0.01$, $\alpha_2 = 0.01$	2.17E+02	2.79E+05

In Figure 6-5 the total number of standard axles that the hot mix asphalt layer can withstand before failure is plotted against the interlayer friction conditions. The general trend shows that the life of the layer is sensitive to the interlayer adhesion conditions. The number of load repetitions reduces as friction between the GB and CTSB diminishes. For instance, by assuming full friction between the AC and GB layers (α_1 = 0.01), the change of friction conditions between the GB and CTSB from full friction (α_2 = 0.01) to partial friction (α_2 = 0.6) induces the reduction of the load repetitions from 2.79E+05 to 1.90E+05. This means an approximate 32% reduction in the layer's life.

From Figure 6-5, it is important to notice the quick reduction of life for a small change of friction parameter in the vicinity of the critical zone. For example, the change in friction parameter $\alpha_2 = 0.6$ to 0.9 induced the decrease of load repetitions at failure from 1.90E+05 to 1.20E+05. This change corresponds to roughly a decrease of 37%. On the other hand, the change of α_2 (in the ideal zone) from 0.1 to 0.3 caused the decrease of load repetition at failure from 2.66E+05 to 2.37E+05 which only corresponds to a decrease of 11%. This behaviour can be explained by the general properties of bound materials. Since all particles of the asphalt layer are bound together, the allowance of limited slip between the AC layer and the GB underneath will not induce much reduction in carrying capacity because the bonding behaviour of the asphalt will still keep all particles unified. As slip conditions increase, the pavement loading might generate free particles between two layers due to abrasion. This results in wearing and deterioration of the layer.

The general observation from the analysis is that the capacity of the asphalt layer to sustain traffic induced loading, is affected by the interlayer adhesion conditions between the GB and CTSB layers. Additionally the rate of decrease in life becomes high as the slip approaches the critical conditions.

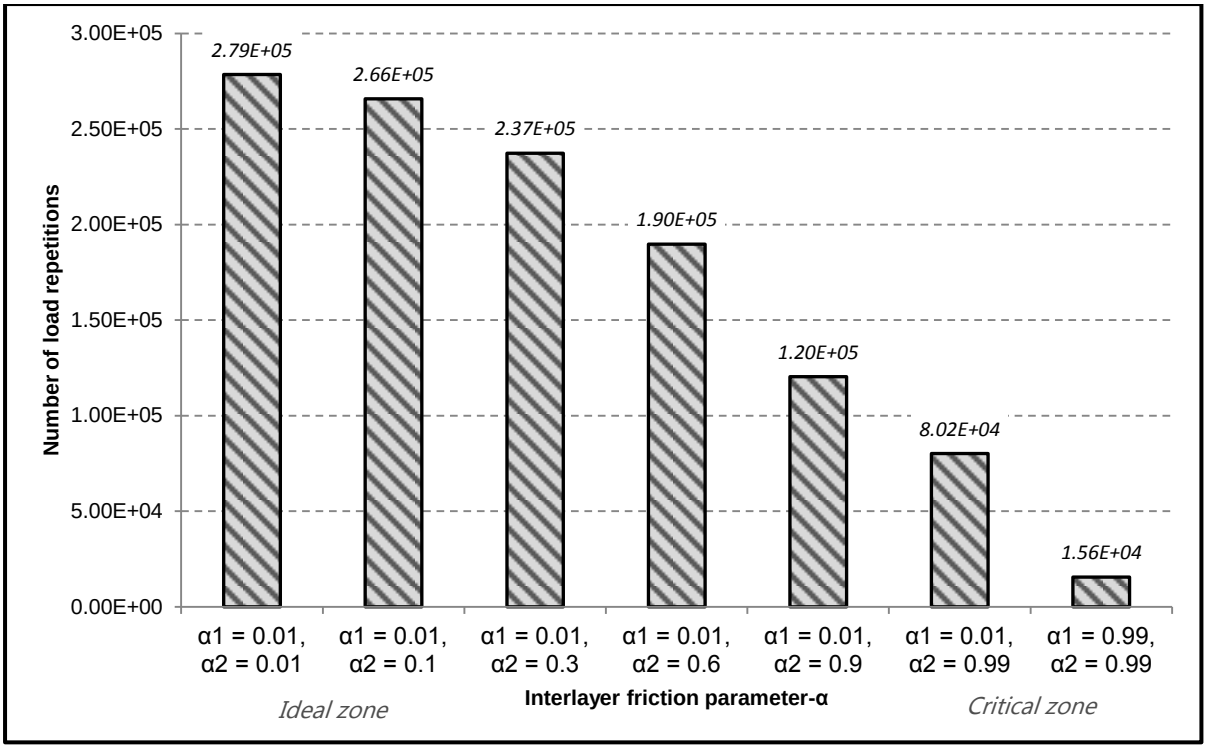

Figure 6-5: The influence of interlayer friction conditions on the life of the asphalt layer

II. Granular Base Layer

The granular base layer fails by gradual shear and permanent deformation due to repeated loading and densification. Principal stresses are the critical parameters which influence failure of the material. The concept of deviator stress ratio, which relates principal stresses to the ultimate shear strength of the material, is used to model the material behaviour.

For the purpose of accurate investigation on stress conditions across the base layer, the entire layer was subdivided into three sub-layers and each one was analysed separately.

Figure 6-6 shows the distribution of deviator stress ratios in the granular base, computed for different interlayer friction conditions.

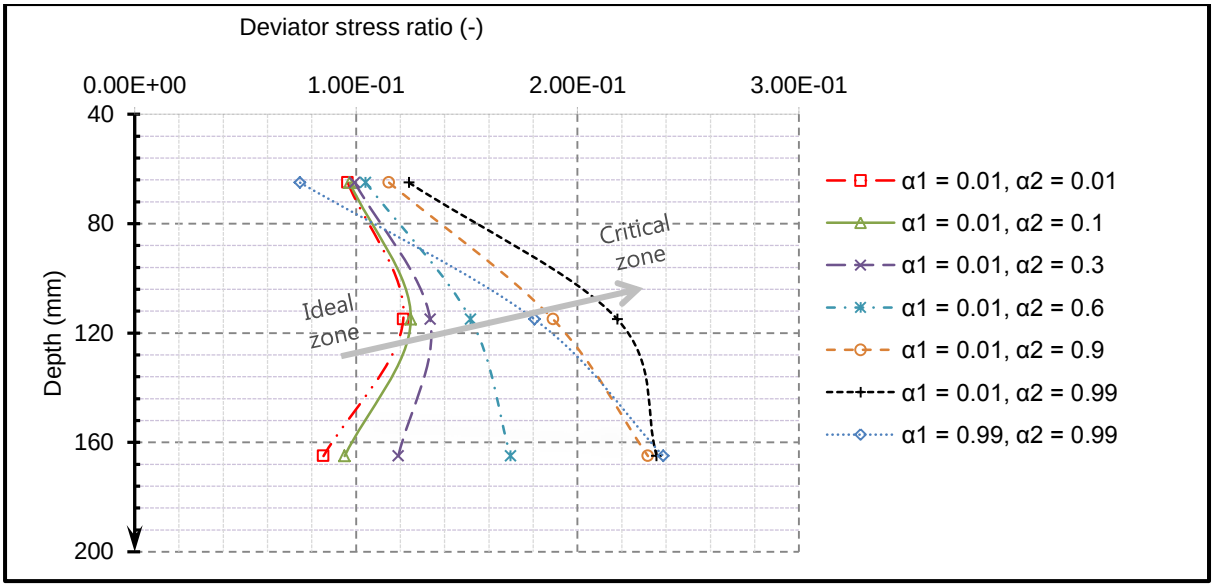

Figure 6-6: Deviator stress distribution in the base layer with variation in interlayer friction

It should be noted from Figure 6-6 that, in spite of the inexplicable results obtained for the worst case scenario ($\alpha_1 = \alpha_2 = 0.99$), the general trend of deviator stress ratios shifts to the right hand side as the interlayer friction parameters – α_2 approach 1. This behaviour demonstrates that the layer becomes more susceptible to shear failure as the interlayer friction diminishes.

The transfer function for a Category A road has been used to calculate the total number of load repetitions that each sub-layer could withstand before its failure. The summary of computed values of safety factor and load carrying capacity related to different interlayer friction conditions are presented in Table 6-6.

It should be noted that, at low friction parameters (i.e. $\alpha_2 < 0.3$), the failure position of the GB layer was not localised in the middle as stipulated by the SAMDM. The third sub-layer was found to be the weakest as revealed by the shear safety factors and corresponding lives presented in Table 6-6 and Figure 6-7. In Figure 6-7(a), lives of the GB is plotted against interlayer friction parameters when the middle sub-layer is unconditionally considered as the weakest. For the plot shown in Figure 6-7(b), the sub-layer with the lowest shear safety factor was considered the weakest.

In spite of the above-mentioned observations, the critical position and layer life were determined based on the SAMDM approach.

Table 6-6: Critical parameter and life of the granular base layer with variation in interlayer friction

Interlayer friction parameter - α	Safety factor against shear failure F		Life of the layer N_A	
	Middle sub-layer	Weakest sub-layer	Middle sub-layer	Weakest sub-layer
$\alpha_1 = 0.99$, $\alpha_2 = 0.99$	1.40	0.36	1.38E+07	2.65E+04
$\alpha_1 = 0.01$, $\alpha_2 = 0.99$	0.67	0.40	1.67E+05	3.37E+04
$\alpha_1 = 0.01$, $\alpha_2 = 0.9$	1.21	0.45	4.40E+06	4.69E+04
$\alpha_1 = 0.01$, $\alpha_2 = 0.6$	2.22	1.67	1.83E+09	7.07E+07
$\alpha_1 = 0.01$, $\alpha_2 = 0.3$	2.92	2.92	1.22E+11	1.22E+11
$\alpha_1 = 0.01$, $\alpha_2 = 0.1$	3.32	3.32	1.39E+12	1.39E+12
$\alpha_1 = 0.01$, $\alpha_2 = 0.01$	3.50	3.50	3.95E+12	3.95E+12

Additionally, both graphs presented in Figure 6-7 highlight the typical response of the granular base when a slight reduction in interlayer friction is allowed in the vicinity of the ideal zone. This reduction of the interlayer friction results in a quick drop of a layer's life.

The magnified perspective can be used to explain the behaviour of the GB when interlayer friction reduces. In fact, when the GB layer is placed on top of the CTSB in such a way that maximum adhesion is achieved, the two layers act in unison and the new equivalent layer thickness yield a significant load carrying capacity as can be visualised in Figure 6-7 for $\alpha_2 = 0.1$. However, if slight slip between the two layers is allowed to occur, immediate release of particles will take place due to unbound behaviour of the granular materials. Therefore the kneading action of the tyre on the pavement surface will induce granular particles to scramble and give way to the CTSB to endure the load. This reaction will quickly deteriorate the base layer as can be noticed in Figure 6-7 whereby the life of the layer was reduced considerably from 1.39E+12 to 1.22E+11 when the interlayer friction parameter was only changed from 0.1 to 0.3. This corresponds to an approximate loss of 91% in load carrying capacity.

From the above observations, it can be concluded that the structural performance of a GB layer is highly sensitive to the achievable interlayer adhesion conditions. A slight reduction in interlayer friction causes a significant reduction in the load carrying capacity of the layer.

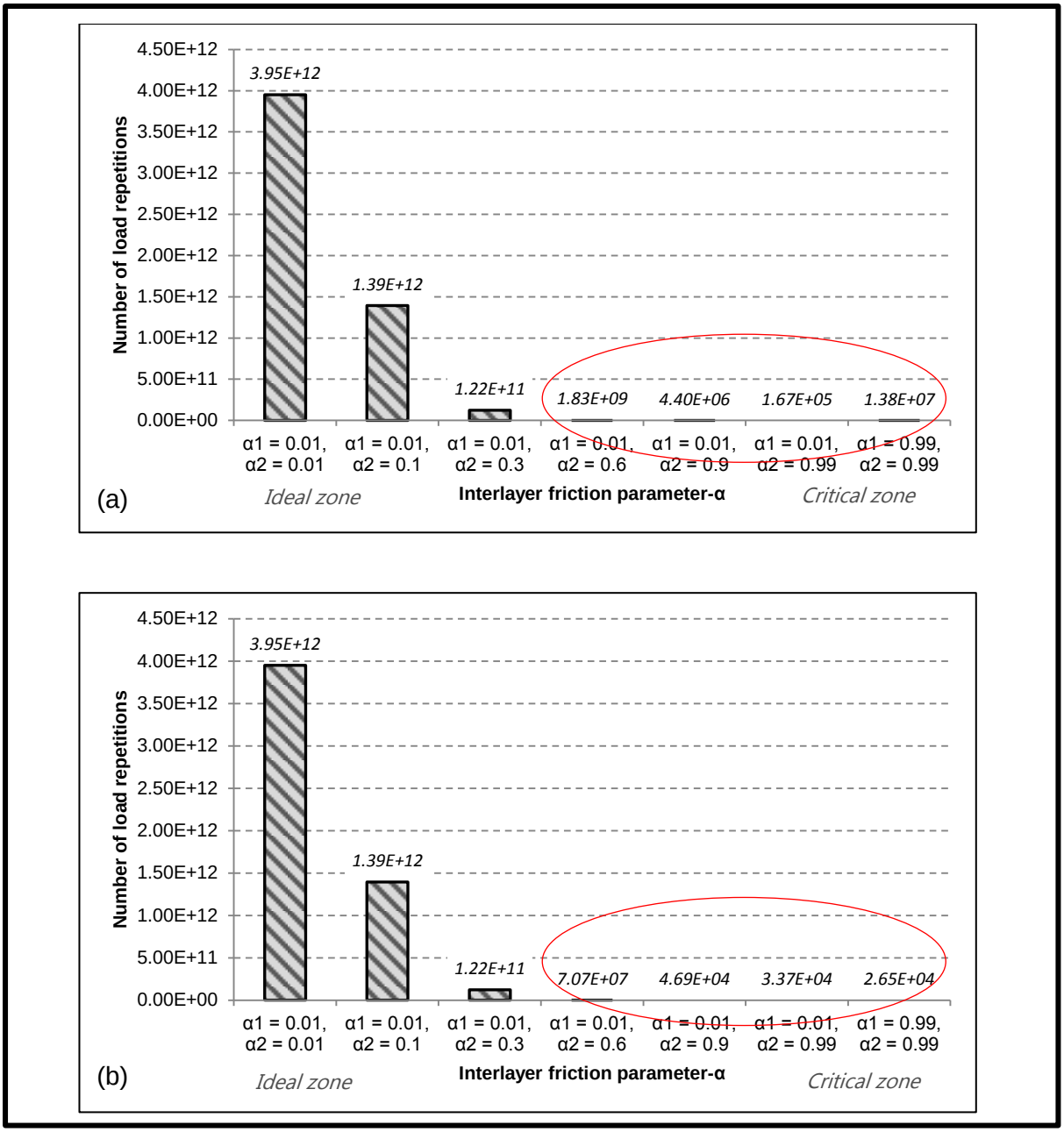

Figure 6-7: The influence of interlayer friction conditions on the life of the granular base layer; (a) estimated life when failure is localised in the middle of the layer; (b) estimated life if failure is localised in the weakest sub-layer.

III. Cement Treated Subbase Layer

Two types of failure modes linked to cement stabilised materials are effective fatigue at the bottom of the layer and crushing on the top. Two crushing conditions are identified, namely crush initiation with approximately 2 mm vertical deformation and advanced crushing with roughly 10 mm vertical deformation on top of the layer. Critical parameters which are used to compute the total number of load applications for failure to occur are; maximum tensile strain ε ($\mu\varepsilon$) at the bottom or within the layer for effective fatigue life and vertical compressive stress σ_v (kPa) on the top of the layer for crushing life.

In Table 6-7 values of the tensile strain in the cement stabilised layer and applied normal stress are presented. Each set of values corresponds to the specific interlayer friction parameter for the GB and CTSB interface. Associated life i.e. effective fatigue, crush initiation and advanced crushing, are also presented.

From Table 6-7, it is clear that, both the tensile strain in the CTSB layer, and vertical compressive stress on top of the layer, increase as the interlayer friction diminishes. This behaviour comes from poor interaction between layers which obstruct smooth distribution of stresses throughout the entire structure. As discussed earlier in this section, when there is no intimate contact between the GB and the CTSB, a considerable part of the load is taken by the CTSB since the GB exhibits low strength at relatively low confining pressure. At an early stage of adhesion (i.e. in the vicinity of the ideal zone), the CTSB can endure the load with limited decrease of life due to overstressing. This can be noticed in Figure 6-8 when α_2 ranges between 0.01 and 0.6. However, when the adhesion shifts to the critical condition, more abrasion and wearing will take place between the GB and CTSB layers. This phenomenon, in combination with brittle behaviour of the cement treated material, results in a quick reduction of the load carrying capacity of the layer. This is well presented in Figure 6-8 whereby the change of α_2 parameter from 0.6 to 0.9 induced the loss of layer life from 6.93E+06 to 1.63E+06. This corresponds to an approximately decrease of 76%.

Table 6-7: Critical parameter and life of the lightly cemented subbase with variation in interlayer friction

Interlayer friction parameter - α	Tensile strain in the cement stabilised layer ε_b ($\mu\varepsilon$)	Vertical stress at top of the CTSB (kPa)	Effective fatigue life N_{eff}	Crush initiation life N_{ci}	Advanced crushing life N_{ca}
α_1 = 0.99, α_2 = 0.99	2.27E+02	841.00	1.23E+05	7.13E+04	3.40E+05
α_1 = 0.01, α_2 = 0.99	2.10E+02	745.80	1.62E+05	1.38E+05	6.57E+05
α_1 = 0.01, α_2 = 0.9	1.93E+02	614.60	2.15E+05	3.43E+05	1.63E+06
α_1 = 0.01, α_2 = 0.6	1.63E+02	406.20	3.55E+05	1.45E+06	6.93E+06
α_1 = 0.01, α_2 = 0.3	1.46E+02	396.90	4.70E+05	1.55E+06	7.39E+06
α_1 = 0.01, α_2 = 0.1	1.37E+02	392.10	5.44E+05	1.60E+06	7.64E+06
α_1 = 0.01, α_2 = 0.01	1.34E+02	390.20	5.76E+05	1.63E+06	7.74E+06

Practically, it is unlikely to find the interlayer friction conditions associated with such an amount of slip ($\alpha_2 = 0.9$). But it is also essential to have an insight understanding of how this parameter affects the life of the layer.

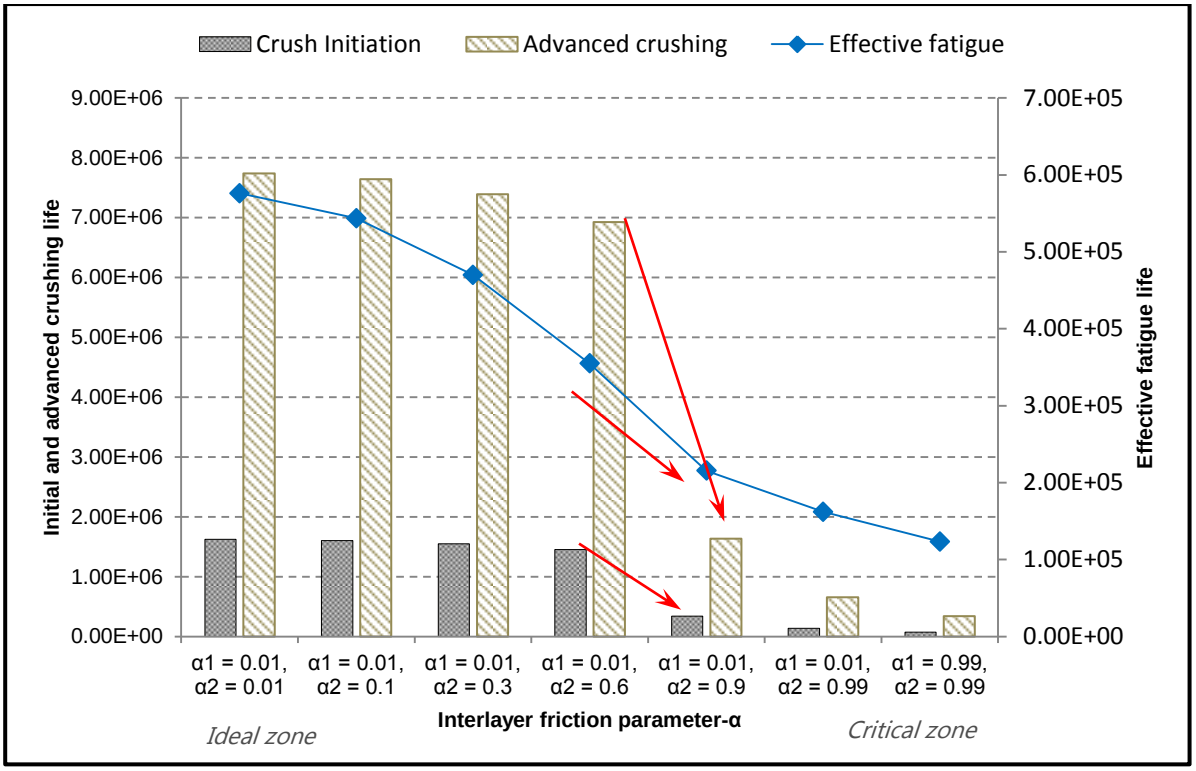

Figure 6-8: The influence of interlayer friction conditions on the performance of the CTSB layer

IV. Subgrade

The failure mode of the subgrade material is permanent deformation due to vertical compressive stress applied at the top of the layer. The induced vertical strain ε ($\mu\varepsilon$) is used to estimate the terminal conditions of the layer, either for 10 mm or 20 mm rut development.

In Table 6-8 values of the vertical strain ($\mu\varepsilon$) computed at the top of the layer are presented for specific interlayer friction conditions. Associated layer lives are also shown for both predefined terminal conditions. All the information presented in Table 6-8 is also plotted in Figure 6-9.

Table 6-8: Critical parameter and life of the subgrade layer with variation in interlayer friction

Interlayer friction parameter - α	Vertical strain at top of the layer ($\mu\varepsilon$)	Life of the layer for 10mm rut N_{10}	Life of the layer for 20mm rut N_{20}
$\alpha_1 = 0.99$, $\alpha_2 = 0.99$	6.53E+02	1.42E+05	1.42E+08
$\alpha_1 = 0.01$, $\alpha_2 = 0.99$	6.12E+02	2.70E+05	2.70E+08
$\alpha_1 = 0.01$, $\alpha_2 = 0.9$	5.43E+02	8.99E+05	8.99E+08
$\alpha_1 = 0.01$, $\alpha_2 = 0.6$	4.46E+02	6.41E+06	6.41E+09
$\alpha_1 = 0.01$, $\alpha_2 = 0.3$	3.98E+02	2.02E+07	2.02E+10
$\alpha_1 = 0.01$, $\alpha_2 = 0.1$	3.74E+02	3.71E+07	3.71E+10
$\alpha_1 = 0.01$, $\alpha_2 = 0.01$	3.65E+02	4.77E+07	4.77E+10

It should be noted from Figure 6-9 that loss of full adhesion between the GB and CTSB layers induced early development of surface ruts due to the deformation of the subgrade material.

In fact, lack of intimate interaction between the GB and CTSB induces high tensile strain at the bottom of the CTSB layer as previously discussed in this section. This develops more pressure on the surface of the layer underneath.

According to this design example, the worst case scenario of the interlayer friction ($\alpha_1 = \alpha_2 = 0.99$) was associated with a layer life of 1.42E+05 standard axles for 10 mm rut and 1.42E+08 standard axle load repetition for 20 mm rut as presented in Table 6-8. If one compares these values with others obtained from top layers as presented in Table 6-5, Table 6-6 and Table 6-7, it becomes clear that, for this particular case, the subgrade is not the most critical layer in the system. However, a reduction in the layer life was recorded when interlayer friction changed from full friction towards complete slip conditions as presented in Figure 6-9.

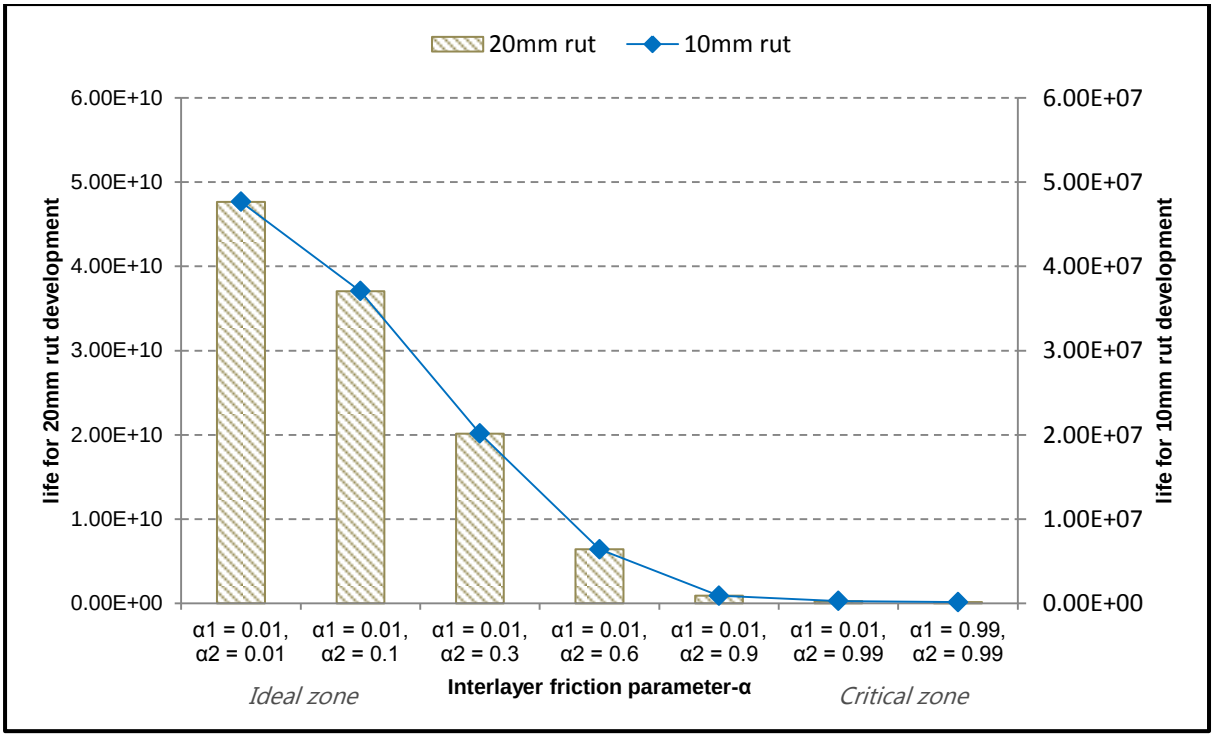

Figure 6-9: Life of the subgrade layer according to different interlayer friction conditions

6.4. CONCLUDING SUMMARY

The objective of this chapter was to establish the influence of interlayer adhesion between the GB and the CTSB, on the overall performance of the pavement. The investigation was based on the structural design of a typical pavement whereby various interlayer friction conditions were selected from ideal to critical conditions.

The analysis of stress-strain distribution was carried out with the BISAR software and pavement performance was estimated by using specific critical parameters and predefined transfer functions.

As mentioned in Chapter 4, the routine construction process of the GB and CTSB involves compaction of the CTSB materials and curing it for 7 days before placing the GB material. The top surface of the subbase layer is not scarified. In this study, this routine field practice was simulated by testing the interlayer when the CTSB layer was not scarified (i.e. quasi-smooth).

The correlation of the achievable adhesion conditions and the interlayer friction parameter used in BISAR software was accomplished by using the correlation chart shown in Figure 6-1. According to the laboratory test results presented in Chapter 5, the achievable adhesion ratios β associated with a quasi-smooth CTSB layer for shear, friction and dilation were 0.7, 0.7 and 0.4 respectively (see Table 6-1). Correlation of these values to the interlayer friction parameter α shows that the interlayer friction conditions of the GB and quasi-smooth CTSB

corresponds to α parameter ranging between 0.5 and 0.7. Figure 6-10 presents the associated number of axle loads for scarified and quasi-smooth CTSB. The total number of standard axles to failure are simulated by α = 0.1 for the scarified CTSB and the average between 0.5 and 0.7 or α = 0.6 for the quasi-smooth CTSB.

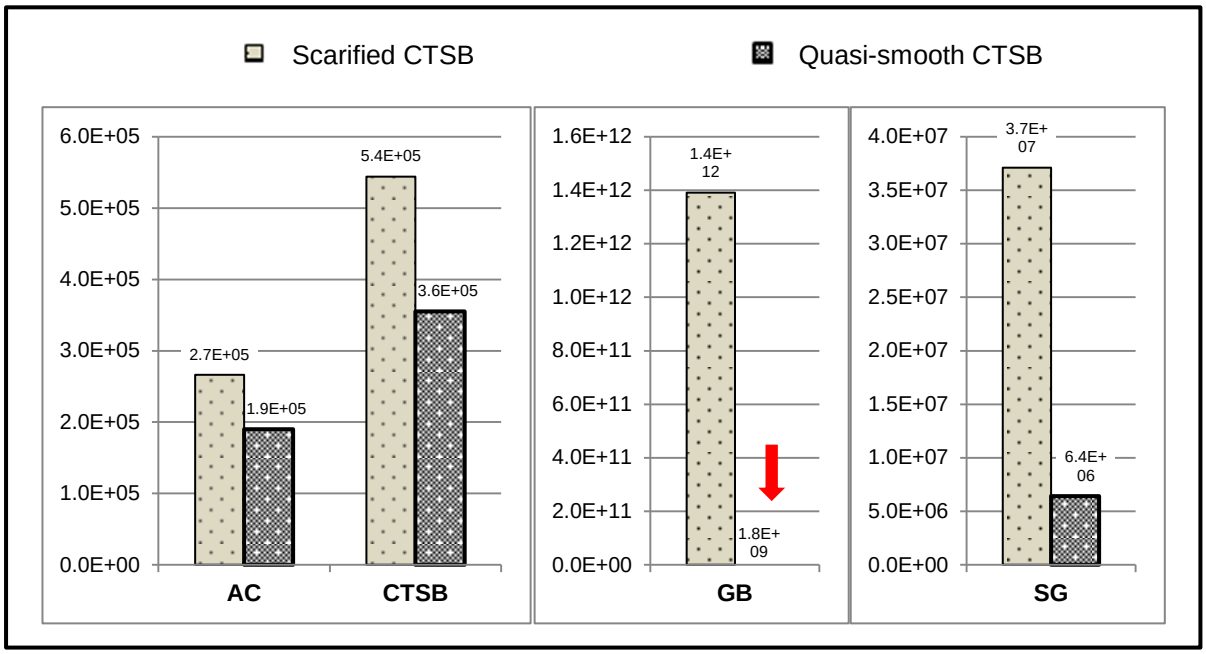

Figure 6-10: Comparison of total number of load repetitions for scarified and quasi-smooth CTSB

Based on the results of the analysis presented in this chapter, the following conclusions can be drawn:

- The distribution of stress and strain in the pavement structure is significantly influenced by the interlayer adhesion conditions. The general trend showed an increase in stress and strain across all layers when the interlayer friction between the GB and the CTSB changes from full friction towards the complete slip. However, the GB was found to be highly sensitive to poor adhesion. This was related to its mechanical behaviour, physical composition and *insitu* conditions.
- The influence of poor adhesion between the GB and the CTSB on the pavement performance was noticeable upon each layer of the pavement structure. The life of every layer showed a substantial decrease when partial friction was allowed. The GB showed early failure compared to other layers.
- From the results of the correlation between the achievable adhesion ratio β and the interlayer adhesion parameter α as presented in Figure 6-10, it is apparent that the interlayer adhesion strength between the GB and the CTSB significantly influences the performance of each individual layer in the pavement structure. The total number of standard axles that every layer can withstand before failure reduces considerably when

the GB is laid on top of non-scarified CTSB. For this design example, the GB layer was found to be more affected by the adhesion conditions.

Chapter 7

CONCLUSIONS AND RECOMMENDATIONS

The main purpose of this study was to investigate the achievable interlayer adhesion strength between the granular base (GB) and the cement treated subbase (CTSB) layers and assess its influence on the general performance of the pavement structure. Various testing methods and analysis approaches presented in Chapter 4 and Chapter 5 were followed to achieve the study objectives. A typical structural design demonstrated in Chapter 6 served as a basis to acquire understanding of the influence of interlayer adhesion on the pavement performance, especially for the routine construction technique used in the field.

This chapter provides a general summary of the main findings since detailed observations are provided in the above-mentioned chapters. Recommendations to further researchers are also presented.

7.1. CONCLUSIONS

- The interlayer shear strength between the cement treated subbase (CTSB) and granular base (GB) increases when the vertical normal pressure increases.
- The increase of moisture content in the pavement structure induces the general decrease of interlayer shear strength between the GB and CTSB.
- Practically the staged construction procedure of CTSB and GB involves laying base materials on a previously hardened CTSB layer. This prohibits the unification of the two layers. However, scarifying the CTSB top surface before curing the layer and laying the GB improves the intimate contact between the two layers and results in unison interaction.
- Generally, most of the laboratory tests, related to the characterisation of pavement construction materials cannot go beyond 19 mm maximum aggregate size due to the restricted size of the testing equipment. Practically, the maximum aggregate size in pavement layers goes up to 37 mm. The shear testing setup used for this study allowed the increase of the maximum size of the aggregate from 19 mm to 26 mm in the CTSB.

  From the general trend of the results, it can be concluded that increasing the maximum aggregate size in the CTSB improves the shear interaction between the GB and CTSB.
- The current construction practice involves laying the GB on top of the CTSB without scarification. According to the results of this study, the associated interlayer shear

strength is significantly lower compared to the inlayer shear strength across the GB. This therefore exhibits the weakness of the interface to sustain shear flow between GB and CTSB in case it is necessary.

- Scarifying the top surface of the CTSB before curing the layer and laying the GB offers the interlayer shear strength which is nearly equal to the inlayer shear strength across the GB layer. This thus confirms high interlayer adhesion due to scarification.
- According to the results of this study, there is no special impact of the CTSB surface conditions on the interlayer shear strength when the pavement structure has high moisture content.
- The distribution of traffic induced stress and strain across the pavement structure is significantly influenced by the interlayer shear strength between the GB and CTSB. The stress-strain pattern in the GB layer is highly sensitive to a slight change in adhesion conditions, comparing to other layers.
- The life of every layer in the pavement structure exhibited a substantial decrease due to the lack of full adhesion between the GB and CTSB. The GB layer showed a faster deterioration in relation to other layers.
- Correlation of the achievable adhesion between the GB and CTSB with the interlayer friction parameter showed that the routine construction process followed in the field induces a significant reduction in the number of standard axle loads that a layer can withstand before reaching specific failure conditions.

In summary, it can be concluded that the interlayer shear condition between the granular base and the cement treated subbase significantly influences the overall pavement performance. The achievable interlayer adhesion depends on the maximum size of the aggregate in the layers, the surface finishing of the cement treated subbase, the confining pressure and the moisture condition. Scarification of the CTSB before laying the GB results in unison interaction between the two layers. This interaction is intensified by the increase of confinement and weakened by water ingress.

7.2. RECOMMENDATIONS

- The direct shear investigation conducted in this study was limited to samples compacted at 100% Mod AASHTO, it is therefore recommended for further researchers to assess the effect of the compaction degree on the interlayer adhesion behaviour by considering various compaction efforts.
- The general trend shows the increase of interlayer adhesion strength when the maximum size of the aggregate in the CTSB increases. However, due to the size of testing equipment, this study was limited to 26mm maximum aggregate. Therefore it is recommended that a testing set-up is developed which can accommodate a typical maximum grain size applicable to a South African pavement structure. This will help to acquire the most practical interlayer conditions between then GB and the CTSB.
- The direct shear set up used for this study allowed approximately 2 mm free space around the specimen. Since for all tests conducted, the sample was vertically confined, this space did not affect the results as long as the sample was well compacted and cured. However, a testing setup allowing both vertical and horizontal confinement should be more suitable.
- Practically, the pavement structure is subjected to multiple dynamic loads. A static load application simulated by the shear box is unlikely to cause the interface to fail. To achieve a detailed analysis of failure mode, it is recommended that a repeated loading system is developed which allows investigating the resilient behaviour of the interface between the GB and the CTSB.
- The practical investigation conducted in this study was based on laboratory prepared samples. To acquire a deep knowledge of interlayer performance, field trials on a trafficked pavement section are recommended.
- After realising the influence of scarification on the improvement of interlayer shear strength between the GB and the CTSB, it is recommended that this practice be incorporated in the routine construction practice.
- To acquire deep clarification on the interlayer shear behaviour, this study should be supplemented by a linear and non-linear finite element analysis.
- With the knowledge of the significant influence of interlayer shear strength on pavement performance, different research projects should be mobilised to deepen the understanding of the subject and to develop coherent and scientifically based views. This will give rise to technical specifications and guidelines to be followed for achieving proper shear interaction in the field.

REFERENCES

Abd El Halim, A., Rickards, I., Haas, R. and Nabi, R. 1997. Evaluation of Design and Construction Effects on Asphalt Pavements Performance through a Portable In-Situ Shear Test Device. *Paper presented at Eighth International Conference on Asphalt Pavements,* 2: 1311-27.

Box, G.E., Hunter, J.S. & Hunter, W.G. 2005. Statistics for Experimenters: Design, Innovation, and Discovery. *AMC,* 10

Burmister, D.M. 1945. The General Theory of Stresses and Displacements in Layered Systems. I. *Journal of Applied Physics,* 16(2).

Canestrari, F., Ferrotti, G., Partl, M.N. & Santagata, E. 2005. Advanced Testing and Characterization of Interlayer Shear Resistance. Transportation Research Record: Journal of the Transportation Research Board, 1929(1).

Canestrari, F. & Santagata, E. 2005. Temperature Effects on the Shear Behaviour of Tack Coat Emulsions used in Flexible Pavements. *International Journal of Pavement Engineering,* 6(1): 39-46.

Choi, Y., Sutanto, M., Collop, A. & Airey, G. 2005. Bond between Asphalt Layers. *Project Report to the UK Highways Agency, Scott Wilson Pavement Engineering Ltd., Nottingham, UK.*

Collop, A., Thom, N. & Sangiorgi, C. 2003. Assessment of Bond Condition using the Leutner Shear Test. *Proceedings of the ICE-Transport,* 156(4): 211-217.

Crispino, M., Festa, B., Giannattasio, P. and Nicolosi, V. 1997. Evaluation of the Interaction between the Asphalt Concrete Layers by a New Dynamic Test. *Paper presented at Eighth International Conference on Asphalt Pavements*, 1: 741-754.

De Beer, M., Maina, J. & Netterberg, F. 2012. Mechanistic Modelling of Weak Interlayers in Flexible and Semi-Flexible Road Pavements: Part 2. *Journal of the South African Institution of Civil Engineering,* 54(1): 43-54.

De Beer, M. & Van der Merwe, C. 1991. *Use of the dynamic cone penetrometer (DCP) in the design of road structures.* Pavement Engineering Technology, Division of Roads and Transport Technology.

Diakhaté, M., Petit, C., Millien, A., Phelipot-Mardelé, A., Pouteau, B. and Goacolou, H. 2007. Comparison of Direct Shear and Torque Tests for Determining Viscoelastic Shear Behaviour of Tack Coats. *Paper presented at Proceedings of the International Conference on advanced characterization of pavement and soil engineering materials,* 282-290.

Diakhaté, M. 2007. Fatigue et comportement des couches d'accrochage dans les structures de chaussée*. Thèse de doctorat. Limoges: Université de Limoges.*

D'Andrea, A. & Tozzo, C. 2012. Interlayer Shear Failure Evolution with Different Test Equipments. Procedia-Social and Behavioral Sciences, 53

D'Andrea, A., Tozzo, C., Boschetto, A. & Bottini, L. 2013. Interface Roughness Parameters and Shear Strength. Modern Applied Science, 7(10).

Ebels, L. 2008. *Characterisation of material properties and behaviour of cold bituminous mixtures for road pavements*. PhD dissertation. Stellenbosch: University of Stellenbosch.

Edwards, J.P. 2007. *Laboratory characterisation of pavement foundation materials.* Doctoral dissertation. Loughborough: Loughborough University.

Freeme, C. 1983. Evaluation of Pavement Behaviour for Major Rehabilitation of Roads. *National Institute for Transport and Road Research Technical Report RP/19/83, Pretoria, CSIR,*

Geocomp. 2012. Shear Trac III system, Load frame system for Running Fully Automated Direct and Interface Shear Tests on Soil and Geosynthetics using Windows XP/Vista/7. User's Manual. Geocomp Corporation. USA

Hariyadi, E.S., Aurum, K.P. and Subagio, B.S. 2013. Theoretical Study of Bonding Condition at the Interface between Asphalt Pavement Layers. *Paper presented at Proceedings of the Eastern Asia Society for Transportation Studies*.

Hu, X. & Walubita, L.F. 2010. Effects of Layer Interfacial Bonding Conditions on the Mechanistic Responses in Asphalt Pavements. *Journal of Transportation Engineering,* 137(1): 28-36.

Hugo, F. & Martin, A. 2004. Significant Findings from Full-Scale Accelerated Pavement Testing. Transportation Research Board (325): 211p

Jaskuła, P. 2014. Influence of Compaction Effectiveness on Interlayer Bonding of Asphalt Layers.

Jenkins, J.K. 2013. Hitchhiker's guide to pavement engineering. Pavement material I unpublished lecture notes. Stellenbosch: Stellenbosch University.

Jooste, F. 2004. A Re-Evaluation of Some Aspects of the Mechanistic-Empirical Design Approach. *Paper presented at Proceedings of the 8th Conference on Asphalt Pavements for Southern Africa (CAPSA'04)*.

Khweir, K. & Fordyce, D. 2003. Influence of Layer Bonding on the Prediction of Pavement Life. *Proceedings of the ICE-Transport,* 156(2): 73-83.

Kruntcheva, M.R., Collop, A.C. & Thom, N.H. 2005. Effect of Bond Condition on Flexible Pavement Performance. *Journal of Transportation Engineering,* 131(11): 880-888.

Kruntcheva, M.R., Collop, A.C. & Thom, N.H. 2004. Feasibility of Assessing Bond Condition of Asphalt Concrete Layers with Dynamic Nondestructive Testing. *Journal of Transportation Engineering,* 130(4): 510-518.

Kruntcheva, M., Collop, A. & Thom, N. 2000. Theoretical and Practical Aspects of the Importance of Bonding in a Pavement Structure. *Project report PGR,* 8

Lambe, T. & Whitman, R. 1969. *Soil Mechanics*. New York: John Wiley & Sons.

LeKarp, F., Isacsson, U. & Dawson, A. 2000. State of the Art. I: Resilient Response of Unbound Aggregates. *Journal of Transportation Engineering,* 126(1): 66-75.

Lepert, P., Poilane, J. and Bats-Villard, M. 1992. Evaluation of various Field Measurement Techniques for the Assessment of Pavement Interface Condition. Paper presented at International Conference on Asphalt Pavements, 7th, 1992, Nottingham, United Kingdom.

Leutner, R. 1979. Untersuchung Des Schichtenverbundes Beim Bituminösen Oberbau. *Bitumen,* 41(3): 84-91.

Mohammad, L.N., Bae, A., Elseifi, M.A., Button, J.W. & Scherocman, J.A. 2009. Interface Shear Strength Characteristics of Emulsified Tack Coats. *Journal of the Association of Asphalt Paving Technologists,* 78: 249-278.

Molenaar, A. 2007. Design of Flexible Pavement, Lecture Note CT 4860 Structural Pavement Design. Delft: Delft University of Technology.

Morton, B.S., Luttig, E., Horak, E. and Visser, A. 2004. The Effect of Axle Load Spectra and Tyre Inflation Pressures on Standard Pavement Design Methods. Paper presented at 8th Conference of Asphalt Pavements of Southern Africa (CAPSA).

Sutanto, MMuslich, S. 2010b. *Assessment of bond between asphalt layers,* PhD dissertation. Nottingham: Nottingham University.

Naudé, W. 1999. Trade in Transport Services: South Africa and the General Agreement on Trade in Services. *Pretoria: Trade and Industrial Policy Strategies* [Online]. Available: http://www.tips.org.za/files/413.pdf [18.10.2014]

Nazarian, S., Baker, M.R. & Crain, K. 1993. *Development and testing of a seismic pavement analyzer* [Online]. Available: http://onlinepubs.trb.org/onlinepubs/shrp/SHRP-H-375.pdf [18.10.2014]

Netterberg, F. & de Beer, M. 2012. Weak Interlayers in Flexible and Semi-Flexible Road Pavements: Part 1. *Journal of the South African Institution of Civil Engineering,* 54(1): 33-42.

Papagiannakis, A. & Masad, E.A. 2008. *Pavement design and materials.* John Wiley & Sons

Peshkin, D. 1994. Pavement Analysis and Design Checks. *National Highway Institute, US Department of Transportation,*

Raab, C. and Partl, M.N. 2004. Interlayer Shear Performance: Experience with Different Pavement Structures. Paper presented at Proceedings of the 3rd Eurasphalt and Eurobitume Congress Held Vienna, May 2004.

Raab, C. & Partl, M. 1999. Methoden zur Beurteilung des Schichtenverbunds von Asphaltbelägen [Methods to determine the bond of asphalt pavements].*ASTRA-Project FA 12/94,*

Raab, C. 2011. *Development of a Framework for Standardisation of Interlayer Bond of Asphalt Pavements,* PhD dissertation. Carleton: Carleton University.

Raab, C., Abd El Halim, A. & Partl, M.N. 2012. Interlayer Bond Testing using a Model Material. *Construction and Building Materials,* 26(1): 190-199.

Raab, C., Partl, M.N. & El Halim, O.A. 2009. Evaluation of Interlayer Shear Bond Devices for Asphalt Pavements. *Baltic Journal of Road and Bridge Engineering,* 4(4): 186-195.

Roffe, J. and Chaignon, F. 2002. Characterisation Tests on Bond Coats: Worldwide Study, Impact, Tests, Recommendations. Paper presented at Proceedings of the 3rd International Conference on Bituminous Mixtures and Pavements, Held Thessaloniki, Greece, November 2002.

Romain, J. 1968. Contraintes, deformations et deflexions dans les systemes quadricouches elastiques. *Institut Francais des Sciences et Technologies des Transports, de l'Aménagement et des Réseaux (IFSTTAR)*,

Romanoschi, S.A. and Metcalf, J. 2002. The Characterization of Pavement Layer Interfaces. Paper presented at Ninth International Conference on Asphalt Pavements.

Ross, G. 2004. *Romance of cape mountain passes.* New Africa Books

Santagata, F.A., Ferrotti, G., Partl, M.N. & Canestrari, F. 2009. Statistical Investigation of Two Different Interlayer Shear Test Methods. *Materials and Structures,* 42(6): 705-714.

SAPEM. 2013. South African Pavement Engineering Manual 1st edition. *South African National Roads Agency Ltd*, Pretoria, Republic of South Africa.

Shell, 1998. BISAR User Manual. Verison3.0, Bitumen Business Group, Shell International Oil Products B.V., Amsterdam, Netherlands.

Shirley, Sponholtz. 2014. *A brief history of road building.* [Online]. Available: http://www.triplenine.org/articles/roadbuilding.asp [16.05.2014]

Sholar, G.A., Page, G.C., Musselman, J.A., Upshaw, P.B. & Moseley, H.L. 2004. Preliminary Investigation of a Test Method to Evaluate Bond Strength of Bituminous Tack Coats (With Discussion). *Journal of the Association of Asphalt Paving Technologists,* 73: 771-806.

Siang, Alvin John Lim Meng, Wijeyesekera, D.C. & Zainorabidin, A. 2013. The Effect of Particle Morphology of Sand on the Relationship between Shear Strength and Dilatancy Characteristics. *Electronic Journal of Geotechnical Engineering,* 18: 1537-1546

Simoni, A. & Houlsby, G.T. 2006. The Direct Shear Strength and Dilatancy of sand–gravel Mixtures. *Geotechnical & Geological Engineering,* 24(3): 523-549.

Simonin, J. and Maisonneuve, P. 1998. Dynamic Investigations in Assessing the Structural Condition of Pavements. Paper presented at Proceedings of 5th International Conference on the Bearing Capacity of Roads and Airfields, Trondheim.

Strategic Highway Research Program, s. a. [Online]. Available:

http://www.ndtoolbox.org/content/bridge/ie-equipment [17.10.2014].

Sutanto, M., Collop, A., Airey, G., Elliott, R. and Choi, Y. 2006. Laboratory Measurement of Bond between Asphalt Layers. Paper presented at Proceedings of the 5th International Conference on Research and Practical Applications Using Wastes and Secondary Materials in Pavement Engineering Held 22-23 February 2006, Liverpool, UK-Vol 1-Day One, Vol 2-Day Two.

Tashman, L., Nam, K. & Papagiannakis, A. 2006. *Evaluation of the influence of tack coat construction factors on the bond strength between pavement layers,*

Theyse, H., De Beer, M., Maina, J. & Kannemeyer, L. 2011. Interim Revision of the South African Mechanistic-Empirical Pavement Design Method for Flexible Pavements.

Theyse, H., De Beer, M., Prozzi, J. & Semmelink, C. 1995. TRH4 Revision 1995, Phase I: Updating the Transfer Functions for the South African Mechanistic Design Method.

Theyse, H., De Beer, M. & Rust, F. 1996. Overview of South African Mechanistic Pavement Design Method. *Transportation Research Record: Journal of the Transportation Research Board,* 1539: 6-17.

Theyse, H. and Muthen, M. 2000. Pavement Analysis and Design Software (PADS) Based on the South African Mechanistic-Empirical Design Method. Paper presented at South African Transport Conference (SATC). Action in Transport for the new Millennium.

Timoshenko, S. & Goodier, J. 1951. *Theory of Elasticity*. New York: Mc Graw-Hill Book Company.

Transportation Officials. 1993. *AASHTO guide for design of pavement structures.* AASHTO

TRH4. 1996. *Structural design of flexible pavements for interurban and rural roads.* Pretoria, South Africa: Department of Transport

TRH14. 1985. *Guidelines for road construction materials.* Pretoria, South Africa: Department of Transport

Tschegg, E.K., Kroyer, G., Tan, D., Stanzl-Tschegg, S.E. & Litzka, J. 1995. Investigation of Bonding between Asphalt Layers on Road Construction. *Journal of Transportation Engineering,* 121(4): 309-316.

Ullidtz, P. 1987. *Pavement analysis. Developments in civil engineering,* Elsevier.

Uzan, J. 1976. Influence of the interface condition on stress distribution in a layered system (abridgement). *Transportation Research Record,* (616): 71-73.

Uzan, J., Livneh, M. and Eshed, Y. 1978. Investigation of Adhesion Properties between Asphaltic-Concrete Layers. Paper presented at Association of Asphalt Paving Technologists Proc.

Walsh, I. & Williams, J. 2001. HAPAS Certificates for Procurement of Thin Surfacing. *Highways and transportation,* 48(7-8).

Whiffin, A. and Lister, N. 1962. The Application of Elastic Theory to Flexible Pavements. Paper presented at International Conference on the Structural Design of Asphalt Pavements.

Willis, J.R. & Timm, D.H. 2007. Forensic Investigation of Debonding in Rich Bottom Pavement. *Transportation Research Record: Journal of the Transportation Research Board,* 2040(1): 107-114.

Ziari, H. & Khabiri, M.M. 2007. Interface Condition Influence on Prediction of Flexible Pavement Life. *Journal of Civil Engineering and Management,* 13(1): 71-76.

APPENDICES

APPENDIX A: MATERIAL CHARACTERISATION AND SHEAR TESTS GRAPHS

A.1. MOD AASHTO COMPACTION FOR G2

A.2. CALIFORNIA BEARING RATIO FOR G5

A.3. DILATION RATE CURVES

APPENDIX B: FACTORIAL DESIGN ANALYSIS

APPENDIX C: CALCULATION OF INTERLAYER SHEAR REACTION MODULUS K_s

APPENDIX D: TEST DATA AND WORK SHEETS FOR DIRECT SHEAR TESTING

APPENDIX A: MATERIAL CHARACTERISATION AND SHEAR TEST GRAPHS

A.1: MOD AASHTO COMPACTION

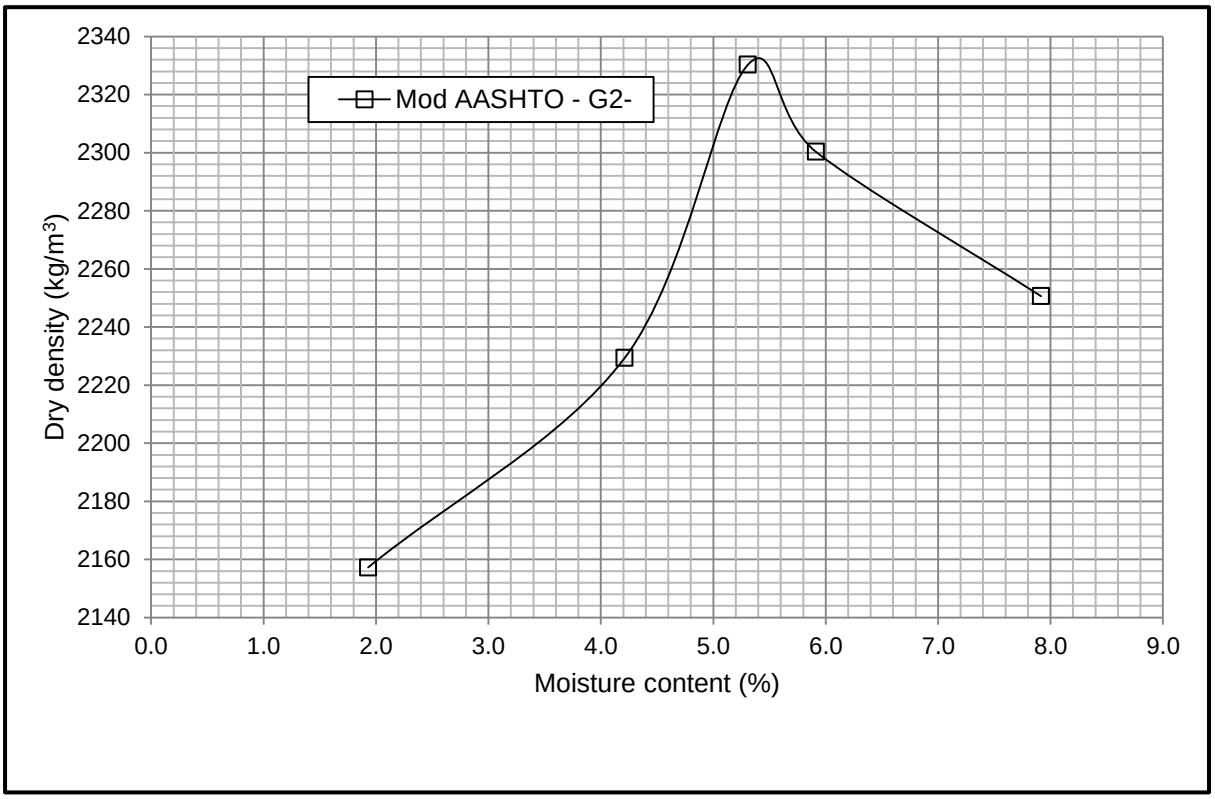

Figure A-1: Mod AASHTO curve for G2

A.2: CALIFORNIA BEARING RATIO FOR G5

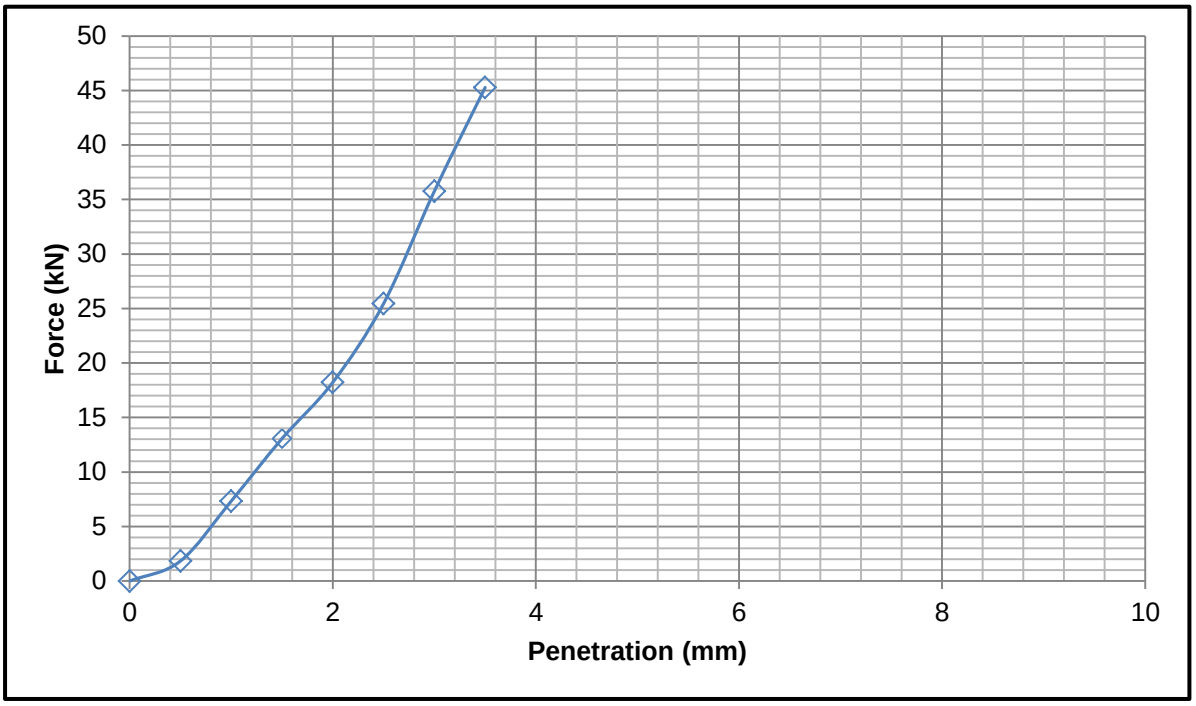

Figure A-2-1: CBR curve, 4.536kg tamper, 457.2 mm drop, 5 layers and 55 blows per layer

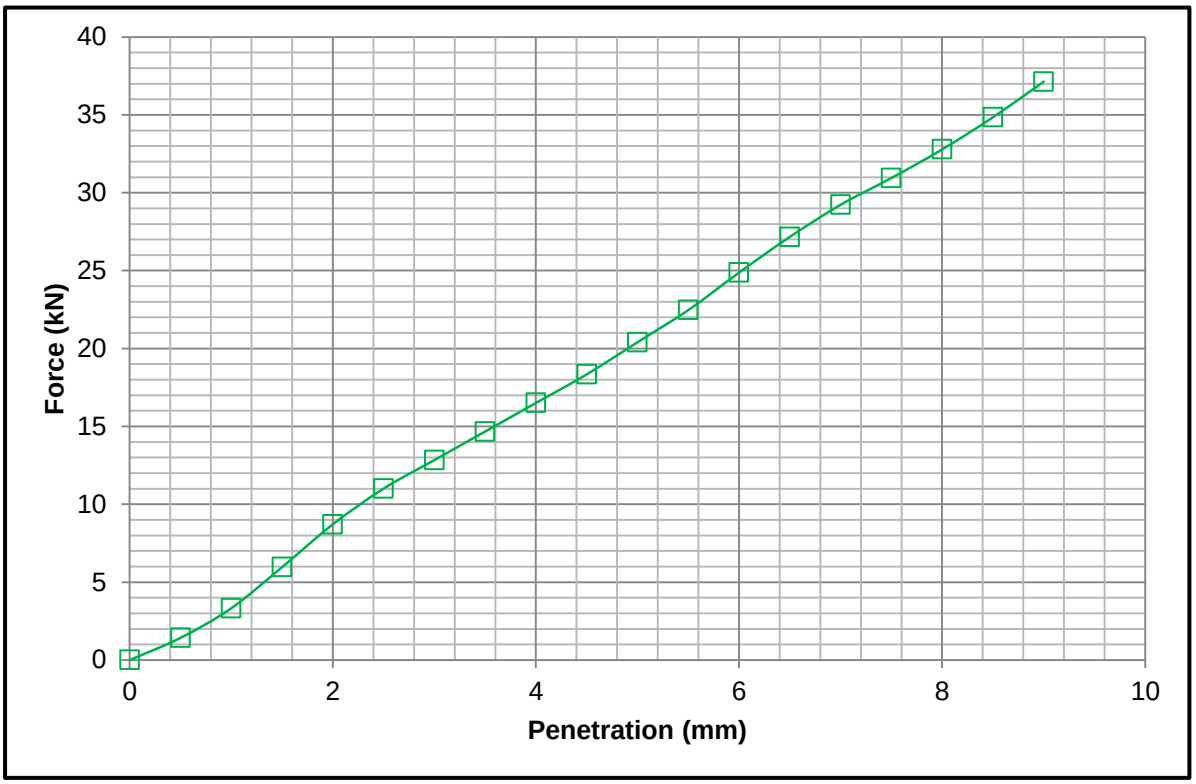

Figure A-2-2: CBR curve, 4.536kg tamper, 457.2 mm drop, 5 layers and 25 blows per layer

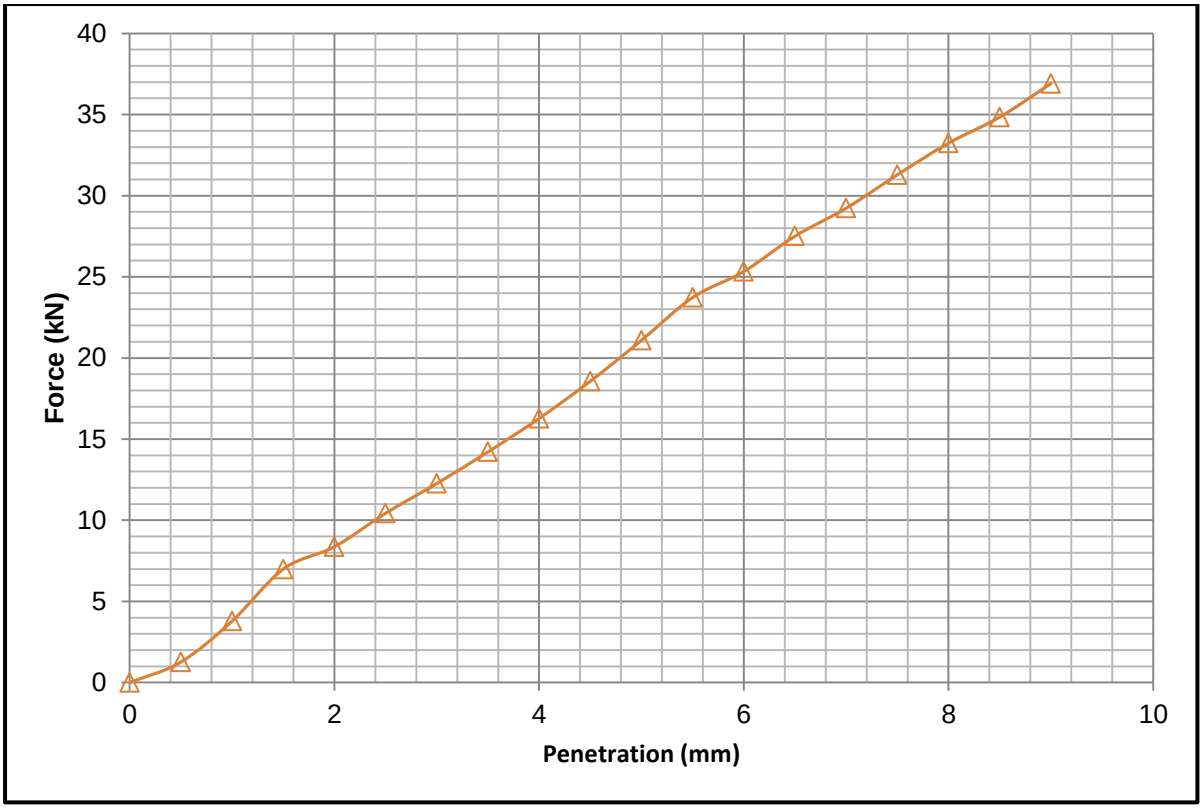

Figure A-2-3: CBR curve, 2.495 tamper, 304.8 mm drop, 3 layers and 55 blows per layer

A.3. DILATION RATE CURVES

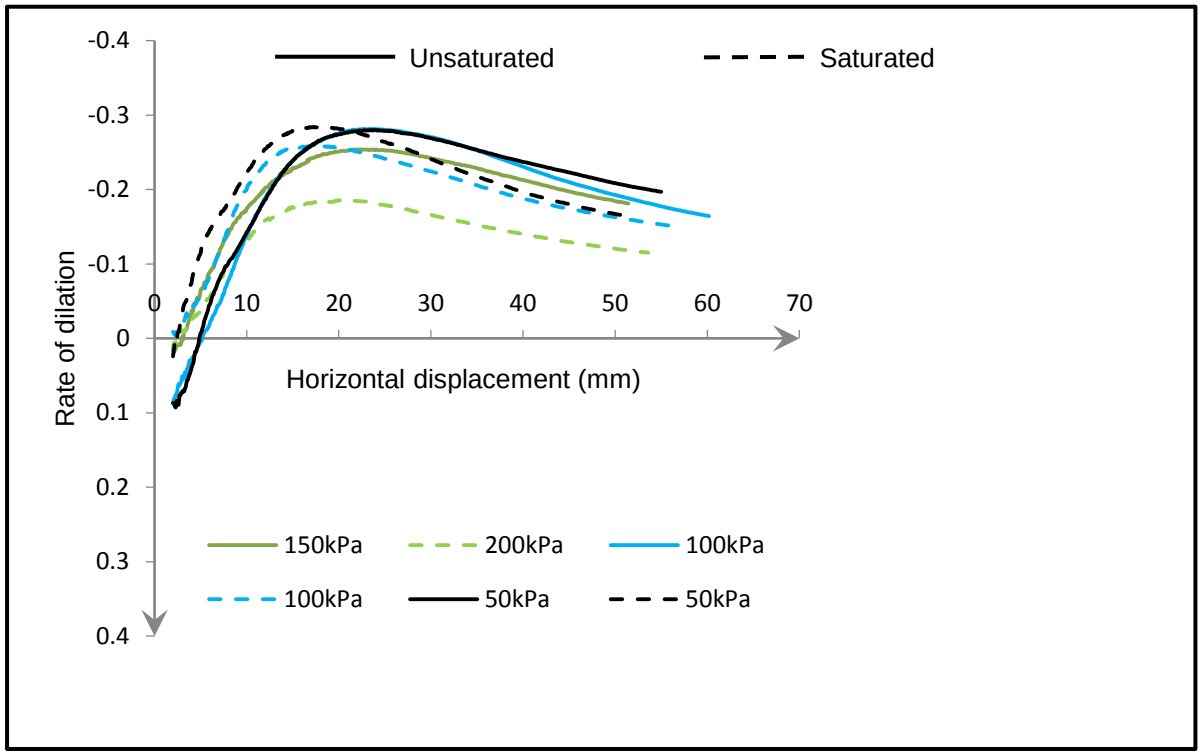

FigureA-3-1: Interlayer shear; CTSB scarified with 19mm maximum aggregate size

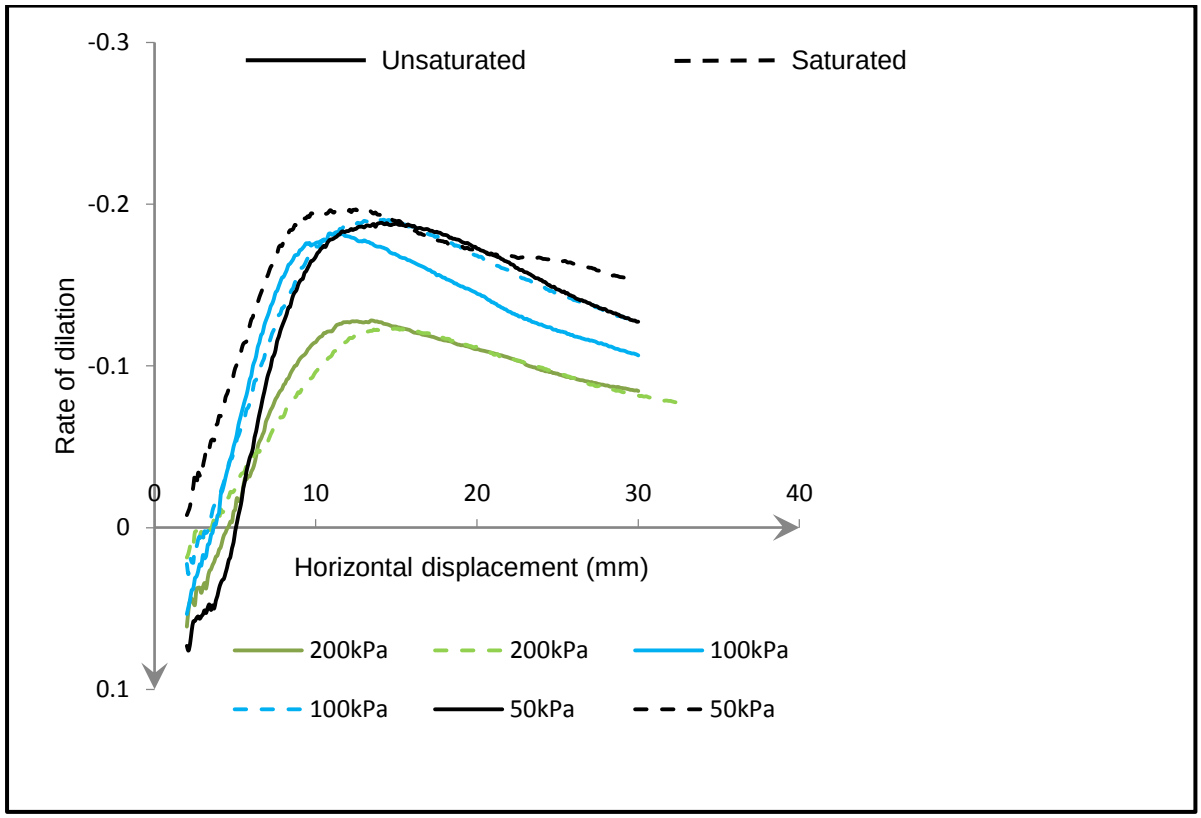

Figure A-3-2: Interlayer shear test; CTSB quasi-smooth with 19mm maximum aggregate size

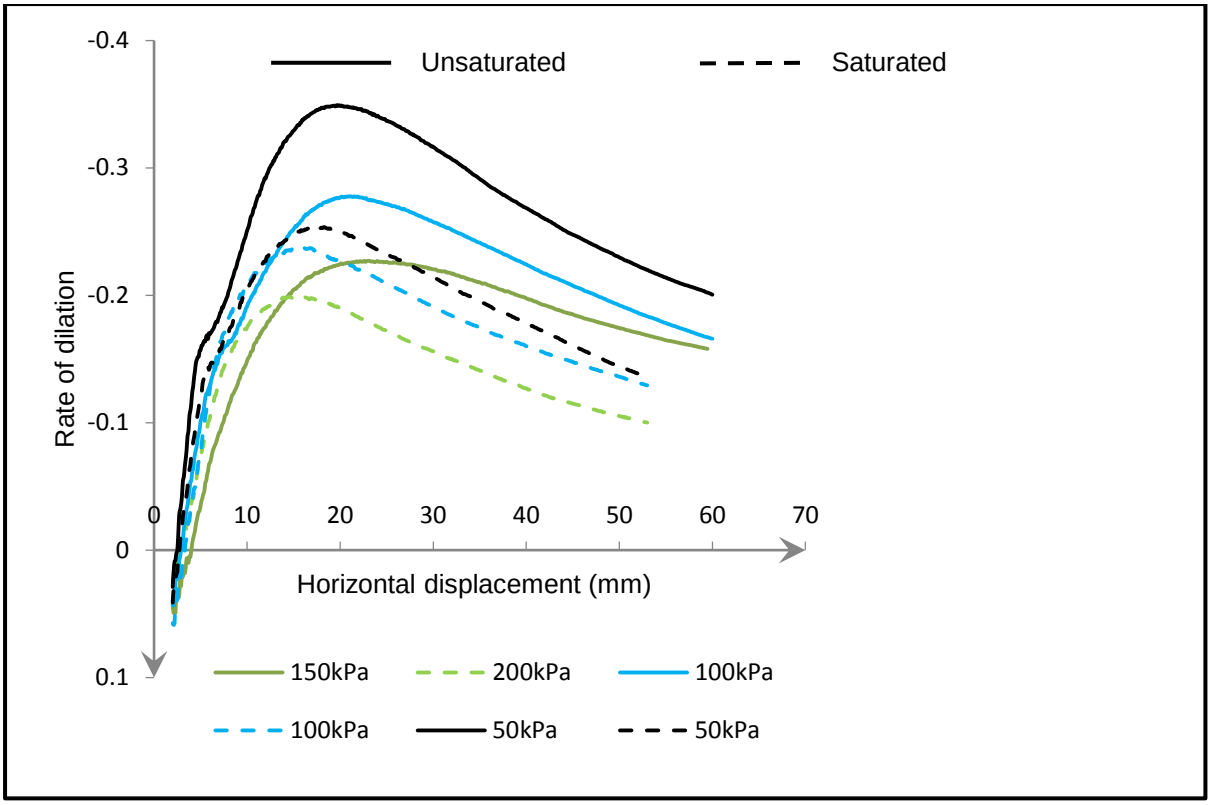

Figure A-3-3: Interlayer shear test; CTSB scarified with 26mm maximum aggregate size

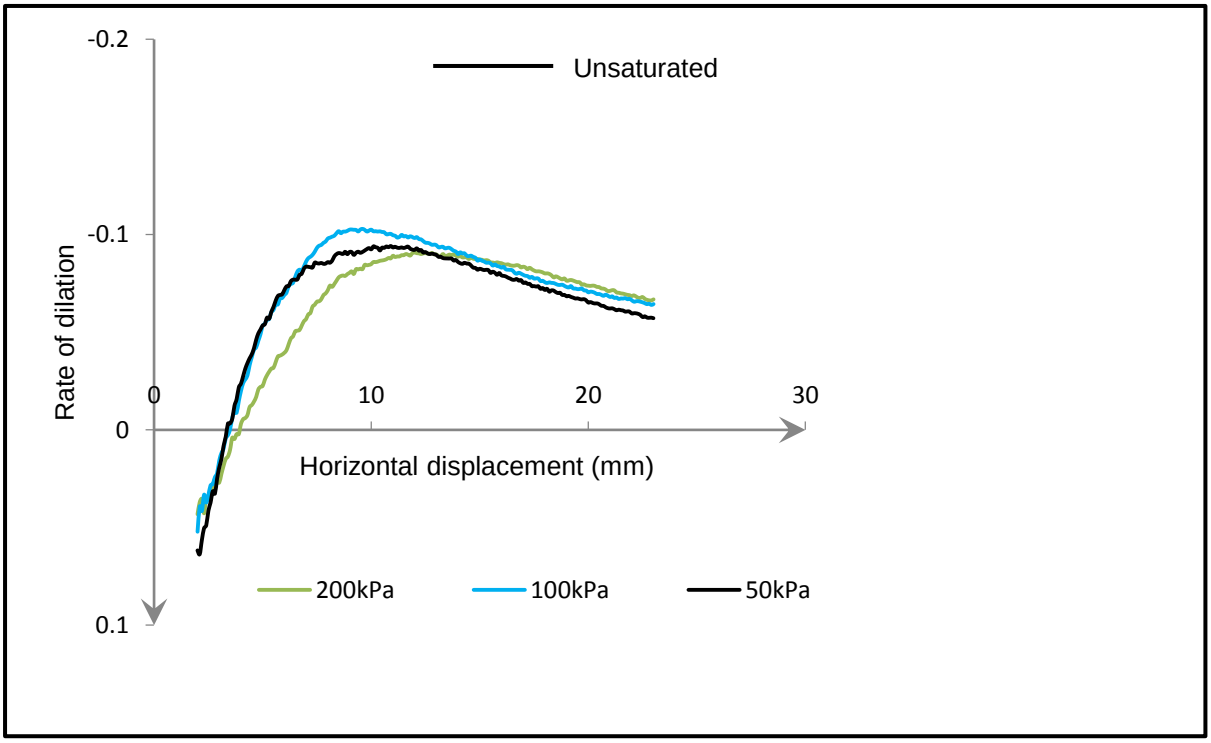

Figure A-3-4: Interlayer shear test; thin plastic at the interface, CTSB with 19mm maximum aggregate

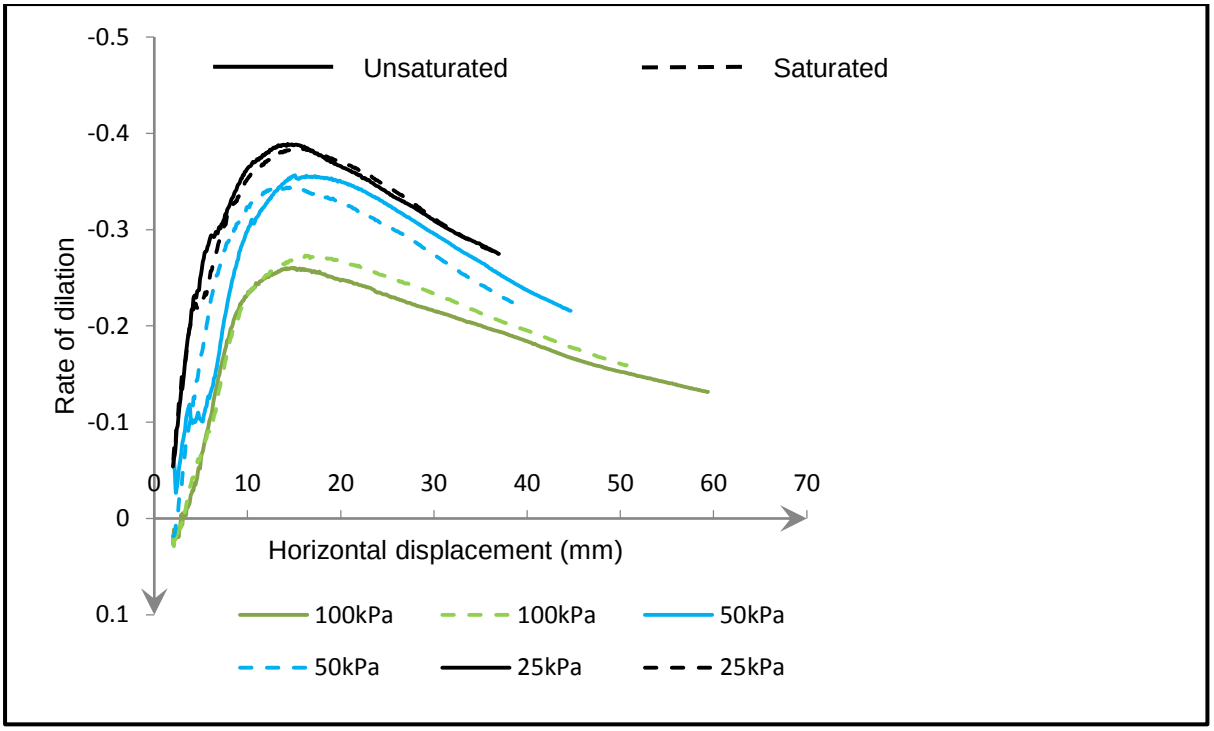

Figure A-3-5: Inlayer shear test; lightly cemented (CTSB)

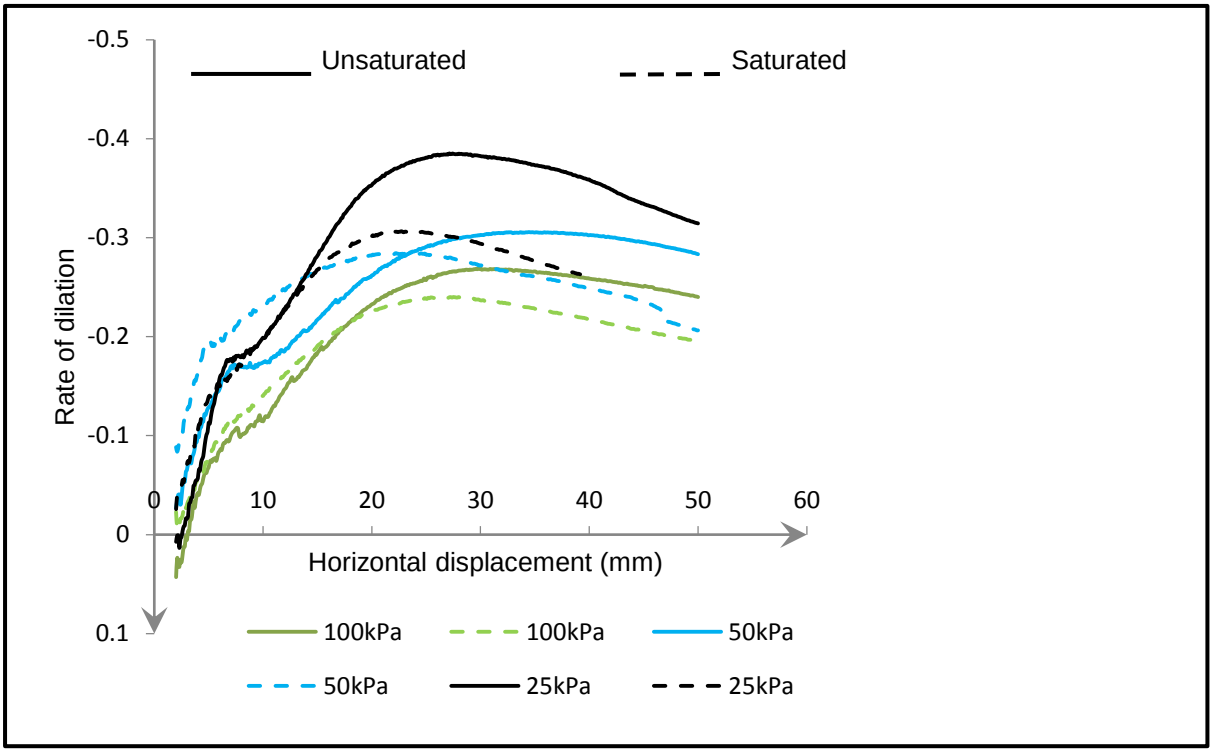

Figure A-3-6: Inlayer shear test; granular material G2

APPENDIX B: FACTORIAL DESIGN ANALYSIS

The factorial design analysis conducted in this study consisted of three variables whereby each variable was analysed at two levels. Two qualitative variables and one quantitative variable were considered. Qualitative variable are CTSB scarification and moisture condition and the quantitative variable is the applied normal pressure. Table B-1 shows a 2^3 data form used to calculate the main effect of each variable on the interlayer shear stress.

Table B-1: Data form for a 2^3 factorial design

Test condition number	Scarification (SC or NS)	Moisture condition (ST or US)	Normal pressure (kPa)	Interlayer shear stress (kPa)
	A	B	C	Y
1	NS	ST	50	100.3
2	SC	ST	50	157.7
3	NS	US	50	133.1
4	SC	US	50	176.4
5	NS	ST	100	173.0
6	SC	ST	100	267.1
7	NS	US	100	191.7
8	SC	US	100	299.7

Calculations of the individual measure of the effect of scarifying the CTSB surface before laying the GB, changing moisture condition and changing normal pressure from 50kPa to 100kPa are shown in Table B-2, Table B-3 and Table B-4 respectively.

Table B-2: Calculation of the main effect of scarification on the CTSB before laying the GB

Individual measure of the effect of scarification		Conditions at which comparison is made	
		Moisture condition	Normal pressure
		B	C
Y2-Y1	57.4	ST	50
Y4-Y3	43.3	US	50
Y6-Y5	94.1	ST	100
Y8-Y7	108	US	100
Main effect of scarification A	**75.7**		

Table B-3: Calculation of the main effect of changing moisture conditions

Individual measure of the effect of Moisture condition		Conditions at which comparison is made	
		Scarification	Normal pressure
		A	C
Y3-Y1	32.8	NS	50
Y4-Y2	18.7	SC	50
Y7-Y5	18.7	NS	100
Y8-Y6	32.6	SC	100
Main effect of Moisture conditions B	**25.7**		

Table B-4: Calculation of the main effect of changing the normal pressure from 50kPa to 100kPa

Individual measure of the effect of Normal pressure		Conditions at which comparison is made	
		Scarification	Moisture condition
		A	B
Y5-Y1	72.7	NS	ST
Y6-Y2	109.4	SC	ST
Y7-Y3	58.6	NS	US
Y8-Y4	123.3	SC	US
Main effect of Normal pressure C	**91**		

Two- factor interactions have been calculated by using Equation B-1 for scarification and moisture conditions, Equation B-2 for moisture conditions and normal pressure, Equation B-3 for scarification and normal pressure. Equation B-4 was used to calculate the three-factor interaction of scarification, moisture conditions and normal pressure.

$$A \times B = \frac{Y_1 + Y_4 + Y_5 + Y_8}{4} - \frac{Y_2 + Y_3 + Y_6 + Y_7}{4} \quad \textbf{(B-1)}$$

$$B \times C = \frac{Y_1 + Y_2 + Y_7 + Y_8}{4} - \frac{Y_3 + Y_4 + Y_5 + Y_6}{4} \quad \textbf{(B-2)}$$

$$A \times C = \frac{Y_1 + Y_3 + Y_6 + Y_8}{4} - \frac{Y_2 + Y_4 + Y_5 + Y_7}{4} \quad \textbf{(B-3)}$$

$$A \times B \times C = \frac{Y_2 + Y_3 + Y_5 + Y_8}{4} - \frac{Y_1 + Y_4 + Y_6 + Y_7}{4} \quad \textbf{(B-4)}$$

APPENDIX C: CALCULATION OF INTERLAYER SHEAR REACTION MODULUS K_s

The theory of interlayer shear reaction modulus has been used by different researchers to characterise the interlayer bonding strength between asphaltic pavement layers (Uzan, 1976; Uzan *et al., 1978;* Kruntcheva *et al.,* 2005). The theory was introduced by Uzan *et al.* (1978) and it is based on Goodman's constitutive law (Goodman *et al.,* 1968).

Figure C shows a typical shear-displacement curve of an interlayer shear test. The curve is characterised by the maximum shear stress τ_p and the associated horizontal displacement U_p. The interlayer shear reaction modulus is defined as the ratio between change in shear stress and horizontal displacement and it is expressed by the Equation C-1

$$\tau = K_s(\Delta U) \qquad \textbf{(C-1)}$$

Whereby:

τ : Maximum shear stress at the interface (MPa)

ΔU: Relative horizontal displacement at the interface (mm) and

K_s: the shear reaction modulus of the interface (MPa/mm).

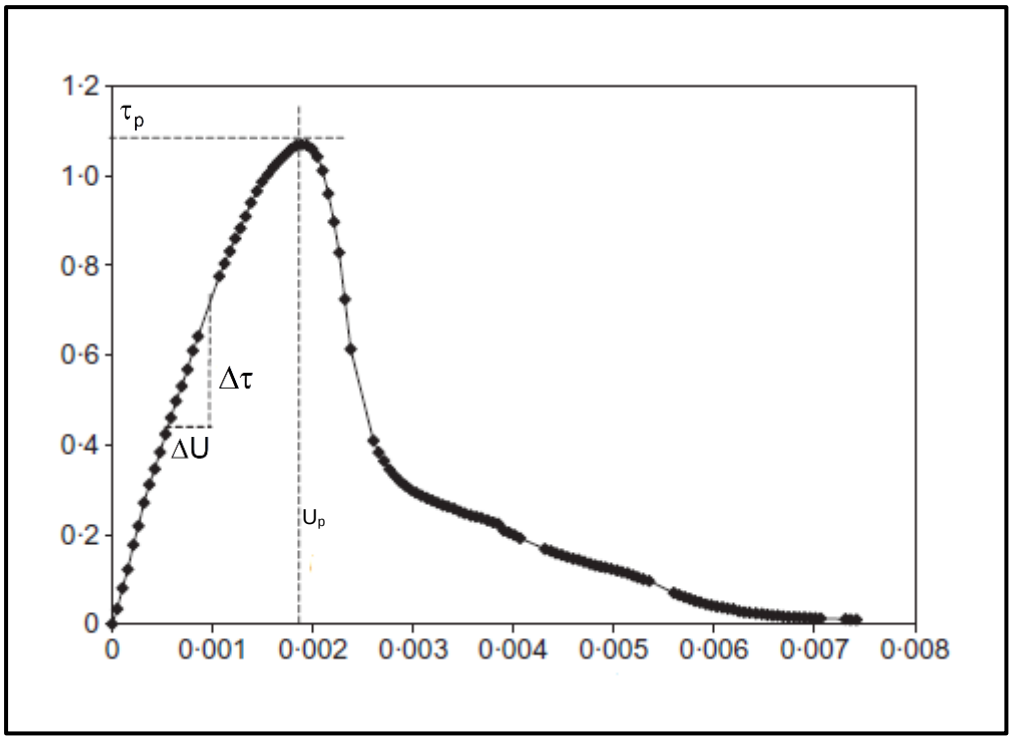

Figure C: General principle of the interlayer shear reaction modulus (Collop *et al.,* 2003)

APPENDIX D: TEST DATA AND WORK SHEETS FOR DIRECT SHEAR TESTING

D.1: INTERLAYER SHEAR TESTING

SPECIMENT SERIAL NUMBER: **Date:**
DESCRIPTION: **Bottom Plate Marking:**

Volume of the layer (m^3)	Height of the layer (mm)
0.00693	77

I. STABILIZED SUBBASE LAYER

1. MIX DESIGN

FULL MIX					HALF MIX
MDD	*OMC*	*AMC*	*WATER TO ADD*		*WATER TO ADD*
kg/m^3	%	%	%	g	g
2301	5.2	0.6	4.6	799	399

1/4 BW of C3 to be compacted (g)
4210

		CEMENT TO ADD			*CEMENT TO ADD*
BD (kg/m^3)	*BW(g)*	%	g		g
2407	16679	1.8	313		156

	C3	G5	C3	G5
Real weight without water (g)	15946	15664	7973	7832
Total weight to scoop (g)	17679	17367	8840	8683

2. DETERMINATION OF COMPACTION MOISTURE CONTENT

Spec SN	*Tin*	*EW (g)*	*FW (g)*	*DW (g)*	*MC (%)*	*Av MC (%)*

Spec SN	*Tin*	*EW (g)*	*FW (g)*	*DW (g)*	*MC (%)*	*Av MC (%)*

2. DATA OF THE SPECIMEN AFTER COMPACTION

							Weight of wooden base (g)		
Spec SN	H (mm)	Av H (m)	CSA (m^2)	Volume (m^3)	W(spec+base) (kg)	Spec Weight (kg)	WD (kg/m^3)	DD (kg/m^3)	Compaction %
1	1. 2. 3. 4.		0.09						

Spec SN	H (mm)	Av H (m)	CSA (m^2)	Volume (m^3)	W(spec+base) (kg)	Spec Weight (kg)	WD (kg/m^3)	DD (kg/m^3)	Compaction %
2	1. 2. 3. 4.		0.09						

Volume of the layer (m^3)	Height of the layer (mm)
0.00765	85

II. GRANULAR BASE LAYER (G2)

1. MIX DESIGN **Date:**

FULL MIX					HALF MIX
MDD	*OMC*	*AMC*	*WATER TO ADD*		*WATER TO ADD*
kg/m^3	%	%	%	g	g
2332	5.4	0.5	4.9	966	483

BD (kg/m^3)	BW (g)
2446	18714

1/4 BW of G2 to be compacted (g)
4718

Real weight without water (g)	17840	8920
Total weight to scoop (g)	19714	9857

2. DETERMINATION OF COMPACTION MOISTURE CONTENT

Spec SN	*Tin*	*EW (g)*	*FW (g)*	*DW (g)*	*MC (%)*	*Av MC (%)*

Spec SN	*Tin*	*EW (g)*	*FW (g)*	*DW (g)*	*MC (%)*	*Av MC (%)*

3. DATA OF THE SPECIMEN AFTER COMPACTION

Spec SN	H (mm)	Av H (m)	CSA (m^2)	Volume (m^3)	W(spec+s/base) (kg)	Spec Weight (kg)	WD (kg/m^3)	DD (kg/m^3)	Compaction %
	1. 2. 3. 4.		0.09						

Spec SN	H (mm)	Av H (m)	CSA (m^2)	Volume (m^3)	W(spec+s/base) (kg)	Spec Weight (kg)	WD (kg/m^3)	DD (kg/m^3)	Compaction %
	1. 2. 3. 4.		0.09						

Weigh of the specimen + Wooden base before compaction of the base layer	1	
	2	

Height of the CTSB before compaction of the base layer	1	
	2	

D.2: INLAYER SHEAR TESTING

SPECIMENT SERIAL NUMBER: **Date:**
DESCRIPTION: **Bottom Plate Marking:**

Volume of the layer (m^3)	Height of the layer (mm)
0.00693	77

I. STABILIZED SUBBASE LAYER

1. MIX DESIGN

FULL MIX					HALF MIX
MDD	*OMC*	*AMC*	*WATER TO ADD*		*WATER TO ADD*
kg/m^3	%	%	%	g	g
2301	5.2	0.6	4.6	799	399

1/4 BW of C3 to be compacted (g)
4210

		CEMENT TO ADD			*CEMENT TO ADD*
BD (kg/m^3)	*BW(g)*	%	g		g
2407	16679	1.8	313		156

	C3	G5	C3	G5
Real weight without water (g)	15946	15664	7973	7832
Total weight to scoop (g)	17679	17367	8840	8683

2. DETERMINATION OF COMPACTION MOISTURE CONTENT

Spec SN	*Tin*	*EW (g)*	*FW (g)*	*DW (g)*	*MC (%)*	*Av MC (%)*

Spec SN	*Tin*	*EW (g)*	*FW (g)*	*DW (g)*	*MC (%)*	*Av MC (%)*

2. DATA OF THE SPECIMEN AFTER COMPACTION

							Weight of wooden base (g)		
Spec SN	H (mm)	Av H (m)	CSA (m^2)	Volume (m^3)	W(spec+base) (kg)	Spec Weight (kg)	WD (kg/m^3)	DD (kg/m^3)	Compaction %
1	1. 2. 3. 4.		0.09						

Spec SN	H (mm)	Av H (m)	CSA (m^2)	Volume (m^3)	W(spec+base) (kg)	Spec Weight (kg)	WD (kg/m^3)	DD (kg/m^3)	Compaction %
2	1. 2. 3. 4.		0.09						

II. GRANULAR BASE LAYER (G2)
SPECIMENT SERIAL NUMBER: **Date:**

Volume of the layer (m^3)	Height of the layer (mm)
0.00693	77

Bottom Plate Marking:

1. MIX DESIGN

FULL MIX					HALF MIX
MDD	*OMC*	*AMC*	*WATER TO ADD*		*WATER TO ADD*
kg/m^3	%	%	%	g	g
2332	5.4	0.5	4.9	880	440

BD (kg/m^3)	BW (g)
2446	16953

1/4 BW of G2 to be compacted (g)
4278

Real weight without water (g)	16161	8080
Total weight to scoop (g)	17953	8976

2. DETERMINATION OF COMPACTION MOISTURE CONTENT

Spec SN	*Tin*	*EW (g)*	*FW (g)*	*DW (g)*	*MC (%)*	*Av MC (%)*

Spec SN	*Tin*	*EW (g)*	*FW (g)*	*DW (g)*	*MC (%)*	*Av MC (%)*

3. DATA OF THE SPECIMEN AFTER COMPACTION

							Weight of wooden base (g)		
Spec SN	H (mm)	Av H (m)	CSA (m^2)	Volume (m^3)	W(spec+base) (kg)	Spec Weight (kg)	WD (kg/m^3)	DD (kg/m^3)	Compaction %
	1. 2. 3. 4.		0.09						

Spec SN	H (mm)	Av H (m)	CSA (m^2)	Volume (m^3)	W(spec+base) (kg)	Spec Weight (kg)	WD (kg/m^3)	DD (kg/m^3)	Compaction %
	1. 2. 3. 4.		0.09						